New Insights into the Regulation of the Innate Immune Response During

Gastrointestinal Infection and Inflammation

By

Yvonne Louise Latour

Dissertation

Submitted to the Faculty of the

Graduate School of Vanderbilt University

in partial fulfillment of the requirements

for the degree of

DOCTOR OF PHILOSOPHY

in

Molecular Pathology and Immunology

December 17, 2022

Nashville, Tennessee

Approved by:

Keith T. Wilson, MD (mentor)
Jeffery C. Rathmell, PhD (committee chair)
Jeremy A. Goettel, PhD
Danyvid Olivares-Villagómez, PhD
Fiona E. Yull, D.Phil

To my family, for their love and encouragement

To Jon, for his unyielding support and belief in me

And finally,

To all the mice that were sacrificed to make this dissertation possible

ACKNOWLEDGEMENTS

There are many people that I would like to thank and acknowledge for their guidance during my time as a graduate student. First, I would like to thank my PhD mentor Dr. Keith T. Wilson for providing an exciting and supportive environment. Keith always maintained an open door, even during the pandemic, and he made it clear that my success and growth as an independent scientist was a priority. This meant that he asked the hardest questions but also knew when to push me and ask, "what's next?". I cannot thank him enough for all his support and training. Next, I would like to thank all members of the Wilson Lab. They have made my time as a student fun and productive. Alain was an immense help in conceptualizing projects and experiments. Carolina, Asim, and Kshipra were always ready with technical help when I needed it. I could not have done all the mouse experiments without Dan and Margaret, especially our karaoke mouse harvests. Kara, Jordan, Kamery, and Thad were always ready to lend a helping hand and an even more helpful ear. And I would also like to thank Lori for being an amazing role model as a woman in science. I would like to acknowledge and thank my committee Dr. Jeffery Rathmell, Dr. Danyvid Olivares-Villagómez, Dr. Fionna Yull, and Dr. Jeremy Goettel for their constructive feedback and new perspectives that they contributed to my research.

Finally, I would like to thank my friends and family. I have made amazing friendships during my time in Nashville. The girls nights, the soccer games, and the many venture outs in Nashville have kept me grounded and made both my time inside and outside if lab enjoyable. Thank you to my father, Larry, for cultivating a love of

TABLE OF CONTENTS

LIST OF TABLES

LIST OF FIGURES

ORIGINAL PUBLICATIONS

Latour YL, Gobert AP, Wilson KT. (2019). The Role of Polyamines in the Regulation of Macrophage Polarization and Function. *Amino Acids*. 52(2):151-160. doi: 10.1007/s00726-019-02719-0; PMID: 31016375; PMCID: PMC6812587.

Gobert AP, Latour YL, Asim M, Finley JL, Verriere TG, Barry DP, Milne GL, Luis PB, Schneider C, Rivera ES, Lindsey-Rose K, Schey KL, Delgado AG, Sierra JC, Piazuelo MB, Wilson KT. (2019). Bacterial Pathogens Hijack the Innate Immune Response by Activation of the Reverse Transsulfuration Pathway. *mBio* 10:e02174-19. doi: 10.1128/mBio.02174-19; PMID: 31662455; PMCID: PMC6819659.

Gobert AP, Boutaud O, Asim M, Zagol-Ikapitte IA, Delgado AG, Latour YL, Finley JL, Singh K, Verriere TG, Allaman MM, Barry DP, McNamara KM, Sierra JC, Amarnath V, Tantawy MN, Bimczok D, Piazuelo MB, Washington MK, Zhao S, Coburn LA, Wilson KT. (2020). Dicarbonyl Electrophiles Mediate Inflammation-Induced Gastrointestinal Carcinogenesis. *Gastroenterology*. 160(4):1256-1268.e9. doi: 10.1053/j.gastro.2020.11.006; PMID: 33189701; PMCID: PMC7956217.

Gobert AP, Finley JL, Latour YL, Asim M, Smith TM, Verriere TG, Barry DP, Allaman MM, Delagado AG, Rose KL, Calcutt MW, Schey KL, Sierra JC, Piazuelo MB, Mirmira RG, Wilson KT. (2020). Hypusination Orchestrates the Antimicrobial Response of Macrophages. *Cell Rep*. 3(11):108510. doi: 10.1016/j.celrep.2020.108510; PMID: 33326776; PMCID: PMC7812972.

Gobert AP, Latour YL, Asim M, Barry DP, Allaman MM, Finley JL, Smith TM, McNamara KM, Singh K, Sierra JC, Delgado AG, Luis PB, Schneider C, Washington MK, Piazuelo MB, Zhao S, Coburn LA, Wilson KT. (2021). Protective Role of Spermidine in Colitis and Colon Carcinogenesis. *Gastroenterology*. 162(7):2138-2143. doi: 10.1053/j.gastro.2021.11.005; PMID: 34767785; PMCID: PMC8881368.

Latour YL, Sierra JC, Finley JL, Asim M, Barry DP, Allaman MM, Smith TM, McNamara KM, Luis PB, Schneider C, Jacobse J, Goettel JA, Calcutt MW, Rose KL, Schey KL, Milne GL, Delgado AG, Piazuelo MB, Paul BD, Snyder S, Gobert AP, Wilson KT. (2022). Cystathionine γ-Lyase Exacerbates *Helicobacter pylori* Immunopathogenesis by Promoting Macrophage Metabolic Remodeling and Activation. *JCI Insight*. 17:e155338. doi: 10.1172/jci.insight.155338. PMID: 35579952; PMCID: PMC9309056.

Latour YL*, Sierra JC*, McNamara KM, Smith TM, Luis PB, Schneider C, Delgado AG, Barry DP, Allaman MM, Calcutt MW, Schey KL, Piazuelo MB, Gobert AP, Wilson KT. (2022). Ornithine Decarboxylase in Gastric Epithelial Cells Promotes the Immunopathogenesis of *Helicobacter pylori* Infection. *J Immunol.* 209 (4) 796-805. doi: 10.4049/jimmunol.2100795; PMID: 35896340; PMCID: PMC9378675.
*These authors contributed equally to this work and are co-first authors

Peek CT, Ford CA, Eichelberger KR, Jacobse J, Torres TP, Maseda D, Latour YL, Piazuelo MB, Johnson JR, Byndloss MJ, Wilson KT, Rathmell JC, Goettel JA, Cassat JE. (2022). Intestinal Inflammation Promotes MDL-1^{+} Osteoclast Precursor Expansion to Trigger Osteoclastogenesis and Bone Loss. *Cell Mol Gastroenterol Hepatol*. 14(4):731-750. doi: 10.1016/j.jcmgh.2022.07.002; PMID: 35835390; PMCID: PMC9420375.

CHAPTER 1

Introduction

1.1 Immunopathogenesis and Inflammation

Immunopathology is a general term to describe disorders that arise from a defective or malfunctioning immune response. These defects can affect either the innate or adaptive immune system and result from autoimmunity (reaction to self), immunodeficiency, or an overactive/hyperactive immune response.[1] Autoimmunity largely occurs when an organism develops self-reactive T cells and autoantibodies, turning the immune system against its own host and attacking the body's tissues. Examples of autoimmune diseases include multiple sclerosis (MS), rheumatoid arthritis (AR), Hashimoto's thyroiditis, and type 1 diabetes mellitus.[2] Immunodeficiencies occur when the immune response is compromised or completely absent due to genetic abnormalities (primary immunodeficiency disease; PID) or by infection with a pathogen, treatment with immunosuppressive drugs, autoimmunity, or malnutrition.[1] Lastly, an overzealous immune response or improper immune regulation can be detrimental to the surrounding tissue and are associated with chronic inflammatory diseases such as inflammatory bowel disease (IBD) and infection with the gastric pathogen *Helicobacter pylori*. Uncovering new mechanisms that regulate inflammation in the context of bacterial infections in the gut will be a focus of this dissertation.

Inflammation is an intricate set of cellular and molecular processes in response to harmful stimuli such as tissue injury or infection. The goal of inflammation is to return to body back to homeostasis, however, as mentioned above, a dysregulated immune response can have pathological consequences. At the onset of the primary insult, dendritic cells and macrophages residing in the afflicted tissue produce mediators including cytokines and chemokines that coordinate the recruitment and activation of other leukocytes to the local area.[3] In incidences of

bacterial infections, pathogen detection is triggered by ligation of pathogen-associated molecular patterns (PAMPs) to Toll-like receptors (TLRs) and nucleotide-binding oligomerization-domain protein (NOD)-like receptors (NLRs) on the surface of and inside the resident immune cells, respectively.[4] Once a threat has been identified, chemokines such as IL-8, CXCL1, CXCL2, and CCL2 and other factors that increase vasodilation and endothelial permeability allow selective extravasation of circulating neutrophils and monocytes into the site of infection.[5]

Neutrophils are professional exterminators and release effectors such as reactive oxygen species (ROS) and proteinases from their granules to kill invading pathogens, but this comes at a cost to the host as these actions do not discriminate and can also cause damage to the tissue. Monocytes contribute to the pool of macrophages and dendritic cells whose differentiation depends on the state of the surrounding microenvironment culminating in a heterogenous population.[6] Under inflammatory conditions, cytokines such as IL-1β, IL-6, and IFNγ drive the monocyte into a proinflammatory macrophage phenotype with antimicrobial abilities. The inflammatory response is deactivated by the presence of IL-10 and transforming growth factor-β (TGFβ) while alternate activation during humoral immunity and tissue repair is mediated by the cytokines IL-4 and IL-13.[7,8] The inflammatory environment is very dynamic and contains multiple stimuli resulting in a spectrum of macrophage phenotypes simultaneously.[6] Macrophages possess the ability to produce antimicrobial molecules, phagocytose microbes and dying cells, present antigens to T cells, and perpetuate the current state of inflammation through cytokine and chemokine release. Under steady state normal conditions, the circulating monocytes can replenish the resident macrophage and dendritic cell population. This is important in tissues such as the stomach and colon where there is high turnover of innate immune cells due to the constant interactions with ingested particles and microbiota at the mucosal surface.[6]

Although not immune cells in the traditional sense, epithelial cells that line mucosal surfaces act as the first line of defense against pathogenic infections by providing a physical barrier, detecting microbial dysbiosis, and regulating the immune response. Tight junctions between cells help limit the movement of commensal microbes and non-invasive pathogens into the underlying tissue while also allowing sampling of the lumen by macrophages and dendritic cells.[9,10] Within the gastrointestinal (GI) epithelium, specialized epithelial cells are distributed throughout the unicellular layer of enterocytes. M cells help sample the luminal environment and translocate

2

material to gut-associated lymphoid tissue. Paneth cells produce and store antibacterial peptides such as defensins while goblet cells release mucins that form the mucus layer that protects the apical surface of the epithelium.[10] GI epithelial cells are also equipped with external and internal pattern recognition receptors (PRRs) to detect certain PAMPS.[11] In response to PAMP recognition, epithelial cells have the autonomous innate immune ability to produce antimicrobial proteins and ROS as well as secret chemokines and cytokines to signal to immune cells that there is an infection, such as pathogenic *Escherichia coli*. Additionally, the close contact and gap junction between epithelial cells also allow for rapid amplification of a distress signal through intercellular communication.[11]

As part of the adaptive branch of immunity, CD4 T cells are another key player in the inflammatory response to pathogens in the gut. Similar to monocytes, naïve CD4 T cells can differentiate into different sub-populations of T helper cells based on the environmental stimuli.[12] Activation of CD4 T cells depends on a specific cytokine combination. Examples include IFNγ + IL-12 giving rise to Th1 cells, IL-4 + IL-2 giving rise to Th2 cells, TGFβ + IL-6 giving rise to Th17 cells, and IL-1β + IL-23 giving rise to Th22 cells. Upon stimulation of the T cell receptor (TCR) by MHCII on antigen presenting cells, co-stimulation of CD28, and cytokine recognition, specific transcriptional factors are upregulated and determine the fate and effector function of the Th cell. Regulatory T cells (Tregs) are essential in maintaining homeostasis in the gut by suppressing inflammatory responses to commensal bacteria and nutrients.[12]

Overall, the body has adapted ways to fight against infectious pathogens and once infection is cleared, has also adapted ways to put a stop inflammation, and repair and restore physiological function to the affected tissue.[13] When inflammation is not resolved due to a defect in the host response or persistent infection by a bacterium that has evolved mechanisms to avoid eradication, such as *H. pylori*, the body can be locked in a chronic inflammatory state. Chronic inflammation becomes a vicious cycle of immune cell infiltration and release of effector molecules that can cause tissue damage and lead to disease.[14] To develop treatments for diseases that arise from chronic inflammation, understanding the physiological pathways that culminate in a state of chronic inflammation are crucial and a central theme of this dissertation.

1.2 *Helicobacter pylori*

H. pylori is a highly prevalent Gram-negative bacterium that infects up to 50% of the world's population.[15] It is transmitted orally and has developed strategies to colonize the gastric mucosa. The majority of individuals will develop chronic gastritis while remaining asymptomatic. A subset of individuals develop more severe gastroduodenal pathologies that stem from the chronic inflammatory state including peptic ulcers, mucosal-associated lymphoid tissue lymphoma, and gastric adenocarcinoma.[16] Evidence of *H. pylori* infection is associated with 89% of gastric cancer cases, the fourth leading cause of cancer mortality, making *H. pylori* the greatest risk factor and the first bacteria to be identified as a cause for cancer.[17,18] It is currently classified as a Group I carcinogen by the World Health Organization.[19] Due to the high prevalence of *H. pylori* colonization and its mostly asymptomatic presence, it has been suggested that *H. pylori* represents a member of the commensal microbiota.[20] However, the lack of clinical and biological markers to reliably predict risk of disease progression maintains *H. pylori* as a significant public health threat and an important field of study.[21]

H. pylori expresses several virulence factors that enhances the risk of cancer development in addition to environmental factors, host genetics, and lifestyle choices.[22–25] The most well studied and potent virulence factor is cytotoxin associated gene A (CagA). CagA is injected into host cells by a type IV secretion system (T4SS) that is encoded by the *cag* pathogenicity island (PAI). Once in the cell, CagA is phosphorylated by host machinery and enhances the miotic activity of gastric epithelial cells.[26] The mechanism in which translocation of CagA contributes cancer development is not completely understood, but CagA$^+$ strains of *H. pylori* are associated with cancer development in humans and gastritis in animal models.[27–29]

Another important toxin is VacA. Unlike CagA, all *H. pylori* strains carry the *vacA* gene with varying levels of expression caused by sequence variation.[30] The most prominent effect of VacA on host cells is the formation and accumulation of vacuoles.[30] In addition, VacA can form pores in the cytoplasmic membrane leaving the host cell open to bacterial infection and can enter the mitochondrial inner membrane and disrupt the transmembrane potential triggering cellular apoptosis of gastric epithelial cells.[31,32]

1.3 *H. pylori* vs. the Host

The stomach is a harsh environment to inhabit, and *H. pylori* has evolved multiple strategies to persist and thrive. The gastric lumen has a pH of 1-2 but, the helical shape and numerous flagella possessed by *H. pylori* allows it to swiftly migrate to the gastric lining and burrow through the mucus layer to sit along the epithelial surface.[33,34] Moreover, *H. pylori* produces urease that raises the pH of the gel formed by gastric mucins and decreases the viscosity making it easier for *H. pylori* to swim.[35,36]

In addition to physical barriers, *H. pylori* has also developed ways to elude and subvert the host immune response that contributes to its success as one of the most prolific human pathogens. Gastric epithelial cells and innate immune cells use PRRs such as TLRs to detect invading pathogens. Slight modifications of the structures of *H. pylori* derived LPS and flagella avoid detection by TLR4 and TLR5, respectively.[37–39] *H. pylori* LPS can activate TLR2, but induces expression of IL-10 that helps suppress the T cell response.[40,41] Translocation of DNA by the T4SS does not trigger a proinflammatory signaling cascade by TLR9, but instead promotes an antiinflammatory outcome.[42] Phagocytosis by neutrophils and macrophages followed by an oxidative burst to facilitate bacterial killing is a key component of the innate immune response to pathogens. *H. pylori* express superoxide dismutase (SOD), catalase, and the highly conserved neutrophil-activating protein (NapA) to combat the respiratory burst of phagocytes and the rising level of ROS in the microenvironment due to the repeated cycle of inflammation. [43–45]

Furthermore, *H. pylori* can manipulate the adaptive immune response by suppressing effector T cell function through preferential activation of Tregs. Chronic gastritis is perpetuated by an influx of Th1 and Th17 cells that are crucial for pathogen control but are no less ineffective at resolving infection.[46–49] Dendritic cells exposed to *H. pylori* induce a Treg response that increases the production of IL-10 and effectively suppresses the effector T helper response.[50] *H. pylori* VacA and γ-glutamyl transpeptidase (GGT) also indirectly contributes to the differentiation of Tregs and inhibit Th cell proliferation by interfering with TCR signaling and inducing cell cycle-arrest.[51–54] The combination of the ability of *H. pylori* to persist in the harsh environment of the gastric niche, circumvent immune recognition, and influence the host response culminates in the chronic inflammatory state that leads to tissue injury, DNA damage, and risk of precancerous lesions.

Macrophages are among the first cells recruited to the gastric lamina propria and play a significant role in the pathogenicity of *H. pylori* infection. Mice injected with dichloromethylene diphosphonate (Cl$_2$MDP)-loaded liposomes had an overall depletion of circulating CD11b$^+$ cells of the monocyte/macrophage lineage and substantial reduction of the recruitment of CD11b$^+$ cells to gastric tissues, normally seen with *H. pylori* infection.[55] This reduction did not affect the colonization or survival of *H. pylori*; however, there was markedly less inflammation suggesting that macrophages are a key contributor to the pathogenicity of *H. pylori*-associated gastritis.[55] This supports one of the hallmarks of *H. pylori* infection: evasion of the elicited innate and adaptive immune response leads to the chronic inflammation responsible for the progression of infection to gastric adenocarcinoma.[16,45,56] Therefore, an aim of this dissertation is to identify pathways within macrophages that contribute to activation as potential targets to limit immunopathogenic consequences.

1.4 Macrophage Polarization and Function

Macrophages are bone marrow-derived monocytes and are the first line of defense against invading pathogens by acting as a surveillance system and are thus a key component of the innate immune response. The fate of macrophages is dependent on environmental factors that stimulate polarization to either classically activated proinflammatory M1 or alternatively activated M2 types. However, this is not a strict dichotomy and macrophages can sit along a spectrum of activation states between M1 and M2. For the purpose of this dissertation, the terms M1 or M2, or proinflammatory and antiinflammatory will be used to describe the general activation state for simplicity. Specific ligands mediate these distinct changes through toll-like receptors. Pathogen-associated molecular markers such as lipopolysaccharide (LPS), damage-associated molecular markers, growth factors, and IFN-γ, a Th1 cytokine, elicit proinflammatory activation, while Th2 cytokines, such as IL-4 and IL-13, elicit the alternative response.[7,8] Nitric oxide (NO) production, through upregulation of inducible NO synthase (NOS2), and nuclear factor kappa-light-chain enhancer of activated B cells (NF-κB) signaling are key characteristic of M1 macrophages.[57] These classically activated M1 macrophages also produce high levels of ROS and proinflammatory cytokines, including TNFα, IL-1β, and IL-12, contributing to pathogen killing and recruitment of other proinflammatory cell types.[58] In contrast, tissue remodeling, wound healing, tumor environment regulation, allergic

reactions, and responses to helminths involve M2 macrophages.[59] These alternatively activated macrophages have enhanced arginase activity and produce IL-10. Due to the high diversity of M2 macrophage functions, the alternatively activated subset can further be subdivided into regulatory macrophages (Mregs), tumor-associated macrophages (TAMs), myeloid-derived suppressor cells (MDSCs), and profibrotic macrophages (M2a).[58,60,61] Each of these M2 subtypes have distinct activators and effector roles, but are overall immunosuppressive. Mregs are both activated by, and secrete IL-10, express neither arginase nor NOS2, but function to suppress the classically activated M1 macrophages.[57,62] Tumor-derived factors within the tumor environment (e.g. hypoxia), in addition to the classic M2 stimuli, promote the differentiation and polarization of TAMs.[63] This contributes to both the initiation and progression of tumor growth by immune suppression and angiogenesis.[63] MDSCs are thought to be the predecessors of TAMs, but have high expression of GR1, a proinflammatory marker, in mice, low expression of F4/80, and have both arginase and NOS2 activity.[64] MDSCs function to suppress the innate and T-cell response in cancer. M2a macrophages express fibronectin and secrete high amounts of IL-4 and IL-13, promoting wound healing and extracellular matrix formation.[65] Once activated, macrophages retain plasticity and can switch from one functional phenotype to another based on environmental signals, but excessive activity of either polarization state can result in tissue damage, inflammatory disease, fibrosis, or tumor growth.[66–71] Thus, elucidating the mechanisms of macrophage regulation is essential for disease management.

A growing body of evidence suggests that macrophages reprogram their metabolism to meet the energetic needs of their current activation state.[72,73] As described above, each polarization state comes with its own set of effector functions and secreted factors. It has been shown that macrophages in a proinflammatory state downregulate oxidative phosphorylation (OXPHOS) while upregulating aerobic glycolysis to generate energy in a more efficient manner and promote the production of proinflammatory cytokines.[74,75] In addition, M1-like macrophages modulate the TCA cycle to reroute intermediates to aid in the production of effector molecules such as ROS, prostaglandin 2 (PGE2), NO, and itaconate.[75–78] When a macrophage enters an M2-like antiinflammatory state, they upregulate OXPHOS while maintaining an intact TCA cycle and rely on glutamine catabolism for energy and effector function.[75,79] Numerous studies have linked inflammatory diseases to changes in immunometabolism.[80]

Thus, macrophage metabolism represents a promising avenue for therapeutic intervention of immunopathogenic disorders.

1.5 *H. pylori* and Macrophage Polyamine Metabolism

Polyamines are naturally occurring, ubiquitously distributed amino acids that are synthesized from L-ornithine by ornithine decarboxylase (ODC; also known as ODC1).[81,82] Once transported into the cell by the solute carrier family 7 member 1/2 (SLC7A1/2), L-arginine is metabolized by arginase to L-ornithine and urea.[81–83] Arginase is present in the cell in two isoforms; arginase 1 (ARG1) is abundantly found in liver and is involved in the urea cycle, and arginase 2 (ARG2) is found in kidney and localizes to the mitochondria. Ornithine is then converted into putrescine by ODC in the cytosol.[84,85] Putrescine can then be converted to spermidine by spermidine synthase (SRM) and spermidine converted to spermine by spermine synthase (SMS) (Figure 1.1). The conversions to spermidine and spermine require the transfer of an aminopropyl group that is donated by the decarboxylated form of S-adenosylmethionine, referred to as dcSAM.[81,82] Methionine is first metabolized to SAM, which can then be decarboxylated to dcSAM by S-adenosylmethionine decarboxylase (SAMDC), which is encoded by the gene *AMD1*. The activity of SAMDC is positively regulated by putrescine and inhibited by spermidine.[82]
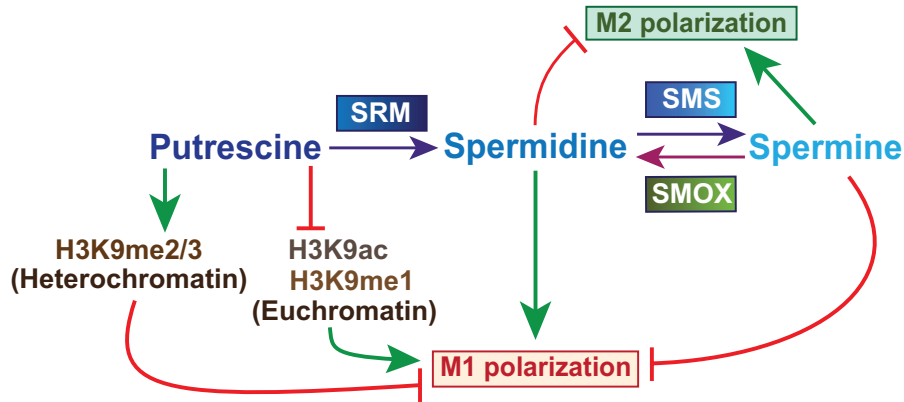
Figure 1.1 Overview of polyamine synthesis and the effect on macrophage polarization. Putrescine is converted to spermidine by spermidine synthase (SRM) and spermidine is converted to spermine by spermine synthase (SMS). Spermine oxidase (SMOX) back-converts spermine to spermidine. Macrophages have two main polarization states; classically activated pro-inflammatory M1 macrophages and alternatively activated, anti-inflammatory and pro-tumoral M2 macrophages. Putrescine inhibits the formation of euchromatin thus downregulating the expression of M1 genes. Spermidine favors M1 polarization while spermine favors M2.

Polyamines play a role in a wide range of cellular functions including cell development, amino acid and protein synthesis, oxidative DNA damage, proliferation, and differentiation.[82] More recently, it has been found that polyamine levels may contribute to alterations of histone modifications and chromatin structure consequently affecting DNA stability and transcription.[69,71,86–89] The overall rate-limiting step of polyamine synthesis, the decarboxylation of L-ornithine by ODC, has been highly studied and inhibition of ODC by difluoromethylornithine (DFMO) has entered clinical trials as a treatment to prevent relapse in patients with neuroblastoma and in patients at high risk of developing colorectal or gastric adenocarcinoma.[84,90–93] Endogenous regulation of ODC is achieved by the induction of antizyme, a natural inhibitor of ODC that is translationally controlled by polyamine levels.[84,90–94] Antizyme directly binds to ODC, triggering its rapid degradation by the proteasome.

Our lab has shown that *H. pylori* induces dysregulation of polyamine synthesis and metabolism that affects disease progression.[91,95–97] Expression of the inducible arginine transporter SLC7A2, also known at cationic amino transporter 2 (CAT2), was found to be upregulated in both mouse and human gastric tissues with *H. pylori*-induced gastritis.[83,96] *H. pylori* infection also upregulates ARG2 and ODC expression in human gastric tissues at both the

mRNA and protein levels, however, ARG1 is not induced.[98,99] This upregulation of ARG2 comes at a cost to the host: ARG2 competes with NOS2 for the availability of L-arginine.[99] In addition, during *H. pylori* infections, the increased activity of ARG2 directly inhibits the translation of NOS2, effectively inhibiting NO production.[99]

In conjunction with upregulation of ARG2, it has been reported that *H. pylori* also induces the increased expression of spermine oxidase (SMOX), an enzyme responsible for the catabolism of spermine to spermidine.[100] This induction is highly dependent on the presence of the *H. pylori* virulence factor CagA, which is also associated with a high risk of developing gastric cancer.[97] Patient gastric tissue and *in vitro* studies using clinical isolates showed higher levels of SMOX expression and risk of developing gastric cancer in correlation with functional CagA secretion.[91,97] The back-conversion of spermine to spermidine is also responsible for the release of H_2O_2, leading to DNA damage and apoptosis. Gerbil studies showed that inhibition of either ODC or SMOX reduced the rate of adenocarcinoma development and DNA damage in cells resistant to apoptosis.[91]

Our lab has shown that the L-arginine metabolic enzymes induced in gastric tissue and epithelial cells are also upregulated in macrophages during *H. pylori* infection. L-arginine is selectively transported into macrophages by SLC7A2 during *H. pylori* infection.[96,101] There is a significant increase of *Arg2*, but not *Arg1*, mRNA expression in *H. pylori*-infected murine macrophages, with the cell line RAW 264.7, and also in primary macrophages.[98,99] Enhanced expression of ARG2 protein levels correlates with the increase in gene expression; ARG1 protein was, again, not induced.[98,99] Past studies demonstrate that the induction or inhibition of arginase and NOS2 inversely vary due to direct competition for available L-arginine. Peritoneal macrophages isolated from *Arg2* knockout mice infected with *H. pylori*, express increased levels of NOS2 and produce more NO compared to infected wild-type (WT) mice.[99] These findings were confirmed *in vivo* using *H. pylori*-infected mice with treatment of the arginase inhibitor *S*-(2-boronoethyl)-L-cysteine (BEC) or ARG2 deletion.[99]

ARG2 impairs the host response to *H. pylori* in addition to competing with NOS2 for the available L-arginine.[102] *Arg2* knockout mice infected with *H. pylori* have decreased bacterial colonization and increased histologic inflammation compared to infected WT mice.[102] Additionally, these mice exhibit enhanced transcription of the genes encoding the pro-inflammatory cytokines IFN-γ, IL-12p40, and IL-17A, and downregulation of the immune regulatory cytokine IL-10.[102] ARG2 deletion also results in an increased influx of macrophages to the

gastric tissues with infection, and these recruited macrophages express higher levels of NOS2 with less evidence of macrophage apoptosis.[102] A more recent study from our laboratory has expanded on these findings and demonstrates the effects of ARG2 on macrophage polarization.[103] Bacterial colonization and gastric inflammation do not differ between *Arg2* knockout and *Arg2;Nos2* double knockout mice, suggesting that the effects of ARG2 *in vivo* are independent of NOS2.[103] *Arg2* knockout mice exhibit enhanced M1 macrophage activation through increased mRNA expression of *Ifng, Il17a, Nos2, Il1b*, and *Tnfa*, and increased production of the pro-inflammatory markers TNF-α, IL-1β, CCL3, CCL4, CCL5, and NO in both gastric tissues and bone marrow-derived macrophages (BMmacs).[103] Loss of ARG2 also modulates changes in the expression of enzymes involved in the polyamine metabolism pathways. The genes encoding ARG1, ODC, SAMDC, diamine acetyltransferase 1 (SAT1), and SMOX are all upregulated in *H. pylori*-infected gastric tissues and BMmacs as a compensatory mechanism for ARG2 deficiency.[103] The decrease of putrescine and increase of spermine by ARG2 deficiency also elicited a more vigorous Th1/Th17 response, indicating that the expression of Th1/Th17 cytokines in the *H. pylori*-infected stomach is dependent on relative polyamine levels.[103] Altogether, these data support the concept that metabolism of L-arginine by arginase drives macrophages away from an M1 response.

To assess the role of chronic inflammation on macrophage function, Chaturvedi et al. isolated gastric macrophages after a 4-month infection with *H. pylori* and re-stimulated them with *H. pylori* lysate.[96] These cells exhibited increased expression of *Slc7a2, Odc*, and *Nos2*.[96] Nevertheless, the increase of mRNA did not result in a corresponding increase in protein levels in macrophages isolated from the infected mice. In fact, there was a decrease in NOS2 protein levels, NO production, and L-arginine uptake compared to cells from uninfected mice, suggesting that polyamine synthesis during chronic infection may favor and maintain an M2-like response, in that M1 responses are blunted.[96] Moreover, in that study it was shown that spermine can impair L-arginine uptake into macrophages, providing one potential mechanism for diminished NOS2 protein expression and NO production as *H. pylori*-stimulated NOS2 protein translation is specifically dependent on L-arginine availability in macrophages.[96,104]

Not only does *H. pylori* induce ARG2, but infection upregulates the expression of ODC in macrophages.[98] Similar to ARG2, the induction of ODC diverts the utilization of L-arginine towards polyamine synthesis and away

from NOS2. Bussière et al. knocked down *Odc* expression with siRNA, demonstrating an inverse relationship with NOS2.[105] *Odc* knockdown increased NOS2 protein expression and NO production, without affecting *Nos2* mRNA levels, which was associated with decreased spermine concentrations within macrophages.[96,105] Inhibiting ODC and putrescine synthesis in *H. pylori*-infected BMmacs with the pharmacological inhibitor DFMO decreased levels of putrescine, supporting the host immune response by enhancing the M1 phenotype without altering M2 activation.[69] These findings are recapitulated *in vivo* with mice treated with DFMO and inoculated with *H. pylori*. [69,96] There is an increase of arginine uptake, *Nos2* translation, and NO production in gastric macrophages. The outcome of this upregulation is decreased *H. pylori* colonization and decreased gastric inflammation in infected mice.[69,96] Supplementation of putrescine in BMmacs rescues ODC inhibition by decreasing M1 macrophage and NLR family, pyrin domain containing (NLRP) 3-driven inflammasome activation demonstrating that putrescine, generated by the induction of ODC, has a role in macrophage function.[69]

In partial contrast to the findings with DFMO, myeloid specific *Odc* knockout (*Odc*$^{\Delta mye}$) mice exhibit decreased *H. pylori* colonization, but increased histological inflammation scores.[69] Using *Odc*$^{\Delta mye}$ mice, Hardbower et al. demonstrated that ODC and putrescine alter histone modifications and attenuate the M1 response.[69] H3K4 monomethylation (H3K4me1) and H3K9 acetylation (H3K9ac) are known histone modifications that enhance euchromatin formation and thus gene expression, while H3K9 di/trimethylation (H3K9me2/3) is associated with decreased gene expression.[106,107] Hardbower et al. found that during *H. pylori* infection of *Odc*$^{\Delta mye}$ BMDM, there is a significant increase of H3K9me1 and H3K9ac, but a decrease of H3K9me2/3.[69] Treatment with BIX 01924, a selective inhibitor of H3K9 methyltransferase, removed the inhibitory methylation of *Odc*$^{fl/fl}$ BMmacs and increased M1 markers, while having no effect on *Odc*$^{\Delta mye}$ BMmacs.[69] In contrast, treatment with anacardic acid, an inhibitor of lysine transferase 2A, reversed the increased M1 expression in *Odc*$^{\Delta mye}$ BMmacs while having no effect in *Odc*$^{fl/fl}$ BMmacs.[69] The histone modification and euchromatin formation of *H. pylori*-infected *Odc*$^{\Delta mye}$ mice leads to an increases of gene expression of macrophage-derived proinflammatory markers *Il1b, Il6, Il12a, Il12b, Tnfa,* and *Nos2* in gastric tissue and stimulated BMmacs.[69] Infection of *Odc*$^{\Delta mye}$ mice resulted in an increase in production of proinflammatory cytokines CCL2, CCL3, CCL4, CCL5, CXCL1, CXCL2, CXCL10, IL-17, and TNF-α.[69] This enhanced M1 macrophage activation was also observed in human THP-1 macrophage-like cells treated with

DFMO.[69] The exogenous addition of putrescine reversed the histone modifications and M1 marker expression observed in $Odc^{\Delta mye}$ BMmacs, highlighting the role of putrescine in macrophage polarization (Fig. 1).[69]

Increased polyamine synthesis provides SMOX with available substrate. Since the catabolism of spermine to spermidine by SMOX produces H_2O_2, this upregulation results in increased macrophage apoptosis of *H. pylori*-infected RAW 246.7 cells.[108] Chemical inhibition of SMOX or detoxification of H_2O_2 with catalase attenuated the infection-induced apoptosis.[108] Our lab also found that knocking down SMOX expression with shRNA decreased arginine uptake by RAW 246.7 macrophages.[95] This resulted in a decrease of *H. pylori* lysate-stimulated production of NO and an increase in *H. pylori* survival.[95] These results were reversed with transfection of a SMOX overexpression vector with subsequent decrease of spermine levels in RAW 246.7 cells and the human moncyte cell line THP-1.[95] Bussière et al. found that increased concentrations of spermine within the cell correlated with decreased NOS2, attributed to a direct inhibition of spermine on the translation of NOS2.[105] In combination, these findings suggest that the macrophage effector function of pathogen killing by NO production is either downregulated by spermine or upregulated by spermidine (Figure 1.2).
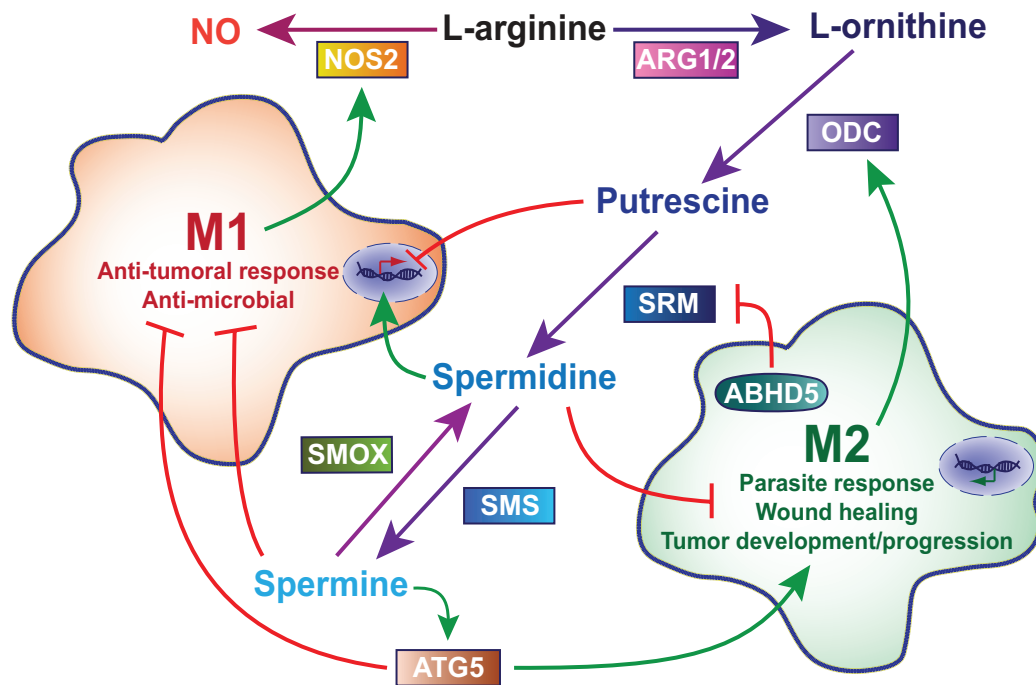
Figure 1.2. Regulation of macrophage function by polyamine synthesis. In general, once activated, M1 macrophages metabolize L-arginine by NOS2 to produce NO while M2 macrophages (Mregs, TAMs, MDSCs, M2a) upregulate the ARG1/2-ODC pathway to produce polyamines, however, both retain the ability to change activation states. Putrescine downregulates transcription of M1 genes including Nos2 and spermine inhibits the translation of NOS2, thus hindering an M1 response. Spermine also supports autophagy via ATG5, which inhibits M1 polarization while promoting M2 polarization. In contrast, spermidine upregulates transcription of *Nos2* and can both directly and indirectly inhibit tumor growth. TAM survival is mediated by upregulation of ABHD5, which suppresses spermidine by inhibiting translation of spermidine synthase (SRM).

Our lab has also recently shown that macrophages upregulate expression of deoxyhypusine synthase (DHPS) during *H. pylori* infection.[109] DHPS is one of two enzymes in the involved in the formation of the unique amino acid hypusine. Hypusine is generated from spermidine by DHPS and deoxyhypusine hydrolase (DOHH) and is located on one protein, the eukaryotic translation initiation factor 5A (EIF5A). Hypusinated EIF5A contributes to protein translation by chaperoning specific mRNAs to ribosomes in addition to alleviating ribosomal pausing.[109] Genetic deletion of *Dhps* in macrophages enhanced *H. pylori* survival and increased gastritis by impairing macrophage translation of proteins involved in antimicrobial activity and autophagy.[109] This study demonstrates that biological processes downstream of the polyamine pathway can regulate macrophage function.

14

1.6 Cystathionine γ-lyase

CTH (previously known as CSE or CGL) is a pyridoxal phosphate (PLP, vitamin B₆)-dependent enzyme that is responsible for the *de novo* generation of cysteine and is a major contributor of hydrogen sulfide (H_2S) production.[110] CTH and cystathionine β-synthase (CBS) make up the mammalian reverse transsulfuration pathway (RTP).[111] The first step of the RTP is the anabolism of cystathionine by CBS using homocysteine and serine (Figure 1.3).[110–113] Cystathionine is then broken down into cysteine and α-ketobutyrate by CTH, producing ammonia. Cysteine can then exit the RTP or be recycled back to cystathionine by either CBS or CTH.[111] The liver is the main site of reverse transsulfuration and expression levels of the two enzymes are tissue specific; under physiological conditions, CBS is mainly found in the central nervous system and CTH in the liver and cardiovascular system.[114,115]
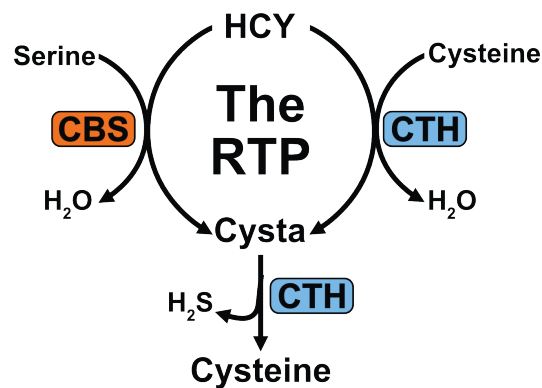
Figure 1.3 The reverse transsulfuration pathway. The RTP is responsible for the conversion of homocysteine (HCY) to cysteine by activity of CBS and CTH.

The RTP is directly downstream of methionine metabolism and methyltransferase reactions. Methionine is an essential sulfur-containing amino acid obtained through diet or the microbiota. The metabolism of methionine fuels multiple metabolic pathways and begins with the generation of S-adenosylmethionine (SAM) by the action of methionine adenosyltransferases (Figure 1.4).[116] SAM is the primary methyl donor used for the methylation of DNA, histone, and proteins.[117] Various methyltransferases facilitate these methylation reactions and produce S-adenosylhomocysteine (SAH) as a byproduct which is further hydrolyzed to homocysteine (HCY) by

adenosylhomocysteinase (AHCY).[117] Homocysteine can reenter the methionine cycle, however, entry into the RTP is irreversible.[118] The levels of SAH and SAM are tightly regulated as changes in the ratio dictate the cellular methylation capacity via binding of excessive SAH to methyltransferase to inhibit activity.[119,120]
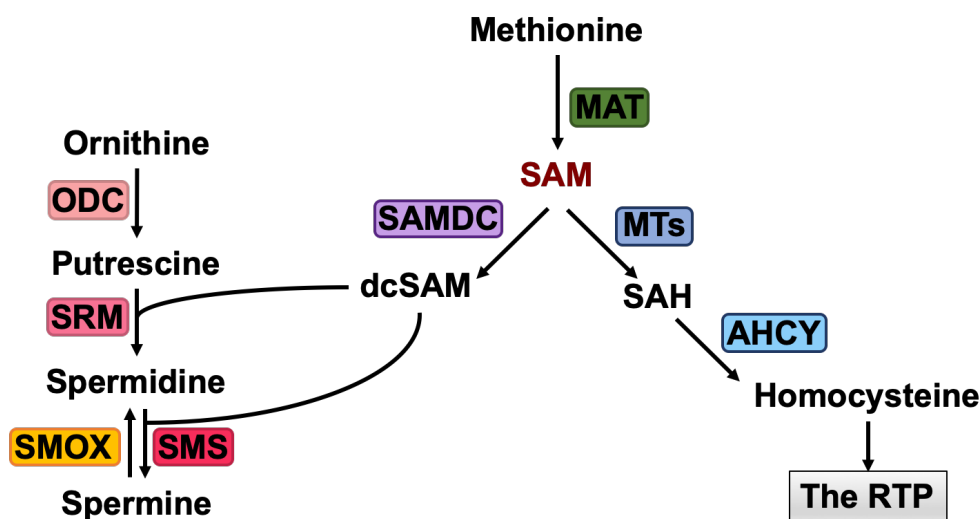
Figure 1.4 The polyamine synthesis pathway is interconnected with the RTP through the common substrate SAM.

The role of CTH and the RTP in inflammation has mainly been studied in the context of H_2S production. H_2S is an extremely diffusible gaseous molecules that has made its way into the ranks of the other gasotransmitters, NO and carbon monoxide. Many steps of the RTP generate H_2S, which has been implicated in cell growth and proliferation, cardiovascular health, and inflammation, however, location and concentration of H_2S are major determinants of its effect.[110,111,115,121,122] Recent advances have made the measurement of bioavailable H_2S more feasible, but due to the ease at which H_2S can diffuse through substrates, the results can often be unreliable.[123] In addition, the study of H_2S in bacterially-induced inflammation can be convoluted since some bacterial species also produce H_2S as protection against antimicrobial activity and expose host cells to exogenous H_2S.[123,124]

The role of H_2S in macrophages has been studied through both chemical and genetic manipulation in models of bacterial infection and sterile inflammation.[125] Overall, the effect of H_2S on macrophage polarization is highly

context dependent.[125] Numerous studies using the RAW264.7 murine macrophage-like cell line challenged with LPS found that exogenous treatment with an H_2S donor skewed the macrophages to an anti-inflammatory phenotype.[126–130] Interestingly, some of the studies noted that exogenous H_2S suppressed the expression of CTH, and thus the generation of endogenous H_2S.[127,130] Furthermore, in vivo knockdown of *Cth* in macrophages was protective and reduced inflammation and tissue injury in both the cecal ligation and puncture model and the polymicrobial model of sepsis.[131,132] In contrast, groups have also found that genetic ablation of *Cth* in macrophages in vitro had the opposite effect and upregulated markers of a proinflammatory phenotype with LPS stimulation.[126,133–135] This suggests that the source of H_2S plays an important role and that treatment with exogenous H_2S may be acting through changes in CTH activity. Many of these studies are limited by using an immortalized cell line that does not reliably recapitulate the dynamic and complex nature of the in vivo system. Additionally, the focus of these previous works on the impact of H_2S on inflammation leaves many questions unanswered questions regarding the cysteine synthesis role of CTH in macrophage function.

Our lab became interested in CTH because of the connection of the RTP with the polaymine pathway. The RTP and polyamine synthesis share SAM as a precursor. Instead of being used for methylation reactions, SAM can be decarboxylated by SAM decarboxylase (SAMDC; previously refered to as AMD1).[82] The decarboxylated form of SAM (dcSAM) can then donate an amino-propyl group to the synthesis of spermidine and spermine (Figure 1.4). As outlined in an earlier section of this chapter, polaymines play a major role in macrophage function and *H. pylori*-induced disease progression. Through the shared reliance on SAM metabolsim, we hypothesized that CTH could modulate polyamine metabolism and thus the macrophage response to *H. pylori*. We demonstrated that CTH expression is upregulated by *H. pylori*-infected macrophages in vitro and in the gastric tissues of *H. pylori* infected indiduals.[136] Through the use of chemical inhibitors and genetic knockdown of CTH, we show that during *H. pylori* infection, the RTP sequesters SAM away from the polyamine pathway leading to an accumulation of putrescine, inhibition of spermidine and spermine synthesis, and enhanced production of cystathionine that all favor bacterial survival and is immunosuppressive.[136] This study provided insight and a basis for further investigation into the role of CTH in the immunopathogenic response to *H. pylori* in vivo.

1.7 Attaching and Effacing *Escherichia coli*

Another potential pathogen of the gastrointestinal tract is *Escherichia coli*, a Gram-negative facultative anaerobe. Most strains of *E. coli* are harmless and reside in the human colon as part of the commensal microbiota. However, pathogenic strains of *E. coli* can cause disease both inside and outside of the intestines. The different strains of intestinal pathogenic *E. coli* are categorized into 5 groups based on virulence factors: Shiga toxin-producing *E. coli* (STEC), enterotoxigenic *E. coli* (ETEC), enteroinvasive *E. coli* (EIEC), enteroaggregative *E. coli* (EAEC), and enteropathogenic *E. coli* (EPEC).[137] EPEC is the leading causes of diarrheal-related deaths, especially in children and the elderly.[138,139] Like *H. pylori*, EPEC is non-invasive, but has evolved strategies to enhance colonization of the GI tract and directly interact with the colonic epithelium. A virulence strategy that sets EPEC apart from other *E. coli* is the ability to form attaching and effacing (A/E) lesions. A type III secretion system (TS33) is encoded by the locus of enterocyte effacement (LEE) along with translocated intimin receptor (Tir), intimin, and other secreted proteins that facilitate the formation of A/E lesion formation on colonic enterocytes.[140–142] Once in contact with a colonocyte, EPEC uses the T3SS to translocate Tir into the host cell and recruit scaffold proteins, talin-1, and actin to bind intimin on the bacterial surface and form a pedestal-like structure.[142,143] EPEC has also development mechanisms to prevent immune activation and subvert eradication by using the T3SS to inject additional virulence factors. These include inactivation of the inflammasome by NleA, direct cleavage of NF-κB subunits by NleC, and downregulation of IL-8 chemokine expression by disruption of MAP kinase pathways.[144,145]

E. coli, including EPEC, have been linked to the initiation and perpetuation of inflammation in IBD patients.[146] In the case of most bacterial infections, the risk of antibiotic resistance and antibiotic overuse is on the rise.[147,148] Taken together, new targets and strategies are needed to both eradicate pathogenic infection and curb the immune response to prevent chronic inflammation and immunopathogenesis, a central theme of this dissertation.

1.8 Talin-1: A Brief Overview

Talin-1 is a large 270 kDa cytoplasmic protein that was first discovered and purified from the smooth muscle of chicken gizzards in 1983, and sits at the interface between the cytoskeleton and the extracellular matrix

(ECM).[149,150] Evidenced by the name, there are two isoforms of talin, with talin-1 being the most dominant and well-studied.[151] Talin-1 can be found in all cell types in all tissues.[151] Talin-2 is mainly expressed in the brain, kidney, and cardiac smooth muscle and unlike talin-1, is not embryonic lethal.[152,153] The talin-1 isoform will be the focus of chapters 3 and chapter 4 of this dissertation. The gene, *Tln1*, encodes a 220-kDa C-terminal rod lined with helical bundles that provide multiple binding sites for actin and vinculin and a 50-kDa N-terminal head containing a FERM (4.1 protein, ezrin, radixin, moesin) domain.[150,154,155] FERM containing proteins are often associated with protein-protein interactions that link the cytoskeleton to transmembrane receptors.[156] The C-terminal rod is made up of 13 helical domains that are arranged to provide mechanical stability and transmit force. Talin-1 has three main biding partners: the cytoplasmic tail of the β-subunit of integrins, f-actin, and vinculin. However, the vinculin binding sites are enclosed in the core of the rod structure and are only exposed during mechanical force.

As a mechanosensory protein, talin-1 relies on physical force to function and transduce signals. Integrin activation is achieved through a conformational change to the extracellular ECM binding domain that requires force for stabilization.[150,157] Once bound to the integrin and tethered to actin, the whole complex can be pulled and revealing the vinculin binding sites.[158] The recruitment of vinculin and other integrin-associated proteins completes the final complex and enhances stabilization. Types of integrin adhesion complexes include focal adhesions, focal complexes, fibrillar adhesions, invadopodia, and hemiadherens junctions.[158] These adhesion complexes contribute to a wide range of physiological functions including immune cell migration, cellular proliferation, and cell survival.[159–169] In addition, talin-1, actin, and vinculin have all been identified in the adhesion complex that is recruited by EPEC to form the pedestals under A/E lesion.[142,143] Our lab has shown that talin-1 is required for actin rearrangements in the intimate attachment of A/E pathogens in vitro and may modulate pathogenicity in vivo.[170] Thus, further elucidation of the role of talin-1 in bacterial infections of the GI tract is needed.

1.9 Conclusions and Research Goal

In conclusion, the immune system is a critical regulator of human health and disease. Within the GI tract, it is responsible for maintaining tolerance against harmless commensal bacteria but must also mount an effective

response to pathogens. When this balance is skewed and the response is dysregulated, tissues can be damaged, chronic inflammation can set in, and the risk of more severe pathologies can rise. Immunopathologies can develop from an intrinsic defect of host immunity or like in the case of *H. pylori* infection, external factors can disrupt normal function. Researchers have spent decades elucidating the physiological mechanism underlying chronic inflammatory diseases such as *H. pylori*-induced gastritis and cancer as well as the initiation and perpetuation of IBD. Despite these efforts, there remains a gap in knowledge in biological pathways within immune cells that can be therapeutically targeted to regulated immune activation and function. The work outlined in this dissertation addresses the overarching goal to identify proteins and their upstream and downstream effectors within cells of the innate immune response as targets for intervention in the context of bacterially induced GI inflammation.

Little is known about the role of CTH in chronic inflammation. Many of the studies assessing the function of CTH in the regulation of macrophage activation use in vitro models and mainly focus on H_2S. This leaves other metabolites of the RTP an open area of research. CTH is intimately tied to multiple metabolic pathways including polyamine synthesis via SAM metabolism. Based on extensive work by the Wilson Lab demonstrating that perturbation of polyamine metabolism has a profound effect on macrophage activation and function, I sought to determine the impact of CTH activity in macrophages during *H. pylori*-induced gastric disease. In Chapter 2, I use ex vivo primary macrophage cultures, in vivo models of acute and chronic inflammation, and a toolbox of omics techniques to establish CTH as an enhancer of macrophage activation. Thus, we propose macrophage CTH as a novel therapeutic target for the control of *H. pylori* immunopathogenesis.

In Chapters 3 and 4, I evaluate other aspects of the immune response within the GI tract. Talin-1 is a ubiquitously expressed scaffold protein that has been implicated in immune cell migration and the formation of A/E lesions on intestinal epithelial cells, but there are limited studies directly assessing the contribution talin-1 to these processes. I used myeloid-specific and epithelial-specific knockout mice to delineate the role of talin-1 in macrophages and colonocytes during pathogenic colitis. These studies revealed a cell-specific role of talin-1 that highlights the potential dichotomy of targeting a single protein.

Overall, this dissertation provides new insights into the innate immune response of the gastrointestinal tract and proposes potential regulators of macrophage trafficking and function in addition to bacterial colonization.

CHAPTER 2

The Role of CTH in Macrophages During *H. pylori*-induced Immunopathogenesis

A version of this chapter was originally published in *JCI Insight:*

2.1 Abstract

Macrophages play a crucial role in the inflammatory response to the human stomach pathogen *Helicobacter pylori*, which infects half of the world's population and causes gastric cancer. Recent studies have highlighted the importance of macrophage immunometabolism in their activation state and function. We have demonstrated that the cysteine-producing enzyme, cystathionine γ-lyase (CTH), is upregulated in humans and mice with *H. pylori* infection. Here we show that induction of CTH in macrophages by *H. pylori* promotes persistent inflammation. $Cth^{-/-}$ mice have reduced macrophage and T-cell activation in *H. pylori*-infected tissues, an altered metabolome, and decreased enrichment of immune-associated gene networks, culminating in decreased *H. pylori*-induced-gastritis. CTH is downstream of the proposed antiinflammatory molecule, S-adenosylmethionine (SAM). While $Cth^{-/-}$ mice exhibit gastric SAM accumulation, WT mice treated with SAM did not display protection against *H. pylori*-induced inflammation. Instead, we demonstrate that *Cth*-deficient macrophages exhibit alterations in the proteome, decreased NF-κB activation, diminished expression of macrophage activation markers, and impaired oxidative phosphorylation and glycolysis. Thus, through altering cellular respiration, CTH is a key enhancer of macrophage activation contributing to a pathogenic inflammatory response that is the universal precursor for the development of *H. pylori*-induced gastric disease.
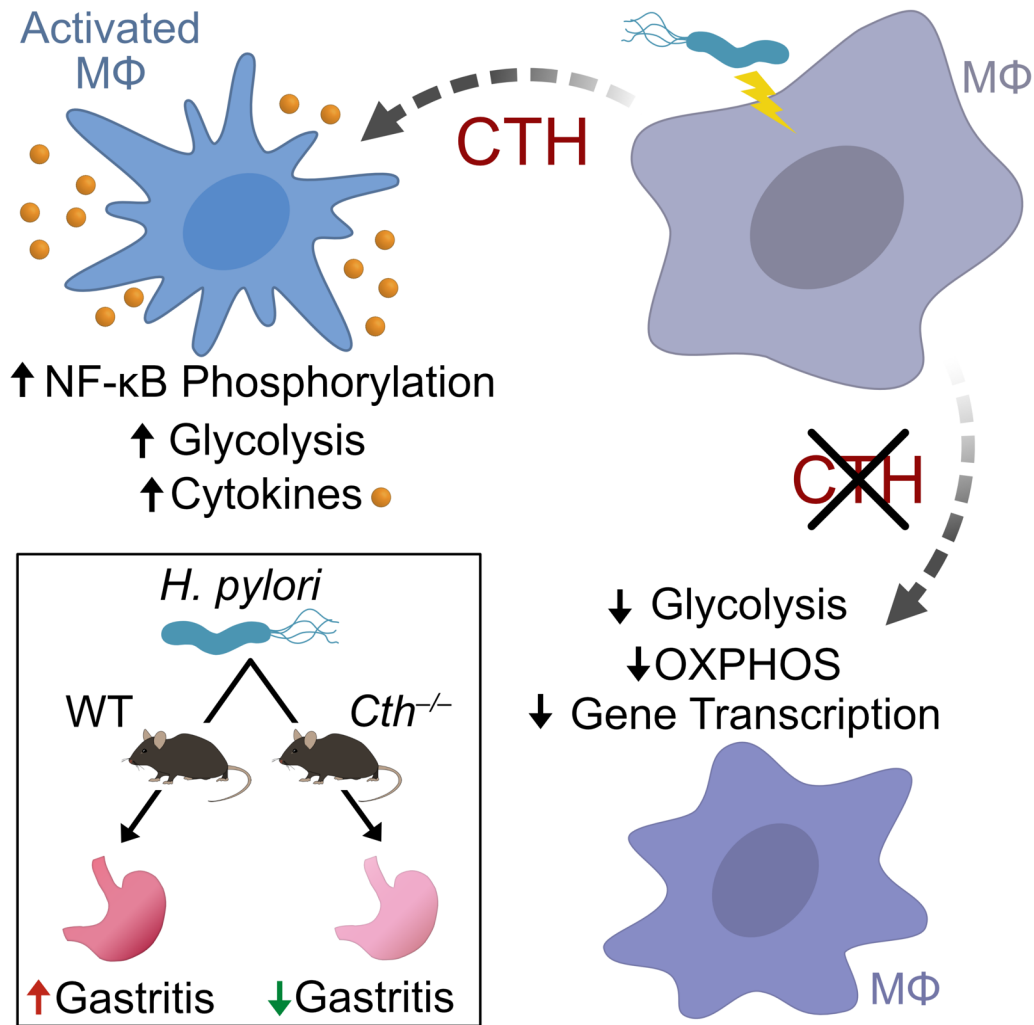
Figure 2.1 Graphical Abstract. Macrophages upregulate the expression of *Cth* when infected with *H. pylori* leading to an increase in glycolysis and M1 activation which is attenuated in the absence of CTH. The abrogated macrophage activation in *Cth*$^{-/-}$ mice provides protection from *H. pylori*-induced gastric inflammation.

2.2 Introduction

Monocyte-derived macrophages are a key component of the innate immune response providing a wide-range of functions, including response to pathogens, antigen presentation, immune regulation, and wound repair.[7,58,61] In reponse to bacterial pathogens such as *Helicobacter pylori*, macrophages exhibit an M1-like phenotype that is characterized by expression of genes encoding chemokines and cytokines that orchestrate the recruitment and

activation of other innate cells as well as a robust adaptive T-cell response that perpetuates inflammation.[24,91,96,97,99,171,172] Proinflammatory macrophages also express enzymes that produce effector molecules such as nitric oxide (NO) and reactive oxygen species (ROS), which help limit the pathophysiology of infection.[69,91,99,109,173] However, these events can contribute to dysregulation of cellular homeostasis and tissue damage. A unique feature of macrophage biology is the ability to maintain plasticity to regulate the proinflamatory response and/or repair damage in responding to environmental cues and metabolic remodeling.[174] Therefore, understanding the molecular mechanisms that dictate and regulate macrophage activation has theapeutic potential that is still largely unexplored.

Cystathionine γ-lyase (CTH, also known as CSE) breaks down cystathionine into cysteine, α-ketobutyrate, and ammonia as the last step of the mammalian reverse transsulfuration pathway (RTP).[110,111] Cystathionine is generated by cystathionine b-synthase (CBS) from homocysteine and serine.[111] Homocysteine is directly downstream of the demethylation of S-adenosylmethionine (SAM) to S-adenosylhomocysteine (SAH), an important step in DNA, histone, and protein methylation (Figure 2.2).[117] Another major role of SAM, a product of methionine metabolism, is the biosynthesis of the polyamines spermidine and spermine by spermidine synthase and spermine synthase, respectively.[82] Both enzymes require the decarboxylated form of SAM (dcSAM), which is synthesized by the enzyme S-adenosylmethionine decarboxylase (SAMDC), to donate an amino-propyl group (Figure 2.2).[82]
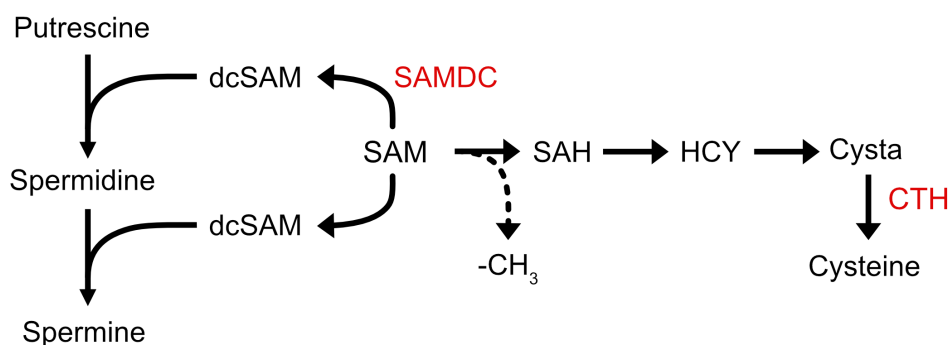
Figure 2.2. SAM Metabolism. Schematic of key metabolites and enzymes (red) downstream of SAM.

23

H. pylori is a Gram-negative bacterium that is estimated to colonize around 4.4 billion people, making it one of the most common bacterial pathogens in humans.[15] *H. pylori* is the strongest risk factor for developing gastric adenocarcinoma, the fourth leading cause of cancer mortality in the most recent 2020 GLOBOCAN data,[17] with 89% of all gastric cancer cases associated with evidence of *H. pylori* colonization.[27,175] While complex regimens of antibiotic treatment are available, the prevalence of antibiotic-resistant strains is on the rise.[176–178] In addition, the benefit of *H. pylori* eradication in cancer prevention relies on low rates of reinfection and sustained negative *H. pylori* colonization status.[179,180]s.[21] *H. pylori* elicits a vigorous, yet generally ineffective innate and adaptive mucosal immune response resulting in a chronic[21] *H. pylori* elicits a vigorous, yet generally ineffective innate and adaptive mucosal immune response resulting in a chronically active inflammatory state that contributes to the progression from gastritis to adenocarcinoma.[22,45,181,182] Thus, new strategies are needed to target the host immune response to reduce antibiotic use and circumvent the risk of antibiotic resistance.

We recently reported that *H. pylori* upregulates expression of CTH in mouse and human gastric macrophages and reduces spermidine and spermine synthesis by limiting SAM availability in macrophages in vitro.[136] We now present evidence that genetic deletion of *Cth* results in reduced gastritis, suppression of both innate and adaptive immune markers, and downregulation of metabolic pathways including those involved in cellular respiration with *H. pylori* or with classical macrophage stimuli. These findings were independent of changes in polyamine metabolism. Additionally, there were changes in adaptive immune responses in the gastric mucosa with *Cth* deletion, but effects on T cells appeared to be independent of any effects of CTH within T cells. Taken together, our data suggest that modulation of CTH activity affects the innate immune response of macrophages and pathogenic gastric inflammation, thus representing a potential target for therapeutic intervention in *H. pylori* pathogenesis.

2.3 Materials and Methods

Animal Studies. $Cth^{-/-}$ mice were generated and provided by Bindu Paul and Solomon Snyder, Johns Hopkins University School of Medicine (Baltimore, MD).[115] C57BL/6 wild-type (WT, also provided by BDP and SHS) and

Cth^{−/−} mice were house-bred and maintained for multiple generations in the same room of our animal facility prior to experiments. Adult age-matched WT and *Cth*^{−/−} mice (8-12 wk) of both sexes were used for isolation of BMmacs and for infection with *H. pylori*. Mice remained in the cages they were weaned in and moved to the same rack for infection studies.

Bone Marrow-Derived Macrophage Culture. Bone marrow cells were isolated from mice of both genotypes as previously described[69] with the following exception; prior to counting, RBCs were lysed with ACK Lysing Buffer (ThermoFisher) for 1 minute. Cells were differentiated into BMmacs for 7 days in complete medium (DMEM media supplemented with 10% FBS, 100 U/ml penicillin/streptomycin, 25 mM HEPES, and 20 ng/ml recombinant macrophage CSF (M-CSF; PeproTech)).

CD4⁺ Splenocyte Culture and Proliferation Analysis. Naïve CD4+ cells were isolated from the spleens of WT and *Cth*^{−/−} mice using the Dynabeads Untouched Mouse CD4 Cells Kit (Thermo Fisher). Cells were seeded into plates pre-coated with 5 µg/mL α-CD3e (Thermo Fisher) and stimulated or not with 2.5 µg/mL of soluble α-CD28 (Thermo Fisher). Cells were maintained for 72 h in complete media (RMPI media supplemented with 10% FBS, 100 U/ml penicillin/streptomycin, 25 mM HEPES, and 50 µM β-mercaptoethanol (βME)).

Proliferation was assessed using CFSE staining and flow cytometry. Briefly, immediately after CD4⁺ splenocyte isolation, cells were incubated with 25 µM CFSE for 5 min at room temperature. Cells were then washed and plated as above. After 72 h, cells were collected and subsequently analyzed by flow cytometry.

Bacteria. The *cagA+ H. pylori* strain PMSS1 and the mouse-adapted *H. pylori* strain SS1 were grown on Trypticase soy agar (TSA) plates containing 10% sheep blood.[96,171,183] Bacteria were harvested directly from plates to infect the macrophages. For *in vivo* infection, *H. pylori* was grown from plates in Brucella broth containing 10% FBS overnight; *H. pylori* was then diluted, grown, and harvested at the exponential phase. *C. rodentium* was grown in Luria-Bertani broth overnight to infect macrophages.[69]

Infection. Mice were infected twice by oral gavage, on day 0 and day 2, with 10^9 *H. pylori* PMSS1 or SS1 in 0.2 mL Brucella broth.[183] Control mice were treated with 0.2 mL Brucella broth alone. Mice were fed *ad libitum* with regular 5L0D chow (LabDiet). Animals were sacrificed after 4 and 8 wk (PMSS1) or 16 wk (SS1). Stomachs were harvested and analyzed as previously described.[69,96,109,173] *H. pylori* gastric colonization was determined by counting the CFUs after plating serial dilutions of homogenized tissues.

Animals were treated or not with 50 mg/kg SAM (S-(5′-adenosyl)-L-methionine chloride dihydrochloride, Sigma-Aldrich) by oral gavage during 4 wk PMSS1 experiments beginning 1 wk p.i..[184] Animals were treated either every other day or every day. Solutions were prepared immediately prior to each treatment. Animals were treated or not with 5 mg/kg SAM486A (Sardomozide, MedChemExpress) by IP injection every other day during 4 wk PMSS1 experiments beginning 1 wk p.i..[185] Control mice were treated with vehicle.

Quantitative Real-Time PCR (RT-PCR). Total RNA was isolated from macrophages using the RNeasy Mini Kit (QIAGEN). RNA was extracted from mouse tissues by homogenization in TRIzol. cDNA was synthesized using the SuperScript IV Reverse Transcriptase (Thermo Fisher) and Oligo dT (Thermo Fisher). mRNAs were amplified by real-time PCR using the PowerUp SYBR Master Mix (Thermo Fisher) and the primers listed in Table 2.2.

Table 2.1: List of RT-PCR primers used for Chapter 2.

Target gene	Sequence (5'-3')
Cth	F: GCCAGTCCTCGGGTTTTGAA
	R: GCAAAGGCCAAACTGTGCTT
Cbs	F: TCATCCTGCCTGACTCTGTG
	R: CAGCTCTTGAACACGCAGAC
Tnf	F: CTGTGAAGGGAATGGGTGTT
	R: GGTCACTGTCCCAGCATCTT
Nos2	F: CACCTTGGAGTTCACCCAGT
	R: ACCACTCGTACTTGGGATGC
Il1b	F: ACCTGCTGGTGTGTGACGTTCC
	R: GGGTCCGACAGCACGAGGCT
Il12a	F: AAATGAAGCTCTGCATCCTGC
	R: TCACCCTGTTGATGGTCACG
Il12b	F: GAAAGACCCTGACCATCACT
	R: CCTTCTCTGCAGACAGAGAC
Cxcl1	F: GCTGGGATTCACCTCAAGAA
	R: CTTGGGGACACCTTTTAGCA
Mip2	F: GCCAAGGGTTGACTTCA
	R: TGTCTGGGCGCAGTG
Arg1	F: AAGAAAAGGCCGATTCACCT
	R: CACCTCCTCTGCTGTCTTCC
Il10	F: CCAAGCCTTATCGGAAATGA
	R: TCACTCTTCACCTGCTCCAC
Ifng	F: GGCCATCAGCAACAACATAAGCGT
	R: TGGGTTGTTGACCTCAAACTTGGC
Il17	F: ATCCCTCAAAGCTCAGCGTGTC
	R: GGGTCTTCATTGCGGTGGAGAG
Il6	F: AGTTGCCTTCTTGGGACTGA
	R: TCCACGATTTCCCAGAGAAC
Tgfb1	F: TCCTTGCCTGCGGAAGTG
	R: GGAGAGCATTGAGCAGTTCGA
Foxp3	F: GAGAGCAGGCAGTTCAGGAC
	R: CGGGAGCATATACCAGGCAC
Chil3	F: ACTTTGATGGCCTCAACCTG
	R: AATGATTCCTGCTCCTGTGG
Actb	F: CCAGAGCAAGAGAGGTATCC
	R: CTGTGGTGGTGAAGCTGTAG

Immunostaining. Immunofluorescent staining for CTH and the macrophage marker CD68 was performed on murine gastric tissues as described[136] using the following antibodies (see Table 2.32: Rabbit polyclonal anti-CTH, 1/100; rabbit polyclonal anti-mouse CD68, 1/100, ready to use; rabbit monoclonal anti-mouse Ly6G, 1/100; rabbit monoclonal anti-mouse CD3, 1/100, ready to use; goat anti-rabbit IgG, Alexa Fluor 488-labeled, 1/400; goat anti-rabbit IgG, Alexa Fluor 555-labeled, 1/500.

Histopathology. Histologic scoring was determined using the modified Sydney System by a gastrointestinal pathologist (MBP) in a blinded manner.[186] Gastritis was assessed on a longitudinal strip of tissue fixed in 10% neutral buffered formalin and stained with H&E. Acute and chronic inflammation were each scored 0–3 in the antrum and corpus regions, and the scores for antrum and corpus were added together for a 0–12 scale.[109]

Gastric Macrophage Isolation and Enrichment Analysis. Macrophages were isolated from the gastric lamina propria as previously described.[85,96,102]n with 1 mg/ml dispase and 0.25 mg/ml of collagenase A at 37°C while shaking. The cells were passed through a 70 μm cell strainer and harvested by centrifugation. Isolated cells were labeled with biotin-conjugated anti-mouse F4/80 antibody, 1/50, at 4°C for 1 h followed by incubation with streptavidin-conjugated beads at 4°C for 1 h. The cells were resuspended in 1 ml of buffer and underwent multiple rounds of washing while applied to a magnet. The positive selection was then collected and immediately used for RNA extraction. Since there are only a small number of gastric macrophages present in uninfected mice, we pooled the F4/80-positive cells from ten mice for each control sample.[85] Macrophage enrichment was assessed by pooling the F4/80-positive cells from three naïve WT mice. Cells were fixed and permeabilized with CytoFix/CytoPerm (BD Biosciences) for 20 mins at 4°C, washed, and then labeled with anti-CD11b-FITC (BD Biosciences), 1/200, and anti-CD68-PE, 1/200, (BioLegend), for 20 min at 4°C in Perm/Wash Buffer. Cells were then washed 3 times and subsequently analyzed using flow cytometry. See Table 2.2 for information regarding antibodies used in this Chapter.

Table 2.2: List of antibodies used for Chapter 2.

Antibody	Company	Identifier
Rabbit polyclonal anti-NOS2	Millipore	Cat# ABN26; RRID: AB_10805939
Rabbit polyclonal anti-MyD88	Cell Signaling	Cat# 3699; RRID:AB_2282236
Rabbit polyclonal anti-NFkB p65	Millipore	Cat# PC138; RRID:AB_2179029
Rabbit monoclonal anti-pNFkB p65 S536	Abcam	Cat# ab76302; RRID:AB_1524028
Rabbit polyclonal anti-CD68	Boster Biological	Cat# PA1518
Rabbit monoclonal anti-CD3	Biocare	Cat# PME324AA
Rabbit monoclonal anti-Ly6G	Abcam	Cat# ab238132
Rabbit polyclonal anti-CTH	MyBioSource	Cat# MBS7047965
Rabbit monoclonal anti-IkBa	Thermo Fisher	Cat# MA5-15153; RRID:AB_10983739
Mouse monoclonal anti-pIkBa S32/36	Thermo Fisher	Cat# MA5-15224; RRID:AB_10981266
Mouse monoclonal anti-5-Methylcytidine	Bio-Rad	Cat# MCA2201; RRID:AB_324056
Mouse monoclonal anti-b-actin	Sigma-Aldrich	Cat# A5316 RRID:AB_476743
Goat anti-rabbit IgG, HRP-labeled	Jackson ImmunoResearch	Cat# 111-035-003; RRID: AB_2313567
Goat anti-mouse IgG, HRP-labeled	Jackson ImmunoResearch	Cat# 115-035-003; RRID: AB_10015289
Goat anti-rabbit IgG, Alexa fluor 488-labeled	Thermo Fisher	Cat# A-11008; RRID: AB_143165
Goat anti-mouse IgG, Alexa fluor 488-labeled	Thermo Fisher	Cat# A-10680; RRID:AB_2534062)
Anti-mouse F4/80, biotin-labeled	Thermo Fisher	Cat# MF48015; RRID:AB_10372665
Donkey anti-mouse IgG, Alexa fluor 555-labeled	Thermo Fisher	Cat# A-31570; RRID: AB_2536180
Anti-mouse CD11b, FITC Conjugate	BD Biosciences	Cat# 557396; RRID:AB_396679
Anti-mouse F4/80, PE Conjugate	Thermo Fisher	Cat# MF48004; RRID:AB_10372666
Anti-mouse CD68, PE Conjugate	BioLegend	Cat# 137014; RRID:AB_10612937
Monoclonal anti-mouse CD3e	Thermo Fisher	Cat# 16-0031-82; RRID:AB_468847
Monoclonal anti-mouse CD28	Thermo Fisher	Cat# 16-0281-81; RRID:AB_468920

RNA sequencing and Analysis. Total RNA was isolated from the F4/80$^+$ gastric macrophages using the RNeasy Micro kit (QIAGEN). Generation and amplification of cDNA was performed using the Ovation RNA-Seq System V2 (Tecan). RNAseq library preparation and Next Generation Sequencing (PE150) were performed using the NEBNext Ultra II Directional RNA Library Prep Kit for Illumina (BioLabs, Inc.) and Illumina NovaSeq6000 with NovaSeq 6000 SP Reagent Kit (Illumina), respectively. Reads were first trimmed to remove the adapter sequence and read quality was checked using *fastp*.[187] Transcripts were quantified and mapped to the indexed mouse genome (M23, GRCm38) using *Salmon*.[188] Transcript-level quantification was then summarized to the gene level, annotated, and prepared for differential gene expression analysis using the R package *tximeta*.[189] The R/Bioconductor package

DESeq2 was then used to identify differentially expressed genes in each condition using Benjamini-Hochberg (BH) adjustment (FDR *p* < 0.05).[190] DAVID was used for pathway analysis and functional annotation of DEGs.[191,192] GSEA was performed using the R packages *clusterProfiler* and *DOSE*.[193,194]

The RNA sequencing data that is included in this Chapter have been deposited in NCBI Gene Expression Omnibus (accession number GEO: GSE158817).

Untargeted Metabolomics. At 8 wk p.i., gastric tissues were processed, and untargeted metabolomics was performed as previously described.[109] Gastric tissues were homogenized by sonication in water:methanol (9:1) containing 50 mM ammonium acetate (pH~6) to yield a tissue density of 50 mg/ml. An aliquot of the homogenate was combined with HPLC-grade methanol, vortexed vigorously, and centrifuged. A portion of the supernatant was diluted with an equal volume of HPLC-grade acetonitrile. A Vanquish ultrahigh performance liquid chromatography (UHPLC) system interfaced to a Q Exactive HF quadrupole/orbitrap mass spectrometer (Thermo Fisher Scientific) was used to acquire discovery metabolomics data. Each sample was first injected in positive ESI mode followed by a second injection in negative mode. All chromatographic separations were performed using a Zic-cHILIC analytical column (3 mm, 2.1 3 150 mm; Merck SeQuant). Mobile phases were made up of 0.2% acetic acid and 15 mM ammonium acetate in (A) water:acetonitrile (9:1) and in (B) acetonitrile:methanol:water (90:5:5). The total chromatographic run time was 20 min, the sample injection volume was 10 ml, and the flow rate was maintained at 300 ml/min. Mass spectra were acquired over a precursor ion scan range of m/z 100 to 1,200 at a resolving power of 30,000 using the following ESI source parameters: spray voltage 5 kV (3 kV in negative mode); capillary temperature 300°C; S-lens RF level 60 V; N_2 sheath gas 40; N_2 auxiliary gas 10; auxiliary gas temperature 100°C. MS/MS spectra were acquired for the five most abundant precursor ions with an MS/MS AGC target of 105, a normalized collision energy of 30, and a maximum MS/MS injection time of 100 ms. Chromatographic alignment, peak picking, and statistical comparisons were performed using XCMS (https://xcmsonline.scripps.edu).[195]

The discovery metabolomics data has been deposited to EMBL-EBI MetaboLights (accession number MetaboLights: MTBLS2851).[196]

Targeted Metabolite Quantification. SAM, dcSAM, SAH, homocysteine, cystathionine, and cysteine were measured at the Vanderbilt Neurochemistry Core as previously described and polyamine concentrations were measured as previously described.[69,136] Briefly, cell pellets or flash frozen tissues were homogenized, and the supernatants were used for the BCA Protein Assay (Pierce) and for liquid chromatography-mass spectrometry (LC-MS). Isotopically-labeled internal standard solutions were used for sample analysis. LC was performed on a 2.0 x 100-mm, 1.7-μm-particle-size CORTECS UPLC Phenyl column (Waters Corporation, Milford, MA USA) using a Waters Acquity I-Class ultraperformance liquid chromatography (UPLC) system. Mobile phase A was 1% aqueous formic acid, and mobile phase B was acetonitrile. Samples were separated by a gradient of 98 to 5% mobile phase A over 11 min at a flow rate of 600 μl/min prior to delivery to a Waters Xevo TQ-S micro triple quadrupole mass spectrometer. The peak height of the endogenous metabolites was compared to the peak height of internal standards for quantitation. All data were analyzed using TargetLynx XS software version 4.1 (Waters Corporation).

Co-Cultures. SAM and SAM486A were added to cells 30 minutes prior to infection. Macrophages were infected with *H. pylori* at a MOI of 100 for 30 min, 6 h, or 24 h. For *C. rodentium*, macrophages were infected at a MOI of 10 for 3 h and then washed and media containing penicillin and streptomycin was added for 21 h more. Media without antibiotics was used for all experiments. LPS/IFN-γ stimulated BMmacs were generated by addition of 10 ng/ml LPS from *E. coli* O111:E4 (Sigma-Aldrich) and 200 U/ml mouse recombinant IFN-γ (PeproTech). IL-4- and IL-10-stimulated BMmacs were generated with 10 ng/ml murine recombinant IL-4 (PeproTech) and 10 ng/ml murine recombinant IL-10 (PeproTech), respectively.

5mC Immunostaining and Flow Cytometry. 5mC immunostaining was performed as previously described[197] with the following exceptions; 24 h p.i., macrophages were washed with PBS and fixed and permeabilized using the CytoFix/CytoPerm kit (BD Bioscience). Chromatin was denatured with 1N HCl for 1 h at 37°C. Non-specific antibody binding was minimized by blocking with Wash Buffer (BD Bioscience) supplemented with 10% FBS for 20 min at 37°C. Cells were then labeled with mouse monoclonal anti-5mC (Bio-Rad), 1/100, for 30 min at room

temperature followed by washing and detection with goat anti-mouse IgG, Alexa Fluor 488-labeled, 1/200, for 45 min at 37°C. Upon completion of staining, 5mC binding was analyzed by flow cytometry; at least 10,000 cells were counted for each sample.

Proteomics and IPA. Macrophages were infected or not with *H. pylori* PMSS1 for 24 h and lysed in 50 mM Tris-HCl pH 7.6, 150 mM NaCl, 1% NP-40, and 2 mM EDTA and protein concentrations were determined by the BCA Protein Assay (Pierce). Samples within each group were combined (15 mg per each lysate), diluted with 100 mM triethylammonium bicarbonate (TEAB), reduced with 5 mL of 200 mM tris(2-carboxyethyl)phosphine (TCEP) at 55°C for 1 h, and carbamidomethylated with 5 mL of 375 mM iodoacetamide for 30 m in the dark at room temperature. Proteins were precipitated with cold acetone, and precipitates were dried and reconstituted in 100 mM TEAB (pH 8.0). Proteins were digested with Trypsin Gold (Promega) overnight at 37°C. Quantitative proteomics analysis was performed using TMT Isobaric Mass Tagging reagents (Thermo Fisher) according to the manufacturer's instructions. Peptides were labeled with TMT reagents with each reconstituted protein sample being labeled with an individual vial of 0.8 mg TMTsixplex reagent (Thermo Fisher). After labeling was complete, labeled peptides from each of the 4 sample groups were combined and fractionation was performed with 40 mg of the combined mixture using the Pierce High pH Reversed-Phase Peptide Fractionation Kit (Thermo Fisher) similar to the manufacturer's recommended protocol for TMT-labeled peptides. Elution steps consisted of the following: 10%, 12.5%, 15%, 17.5%, 20%, 22.5%, 25%, 50%, and 80% acetonitrile with 0.1% triethylamine. Eluted fractions were dried via vacuum centrifugation in a SpeedVac concentrator, and peptides were reconstituted in 0.1% formic acid for analysis by LC-coupled tandem mass spectrometry (LC-MS/MS). An analytical column was packed with 30 cm of C18 reverse phase material (Jupiter, 3 μm beads, 300 Å, Phenomenox) directly into a laser-pulled emitter tip. Peptides were loaded on the capillary reverse phase analytical column (360 μm O.D. x 100 μm I.D.) using a Dionex Ultimate 3000 nanoLC and autosampler. The mobile phase solvents consisted of 0.1% formic acid, 99.9% water (solvent A) and 0.1% formic acid, 99.9% acetonitrile (solvent B). Peptides were gradient-eluted at a flow rate of 400 nL/min, using a 155-min gradient. The gradient consisted of the following: 5-30% B in 125 min, 30-50% B in

10 min, 50-70% B in 4 min, 70% B for 2 min; 70-2% B in 2 min, followed by column equilibration. A Q Exactive Plus mass spectrometer (Thermo Scientific), equipped with a nanoelectrospray ionization source, was used to mass analyze the eluting peptides using a data-dependent method. The instrument method consisted of MS1 using an MS AGC target value of 3×10^6, followed by up to 15 MS/MS scans of the most abundant ions detected in the preceding MS scan with an MS2 AGC target of 1×10^5. Dynamic exclusion was set to 20 s, HCD collision energy was set to 30 nce, and peptide match and isotope exclusion were enabled. For the final two fractions, the peptides were eluted from the reverse phase analytical column using a gradient of 5-50% B in 125 min, followed by 50-95% B in 12 min, 95% B for 1 min, 95-5% B in 2 min, and column equilibration at 2% B.

For identification of peptides, HCD tandem mass spectra were searched in Proteome Discoverer 2.1 (Thermo Scientific) using SequestHT for database searching against a subset of the UniprotKB protein database (www.uniprot.org) containing *Mus musculus* protein sequences. The factory default templates in Proteome Discoverer were used for processing and consensus workflows, which included the PWF_QE_Reporter_Based_Quan_SequestHT_Percolator processing workflow and the CWF_Comprehensive_Enhanced Annotation_Quan_Results export consensus workflow. Search parameters included trypsin cleavage rules with two missed cleavage sites, carbamidomethyl (C) and TMTsixplex (K, N-terminus) as static modifications, and a dynamic modification of oxidation (M). Percolator validation was performed with a target false discovery rate (FDR) setting of 0.01 for high confidence protein identifications. A few exceptions to the consensus workflow default settings were used, including an average reporter S/N threshold of 10, and no scaling or normalization modes were applied. After peptides were identified and proteins were quantified, the results were then filtered to include those proteins for which a minimum of two unique peptides were identified. Log_2 protein ratios calculated in Proteome Discoverer were then fit to a normal distribution using non-linear (least squares) regression, and the mean and standard deviation values derived from the Gaussian fit of the ratios were used to calculate *p* values. Subsequently, *p* values were corrected for multiple comparisons by the Benjamini-Hochberg (B-H) method.[198] Statistically significant changes were determined using the B-H method with an alpha (α) level of 0.05 (<5% FDR).[198198]

The proteomics data has been deposited to the ProteomeXchange Consortium via the PRIDE partner repository (accession number ProteomeXchange Consortium: PXD026831).[199]

Ingenuity Pathway Analysis software (IPA, QIAGEN) was used to determine canonical signaling pathways and functional implications of the differential proteome expression. The statistical significance for each assignment was expressed by a corresponding *p*-values calculated using Fisher's exact test.

Western Blot. Macrophages were washed with PBS and lysed using ice cold CellLytic M Reagent (Sigma-Aldrich) supplemented with the Protease Inhibitor Cocktail (Set III, Calbiochem) and the Phosphatase Inhibitor Cocktail (Set I, Calbiochem). Protein concentrations were determined using the BCA Protein Assay (Pierce). Proteins were separated by SDS-PAGE on a 4-20% gel and transferred to nitrocellulose membranes. Membranes were blocked with 5% w/v milk in TBS with 0.1% Tween-20 for 1 h, and then incubated with primary antibody overnight at 4°C in either 5% w/v milk in TBS with 0.1% Tween-20 or 5% w/v BSA in TBS with 0.1% Tween-20 (based on the manufacturer's recommendations) followed by incubation with secondary antibody in 5% w/v milk in TBS with 0.1% Tween-20 for 1 h. Protein bands were visualized using SuperSignal West Pico PLUS Chemiluminescent Substrate (Pierce) and HyBlot CL Autoradiography Film (labForce). Densitometric analysis of Western blots was performed with Fiji.[200] See **Table 2.3** for information regarding antibodies used in this Chapter.

Measurement of NO. NO (NO_2^-) concentrations were assessed 24 h p.i. with *H. pylori* by the standard Griess reaction (Promega).[69]

Flow Cytometry for CD11b and F4/80. Macrophages were infected or not with *H. pylori* PMSS1 for 24 h and then washed 3 times with PBS. Cells were fixed and permeabilized with CytoFix/CytoPerm (BD Biosciences) for 20 mins at 4°C, washed, and then labeled with anti-CD11b-FITC (BD Biosciences), 1/200, and anti-F4/80-PE, 1/200, (Thermo Fisher), for 20 min at 4°C in Perm/Wash Buffer. Cells were then washed 3 times and subsequently analyzed using flow cytometry. See *Table 2.3* for information regarding antibodies used in this Chapter.

Glutathione Detection. Macrophages were infected or not with *H. pylori* PMSS1 for 24 h and then washed 3 times with PBS. Cells were then seeded into a white opaque 96-well assay plate at 1×10^4 cells per 50 µl. Glutathione levels were assessed using the GSH-Glo Glutathione Assay kit (Promega) per the manufacturer's directions for cells in suspension.

Measurement of mitochondrial superoxide. Macrophages were infected or not with *H. pylori* PMSS1 for 24 h and then washed 3 times with Hank's balanced salt solution (HBSS) with calcium and magnesium. The cells were then incubated with HBSS containing 5 µM MitoSOX™ Red (Thermo Fisher) for 15 min at 37°C, washed once, and subsequently analyzed utilizing flow cytometry.

Cellular Respiration Profiling. Oxygen consumption rate (OCR) and extracellular acidification rate (ECAR) were measured using the Seahorse XFe96 Analyzer (Agilent). Differentiated BMmacs were seeded at 1×10^5 cells per well in Seahorse XFe96 Cell Culture Microplates (Agilent) and infected or not with *H. pylori* PMSS1 (MOI 100) for 24 h. Cells were washed and incubated in Mitochondrial Stress Test Assay medium (1 mM sodium pyruvate, 2 mM glutamine, and 10 mM glucose in XF DMEM Medium (Agilent)) or Glycolysis Stress Test Assay medium (2 mM glutamine in XF DMEM Medium (Agilent)) for 45 min at 37°C in the absence of CO_2. Mitochondrial oxidative phosphorylation and glycolytic function were assessed per the Mitochondrial Stress Test and Glycolysis Stress Test assay manuals (all Agilent). Briefly, for the Mitochondrial Stress Test assay, OCR was measured under basal conditions and after the sequential addition of the following drugs: 15 µM oligomycin (Cayman Chemical), 10 µM fluoro-carbonyl cyanide phenylhydrazone (FCCP, Cayman Chemical), and 5 µM rotenone with 5 µM antimycin A (both Sigma-Aldrich). For the Glycolysis Stress Test assay, ECAR was measured under basal condition and after the sequential addition of the following drugs: 10 mM glucose (Agilent), 10 µM oligomycin (Cayman Chemical), and 500 mM 2-deoxy-glucose (2-DG, Cayman Chemical). The drugs were loaded into calibrated XFe96 sensor

cartridges (Agilent) and measurements were normalized to cell count. See Table 2.4 for information regarding reagents used in this Chapter.

Statistics. All the data shown represent the mean ± SEM. A minimum of three biological replicates were used for in vitro studies. Statistical analysis was performed in GraphPad Prism 9.2 (GraphPad Software) and significance was set at $p < 0.05$. Where data were normally distributed, Student's t test and one-way ANOVA with the Newman-Keuls or Dunnett's post hoc test were used to determine significant differences between two groups or multiple test groups, respectively. Where data was not normally distributed, a one-way ANOVA with the Kruskal-Wallis test, followed by a Mann-Whitney U test, was performed, unless otherwise noted.

Study Approval. Mice were used under the protocols M1900034, V1800106, and V2000018 approved by the Institutional Animal Care and Use Committee at Vanderbilt University and Institutional Biosafety Committee, and the Research and Development Committee of the Veterans Affairs Tennessee Valley Healthcare System. Procedures were performed in accordance with institutional policies, AAALAC guidelines, the AVMA Guidelines on Euthanasia, NIH regulations (Guide for the Care and Use of Laboratory Animals), and the United States Animal Welfare Act (1966).

Table 2.3: List of reagents/kits used for Chapter 2.

Reagent/Kit	Company	Identifier
Recombinant Murine M-CSF	PeproTech	Cat# 315-02
Dynabeads Untouched Mouse CD4 Cell Kit	Thermo Fisher	Cat# 11415D
LPS from *E. coli* O127:B8	Sigma-Aldrich	Cat# L4516
Recombinant Murine IFNg	PeproTech	Cat# 315-05
Recombinant Murine IL-4	PeproTech	Cat# 214-14
Recombinant Murine IL-10	PeproTech	Cat# 210-10
Oligo dT	Thermo Fisher	Cat#18418020
PowerUp SYBR Green Master Mix	Thermo Fisher	Cat# A25741
CellLytic M	Sigma-Aldrich	Cat# C2978
Protease Inhibitor Cocktail Set III	Calbiochem	Cat# 539134
Phosphatase Inhibitor Cocktail Set I	Calbiochem	Cat# 539131
SuperSignal West Pico PLUS Chemiluminescent Substrate	Thermo Fisher	Cat# 34577
S-(5-Adenosyl)-L-methionine chloride dihydrochloride	Sigma-Aldrich	Cat# A7007
Sardomozide	MedchemExpress	Cat# HY-13746
Streptavidin Particles Plus - DM	BD Biosciences	Cat# 557812
CytoFix/CytoPerm	BD Biosciences	Cat# 554714
GSH-Glo Glutathione Assay	Promega	Cat# V6911
MitoSOX™ Red Mitochondrial Superoxide Indicator	Thermo Fisher	Cat# M36008
Seahorse XFe96 FluxPak mini	Agilent	Cat# 102601-100
Seahorse XF DMEM	Agilent	Cat# 1035575-100
Seahorse XF 100 mM pyruvate	Agilent	Cat# 103578-100
Seahorse XF 1.0 M glucose	Agilent	Cat# 103577-100
Seahorse XF 200 mM glutamine	Agilent	Cat# 103579-100
Oligmycin Complex	Cayman Chemical	Cat# 11341
FCCP	Cayman Chemical	Cat# 15218
Rotenone	Sigma-Aldrich	Cat# R8875
Antimycin A	Sigma-Aldrich	Cat# A8674
2-DG	Cayman Chemical	Cat# 14325
TMTsixplex	Thermo Fisher	Cat# 90061
RNeasy Mini Kit	QIAGEN	Cat# 74106
RNeasy Micro Kit	QIAGEN	Cat# 74004
Superscript IV Reverse Transcriptase	Thermo Fisher	Cat# 18090010
BCA Protein Assay Kit	Pierce	Cat# 23225
Griess Reagent System	Promega	Cat# G2930
Fixation/Permeabilization Solution Kit	BD Biosciences	Cat# 554714
Pierce™ High pH Reversed-Phase Peptide Fractionation Kit	Thermo Fisher	Cat# 84868
CFSE	Thermo Fisher	Cat# 65-0850-84

2.4 Results

Deletion of Cth reduces gastritis in acute models of *H. pylori* pathogenesis.

We determined that CTH expression was localized to gastric macrophages in *H. pylori*-infected human stomach tissues and persists at an increased level during progression along the histological cascade towards carcinogenesis.[136] Thus, we used *Cth*-deficient mice to determine the role of CTH in vivo during *H. pylori* infection.[115] First, we confirmed that *Cth* mRNA expression is eliminated in the gastric tissues of *Cth*^{−/−} mice with and without *H. pylori* infection (Figure 2.2A). Immunofluorescence of infected gastric tissues from wild-type (WT) mice showed colocalization of CTH with CD68^{+} gastric macrophages (Gmacs) (Figure 2.2B); deletion of *Cth* led to loss of *H. pylori*-stimulated CTH protein in CD68^{+} Gmacs (Figure 2.2B). Then, to assess the effect of CTH in vivo, we used well established models of *H. pylori* infection: C57BL/6 WT and *Cth*^{−/−} mice were infected with *H. pylori* strain PMSS1 for 4 or 8 wk.[69,183] Animals lacking *Cth* demonstrated significantly decreased histologic gastritis at 4 wk (Appendix A, Figure 1, A and B) and 8 wk (Figure 2.2, C and D), and no difference in histology in uninfected mice (Appendix A, Figure 1A). Consistent with our previous studies in other mutant mice, decreased levels of gastritis were associated with increased levels of gastric colonization by *H. pylori* in *Cth*^{−/−} mice (Figure 2.2,E and F, and Supplemental Figure 1C).[69,102,173,201] Expression of the genes encoding for 1) the proinflammatory marker, tumor necrosis factor alpha (TNF-α), 2) the antiinflammatory marker, arginase 1 (ARGI1), and 3) the Th1 cytokine, interferon gamma (IFN-γ), were all significantly downregulated in *Cth*^{−/−} mice infected with *H. pylori* PMSS1 for 4 wk when compared to infected WT mice (Appendix A, Figure 1, D and E).

Figure 2.2. Deletion of *Cth* reduces gastritis in an acute model of *H. pylori* pathogenesis. WT and *Cth*[^−/−] mice were infected or not with *H. pylori* PMSS1 for 8 wk. (**A**) CTH mRNA expression in gastric tissues of WT and *Cth*[^−/−] mice infected or not with *H. pylori*; *n* = 3-7 mice per genotype. (**B**) Representative immunofluorescence images of CTH (green) co-localized (yellow) with the macrophage marker CD68 (red) from WT and *Cth*[^−/−] mice infected or not with *H. pylori*; *n* = 3 mice per genotype. DAPI (blue). (**C**) H&E images from infected mice; arrowheads highlight inflammatory cells. (**D**) Histologic gastritis scores, each symbol is a different mouse, data pooled from 2 independent experiments. (**E**) *H. pylori* colonization in gastric tissues from *D*. (**F**) Correlation between gastritis in *D* and *H. pylori* colonization in *E*. All values are means ± SEM. Statistical analyses where shown: (**A**) and (**D**), One-way ANOVA with Kruskal-Wallis test, followed by a Mann-Whitney *U* test; (**E**), Student's *t* test; (**F**), Correlation and significance determined by Pearson's product-moment correlation test; **$p < 0.01$. Scale bars in (**B**) and (**C**), 50 μm.

CTH mediates induction of immune response-specific gene sets.

Because *H. pylori* infection produces a chronic inflammatory state in humans, we utilized an established mouse model of chronic *H. pylori* infection to assess differential gene expression, in which mice were infected with *H. pylori* strain SS1 for 16 wk.[69,173] Similar to the acute *H. pylori* infection models, $Cth^{-/-}$ mice exhibited significantly decreased histologic gastritis (Figure 2.3, A and B) and increased *H. pylori* colonization (Figure 2.3C). Furthermore, the expression of the genes encoding for the proinflammatory markers TNF-α, chemokine (C-X-C motif) ligand 1 (CXCL1; the murine homologue of the neutrophil chemokine IL-8), IL-12B, and for the Th17 marker IL-17, and the Th1 marker IFN-γ were downregulated in $Cth^{-/-}$ mice chronically infected with *H. pylori* SS1 for 16 wk compared to infected WT animals (Figure 2.3D). Similarly, the transcript of the antiinflammatory marker *Il10*, was also higher in WT mice versus $Cth^{-/-}$ mice during *H. pylori* infection (Figure 2.3E). CTH expression was not induced in Ly6G$^+$ neutrophils (Appendix A, Figure 2) or CD3$^+$ lymphocytes (Appendix A, Figure 3A) found in the gastric tissues of infected WT mice. Although WT CD4$^+$ splenocytes express increased levels of *Cth* mRNA with co-stimulation of CD3 and CD28 (Appendix A, Figure 3B), $Cth^{-/-}$ splenocytes did not exhibit differences in cytokine or T cell transcription factor expression or proliferation compared to WT splenocytes (Appendix A, Figure 3, C-E). Thus, CTH is not upregulated in either gastric neutrophils or T cells with *H. pylori* infection, and CTH does not have a primary effect on T cell function. However, our data demonstrate that CTH expression contributes to the gastric immune response to *H. pylori* and affects the macrophage innate response and hence, the adaptive T cell response.
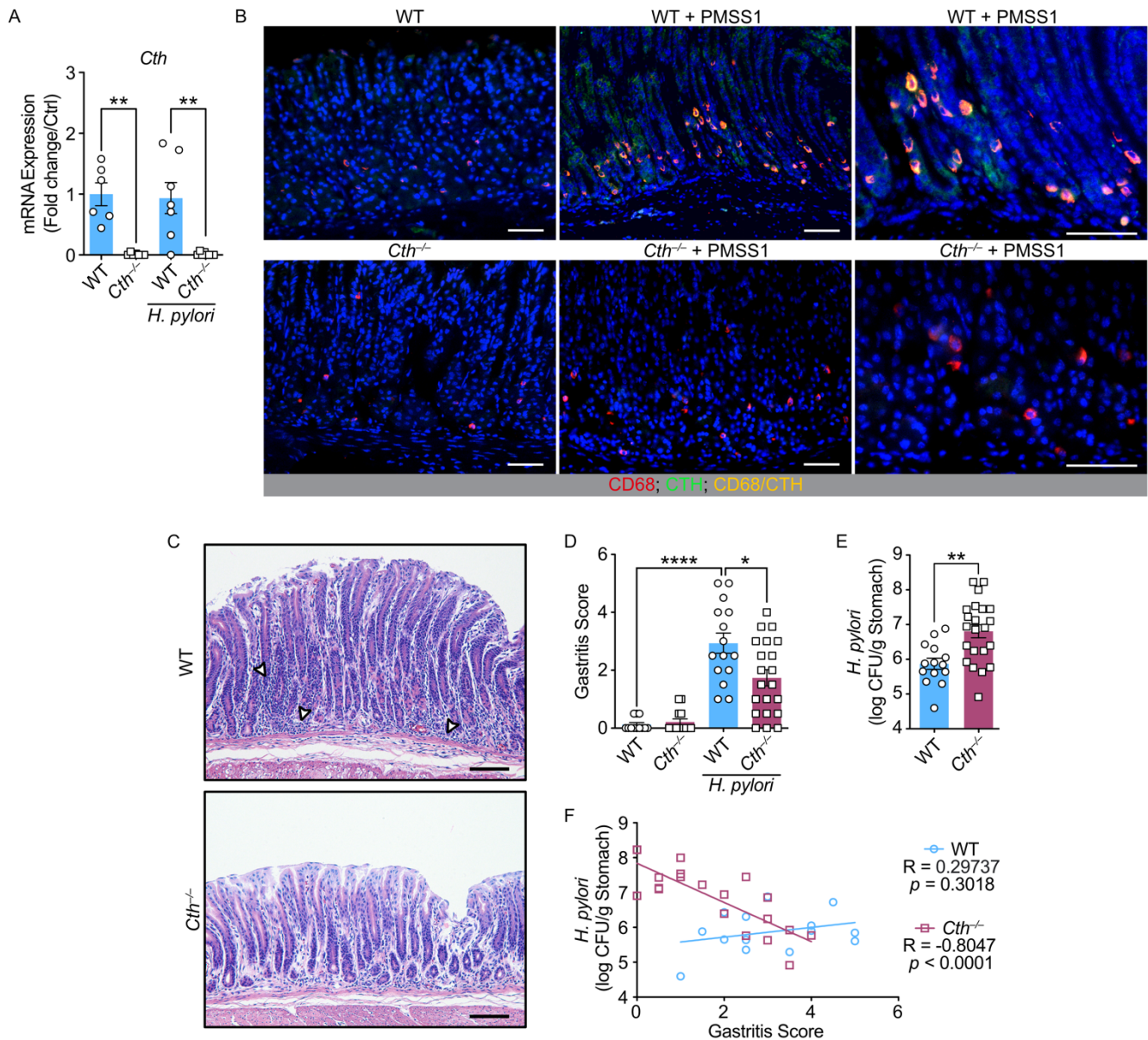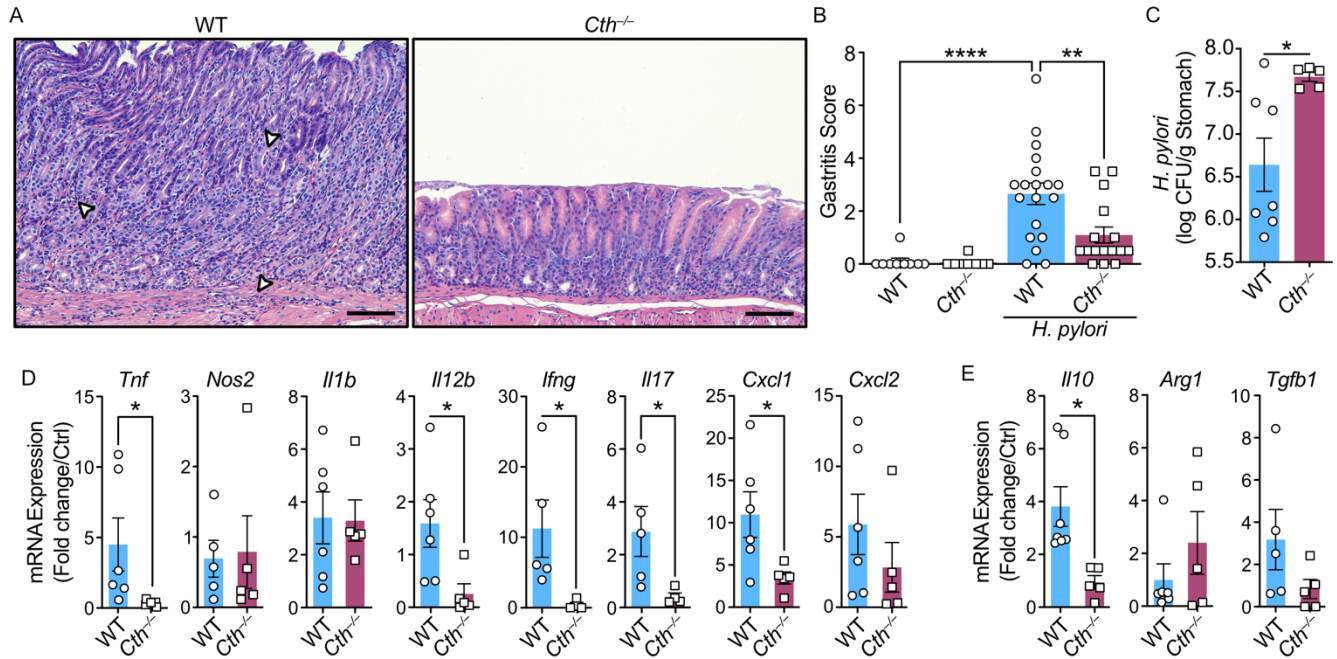
Figure 2.3. Deletion of *Cth* reduces gastritis in a chronic model of *H. pylori* pathogenesis. WT and *Cth*^{−/−} mice were infected or not with *H. pylori* SS1 for 16 wk. (A) H&E images from infected mice; arrowheads highlight inflammatory cells. (B) Histologic gastritis scores, each symbol is a different mouse, data pooled from 2 independent experiments. (C) *H. pylori* colonization in gastric tissues from *B*. (Tissues from one of the experiments was used for RNA sequencing). mRNA expression of (D) proinflammatory and (E) antiinflammatory markers in gastric tissues; *n* = 5-6 *H. pylori* infected mice per genotype. (B-E) All values are means ± SEM. Statistical analyses where shown: (B), (D) and (E), One-way ANOVA with Kruskal-Wallis test, followed by a Mann-Whitney *U* test; (C) Student's *t* test. *$p < 0.05$. Scale bars in (A), 50 μm.

To evaluate global changes in the transcriptome of Gmacs, we isolated F4/80$^+$ cells (Appendix A, Figure 4A) from the gastric tissues of WT and $Cth^{-/-}$ mice infected with *H. pylori* SS1 for 16 wk and performed RNA sequencing (RNAseq). Hierarchical clustering and heatmap analysis highlighted differential transcript abundance between genotype and infection status (Appendix A, Figure 4B). Principal-component analysis (PCA) demonstrated a distinct distribution of transcript profiles from WT and $Cth^{-/-}$ Gmacs that was dependent on *H. pylori* infection (Appendix A, Figure 4C). Overall, there were 24,781 transcripts identified that were present in two or more samples. Of the total transcripts, 17,246 were known mRNAs and 7,535 were unknown. Using a false discovery rate (FDR) of 0.1, we identified differentially expressed genes (DEGs), downregulated and upregulated, between Gmacs from infected $Cth^{-/-}$ and WT mice (Figure 2.4A). Gene ontology (GO) term gene set enrichment analysis (GSEA) of the significant DEGs between Gmacs from infected $Cth^{-/-}$ versus WT mice evidenced suppression of gene sets associated with immunity and response to stimuli (Figure 2.4B). Notably, gene level expression analysis of the GO term "Immune system process" revealed consistently reduced expression in Gmacs from infected $Cth^{-/-}$ mice compared to WT mice (Figure 2.4, C and D).
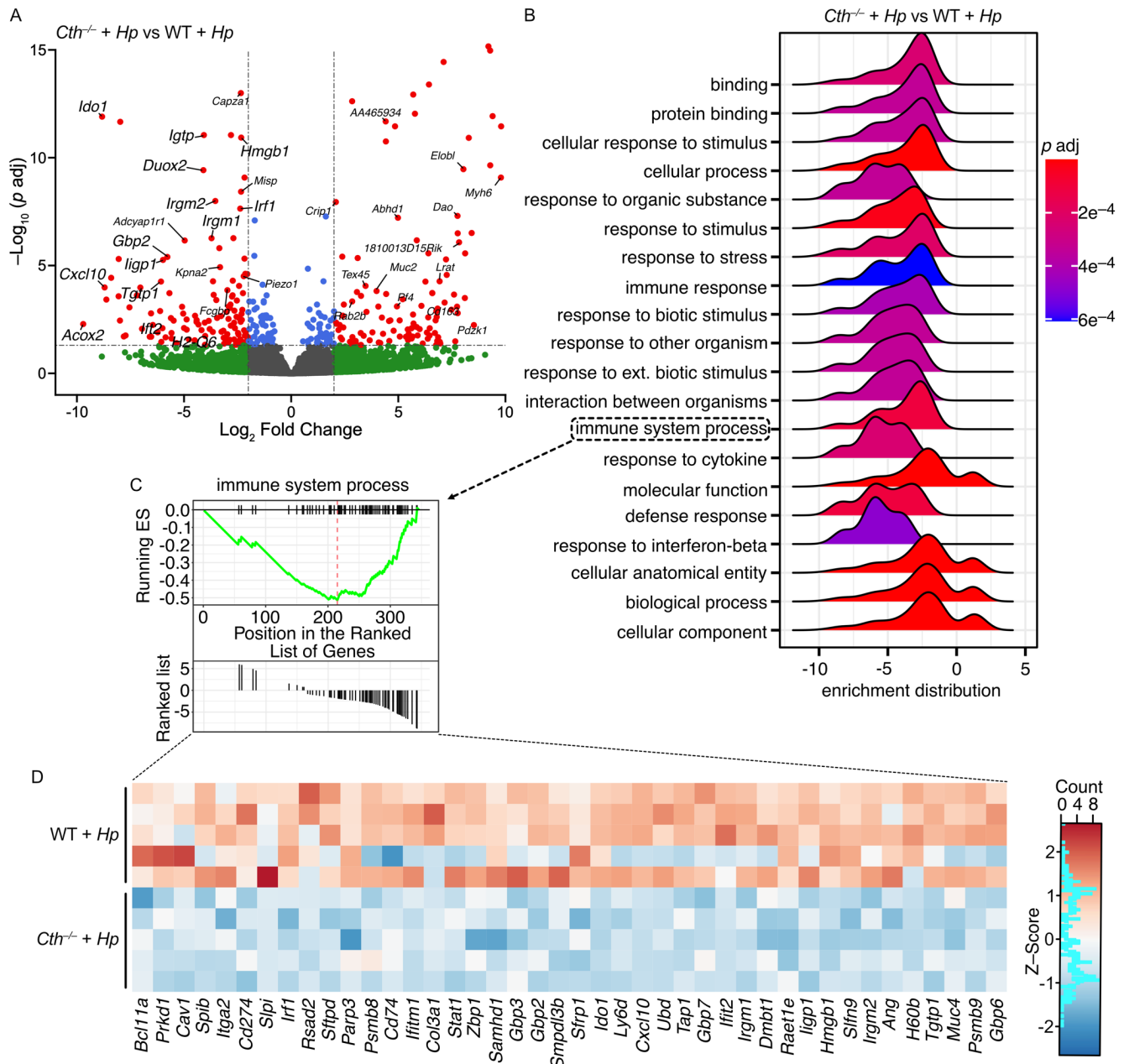
Figure 2.4. CTH mediates induction of immune response-specific gene sets. Transcriptomic analysis using RNAseq of F4/80+ enriched gastric cells (Gmacs); $n = 5$ individual infected mice per genotype. (A) Volcano plot of differentially expressed genes (DEGs) in $Cth^{-/-}$ Gmacs compared to WT Gmacs from infected mice (Fold change > 2, FDR < 0.05). Immune associated genes are enlarged. Grey dots, not significant; green dots, Log2 fold change > 2; blue dots, adjusted p value < 0.05; red dots, Log2 fold change > 2 and adjusted p value < 0.05. (B) Ridge plot displaying GSEA of differentially expressed genes in infected $Cth^{-/-}$ compared to infected WT Gmacs (Log2 fold change >2, FDR < 0.05). (C) Enrichment score plot of the gene set "Immune system process" identified in *A*. (D) Heatmap showing the gene level expression of genes within the "immune system process" gene set shown in *B*.

43

We next determined how the response to infection differs between WT and *Cth*-deficient mice when compared to their respective uninfected controls. We performed differential gene expression analysis to compare the response to infection between genotypes. There were 37 downregulated genes shared by WT and *Cth*$^{-/-}$ Gmacs and 145 genes that were induced in both WT and *Cth*$^{-/-}$ cells during infection (Supplemental Figure 5A). Immune-related genes upregulated by infection in WT Gmacs include *Irgm1*, *Irgm2*, *Ifit1*, and *Ido1* in addition to upregulated *Cth* expression (Figure 2.5A). In contrast, immune-related genes were either not induced or downregulated by infection, such as *Ifit2*, *Cybb*, and *Fcna*, in *Cth*$^{-/-}$ Gmacs (Figure 2.5B). Pathway analysis of significant DEGs using the Database for Annotation, Visualization, and Integrated Discovery Bioinformatics Resource revealed 4 downregulated pathways from the Kyoto Encyclopedia of Genes and Genome Pathways database in the transcriptome of *Cth*$^{-/-}$ mice compared to WT mice (Appendix A, Figure 5B). We also assessed function-associated keywords and identified 26 downregulated keywords (Appendix A, Figure 5C). Downregulated pathways and keywords in cells from infected *Cth*$^{-/-}$ mice compared to WT mice included the following pathways: "Metabolic Pathways" and downregulated keywords: "Immunity", "S-adenosyl-L-methionine", and "Methyltransferase" (Figure 2.5C and Appendix A, Figure 5, B and C). Downregulation of these pathways suggests that Gmacs from *Cth*$^{-/-}$ mice have altered immune function and impaired metabolic activation compared to WT. Furthermore, the downregulation of genes associated with SAM and methyltransferases is consistent with our hypothesis that CTH activity has the capability to modulate the reactions upstream of the RTP.
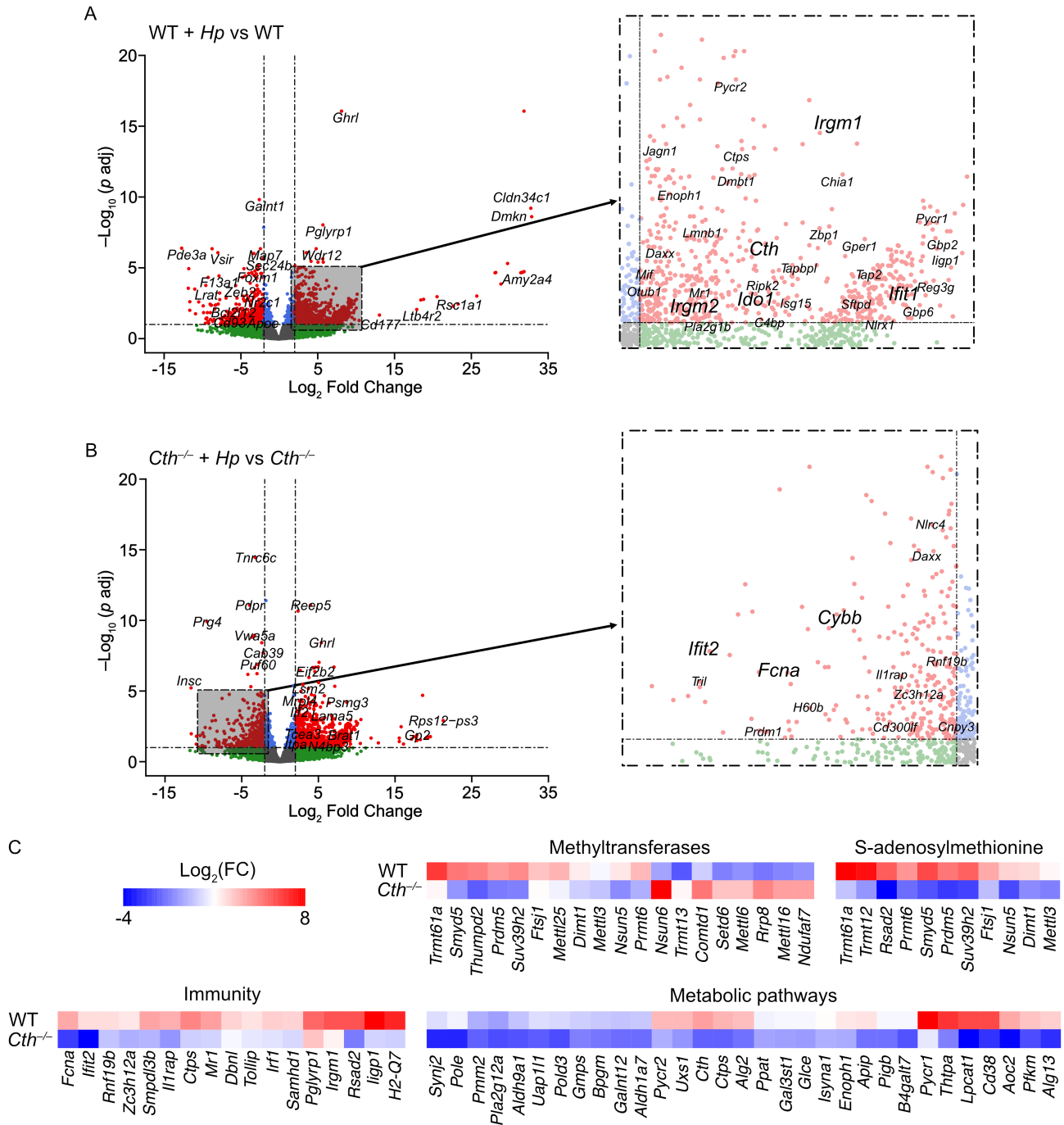
Figure 2.5. Identification of *H. pylori*-regulated genes in gastric macrophages. (**A-B**) The volcano plots show differential gene signatures in Gmacs from infected mice compared to uninfected mice (Fold change > 2, FDR < 0.05). Grey dots, not significant; green dots, Log$_2$ fold change > 2; blue dots, adjusted *p* value < 0.05; red dots, Log$_2$ fold change > 2 and adjusted *p* value < 0.05. Genes of interest are enlarged. (**A**) Gmacs from *H. pylori*-infected WT mice compared to uninfected WT mice. (**B**) Gmacs from *H. pylori*-infected *Cth*$^{-/-}$ mice compared to uninfected *Cth*$^{-/-}$ mice. (**C**) Heatmaps displaying significantly altered pathways of DEGs in *Cth*$^{-/-}$ Gmacs compared to WT Gmacs of infected mice when compared to uninfected controls (interaction *p* < 0.01). Fold change is infected/control per genotype.

45

CTH promotes the metabolism of SAM through the RTP during *H. pylori* infection.

To relate the transcriptional changes to metabolic signatures, we next performed an untargeted global metabolomic analysis of the gastric tissues from infected WT and *Cth*$^{-/-}$ mice. Overall, there were 1,300 positively charged metabolites and 734 negatively charged metabolites significantly affected by CTH in infected mice (Appendix A, Figure 6, A and B). Pathway analysis evidenced metabolic pathways involving SAM metabolism, namely "(S)-reticuline biosynthesis", "spermidine biosynthesis", "spermine biosynthesis", and "L-serine degradation", were significantly affected by deletion of *Cth* in infected mice (Figure 2.6A). We also found that pathways involved in energy production such as the TCA cycle and glycolysis were affected by the deletion of *Cth* (Figure 2.6A). We then used targeted metabolomics to verify our findings. Specifically, dcSAM, SAM, and cystathionine levels were measured by LC-MS in the tissues of WT and *Cth*$^{-/-}$ mice infected or not with *H. pylori* (Figure 2.6B). Levels of dcSAM remained relatively similar; however, SAM levels were significantly accumulated in naïve *Cth*$^{-/-}$ mice and significantly decreased in with infection with no change in SAM levels in the WT mice (Figure 2.6B). Importantly, levels of cystathionine, the substrate for CTH, were markedly increased in the *Cth*$^{-/-}$ mice, confirming that CTH activity was lost (Figure 2.6B). Because there was an abundance of SAM in naïve *Cth*$^{-/-}$ gastric tissues, we investigated whether SAM availability directly regulates the macrophage response to *H. pylori*. We treated bone marrow-derived macrophages (BMmacs) with SAM in the absence or presence of *H. pylori* for 24 h. We confirmed that exogenous SAM treatment results in accumulation of SAM and cystathionine in the BMmacs, which decreased with infection (Appendix A, Figure 7A). Analysis of mRNA expression revealed that treatment with SAM significantly reduced expression of *Tnf* and *Il12b*, while increasing expression of *Il1b* and *Il6*, having no effect on *Nos2* and the p35 subunit of IL-12 (*Il12a*), and increasing expression of the prototypical markers of antiinflammatory macrophages, *Arg1*, and transforming growth factor, beta 1 (*Tgfb1*) (Appendix A, Figure 7, B-E). To assess the in vivo effect of SAM on *H. pylori*-induced disease, WT mice were orally gavaged with SAM starting 1 wk post-infection (p.i.) (Appendix A, Figure 7F). There was no change in gastritis score or colonization following SAM treatment (Appendix A, Figure 7, G and H).
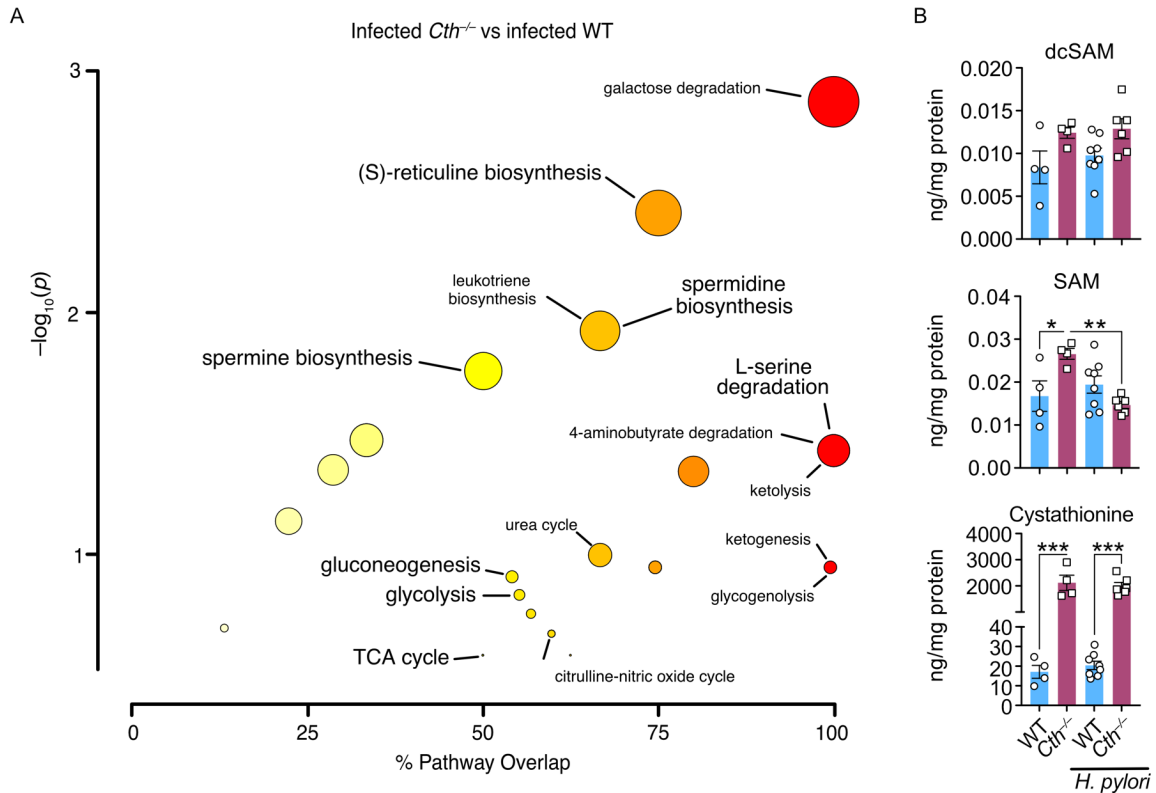
Figure 2.6. CTH promotes the metabolism of SAM through the RTP during *H. pylori* infection. (**A**) Bubble plot of metabolomic analysis of gastric tissues from WT and *Cth*$^{-/-}$ mice at 8 wk p.i. with *H. pylori* PMSS1 (FDR < 0.05). Pathways involving SAM metabolism or energy production are enlarged. The x-axis and node color represent pathway overlap and the y-axis and node radius represent *p* value; *n* = 8 infected mice per genotype. (**B**) Abundance of dcSAM, SAM, and cystathionine in the gastric tissues of WT and *Cth*$^{-/-}$ mice at 4 wk p.i. with *H. pylori* PMSS1; *n* = 4 uninfected and 6-8 infected mice per genotype. All values are means ± SEM. Statistical analyses where shown: One-way ANOVA with Newman-Keuls post hoc test; **$p < 0.01$ and ***$p < 0.001$.

CTH is downstream of SAM, which is needed for the biosynthesis of dcSAM, and thus for spermidine and spermine production. We have previously shown that polyamines can regulate *H. pylori*-induced macrophage activation and thus affect disease progression.[58,69,91,97,102] To determine if CTH may affect *H. pylori*-induced immune activation by a mechanism linked to polyamines, we next measured polyamine levels in the gastric tissues of WT and *Cth*$^{-/-}$ mice infected or not with *H. pylori*. We found that there were no significant differences in putrescine, spermidine, or spermine levels between WT and *Cth*$^{-/-}$ mice (Appendix A, Figure 8A). This may be explained by the absence of any changes in the mRNA expression levels of enzymes within the polyamine pathway in the gastric

tissues (Appendix A, Figure 8B). We next directed the consumption of SAM towards the RTP and away from polyamine synthesis using the SAMDC inhibitor, SAM486A (also known as CGP 48664 and commercially as Sardomozide).[202] Inhibition of SAMDC in BMmacs resulted in a significant accumulation of putrescine with and without *H. pylori* infection (Appendix A, Figure 8C). Spermidine levels remained relatively the same independent of treatment or infection, while spermine levels significantly decreased in *H. pylori*-infected cells following SAMDC inhibition (Appendix A, Figure 8C). BMmacs treated with SAM486A and infected with *H. pylori* for 24 h displayed significantly increased expression of *Tnf* but decreased expression of *Il12b* compared to the untreated infected BMmacs (Appendix A, Figure 8D). To assess the in vivo effect of SAMDC inhibition on *H. pylori*-induced disease, beginning 1 wk p.i., C57BL/6 mice were administered SAM486A by intra-peritoneal (IP) injection every other day for the remainder of the 4 wk infection (Appendix A, Figure 8E).[185] As expected, SAM486A treatment led to an increase of putrescine levels in the gastric tissues from the mice (Appendix A, Figure 8F). In contrast, the levels of spermidine and spermine did not change with either infection or treatment with SAM486A (Appendix A, Figure 8F), suggesting another mechanism maintains polyamine levels in the stomach. Mice treated with SAM486A had no change in gastritis scores or *H. pylori* colonization (Appendix A, Figure 8, G and H). In summary, SAM supplementation and SAMDC inhibition had moderate effects on macrophage gene expression in vitro, however, this did not translate to in vivo effects, suggesting that SAM, SAMDC, and polyamines do not mediate the effects of CTH on *H. pylori*-induced inflammation and that other mechanisms should be identified.

CTH suppresses DNA methylation and supports activated macrophage gene expression.

We observed that expression of CTH is specifically induced by *H. pylori* in BMmacs compared to another Gram-negative bacterium, *Citrobacter rodentium*, or the classical stimuli of M1-like macrophages, LPS+IFN-γ; M2-like macrophages, Il-4; or Mreg-like macrophages, IL-10 (Figure 2.7A). Currently available inhibitors of CTH are moderately selective, but are active against other PLP-dependent enzymes.[203] Therefore, to assess the role of CTH in macrophages, we generated BMmacs from WT and *Cth*^{-/-} mice (Figure 2.7B and Appendix A, Figure 9A). We confirmed that CTH was not expressed in *Cth*^{-/-} BMmacs (Appendix A, Figure 9B) and that there was no change in expression of *Cbs* in the absence of CTH or after *H. pylori* infection (Appendix A, Figure 9C). Homocysteine,

the substrate for transsulfuration, was significantly higher in $Cth^{-/-}$ BMmacs independent of infection and cystathionine levels were the same between WT and $Cth^{-/-}$ BMmacs with or without infection (Figure 2.7C and Appendix A, Figure 9D). SAM levels were significantly higher in WT infected BMmacs compared to the uninfected control, while SAM was significantly decreased in $Cth^{-/-}$ BMmacs with and without *H. pylori* infection (Figure 2.7C and Appendix A, Figure 9D). DNA methylation was significantly increased in infected $Cth^{-/-}$ BMmacs 6 h p.i. with *H. pylori* (Figure 2.7, D and E). At 24 h p.i., DNA methylation was reduced to almost uninfected WT levels, however, $Cth^{-/-}$ BMmacs had significantly higher levels of DNA methylation compared to WT, independent of infection (Appendix A, Figure 9, E and F).

We next assessed whether the increase in DNA methylation affected gene expression. Levels of proinflammatory macrophage markers *Tnf*, *Nos2*, *Cxcl10*, *Il1b*, *Il6, and Il12b* were significantly reduced in $Cth^{-/-}$ BMmacs 6 h p.i. with *H. pylori* (Figure 2.7F). The decreased *Nos2* mRNA expression in infected $Cth^{-/-}$ BMmacs correlated with decreased levels of NOS2 protein and NO production (Figure 7, G and H). Expression of the antiinflammatory markers *Chil3* and *Tgfb1*, but not *Arg1* and *Il10*, were decreased in $Cth^{-/-}$ BMmacs at 6 h p.i. with *H. pylori* (Figure 2.7I). At 24 h p.i. with *H. pylori*, expression of *Tnf, Arg1*, *Tgfb1* were significantly reduced in $Cth^{-/-}$ BMmacs (Appendix A, Figure 9, G and H). This supports the idea that CTH can regulate macrophage gene expression through DNA methylation.

We have previously shown that *H. pylori* enhances macrophage gene expression through NF-κB activation.[85,173] We next found that WT and $Cth^{-/-}$ BMmacs had similar levels of MyD88 expression (Figure 2.7J), which is directly linked to toll-like receptor signaling upstream of NF-κB activation. In contrast, phosphorylation of the NF-κB p65 subunit, RELA, at Ser-536 that was activated by *H. pylori* infection in WT BMmacs, was significantly decreased in $Cth^{-/-}$ cells (Figure 2.7J). NF-κB activation and nuclear translocation is regulated by the phosphorylation of inhibitor of κ light polypeptide gene enhancer in B cells, inhibitor α (NFKBIA, also known as IκBα) and subsequent degradation. There was no difference in the phosphorylation or total levels of NFKBIA (Appendix A, Figure 9I). These findings suggest that CTH is important in early signaling cascades in macrophages by enhancing the phosphorylation of NF-κB, independent of NFKBIA degradation.
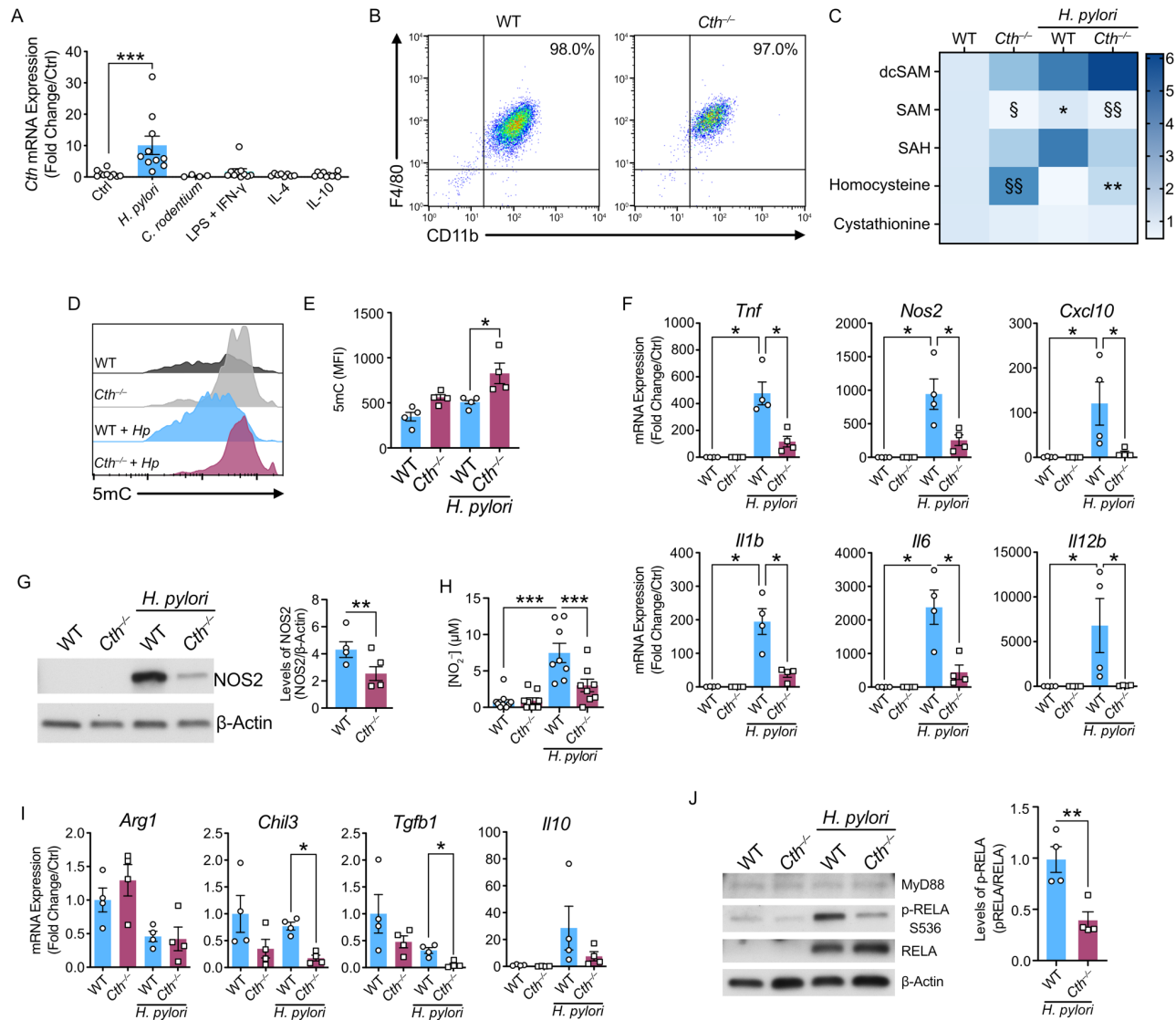
Figure 2.7. CTH suppresses DNA methylation and supports M1 macrophage gene expression. (**A**) Expression of *Cth* by WT BMmacs 24 h post-challenge; *n* = 4-10 biological replicates from 3 independent experiments. (**B**) Representative plot of CD11b and F4/80 expression of WT and *Cth*^{–/–} BMmacs 24 h p.i. with *H. pylori*. (**C**) Fold change of metabolite levels in BMmacs 24 h p.i. with *H. pylori* compared to control; *n* = 4 biological replicates. (**D**) Representative plot and (**E**) and MFI quantification of 5mC staining in WT and *Cth*^{–/–} BMmacs 6 h p.i. with *H. pylori*; *n* = 4 biological replicates. (**F**) Expression of proinflammatory macrophage activation markers by WT and *Cth*^{–/–} BMmacs 6 h p.i. with *H. pylori*; *n* = 4-10 biological replicates per genotype from 3 independent experiments. (**G**) NOS2 protein immunoblot and densitometric analysis of WT and *Cth*^{–/–} BMmacs 24 h p.i. with *H. pylori*; *n* = 4 biological replicates per genotype. (**H**) NO$_2^-$ concentration in supernatants from WT and *Cth*^{–/–} BMmacs; *n* = 8 biological replicates from 2 independent experiments. (**I**) Expression of antiinflammatory macrophage activation markers by WT and *Cth*^{–/–} BMmacs 6 h p.i. with *H. pylori*; *n* = 4-10 biological replicates per genotype from 3 independent experiments. (**J**) pRELA protein immunoblot and densitometric analysis of WT and *Cth*^{–/–} BMmacs 30 min p.i. with *H. pylori*; *n* = 3-4 biological replicates from 2 independent experiments. All values are means ± SEM. Statistical analyses where shown: (**A**), 1-way ANOVA with Dunnett's test; (**C**) One-way ANOVA with Newman-Keuls post hoc test; (**E**), (**F**), (**H**), and (**I**) One-way ANOVA with Kruskal-Wallis test, followed by a Mann-Whitney *U* test; (**J**) Student's *t* test; *p < 0.05, **p < 0.01, and ***p < 0.001 vs. uninfected; §*p* < 0.05 and §§*p* < 0.01 vs. WT.

The role of CTH in the macrophage proteome.

To further determine the role of CTH in the macrophage response to *H. pylori*, we analyzed the proteome of WT and *Cth*$^{-/-}$ BMmacs. Using a 4-plex tandem mass tag Isobaric Mass Tagging-based approach, we identified 213 proteins in WT BMmacs and 142 proteins in *Cth*$^{-/-}$ BMmacs that were upregulated with infection, with 101 of those proteins shared between the two genotypes (Figure 2.8A). In addition, we identified 75 proteins in WT BMmacs and 45 proteins in *Cth*$^{-/-}$ BMmacs that were downregulated with infection, with 29 of those proteins shared between the two genotypes (Figure 2.8A). We then assessed the *H. pylori*-induced proteome of WT BMmacs using Ingenuity Pathway Analysis (IPA) (Figure 2.8B). The pathway most significantly activated by infection was "Metabolism of reactive oxygen species" with a z-score of 3.51 (Figure 2.8B). We next assessed alterations in the *H. pylori*-induced proteome in the absence of CTH. *Cth*$^{-/-}$ BMmacs infected with *H. pylori* compared to uninfected *Cth*$^{-/-}$ BMmacs exhibited upregulation of only 27 of the 89 pathways (30%) activated by *H. pylori* infection in WT BMmacs (Figure 2.8C) and downregulation of only 2 of the 8 pathways (25%) inhibited by *H. pylori* infection in WT BMmacs (Appendix A, Figure 10). While "Synthesis of reactive oxygen species" and "Production of reactive oxygen species" are present in both WT and *Cth*$^{-/-}$ BMmacs, importantly, the "Metabolism of reactive oxygen species" is not present in the pathways induced by *H. pylori* in *Cth*$^{-/-}$ BMmacs (Figure 2.8, B and C). Thus, CTH has the capacity to regulate protein expression in macrophages and contribute to macrophage activation and functions.
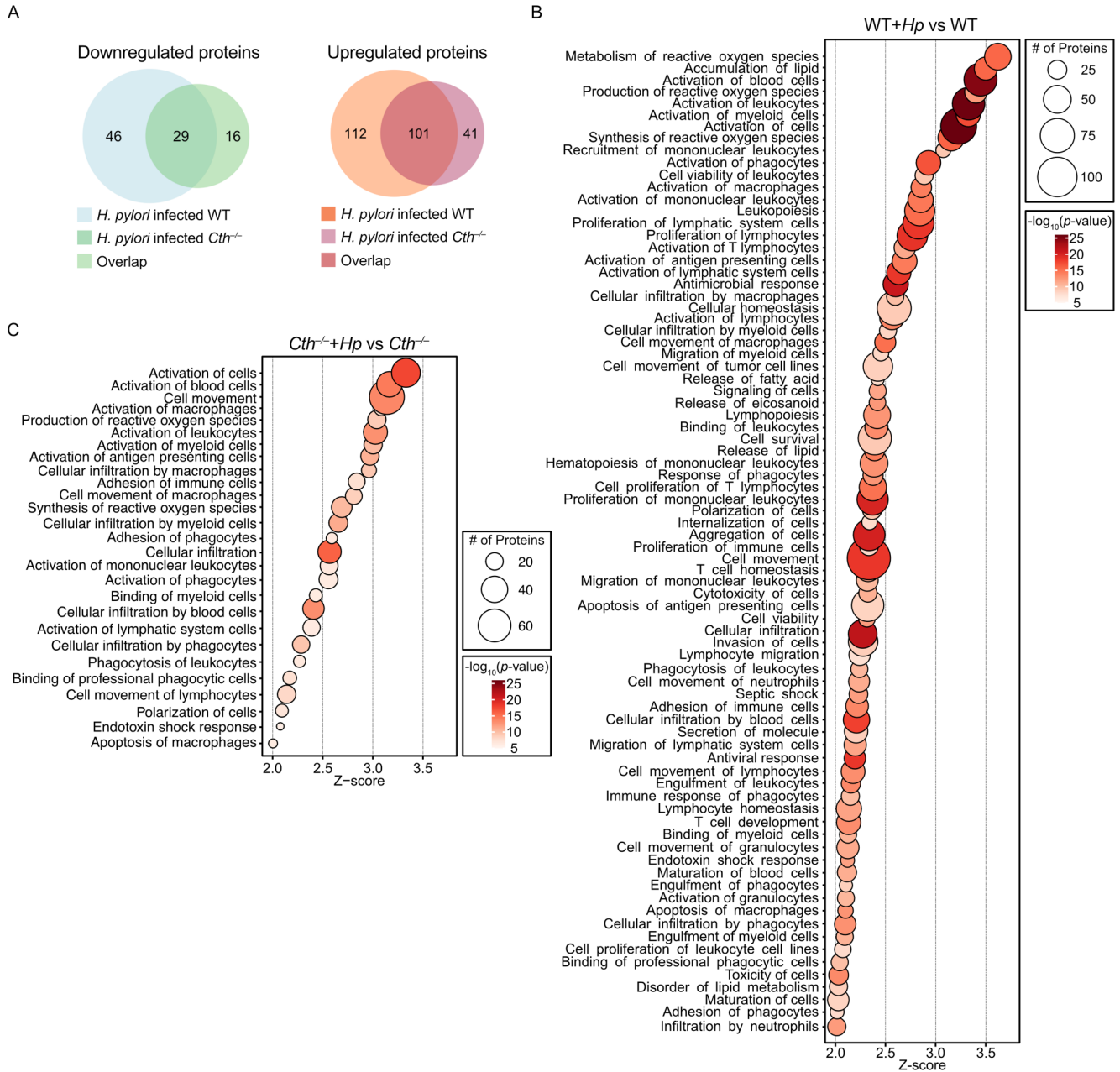
Figure 2.8. CTH modifies macrophage activation patterns of proteins during *H. pylori* infection. Proteomic analysis of BMmacs from WT and *Cth*^{−/−} mice infected or not with *H. pylori* for 24 h, *n* = 4 biological replicates per genotype. (**A**) Venn diagram showing commonly downregulated and upregulated proteins. (**B**) Enrichment analysis of pathways activated by *H. pylori* infection in WT BMmacs. (**C**) Enrichment analysis of the pathways in B activated by *H. pylori* infection in *Cth*^{−/−} BMmacs. (FDR <0.05, z-score >2).

CTH supports mitochondrial respiration while promoting glycolysis in *H. pylori*-infected macrophages.

To elucidate the mechanism by which CTH supports macrophage activation and contributes to *H. pylori*-induced disease, we investigated the downstream metabolic effects of *Cth* deletion in macrophages. Since the metabolomic pathway analysis indicated changes in glycolysis and the TCA cycle, we conducted extracellular flux assays on WT and *Cth*$^{-/-}$ BMmacs to assess mitochondrial function and cellular respiration. As expected, glycolysis and glycolytic capacity were increased with *H. pylori* infection in WT BMmacs, while *Cth*$^{-/-}$ BMmacs had impaired glycolysis and glycolytic capacity in naïve cells or those exposed to *H. pylori* (Figure 2.9A). WT BMmacs stimulated with LPS+IFN-γ for 24 h had decreased oxygen consumption rate (OCR) but increased extracellular acidification rate (ECAR) (Appendix A, Figure 11, A and B), whereas WT BMmacs stimulated with IL-4 for 24 h displayed both increased OCR and increased ECAR (Appendix A, Figure 11, C and D). Mitochondrial oxidative phosphorylation (OXPHOS) was decreased (Figure 2.9, B) and ECAR was increased with *H. pylori* infection in WT BMmacs (Figure 9C). *Cth*$^{-/-}$ BMmacs displayed increased OCR and ECAR 24 h post-challenge with *H. pylori* (Figure 9, B and C) or with LPS+IFN-γ (Appendix A, Figure 11, A and B), but did not change with IL-4 stimulation (Supplemental Figure 11, C and D). Uninfected *Cth*$^{-/-}$ BMmacs exhibited lower basal and maximal respiration than uninfected WT BMmacs, that did not change with infection unlike the WT BMmacs (Figure 2.9D). Elevated ECAR levels with *H. pylori* infection or LPS+IFN-γ stimulation confirmed that the *Cth*$^{-/-}$ BMmacs were still viable (Figure 2.9C and Appendix A, Figure 11B). The decreased mitochondrial respiration also resulted in decreased mitochondrial ATP production and spare respiratory capacity (SRC), an indicator of metabolic plasticity, in the *Cth*$^{-/-}$ BMmacs (Figure 2.9D), suggesting that *Cth*$^{-/-}$ BMmacs do not exhibit metabolic activation in response to infection.

Since mitochondrial activity contributes to the production of ROS that macrophages generate to combat pathogens, we measured mitochondrial superoxide levels, an indicator of mitochondrial ROS (mitoROS). We found that *H. pylori*-infected *Cth*$^{-/-}$ BMmacs exhibited a significant accumulation of mitoROS compared to uninfected controls and infected WT cells at 24 h p.i. (Figure 2.9, E and F). We next measured the amount of intracellular antioxidant, glutathione (GSH), and found that GSH levels were low in *Cth*$^{-/-}$ BMmacs at baseline and remained

unchanged with infection, while GSH decreased with infection in WT BMmacs (Figure 2.9G). Cysteine, the direct product of CTH activity, is a semi-essential amino acid that is the main precursor for generation of GSH.[110,111] Cysteine levels were significantly elevated in infected WT BMmacs compared to control and infected $Cth^{-/-}$ BMmacs (Figure 2.9H), consistent with loss of CTH activity in $Cth^{-/-}$ BMmacs, and increased CTH activity with *H. pylori* infection in WT cells. These results suggest that macrophages upregulate CTH expression during *H. pylori* infection to maintain redox homeostasis.

Taken together, these studies demonstrate that the loss of CTH in macrophages leads to metabolic suppression and impaired immune activation that underlies the decrease in *H. pylori*-induced gastritis observed in $Cth^{-/-}$ mice.
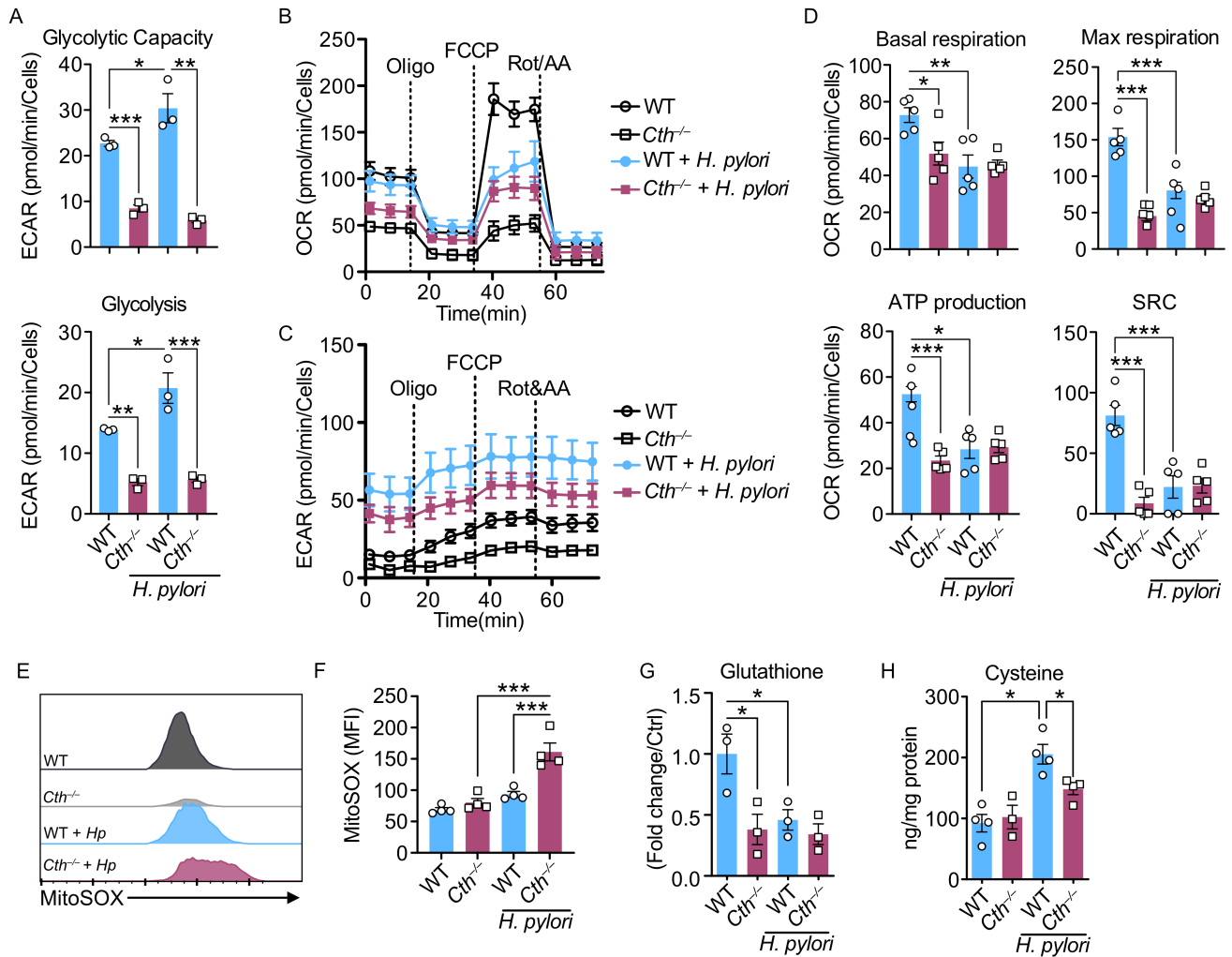
Figure 2.9. CTH contributes to macrophage activation by enhancing mitochondrial function and glycolysis in *H. pylori*-infected macrophages. (**A**) Rate of glycolysis and glycolytic capacity of WT and *Cth*^{−/−} BMmacs 24 h p.i. with *H. pylori*; $n = 3$ mice per genotype. (**B**) Oxygen consumption rate (OCR) and (**C**) extracellular acidification rate (ECAR) of WT and *Cth*^{−/−} BMmacs 24 h p.i. with *H. pylori*; $n = 5$ from 2 independent experiments. Vertical dashed lines indicated the sequential addition of oligomycin (Oligo), FCCP, and Rot/AA. (**D**) Basal respiration, maximal respiration, ATP production, and SRC derived from *B*. (**E**) Representative plot and (**F**) MFI quantification of MitoSOX Red staining in WT and *Cth*^{−/−} BMmacs 24 h p.i. with *H. pylori*; $n = 4$ biological replicates. (**G**) Glutathione levels in WT and *Cth*^{−/−} BMmacs 24 h p.i. with *H. pylori*; n = 3 biological replicates. (**H**) Cysteine levels in WT and *Cth*^{−/−} BMmacs 24 h p.i. with *H. pylori*; n = 4 biological replicates. All values are means ± SEM. Statistical analyses where shown: One-way ANOVA with Newman-Keuls post hoc test; *$p < 0.05$, **$p < 0.01$, and ***$p < 0.001$.

2.5 Discussion

Macrophages are a fundamental component of the host immune response with the capacity to transition along the spectrum of proinflammatory to antiinflammatory polarization as environmental signals and stimuli change.[7,58] In inflammatory pathologies, such as *H. pylori*-induced gastritis, overzealous immune responses can lead to more severe disease outcomes, such as gastric cancer.[24] Therefore, identification of alternative strategies that target the host to limit chronic inflammatory conditions are needed to prevent disease progression. Our study demonstrates that CTH impacts metabolic activation and polarization of macrophages in response to *H. pylori* infection. Moreover, we utilized unbiased "omics" approaches to probe the global effects of CTH in the host response to *H. pylori* and consistently found evidence of a heightened immune response and enhanced cellular respiration in the presence of CTH that contributes to *H. pylori*-induced disease.

Several previous studies have investigated the role of CTH in inflammation within the context of H_2S production, however, there is not a consensus and results often depend on exogenous versus endogenous enzymatic H_2S derivation, with the latter being much less understood.[125,204] This variation in findings highlights the need to further characterize the role of CTH in different models of inflammation. Using a genetic model of *Cth* deletion, here we have shown that $Cth^{-/-}$ mice have significantly attenuated gastritis in models of acute and chronic *H. pylori* infection. In this study, we did not measure H_2S since many bacterial pathogens, including *H. pylori*,[205] produce H_2S and host cells maintain the ability to produce H_2S in the absence of CTH through CBS or 3-mercaptopyruvate sulfurtransferase activity.[111] Instead, we measured homocysteine, cystathionine, and cysteine levels as direct measures of CTH activity. Our work further supports the idea that CTH is a modulator of immune cell function and we have identified, for the first time, the role of CTH in the stomach in the context of *H. pylori* infection. In future studies, it would be interesting to examine the interplay between CTH and the gut microbiome.

Our previous findings demonstrated that exogenous overexpression of the human *CTH* gene in RAW 264.7 cells inhibited markers of macrophage activation.[136] However, determining the effect of CTH inhibition on macrophage activation was not feasible in the prior study, as we found that *Cth* siRNA diminished the number of live *H. pylori* in infected cells, potentially limiting the macrophage response, and that the CTH inhibitor,

aminooxyacetic acid, directly kills *H. pylori*.[136] In addition, the CTH inhibitor has off-target activity.[136,203] In the current study, genetic knockout of *Cth* led to decreased macrophage activation during *H. pylori* infection. Transcriptomic analysis of gastric macrophages revealed that multiple gene sets involved in immune function were downregulated with *Cth* deletion. This was also reflected in the proteome of macrophages from *Cth*$^{-/-}$ versus WT mice infected ex vivo with *H. pylori*.

Because CTH has been mainly studied as a producer of H_2S, there is a gap in knowledge about how CTH may influence the metabolic pathways directly upstream of its activity. Our analysis of untargeted metabolomics identified SAM metabolism and cellular respiration as pathways regulated by CTH. SAM supplementation has been shown to reduce airway inflammation and M1-like macrophages exhibit reduced DNA methylation.[206–208] However, SAH, the product of methyl donation by SAM, can bind to methyltransferases and inhibit methylation reactions.[119,120] Although SAM supplementation suppressed proinflammatory and enhanced antiinflammatory gene expression in vitro, there was no protection from *H. pylori* gastritis in vivo. Directly linked to SAM metabolism is the polyamine pathway. Based on the increased gastritis in mice with myeloid-specific deletion of ODC during *H. pylori* infection,[69] we anticipated that inhibition of SAMDC would result in the accumulation of putrescine and decreased inflammation. However, we observed that SAMDC inhibition increased putrescine levels in the stomach of mice without affecting gastritis, suggesting that putrescine accumulation alone is not sufficient to regulate gastritis. Similarly, we hypothesized that deletion of CTH might free up SAM for the metabolism of putrescine into spermidine and increase inflammation. However, loss of CTH did not alter polyamine levels sufficiently enough to impact gastritis.

There is a growing body of literature describing the metabolic needs of immune cells, and in particular, the role of metabolism in macrophage differentiation and activation.[72,73] During macrophage stimulation, polarizing macrophages remodel their metabolism to meet energetic needs. Proinflammatory macrophages repress oxidative phosphorylation in favor of glycolysis to aid in the production of cytokines and reactive oxygen species.[74] In contrast, antiinflammatory M2 macrophages enhance mitochondrial oxidative phosphorylation while still consuming glucose.[79] We found that macrophages lacking CTH have impaired ability to metabolically adapt to external stimuli. ROS and nitrogen species are important effector molecules produced by macrophages to combat

pathogens and regulate polarization,[209] however, high levels can be detrimental and cause cellular dysfunction, including mitochondrial impairment.[210] This supports our findings that loss of CTH results in depleted intracellular cysteine and GSH, and contributes to high levels of mitochondrial superoxide and reduced mitochondrial function. Beyond the altered gene expression of macrophage cytokines, our data highlight an unexpected role of CTH in macrophage metabolism and respiration.

Lastly, in the context of *H. pylori* infection, regulation of TNF-α transcription has been shown to be dependent on alternative activation of NF-κB through the phosphorylation of the p65 subunit, RELA, at Ser-536 that does not involve NFKBIA degradation.[209] We found that deletion of *Cth* led to decreased TNF-α expression during infection with *H. pylori*, in vitro and in vivo, and with LPS + IFNγ stimulation. The impaired cytokine production may be linked to the observed decrease in phosphorylation of RELA at Ser-536 in the infected $Cth^{-/-}$ macrophages, especially since there were no differences in phospho- or total NFKBIA levels between the infected cells. Since many kinases are involved in the phosphorylation of p65, future studies using various receptor and signaling cascade inhibitors may enhance the understanding of the mechanism connecting CTH with the early macrophage responses.

In summary, our findings outline the role of CTH in regulating the macrophage-facilitated response to *H. pylori*. Increased expression of CTH by macrophages contributes to inflammation in the gastric tissues of mice and markers of proinflammatory macrophages ex vivo in the context of *H. pylori* infection. Using genetic deletion of *Cth*, we determined that CTH can affect macrophage function via enhanced gene and protein expression through NF-κB phosphorylation and suppression of DNA methylation and maintenance of mitochondrial function through redox homeostasis. This in turn can affect the adaptive immune response in T cells, though *Cth* deletion does not appear to affect T cell function in a cell autonomous manner. Due to the limitations of current chemical inhibitors of CTH, exploring the full spectrum of pathways related to CTH is essential in the discovery of therapeutic targets that can help reduce the burden of chronic gastritis and risk of gastric cancer in humans.

CHAPTER 3

The Role of Talin-1 in Macrophages During *C. rodentium*-induced Colitis

3.1 Abstract

The intestinal immune response is crucial in maintaining a healthy gut, but the enhanced migration of monocyte-derived macrophages in response to pathogens is a major contributor to disease pathogenesis. The goal of this study was to uncover a mechanism by which intestinal macrophages promote inflammation. Integrins are ubiquitously expressed cellular receptors that are highly involved in immune cell adhesion to endothelial cells while in the circulation and help facilitate extravasation into tissues. Here we show that specific deletion of the gene encoding talin-1, an integrin-activating scaffold protein, from cells of the myeloid lineage reduces epithelial damage, attenuates colitis, downregulates the expression of macrophage markers, and diminishes the presence of CD68-positive cells in the colonic mucosa of mice infected with the enteric pathogen *Citrobacter rodentium*. Bone marrow-derived macrophages lacking expression of *Tln1* did not exhibit a cell autonomous phenotype; there was no impaired proinflammatory gene expression, nitric oxide production, phagocytic ability, or surface expression of CD11b, CD86, or major histocompatibility complex II (MHCII) in response to *C. rodentium*. Thus, we demonstrate that talin-1 plays a role in the manifestation of infectious colitis by increasing macrophage recruitment, with an effect that is independent of macrophage activation.
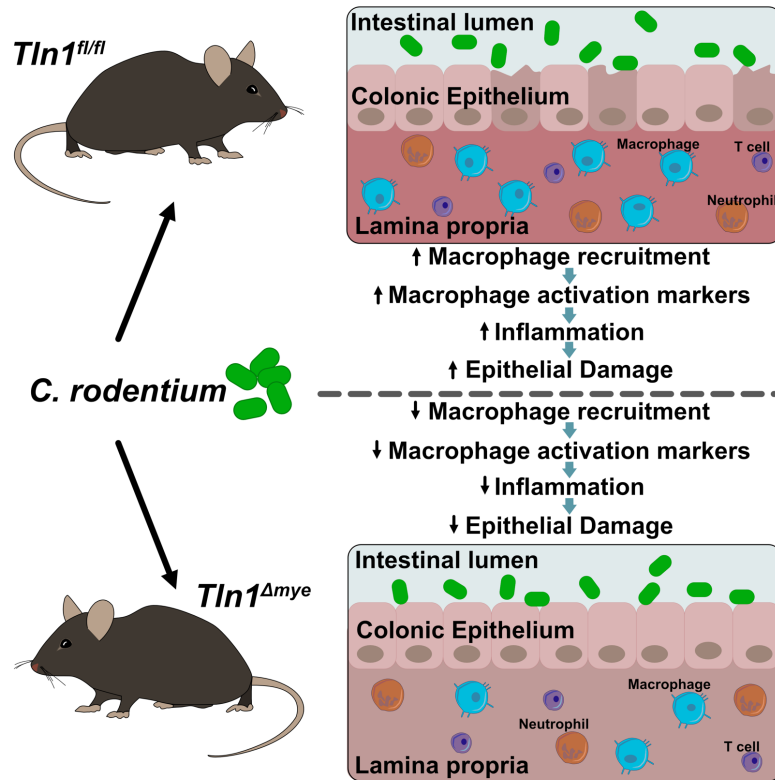
Figure 3.1. Graphical Abstract. Talin-1 contributes to the recruitment of macrophages during infection by the enteric murine pathogen *Citrobacter rodentium* and thus the pathogenic inflammatory response.

3.2 Introduction

Macrophages are an essential component of the intestinal immune response. Under normal conditions, the intestinal lamina propria is home to the largest population of mononuclear leukocytes in the body with macrophages being the most abundant subpopulation.[211] Intestinal macrophages are unique compared to other tissue macrophages in that they are continuously replenished from circulating blood monocytes as they help maintain epithelial renewal and immune homeostasis in the presence of the gut microbiota.[211] Inflammatory conditions of the intestines are often the result of perturbation of the normal gut flora, pathogenic infection, or an inherent dysregulation of the immune response. During infection with pathogenic bacteria, such as enteropathogenic *Escherichia coli* (EPEC) and Shiga toxin-producing *E. coli*, the enhanced immune cell recruitment and activation can be both protective and deleterious, and is a major cause of the resulting pathology.[212]

Recruited circulating monocytes enter tissues through integrin binding to adhesion molecules on endothelial cells.[213–215] Integrin ligand affinity and activation is facilitated by talin-1, a cytoskeletal scaffold protein that interacts with the cytoplasmic domain of the β-subunit of integrins and induces a confirmational change to the extracellular domain.[150,157] In this study, we sought to elucidate the role of talin-1 in macrophages during colonic infection by *Citrobacter rodentium*, the rodent equivalent of EPEC, a well-established model of infectious colitis.[109,170,216] Myeloid cell-specific knockdown of *Tln1* resulted in decreased epithelial damage and inflammation that was associated with decreased transcript levels of macrophage markers and less macrophages recruited to the infected tissues. This outcome was independent of a cell-autonomous effect of talin-1 in macrophage activation and function ex vivo. Overall, we demonstrate that talin-1 regulates the recruitment of macrophages in response to the enteric murine pathogen *C. rodentium* and facilitates the inflammatory response.

3.3 Materials and Methods

Mice. C57BL/6 *Tln1*$^{fl/fl}$ mice were provided by Dr. Roy Zent at Vanderbilt University Medical Center (Nashville, TN).[217] *Tln1*$^{fl/fl}$ mice were crossed with C57BL/6 *Lyz2*$^{cre/cre}$ mice and the resulting offspring were crossed to generate *Tln1*$^{fl/fl}$;*Lyz2*$^{+/+}$ (*Tln1*$^{fl/fl}$) and *Tln1*$^{fl/fl}$;*Lyz2*$^{cre/cre}$ (*Tln1*^{Δmye}) littermates.[218,219] All experiments were approved by the IACUC at Vanderbilt University and Institutional Biosafety Committee and the Research and Development Committee of the Veterans Affairs Tennessee Valley Healthcare System under the protocol V2000018.

Generation of bone marrow-derived macrophages. Bone marrow-derived macrophages (BMmacs) were generated as described.[220]

Infection with *C. rodentium*. Male adult (6-12 wk) littermates were orally inoculated by gavage with 5×10^8 *C. rodentium* strain DBS100.[170,216] Control mice received sterile Luria-Bertani broth alone. Animals were monitored and weighed daily for 14 days. Mice were sacrificed, and the colons were removed, measured, cleaned, weighed, and Swiss-rolled for fixation in 10% neutral buffered formalin for histology. Prior to fixation, three proximal and

distal pieces were collected; two pieces were flash frozen and the third was weighed, homogenized, serially diluted, and cultured on McConkey agar plates to determine bacterial colonization by counting the colony forming units (CFUs). Hematoxylin and eosin (H&E) stained slides were scored in a blinded manner by a gastrointestinal pathologist (MBP) for histologic injury (0–21), a composite of the total inflammation (0-18) plus epithelial injury (0-3).[170]

BMmacs were infected with *C. rodentium* at a multiplicity of infection (MOI) of 10 for 3 h in antibiotic-free media. The cells were then washed and provided media containing penicillin and streptomycin for an additional 3 h (mRNA) or 21 h (protein, flow cytometry).

mRNA Analysis. Total RNA was isolated from BMmacs and the flash frozen colonic tissues using the RNeasy Mini Kit (QIAGEN). Total RNA samples were reverse transcribed into cDNA using the SuperScript III Reverse Transcriptase (Thermo Fisher), Oligo (dT) primers (Thermo Fisher), and dNTP Mix (Applied Biosystems). Quantitative real-time PCR (qRT-PCR) was performed using the PowerUp SYBR Green Master Mix (Applied Biosystems). The primers are listed in Table 3.1.

Table 3.1: List of qRT-PCR primers used for Chapter 3.

Target gene	Sequence (5'-3')
Tln1	F: GGCCCTCCCAACGACTTT
	R: AGCCTCTAGCCAGATGCCTTT
Tnf	F: CTGTGAAGGGAATGGGTGTT
	R: GGTCACTGTCCCAGCATCTT
Il1b	F: ACCTGCTGGTGTGTGACGTTCC
	R: GGGTCCGACAGCACGAGGCT
Il6	F: AGTTGCCTTCTTGGGACTGA
	R: TCCACGATTTCCCAGAGAAC
Il23a	F: CCAGCAGCTCTCTCGGAATC
	R: TCATAGTCCCGCTGGTGC
Cxcl10	F: GGTCTGAGTGGGACTCAAGG
	R: GTGGCAATGATCTCAACACG
Arg1	F: AAGAAAAGGCCGATTCACCT
	R: CACCTCCTCTGCTGTCTTCC
Tnfsf14	F: CTGCATCAACGTCTTGGAGA
	R: GATACGTCAAGCCCCTCAAG
Ifng	F: GGCCATCAGCAACAACATAAGCGT
	R: TGGGTTGTTGACCTCAAACTTGGC
Il17a	F: ATCCCTCAAAGCTCAGCGTGTC
	R: GGGTCTTCATTGCGGTGGAGAG
Il22	F: TTGAGGTGTCCAACTTCCAGCA
	R: AGCCGGACGTCTGTGTTGTTA
Actb	F: CCAGAGCAAGAGAGGTATCC
	R: CTGTGGTGGTGAAGCTGTAG

Western Blot and Densitometric Analysis. Protein isolation, SDS-PAGE separation, nitrocellulose membrane transfer, and band visualization were performed as previously described.[220] The membranes were incubated with a rabbit anti-talin-1 (Cell Signaling) or a mouse anti-β-actin (Sigma) followed by HRP-labeled goat anti-rabbit IgG (Jackson ImmunoResearch) or HRP-labeled goat anti-mouse IgG (Promega), respectively. Densitometric analysis was performed with Fiji (ImageJ).[200]

Immunohistochemistry and Analysis. Paraffin-embedded Swiss-rolled murine colon tissues were processed as previously described[221] and incubated overnight at 4° C using the following antibodies: anti-CD68 (Biocare Medical), anti-Ly6G (abcam), anti-CD11c (Cell Signaling), or anti-CD3 (Abcam). All slides were imaged and analyzed using a Cytation C10 Confocal Imaging Reader and Gen 5+ software (Agilent BioTek). The average number of CD68-, Ly6G-, Cd11c-, and CD3-positive cells was quantified by the Cell Analysis function of the Gen 5+ software and was limited to the mucosa to reduce inclusion of non-specific staining and normalized to tissue surface area.

Gentamicin Assay. BMmacs were infected at an MOI of 10 for 1 h prior to washing, counting, and treating with 200 g/mL gentamicin for 1 h.[136] The cells were then lysed with 0.1% saponin for 30 mins at 37°C and the lysate was serially diluted and cultured on McConkey agar plates. CFUs were counted and normalized to cell count.

Flow cytometry. BMmacs infected or not with *C. rodentium* for 24 h were washed with PBS and fixed with CytoFix (BD Biosciences) for 20 min at 4°C, washed, and then labeled with anti-CD11b (BD Biosciences), anti-CD86 (Invitrogen), and anti-MHCII (Invitrogen).

Statistics. All the data shown represent the mean ± SEM unless otherwise noted. GraphPad Prism 9.4 (GraphPad Software) was used to perform statistical analyses and significance was set at $P < 0.05$.

3.4 Results and Discussion

Mice lacking talin-1 in the myeloid cell lineage exhibit less epithelial damage and inflammation during pathogenic colitis

We first confirmed knockdown of *Tln1* mRNA (Figure 3.2A) and talin-1 protein (Figure 3.2, B and C) in BMmacs isolated from *Tln1$^{\Delta mye}$* mice infected or not ex vivo with *C. rodentium*. Note that *C. rodentium* infection

had no effect on the expression of *Tln1* mRNA (Figure 3.2A) or talin-1 protein (Figure 3.2, B and C) in *Tln1^{fl/fl}$

BMmacs. Male mice were then infected via oral gavage with $5x10^8$ CFUs of *C. rodentium* and monitored for 14

days. We did not observe differences in body weight loss (Figure 3.3A), colon weight (Figure 3.3B), or bacterial

burden (Figure 3.3C) between *Tln1^{fl/fl}* and *Tln1^{Δmye}* mice. Consistent with previous studies, infection with *C.*

rodentium resulted in mucosal hyperplasia[222,223], erosion and ulceration of the epithelium, and immune cell invasion

of the mucosa and submucosa (Fig 3.3D).[141,224] Notably, histologic injury scores were attenuated in *Tln1^{Δmye}* mice

compared to *Tln1^{fl/fl}* littermates (Figure 3.3E), due to a reduction in both components of the composite score,

epithelial damage and total inflammation (Figure 3.3F). These results suggest that talin-1 in myeloid cells

contributes to *C. rodentium* pathogenesis and are supported by the findings that mice that have a weakened response

of neutrophils and/or macrophages, but have an intact lymphoid cell compartment, exhibit decreased colitis and

epithelial damage yet can still control bacterial growth.[225,226] In contrast, immunocompromised mice or mice that

lack an effective type 3 T cell or innate lymphoid cell response are unable to control the bacterial burden and exhibit

higher rates of mortality.[227–229]
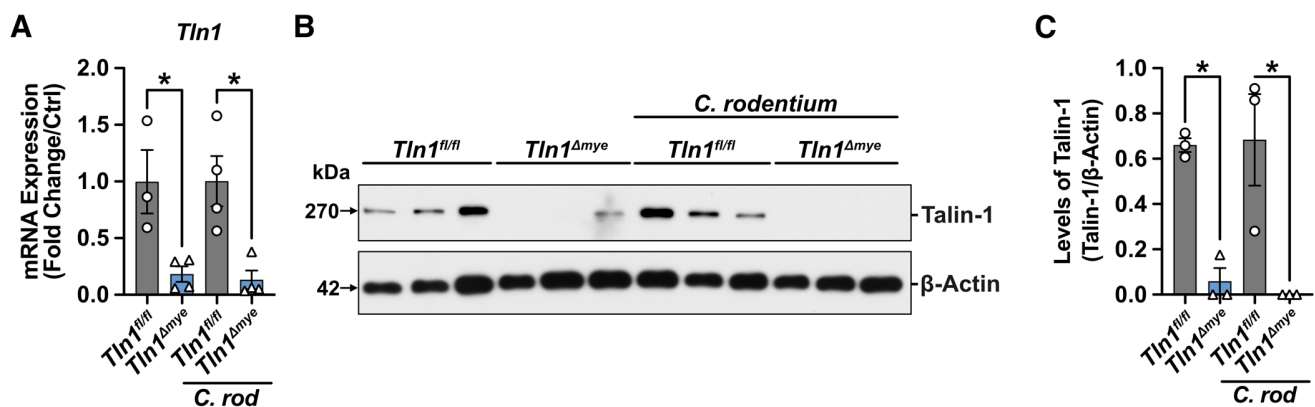
Figure 3.2. Myeloid cell-specific deletion of *Tln1*. BMmacs were generated form *Tln1^{fl/fl}* and *Tln1^{Δmye}* mice and infected with *C. rodentium*. (**A**) Expression of *Tln1* mRNA determined by qRT-PCR 6 h post-infection; $n = 3-4$ mice per genotype. (**B**) Western blot of talin-1 protein (270 kDa) expression and (**C**) densitometry analysis at 24 h post-infection; $n = 3$ mice per group. All values are reported as mean ± SEM. Statistical analyses, where shown; *$P<0.05$ and **$P<0.01$ determined by 1-way ANOVA and Tukey post hoc test.
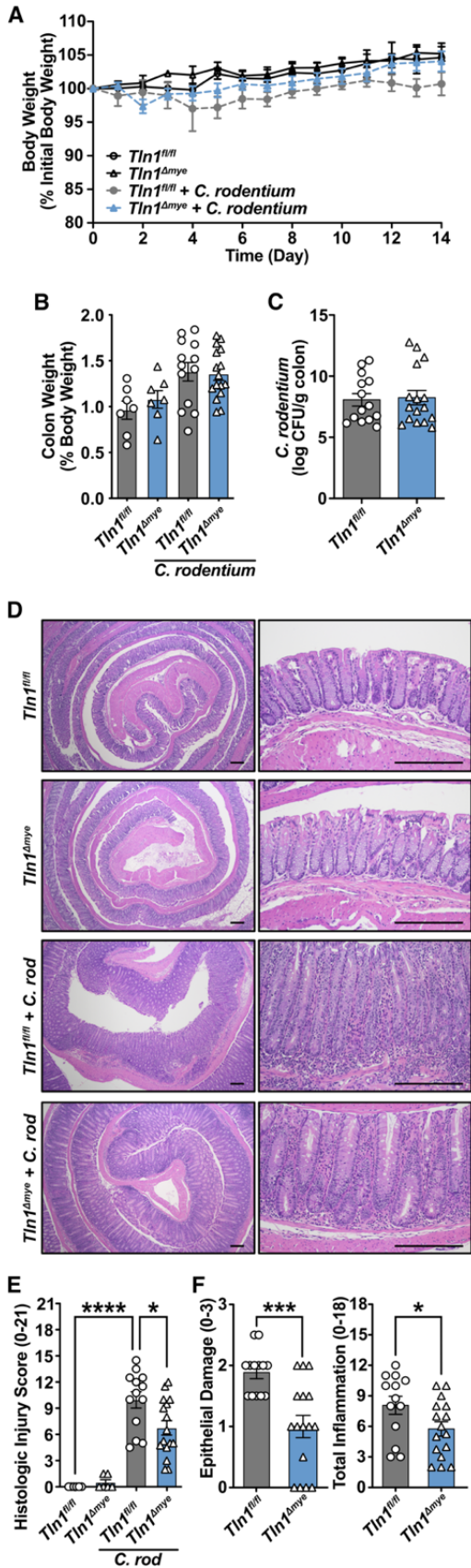
Figure 3.3. Loss of talin-1 in myeloid cells protects mice from *C. rodentium* induced injury. *Tln1^{fl/fl}* and *Tln1^{Δmye}* male littermates were orally inoculated with 5x10^8 CFU of *C. rodentium* by gavage and observed for 14 days. *n* = 7 uninfected mice and *n* = 13-16 infected mice per genotype. Data pooled from 2 independent experiments. (**A**) Daily body weights depicted as a percent of initial body weight. (**B**) Colon weights depicted as a percent of body weight on day 14 post-infection. (**C**) *C. rodentium* colonization of the colon determined by counting CFUs from serial dilutions of homogenized tissues and normalized to tissue weight on day 14 post-infection. (**D**) Representative H&Es of Swiss-rolled fixed tissues. (**E**) Histologic injury score assessed by a pathologist using the H&E-stained tissues and is the sum of (**F**) epithelial damage and total inflammation. All values are reported as mean ± SEM. Statistical analyses, where shown; *$P<0.05$ and ****$P<0.0001$ determined by (**E**) 1-way ANOVA and Tukey post hoc test and (**F**) Student's *t* test.

Mice with myeloid cell-specific deletion of *Tln1* express lower levels of macrophage markers and recruit less macrophages in the colon with *C. rodentium* infection

We next assessed the expression of genes encoding for immune effectors typically associated with *C. rodentium* infection in the colon. Markers of proinflammatory macrophages, namely tumor necrosis factor (*Tnf*), interleukin (IL)-1β (*Il1b*), *Il6*, *Il23a*, and C-X-C ligand 10 (*Cxcl10*) were induced with infection in *Tln1^{fl/fl}* mice and significantly decreased in the colon tissues from infected *Tln1^{Δmye}* mice compared to infected *Tln1^{fl/fl}* mice (Figure 3.4A). Additionally, the levels of the transcripts encoding the antiinflammatory macrophage markers, specifically arginase 1 (*Arg1*) and tumor necrosis factor super family 14 (*Tnfsf14; Light*) were also significantly decreased in infected *Tln1^{Δmye}* colon tissues (Figure 3.4B). We observed a significant reduction in the expression of the Th1 T cell marker interferon-γ (*Ifng*) with no change in the expression of the Th17 marker *Il17a*, or the Th22 marker *Il22* in infected *Tln1^{Δmye}* colon tissues (Figure 3.4C). In accordance with our findings that there were no differences between the *C. rodentium* colonization of *Tln1^{fl/fl}* and *Tln1^{Δmye}* mice, but decreased colitis, IL-22 and IL-17 are important for controlling bacterial growth, but not disease development.[229–232]

Numerous studies have demonstrated that talin-1 is essential for the migration and recruitment of leukocytes, including neutrophils, dendritic cells, and T cells to sites of inflammation.[166–169] Thus, we next assessed the population of immune cells present in the colon via immunohistochemistry and quantification of positively-stained cells. Consistent with the gene expression we observed, the number of CD68+ macrophages in the colon were increased with infection in *Tln1^{fl/fl}* tissues, but were significantly less abundant in infected *Tln1^{Δmye}* mice (Figure 3.5A). Interestingly, there was no differences in the number of Ly6G+ neutrophils or CD11c+ dendritic cells between *Tln1^{fl/fl}* and *Tln1^{Δmye}* mice with infection (Figure 3.5, B and C). The *Lyz2*-flox system is used to target specific gene deletions in cells of the myeloid cell lineage and affects macrophages, neutrophils, and dendritic cells to varying degrees[218,219] suggesting that talin-1 is important for the recruitment of macrophages, but not dendritic cells or neutrophils during *C. rodentium* infection. In addition, the number of CD3+ cells were similar in *Tln1^{Δmye}* mice compared to *Tln1^{fl/fl}* mice with infection, matching the comparable expression of *Il17a* and *Il22* (Figure 3.5D).
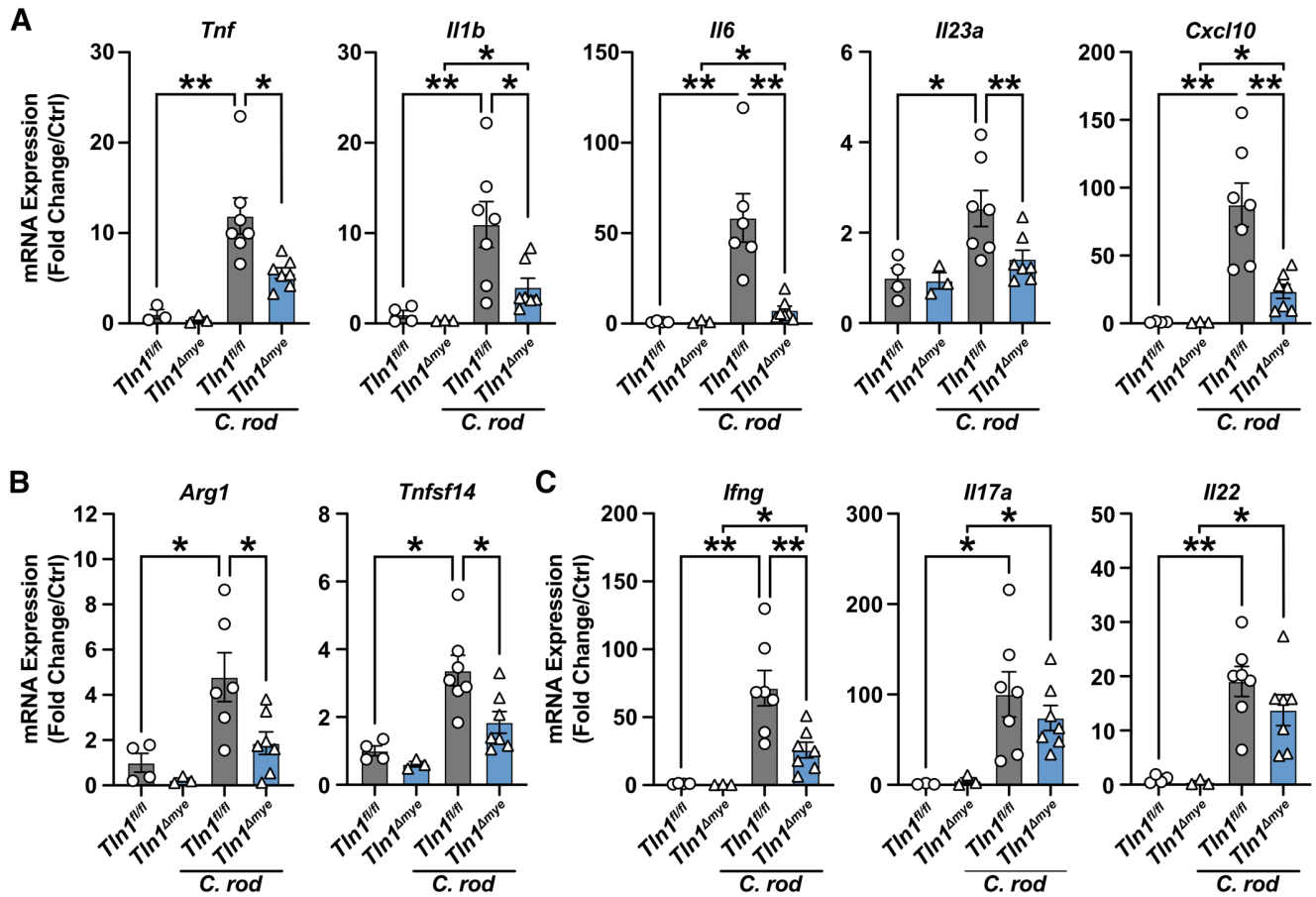
Figure 3.4. Knockdown of talin-1 in myeloid cells reduces expression of macrophage markers in vivo. Whole tissue mRNA expression of (**A**) proinflammatory, (**B**) antiinflammatory, and (**C**) T cell markers analyzed by qRT-PCR. n = 3-4 uninfected mice and n = 6-7 infected mice per genotype. Each symbol is a different mouse. All values are reported as mean ± SEM. Statistical analyses, where shown; *$P<0.05$ and **$P<0.01$ determined by 1-way ANOVA with Tukey post hoc test or Kruskal-Wallis test, followed by Mann-Whitney U tests.
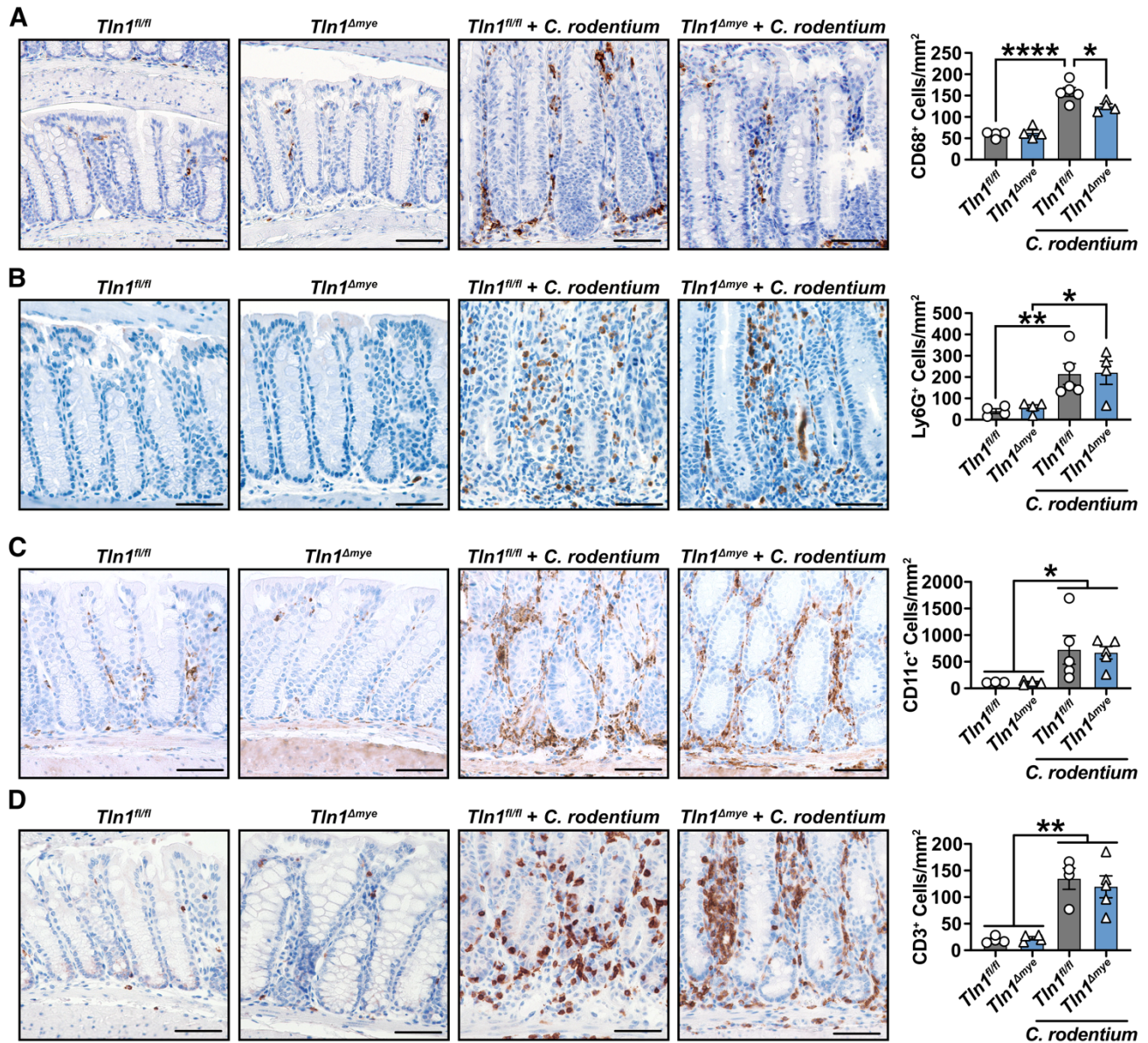
Figure 3.5. Myeloid cell talin-1 contributes to macrophage recruitment in response to infection. Representative immunohistochemistry images and the quantification of positive cells per mm^2 of colon tissues immunoperoxidase-stained for (**A**) CD68, (**B**) Ly6G, (**C**) CD11c, and (**D**) CD3. $n = 4$ uninfected mice and $n = 5$ infected mice per genotype. All values are reported as mean ± SEM. Statistical analyses, where shown; *$P<0.05$, **$P<0.01$, and ****$P<0.01$ determined by 1-way ANOVA and Tukey post hoc test. Scale bars represent 100 µm.

Loss of talin-1 does not have a cell-intrinsic effect on macrophage activation and function ex vivo

Thus far, we have demonstrated that $Tln1^{\Delta mye}$ mice exhibit decreased histologic injury and diminished recruitment of CD68^{+} macrophages during *C. rodentium* infection in vivo. Therefore, we wanted to evaluate whether talin-1 has a role in macrophage activation and function. Previously, it has been shown that *Tln1*-deficient dendritic cells express lower levels of proinflammatory genes when challenged with TLR agonists resulting in compromised immunity during skin infection.[167] BMmacs derived from $Tln1^{fl/fl}$ and $Tln1^{\Delta mye}$ mice displayed similar levels of induced *Tnf, Il1b*, *Il6*, and *Il23a* transcripts after infection with *C. rodentium* (Figure 3.6A). In addition, *Tln1*-deficient BMmacs retained the ability to produce nitric oxide (Figure 3.6B), a commonly used marker to evaluate the activation and polarization of inflammatory macrophages.[103,220] These data suggest that the decreased gene expression and inflammation that we observed in the tissues of $Tln1^{\Delta mye}$ mice during *C. rodentium* infection in vivo is not due to impaired macrophage activation.

Talin-1 has also been implicated in the phagocytic ability of macrophages; however, this is dependent on the integrin β-subunit and the target of the engulfment. Talin is dispensable for integrin β_5-mediated phagocytosis of apoptotic cells[233] while talin is required for the integrin β_2-mediated phagocytosis of C3bi-opsinized red blood cells.[234] We found that *Tln1*-deficient BMmacs engulfed the same number of *C. rodentium* as $Tln1^{fl/fl}$ BMmacs (Figure 3.6C), signifying that talin-1 is not required for the phagocytosis of *C. rodentium* by macrophages.

Macrophages have the dual responsibility of directly killing pathogens and acting as professional antigen presenting cells to activate and directs T cells.[58] Talin-1 has been shown to be involved in T cell activation in an antigen presenting cell contact-dependent manner through stabilization of the immune synapse.[235] To assess the role of talin-1 in the activation of macrophages in the context of antigen presentation, we measured the surface expression of MHCII and the co-stimulatory molecule, CD86. First, we confirmed that $Tln1^{fl/fl}$ and $Tln1^{\Delta mye}$ mouse-derived BMmacs expressed similar levels of CD11b, a β_2 integrin, and interestingly, *Tln1*-deficient BMmacs expressed higher levels of CD11b compared to $Tln1^{fl/fl}$ BMmacs with and without infection (Appendix B, Figure 1). The CD11b^{+} *Tln1*-deficient BMmacs also expressed significantly higher levels of CD86 (Figure 3.6D), but not MHCII (Figure 3.6E), compared to $Tln1^{fl/fl}$ BMmacs with infection. Collectively, our data demonstrate that loss of

macrophage talin-1 is protective in the *C. rodentium* model of infectious colitis through a non-cell-autonomous manner.

In summary, the results from this present study indicate that talin-1 within macrophages affects recruitment, but not activation in the context of pathogenic colitis. Our data indicate that the expression of talin-1 by macrophages contributes to *C. rodentium*-induced inflammation, with the increased number of colonic macrophages leading to more generation of inflammatory mediators, while failing to help eradicate the pathogen. These findings provide further insight into the development of bacterially-induced colitis and highlights a potential target to control macrophage movement into tissues that leads to the propagation of inflammation.
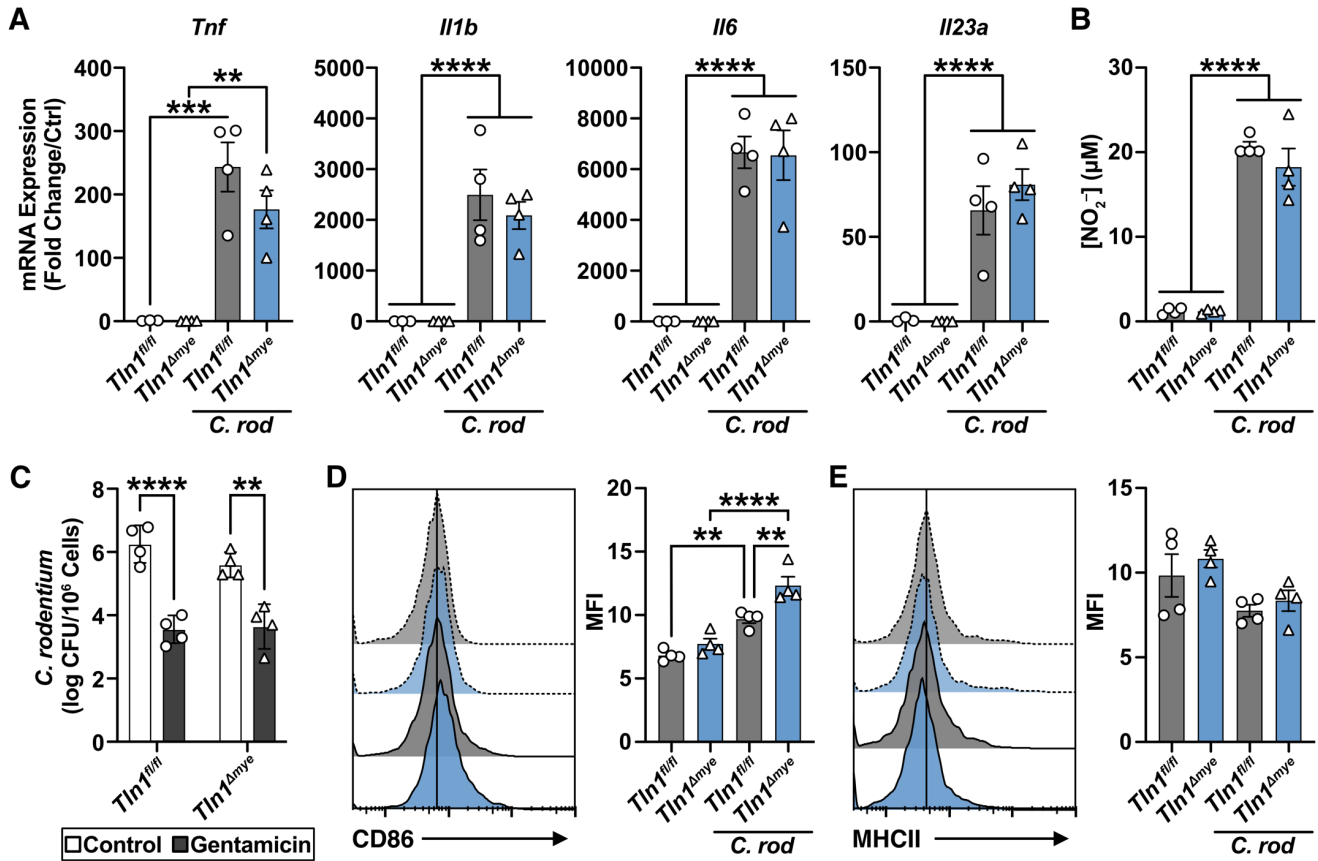
Figure 3.6. Talin-1 does not contribute to macrophage activation or phagocytic ability ex vivo. BMmacs derived from $Tln1^{fl/fl}$ and $Tln1^{\Delta mye}$ mice were infected or not with *C. rodentium*, $n=$ 3-4 mice per genotype. (**A**) Expression of proinflammatory macrophage markers at 6 h post-infection. (**B**) The concentration of NO_2^- in cell supernatants 24 h post-infection. (**C**) The amount of *C. rodentium* phagocytosed by $Tln1^{fl/fl}$ and $Tln1^{\Delta mye}$ BMmacs 1 h post-infection determined by gentamicin assay. (**D-E**) Representative flow plots and graphs depicting the surface expression and mean fluorescence intensity (MFI) of (**D**) CD86 and (**E**) MHCII on BMmacs 24 h post-infection. All values are reported as mean ± SEM. Statistical analyses, where shown; *$P<0.05$, **$P<0.01$, and ****$P<0.01$ determined by 1-way ANOVA and Tukey post hoc test.

CHAPTER 4

The Role of Talin-1 in the Colonic Epithelium During *C. rodentium* Infection

4.1 Abstract

Pathogenic enteric *Escherichia coli* present a significant burden to global health. Food-borne enteropathogenic *E. coli* (EPEC) and Shiga toxin-producing *E. coli* (STEC) utilize attaching and effacing (A/E) lesions and actin-dense pedestal formation to colonize the gastrointestinal tract. Talin-1 is a large structural protein that links the actin cytoskeleton to the extracellular matrix though direct influence on integrins. Here we show that mice lacking talin-1 in intestinal epithelial cells ($Tln1^{\Delta epi}$) have heightened susceptibility to colonic disease caused by the A/E murine pathogen *Citrobacter rodentium*. $Tln1^{\Delta epi}$ mice exhibit decreased survival, and increased colonization, colon weight, and histologic colitis compared to littermate $Tln1^{fl/fl}$ controls. These findings were associated with decreased actin polymerization and increased infiltration of innate myeloperoxidase-expressing immune cells, but more bacterial dissemination deep into colonic crypts. Further evaluation of the immune population recruited to the mucosa in response to *C. rodentium* revealed that loss of *Tln1* in colonic epithelial cells (CECs) results in impaired recruitment and activation of T cells. *C. rodentium* infection-induced colonic mucosal hyperplasia was exacerbated in $Tln1^{\Delta epi}$ mice compared to littermate controls. We demonstrate that this is associated with decreased CEC apoptosis and crowding of proliferating cells in the base of the glands. Taken together, talin-1 expression by CECs is important in the regulation of both epithelial renewal and the inflammatory T cell response in the setting of colitis caused by *C. rodentium*, suggesting that this protein functions in CECs to limit, rather than contribute to the pathogenesis of this enteric infection.

4.2 Introduction

The colonic epithelium plays a pivotal role in the delicate balance between gut homeostasis and disease. Colonic epithelial cells (CECs) line the lumen of the colon and provide the initial barrier between the microbiome and the

rest of the body.[236] *Escherichia coli,* a prominent member of the human colonic microbiota, usually maintains a commensal relationship with the host, however, enteropathogenic *E. coli* (EPEC) are leading causes of diarrheal-related deaths, especially in children and the elderly.[138,139] One mode of EPEC pathogenesis is through attaching and effacing (A/E) lesions, a strategy shared by other bacteria, such as Shiga toxin-producing *E. coli* (STEC) and the naturally occurring mouse-restricted pathogen, *Citrobacter rodentium.*[140,141] The virulence factors that induce A/E lesion formation are encoded by the locus of enterocyte effacement (LEE), which includes genes encoding for a type III secretion system (T3SS) secreted proteins, the adhesin intimin, and its receptor termed translocated intimin receptor (Tir).[140–142] The formation of pedestal-like structures underneath the intimately adhered bacteria are composed of the bacterial translocated effectors and the recruited host cytoskeletal and focal adhesion proteins α-actinin, vinculin, and talin-1.[142,143]

Talin-1, encoded by the gene *Tln1*, is a ubiquitously expressed mechanosensory scaffold protein that was first discovered in chicken gizzards.[149,150] The homo-dimeric talin-1 molecule is comprised of two subunits; a 50-kDa N-terminal head containing a FERM domain and a 220-kDa C-terminal rod lined with helical bundles that provide multiple binding sites for actin and vinculin.[150,154,155] The family of proteins that possess a FERM domain are often associated with protein-protein interactions that link the cytoskeleton to transmembrane receptors.[156] The head of talin-1 has been shown to bind to the cytoplasmic domain of the β-subunit of integrins and facilitates a conformational change to the extracellular domain that increases integrin binding affinity.[150,157] The tail of talin-1 tethers to F-actin and through inside-out signaling, promotes focal adhesion assembly and increases forces exerted on the extracellular matrix (ECM).[159–163]

Increasing evidence suggests that talin-1 is essential for A/E lesion pedestal formation and actin polymerization.[237,238] We have recently shown that suppression of talin-1 expression in vitro results in decreased actin rearrangement in immortalized young adult mouse colon (YAMC) cells.[239] Therefore, our aim in this study was to determine the role of talin-1 in CECs during pathogenic enteric bacterial infection in vivo. Cell-specific knockdown of *Tln1* in intestinal epithelial cells in mice resulted in increased *C. rodentium* colonization with increased depth of infection in the colonic epithelial glands, associated with decreased actin condensation, enhanced

neutrophil infiltration, and impaired T cell response, together resulting in increased clinical and histologic evidence of colitis. In addition, we demonstrate that genetic loss of *Tln1* contributes to colonic crypt hyperplasia. This effect was associated with reduced apoptosis of surface CECs and reduced proliferation along the upper zone of the crypts. Taken together, these findings implicate talin-1 as a regulator of CEC response and T cell recruitment during infectious colitis that restricts *C. rodentium* pathogenesis.

4.3 Materials and Methods

Mice. C57BL/6 *Tln1$^{fl/fl}$* mice were generated by Petrich *et al.* and provided to us by Dr. Roy Zent at Vanderbilt University Medical Center (Nashville, TN).[217,240] The *Tln1$^{fl/fl}$* mice were then crossed with C57BL/6 *Vil1$^{cre/+}$* mice and the resulting offspring were backcrossed to *Tln1$^{fl/fl}$* mice to generate *Tln1$^{fl/fl}$*;*Vil1$^{+/+}$* and *Tln1$^{fl/fl}$*;*Vil1$^{cre/+}$* (*Tln1$^{\Delta epi}$*) mice.[241] The mouse colony was maintained and housed in a specific-pathogen free facility with ventilated cage racks and a 12h/12h light/dark cycle. Mice were fed *ad libitum* with 5L0D chow (LabDiet) and provided continuous water. All experiments were approved IACUC at Vanderbilt University and Institutional Biosafety Committee and the Research and Development Committee of the Veterans Affairs Tennessee Valley Healthcare System under the protocol V2000018. Procedures were performed in accordance with institutional policies, AAALAC guidelines, the American Veterinary Medical Association Guidelines on Euthanasia, NIH regulations (Guide for the Care and Use of Laboratory Animals; National Academies Press, 2011), and the US Animal Welfare Act (1966).

Isolation of Colonic Epithelial Cells. Epithelial cells were isolated from the colonic mucosa as previously described.[239,242] Briefly, colons were excised, cut longitudinally, washed with PBS, cut into 2 mm pieces, placed in dissociation buffer containing 3 mM DTT and 0.5 mM EDTA, and incubated on ice for one hour. The pieces were then vigorously shaken in PBS and the cells were passed through a 70 μm cell strainer.

mRNA Analysis. Total RNA was isolated from CECs and colonic tissues using the RNeasy Mini Kit (QIAGEN), according to the manufacturer's instructions. Equal amounts of total RNA were reverse transcribed into cDNA using the SuperScript III Reverse Transcriptase (Thermo Fisher), Oligo (dT) primers (Thermo Fisher), and dNTP Mix (Applied Biosystems). Quantitative real-time PCR was performed using the PowerUp SYBR Green Master Mix (Applied Biosystems) and the primers listed in Table 4.1.

Table 4.1: List of qRT-PCR primers used for Chapter 4.

Target gene	Sequence (5'-3')
Tln1	F: GGCCCTCCCAACGACTTT
	R: AGCCTCTAGCCAGATGCCTTT
Ccl5	F: GGCCATCAGCAACAACATAAGCGT
	R: ACACACTTGGCGGTTCCT
Ccl20	F: CGACTGTTGCCTCTCGTACA
	R: AGGAGGTTCACAGCCCTTTT
Ifng	F: GGCCATCAGCAACAACATAAGCGT
	R: TGGGTTGTTGACCTCAAACTTGGC
Il17a	F: ATCCCTCAAAGCTCAGCGTGTC
	R: GGGTCTTCATTGCGGTGGAGAG
Il22	F: TTGAGGTGTCCAACTTCCAGCA
	R: AGCCGGACGTCTGTGTTGTTA
Tnf	F: CTGTGAAGGGAATGGGTGTT
	R: GGTCACTGTCCCAGCATCTT
Actb	F: CCAGAGCAAGAGAGGTATCC
	R: CTGTGGTGGTGAAGCTGTAG

Western Blot and Densitometric Analysis. Isolated CECs or colonic tissues were lysed using ice cold CellLytic MT Reagent (Sigma-Aldrich) supplemented with the Protease Inhibitor Cocktail (Set III, Calbiochem) and the Phosphatase Inhibitor Cocktail (Set I, Calbiochem). The BCA Protein Assay (Pierce) was used to measure total protein concentrations. Proteins were separated by SDS-PAGE on a 4-20% gel, transferred to nitrocellulose membranes, and blocked with 5% w/v milk in TBS with 0.1% Tween-20 for 1 h. Membranes were incubated with

a rabbit anti-Talin-1 mAb (Cell Signaling, C45F1; 1:2000) overnight at 4°C in 5% w/v BSA in TBS with 0.1% Tween-20 (based on the manufacturer's recommendations) or a mouse anti-β-actin mAb (Sigma, A1978; 1:10000) in 5% w/v milk in TBS with 0.1% Tween-20 for 30 min at room temperature. Protein bands were visualized by incubating the membrane with HRP-labeled goat anti-rabbit IgG (Jackson ImmunoResearch, 111-035-003; 1:5000) or HRP-labeled goat anti-mouse IgG (Promega, W402B; 1:20000), respectively, and using SuperSignal West Pico PLUS Chemiluminescent Substrate (Pierce) and HyBlot CL Autoradiography Film (labForce). Densitometric analysis of Western blots was performed with Fiji (ImageJ).[200]

***C. rodentium* Colitis.** *C. rodentium* strain DBS100 was cultured overnight in Luria-Bertani (LB) broth shaking at 37° C. Adult male *Tln1$^{fl/fl}$* and *Tln1$^{\Delta epi}$* littermates (6-12 wk) are inoculated by oral gavage with 5x10^8 *C. rodentium* in 0.2 mL LB broth.[216,239,243] Control mice received 0.2 mL of sterile LB broth alone. Mice were weighed and monitored daily and animals that showed signs of distress, lost more than 20% of initial body weight, or became moribund were euthanized. At 14 days post-inoculation, mice were sacrificed, and the colons were removed, measured, cleaned, weighed, and Swiss-rolled for fixation in 10% neutral buffered formalin and subsequent histology. Three proximal and distal pieces were collected prior to fixation. Two pieces were flash frozen for RNA and protein isolation and analysis and the third was used to determine bacterial colonization by counting the colony forming units (CFUs) after plating serial dilutions of homogenized tissue on McConkey agar plates. *C. rodentium* colonization of the spleen was determined as above.

Immunofluorescence. Immunofluorescent staining for *C. rodentium* was performed on paraffin-embedded Swiss-rolled murine colon tissues using the following antibodies: rabbit polyclonal anti-*C. koseri*, (cross-reacts with *C. rodentium*) (Abcam; 1:50), and Alexa Fluor 488-labeled goat anti-rabbit IgG (1:400; Life Technologies) or Alexa Fluor 555-labeled goat anti-rabbit IgG (1:400; Life Technologies) and pseudo-colored green during imaging.[239] Slides were washed, dried, and mounted using VECTASHIELD HardSet™ Antifade Mounting Medium with DAPI

(Fisher Scientific). Fluorescently stained slides were imaged using a Cytation C10 Confocal Imaging Reader and Gen 5+ software (Agilent BioTek).

FAS Test. Phalloidin CF488A (Biotium; 1:50) was included in the secondary antibody incubation step of *C. rodentium* immunofluorescence staining and pseudo-colored white during imaging.

Histologic Score. Paraffin-embedded Swiss-rolled colons were sectioned (5 μm), stained with hematoxylin (H&E), and examined in a blinded manner by a gastrointestinal pathologist (MBP). The histologic injury score (0–21) is the combination of epithelial injury score (0–3) plus total inflammation (0-18), which is the extent of inflammation (0-3) multiplied by the sum of acute and chronic inflammation (0–3 for each) scores multiplied by extent of inflammation (0–3) as described. [239]

Immunohistochemistry and Analysis. Immunoperoxidase staining for Ki-67, myeloperoxidase (MPO), CD3, and cleaved caspase-3 were performed on paraffin-embedded Swiss-rolled murine colon tissues. Sections were deparaffinized, antigens retrieved with citrate buffer, and quenched with H_2O_2. Tissues were then incubated overnight at 4° C using the following antibodies: prediluted rabbit polyclonal anti-Ki-67 (Biocare, PRM325AA), prediluted rabbit monoclonal anti-MPO (Biocare, PP023AA), rabbit polyclonal anti-CD3 (Abcam, ab5690; 1:150), or rabbit monoclonal anti-cleaved caspase-3 (Cell Signaling, 9664; 1:400). Primary antibodies were detected with anti-rabbit HRP Polymer (DAKO), color was developed using 3,3′-diaminobenzidine (DAB+), and tissues were counterstained by hematoxylin. All slides were imaged and analyzed using a Cytation C10 Confocal Imaging Reader and Gen 5+ software (Agilent BioTek). Crypt length and the proportion of the crypt that contained Ki-67 positive nuclei were determined by measuring the distance from the base of the crypt to the luminal surface and the last positive nuclei from 3 mid-powered fields, respectively. The average number of CD3-positive cells was quantified by the Cell Analysis function of the Gen 5+ software (Agilent BioTek) and was limited to the mucosa to reduce inclusion of non-specific staining. The proportion of apoptotic mucosa per 5 high-powered fields was

quantified by measuring the total height of the mucosa and the height of the region containing positive cleaved caspase-3 staining.

The average number of MPO-positive cells per 5 high-powered fields was quantified by a gastrointestinal pathologist (MBP) in a blinded manner.

Generation of Colonoids. Colons were extracted from $Tln1^{fl/fl}$ and $Tln1^{\Delta epi}$ mice, washed with PBS, cut into 5-6 pieces, and incubated in chelating buffer (10 mM EDTA in PBS) at 4° C for 30 min while rocking. The tissues were then vigorously shaken in fresh dissociation buffer (1% w/v D-sorbitol and 1.5% w/v sucrose in PBS) and repeated until a clean fraction of crypts was obtained. The isolated crypts were embedded in Matrigel matrix (Corning, 356231) and maintained in 50% L-WRN conditioned media with 100 U/ml penicillin/streptomycin, 10 µg/ml Gentamicin (Gibco), 10 µM Y27632 (Tocris, 1254), and 10 µM SB431542 (Tocris, 12614). Gentamicin and Y27632 are not included after the first passage.

Statistics. All the data shown represent the mean ± SEM unless otherwise noted. GraphPad Prism 9.4 (GraphPad Software) was used to perform statistical analyses and significance was set at $P < 0.05$. For normally distributed data, a 2-tailed Student's t test or a 1-way ANOVA with the Tukey or Šídák's post hoc test were performed to compare differences between two or more test groups, respectively. Non-normally distributed data was analyzed by a 1-way ANOVA with the Kruskal-Wallis test, followed by a Mann-Whitney U test, unless otherwise noted. The Log-rank (Mantel-Cox) test was used to assess differences between the Kaplan-Meier curves of survival. Differences in daily body weights were analyzed by a 2-way ANOVA and Tukey post hoc test.

4.4 Results

$Tln1^{\Delta epi}$ mice have increased susceptibility to *C. rodentium* infection.

Talin-1 has been implicated in the formation of attaching and effacing lesions in response to EPEC and *C. rodentium*, but this has not been directly studied in vivo.[238,239] To evaluate the role of talin-1 in epithelial cells during

pathogenic colitis, we used $Tln1^{\Delta epi}$ and littermate control $Tln1^{fl/fl}$ mice.[240,241] We first confirmed knockdown of $Tln1$ mRNA (Figure 4.1a) and talin-1 protein expression in isolated CECs (Figure 4.1, b and c). Next, we inoculated $Tln1^{\Delta epi}$ mice and their $Tln1^{fl/fl}$ littermate controls via oral gavage of $5x10^8$ CFUs of *C. rodentium* for 14 days, as we described.[216,239,243] $Tln1^{\Delta epi}$ mice were more susceptible to *C. rodentium*-induced disease, exhibiting decreased survival (Figure 4.1d) and increased body weight loss (Figure 4.1e) compared to infected $Tln1^{fl/fl}$ mice. $Tln1$ mRNA and talin-1 protein levels remained significantly reduced in whole tissues of $Tln1^{\Delta epi}$ mice with and without infection (Figure 4.1, f-h).
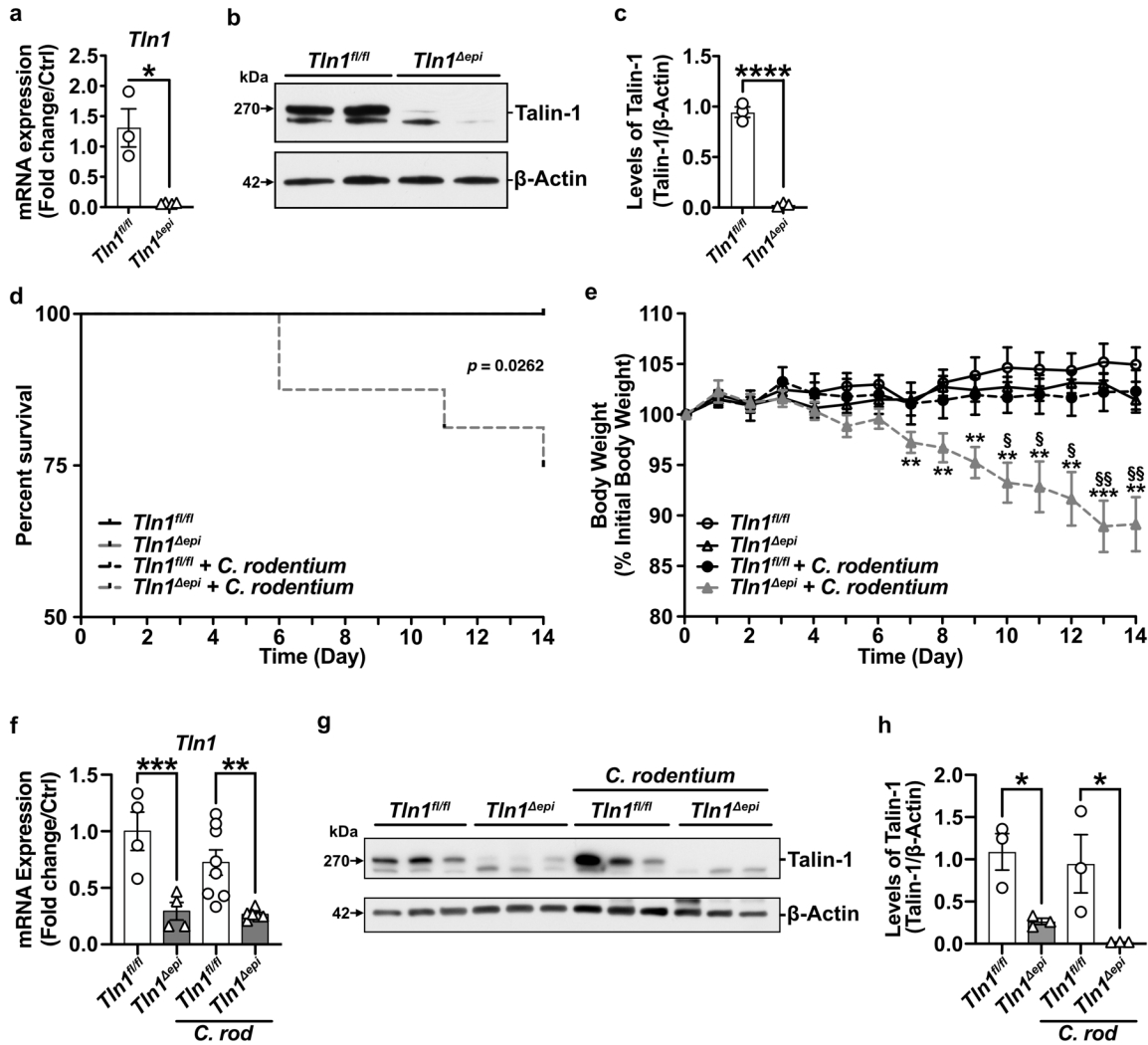
Figure 4.1. Epithelial-specific deficiency of talin-1 enhances susceptibility to *C. rodentium*-induced death and weight loss. (a-c) Colonic epithelial cells were isolated from *Tln1^fl/fl* and *Tln1^Δepi* mice. (a) *Tln1* mRNA expression was determined by RT-qPCR; n = 3-4 per genotype. (b) Representative Western blot of talin-1 protein (270 kDa) expression. (c) Densitometry analysis of talin-1 protein expression; n = 3 mice per group. (d-f) *Tln1^fl/fl* and *Tln1^Δepi* mice were infected with 5×10^8 CFU of *C. rodentium* by oral gavage and monitored daily for 14 days; n = 8-9 uninfected mice and n = 12-15 infected mice per genotype. Data pooled from 2 independent experiments. (d) Kaplan-Meier curves of uninfected and infected mice. (e) Daily body weights depicted as percent of initial body weight. (f) *Tln1* mRNA expression in whole colon tissues determined by RT-qPCR; n = 4 uninfected mice and n = 6-8 infected mice per genotype. (g) Western blot of talin-1 protein (270 kDa) and (h) densitometry analysis; n = 3 mice per group. All values are reported as mean ± SEM. Statistical analyses, where shown; *$P<0.05$, **$P<0.01$, ***$P<0.001$, and ****$P<0.0001$ determined by (a and c) Student's *t* test, (d) Log-rank (Mantel-Cox) test, (e) 2-way ANOVA and Tukey test, $^§P < 0.05$ and $^{§§}P < 0.01$ compared to infected *Tln1^fl/fl* littermate controls, (f and h) 1-way ANOVA and Šídák's test compared to *Tln1^fl/fl*.

Epithelial talin-1 contributes to pathogen containment by facilitating actin rearrangement and attachment of *C. rodentium* to the epithelium.

It has been suggested that talin-1, a focal adhesion molecule, is necessary for the binding of A/E pathogens and we have reported that diminution of *Tln1* mRNA transcripts results in decreased intimate attachment of *C. rodentium* to colonic epithelial cells in vitro.[143,238,239] Therefore, we assessed the burden and localization of *C. rodentium* in *Tln1^fl/fl* and *Tln1^Δepi* mice infected for 14 days. Mice with epithelial deletion of *Tln1* exhibited a 1.6 log-order increase of *C. rodentium* CFU per gram of colon tissue (Figure 4.2a). To determine whether the increase in *C. rodentium* colonization in the colon led to increased bacterial dissemination to other organs, we harvested the spleens and assessed viable bacteria. There was no difference between bacterial burden in the spleens of infected *Tln1^Δepi* mice compared to *Tln1^fl/fl* mice (Figure 4.2b). This suggests that epithelial loss of talin-1 does not decrease gut barrier function. Immunofluorescence and confocal microscopy revealed that in *Tln1^fl/fl* mice, *C. rodentium* was restricted to the apical surface that lines the colon lumen (Figure 4.2c). In contrast, in mice deficient in epithelial talin-1, *C. rodentium* extended along the epithelial cells that line the sides of the crypts and into the base (Figure 4.2c). *C. rodentium*-induced actin polymerization, visualized using fluorescence actin staining (FAS) and confocal microscopy, was decreased in *Tln1*-deficient epithelial cells (Figure 4.2d). In addition, detachment of numerous *C. rodentium*-bound epithelial cells was apparent in *Tln1^fl/fl* mice and this was abolished in the *Tln1^Δepi* mice (Figure 4.2d) suggesting that talin-1 is essential for cytoskeletal polymerization and subsequent shedding of compromised epithelial cells.
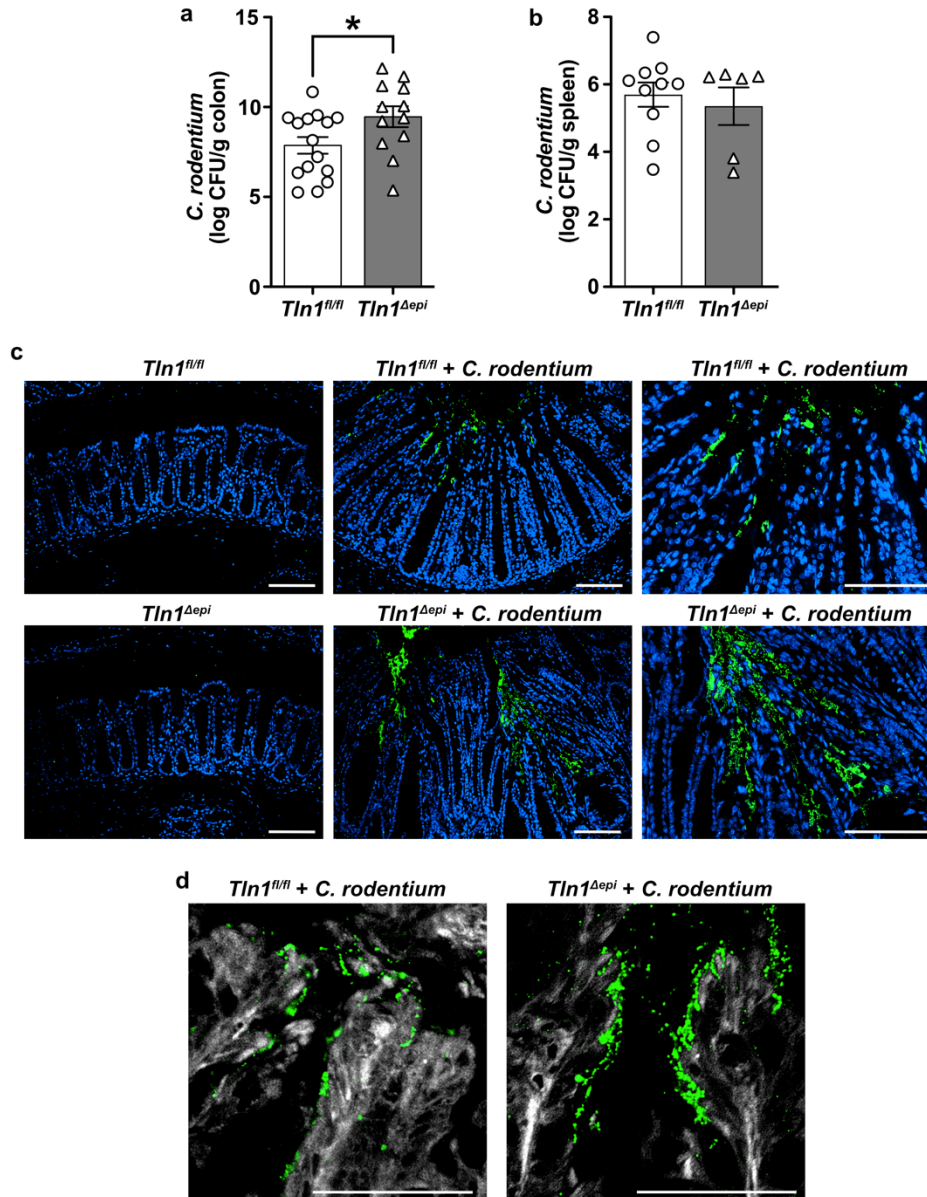
Figure 4.2. Epithelial-specific talin-1 contributes to pathogen containment by facilitating actin rearrangement and attachment of *C. rodentium* to the epithelium. (a-b) Bacterial burden was assessed by culturing serial dilutions of homogenized tissues and normalizing to tissue weight on day 14 post-infection (p.i.). (a) *C. rodentium* colonization of the colon; $n = 15$ infected *Tln1^{fl/fl}* mice and $n = 12$ infected *Tln1^{Δepi}* mice. Data pooled from 2 independent experiments. *$P < 0.05$ determined by Student's *t* test. (b) *C. rodentium* colonization of the spleen, $n = 10$ infected *Tln1^{fl/fl}* mice and $n = 6$ infected *Tln1^{Δepi}* mice. (c) Representative immunofluorescence images of *C. rodentium* (green) and DAPI (blue) in colon tissues of uninfected and infected mice; $n = 4$ mice per group. (d) Representative images of fluorescence actin staining (FAS, white) co-stained with *C. rodentium* (green) in colon tissues of uninfected and infected mice; $n = 4$ mice per group. All values are reported as mean ± SEM. Statistical analyses, where shown; *$P<0.05$ determined by Student's *t* test. (c-d) Scale bars represent 100 μm.

Talin-1 moderates *C. rodentium*-induced colitis.

Animals lacking epithelial *Tln1* exhibited enhanced immune cell infiltration and hyperplasia (Figure 4.3a), which led to significantly increased histologic injury scores (Figure 4.3b) compared to *Tln1$^{fl/fl}$* littermate controls infected with *C. rodentium*. The histologic injury score is a composite of the epithelial damage and total inflammation (Figure 4.3c). While there was exacerbated hyperplasia of the colonic glands (Figure 4.3c), there was no difference in the score for epithelial damage between infected *Tln1$^{fl/fl}$* and *Tln1$^{\Delta epi}$* mice, and the increased histologic injury score was driven by a significant increase in total inflammation (Figure 4.3c). Consistent with the increase in inflammation, the colon weight to length ratio was higher in infected animals and significantly increased in *Tln1$^{\Delta epi}$* mice compared to *Tln1$^{fl/fl}$* littermate controls (Figure 4.3d).
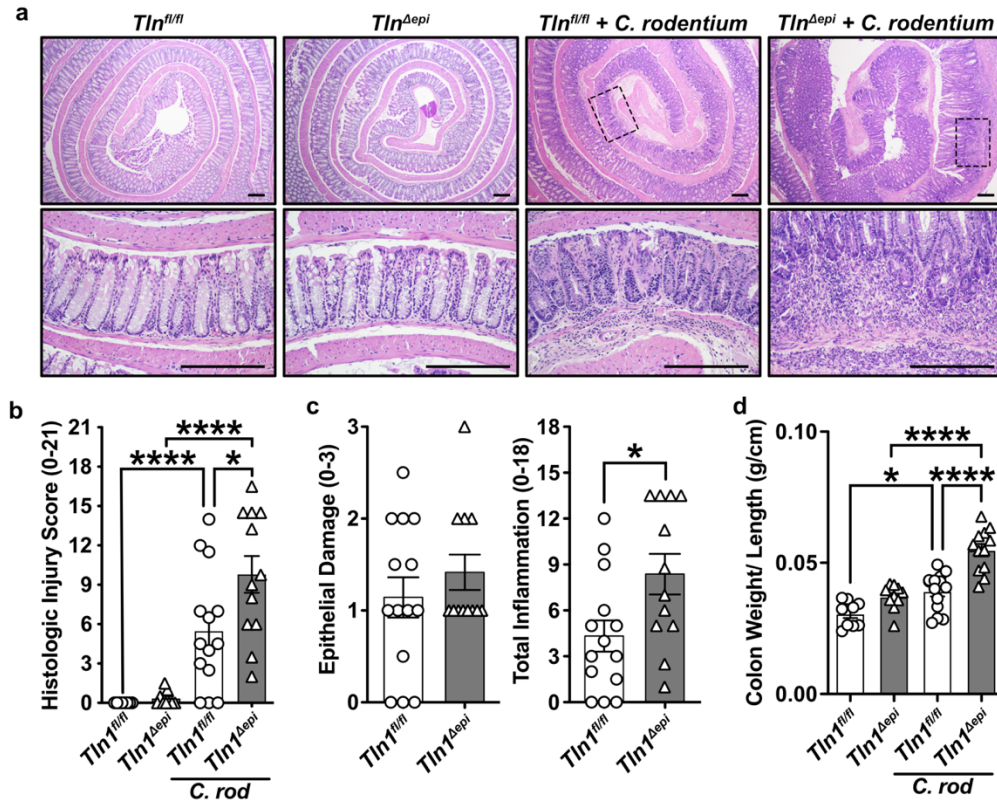
Figure 4.3. Talin-1 moderates *C. rodentium*-induced acute inflammation. *Tln1^{fl/fl}* and *Tln1^{Δepi}* mice were infected with $5x10^8$ CFU of *C. rodentium* by oral gavage for 14 days. Data pooled from 2 independent experiments. (a) Representative H&E images of the Swiss-rolled colon tissues from uninfected and infected mice. (b) Histologic injury scores derived from the H&E-stained tissues; *n* = 8-9 uninfected mice and *n* = 12-15 infected mice per genotype. (c) Epithelial damage scores and total inflammation scores that were used to generate the histologic injury score in *b*. (d) Colon weight as a proportion of body weight on day 14 post-inoculation. Each symbol is a different mouse. All values are reported as mean ± SEM. Statistical analyses, where shown; *$P<0.05$, **$P<0.01$, and ****$P<0.0001$ determine by (b and d) 1-way ANOVA with Tukey test; (c) Student's *t* test. (a) Scale bars represent 200 μm.

Knockdown of talin-1 in epithelial cells heightens neutrophil recruitment but diminishes the T cell response to pathogenic bacteria.

To further evaluate the differences in the inflammatory response between *Tln1^{fl/fl}* and *Tln1^{Δepi}* mice, we assessed the immune cell populations by immunohistochemistry. Colon tissues were immunostained for MPO-expressing neutrophils and monocytic cells (Figure 4.4a). The number of MPO-positive cells was significantly increased in infected *Tln1^{Δepi}* mice compared to uninfected *Tln1^{Δepi}* mice and infected *Tln1^{fl/fl}* mice (Figure 4.4b).

85

In contrast, the elevated number of CD3$^+$ cells in the mucosa of infected $Tln1^{fl/fl}$ mice was significantly reduced in the tissues of infected $Tln1^{\Delta epi}$ mice (Figure 4.5, a and b). Concomitantly, mRNA expression of T cell-attracting chemokines *Ccl5* and *Ccl20* was induced in $Tln1^{fl/fl}$ mice with infection and was diminished in infected $Tln1^{\Delta epi}$ mice (Figure 4.5c). Additionally, the tissues of $Tln1^{\Delta epi}$ mice expressed significantly reduced levels of the transcripts coding for the Th1 marker interferon (IFN)-γ and the Th17 markers IL-17 and IL-22 (Figure 4.5d). Thus, these data suggest that the role of talin-1 within epithelial cells includes recruitment and activation of T cells, such that when *Tln1* is deleted, there is loss of host defense associated with activated T cells.
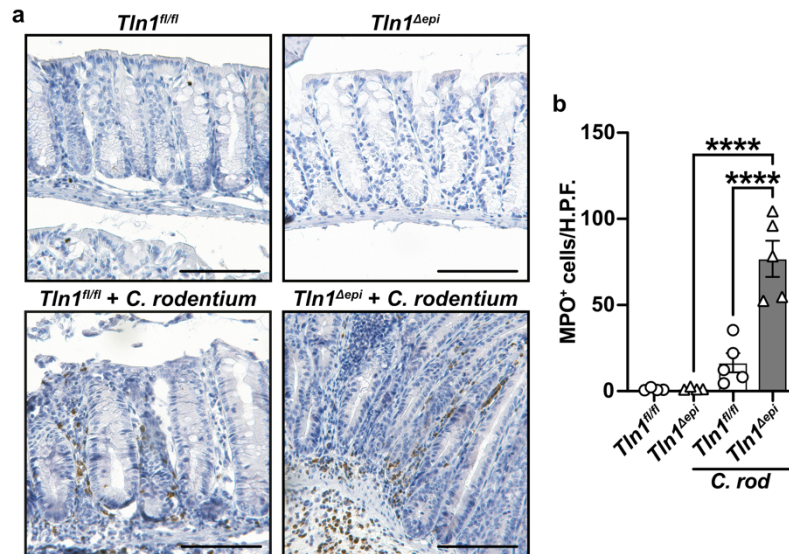
Figure 4.4. Knockdown of talin-1 in epithelial cells heightens neutrophil recruitment but diminishes the T cell response to pathogenic bacteria. (a) Representative images of colon tissues immunoperoxidase-stained for MPO and (b) the quantification of MPO$^+$ cells per high-powered field (H.P.F.). $n = 4$ uninfected mice and $n = 5$ infected mice per genotype. Each symbol is a different mouse. All values are reported as mean ± SEM. Statistical analyses, where shown; **$P<0.01$ and ****$P<0.0001$ determined by 1-way ANOVA and Tukey test. Scale bars represent 100 μm.
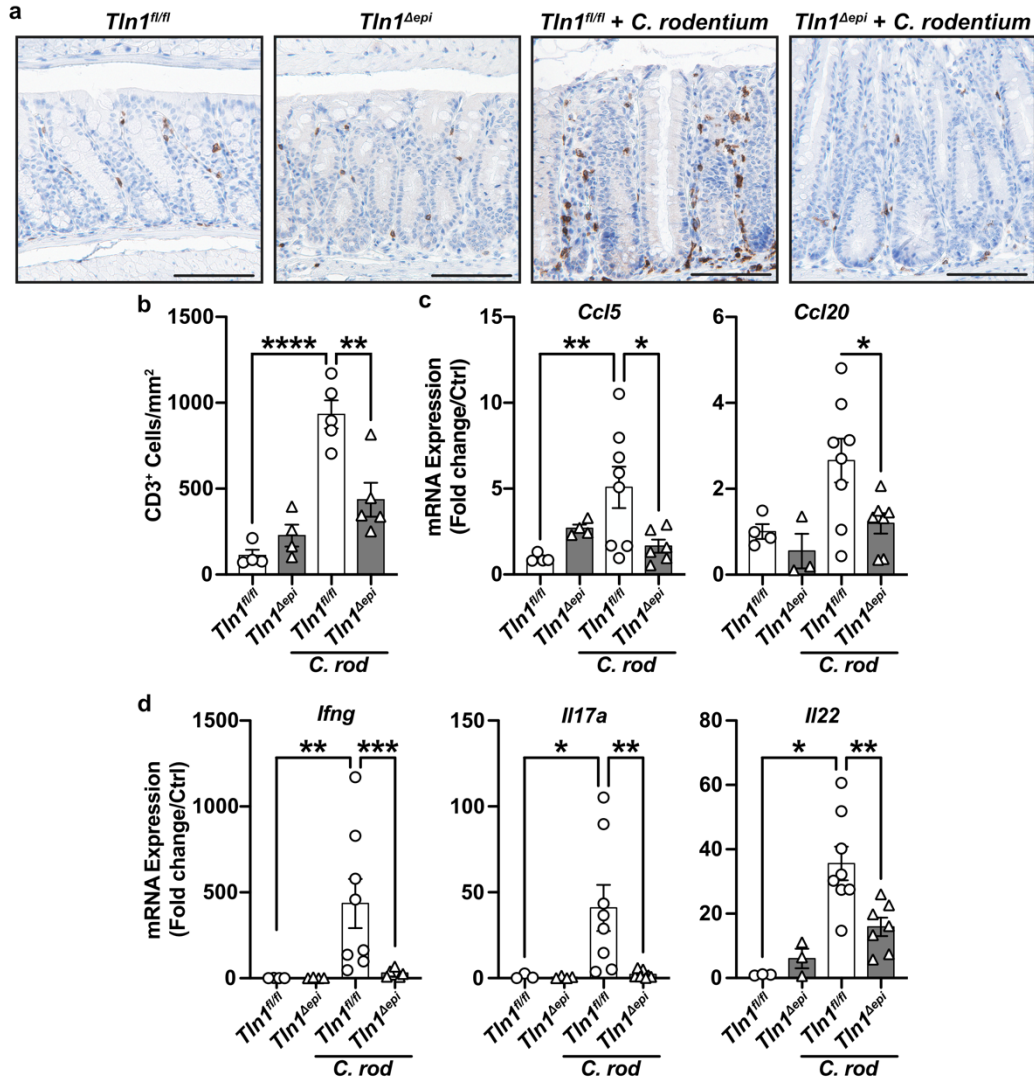
Figure 4.5. Knockdown of talin-1 in epithelial cells reduces T cell infiltration and activation in the colonic mucosa. (a) Representative images of colon tissues immunoperoxidase-stained for CD3 and (b) the quantification of CD3$^+$ cells per mm^2. $n = 4$ uninfected mice and $n = 5$ infected mice per genotype. (c) mRNA expression of T cell chemokines analyzed by RT-qPCR. (d) mRNA expression of markers of T cell activation analyzed by RT-qPCR. (c and d) $n = 4$ uninfected mice and $n = 8$ infected mice per genotype. Each symbol is a different mouse. All values are reported as mean ± SEM. Statistical analyses, where shown; **$P<0.01$ and ****$P<0.0001$ determined by (b) 1-way ANOVA and Tukey test and (c-d) 1-way ANOVA with Kruskal-Wallis test, followed by a Mann-Whitney U test. Scale bars represent 100 μm.

Loss of epithelial-specific talin-1 enhances pathogen-induced colonic hyperplasia and suppresses epithelial apoptosis.

A hallmark of *C. rodentium* infection is crypt hyperplasia, which is characterized by rapid turnover of the epithelial cells lining the crypts and thickening of the colonic mucosa.[141,222] Therefore, we assessed cellular proliferation in the colonic mucosa of *Tln1fl/fl* and *Tln1Δepi* mice by immunostaining for Ki-67. *C. rodentium* induced increased Ki-67 expression in both *Tln1fl/fl* and *Tln1Δepi* mice when compared to uninfected control mice (Figure 4.6a). In the infected *Tln1fl/fl* mice, the proliferating cells extended from the base of the crypt to the luminal surface while in the *Tln1Δepi* mice, the positive nuclei did not extend to the lumen and crowded at the base of the crypt (Figure 4.6a). Infected *Tln1fl/fl* and *Tln1Δepi* mice had significantly longer crypts compared to uninfected controls and the crypts were further elongated in the infected *Tln1Δepi* mice (Figure 4.6b). Consistent with the photomicrographs of Figure 6a, image analysis confirmed that the proportion of the crypt length in which the Ki-67$^+$ cells extended was significantly reduced in infected *Tln1Δepi* mice (Figure 4.6c).

To determine the fate of the mature epithelial cells, we assessed apoptosis by immunostaining for cleaved caspase-3. Uninfected mice from each genotype displayed a baseline level of apoptosis that encompassed a single layer of luminal surface cells, which was then increased in *C. rodentium*-infected *Tln1fl/fl* mice (Figure 4.7a). This increase was absent in the *Tln1Δepi* mice with infection (Figure 4.7a), quantified as the proportion of the mucosa containing apoptotic cleaved caspase-3-positive cells (Figure 4.7b). The mRNA expression of the gene encoding TNF-α, a stimuli of apoptotic cell shedding, was significantly reduced in infected *Tln1Δepi* mice compared to infected *Tln1fl/fl* mice (Figure 4.7c).[244] These data along with the decrease in actin polymerization and shedding of *C. rodentium*-bound cells suggest that talin-1 is important for epithelial cell movement and regeneration in response to challenge, and that this activity is protective during infection.
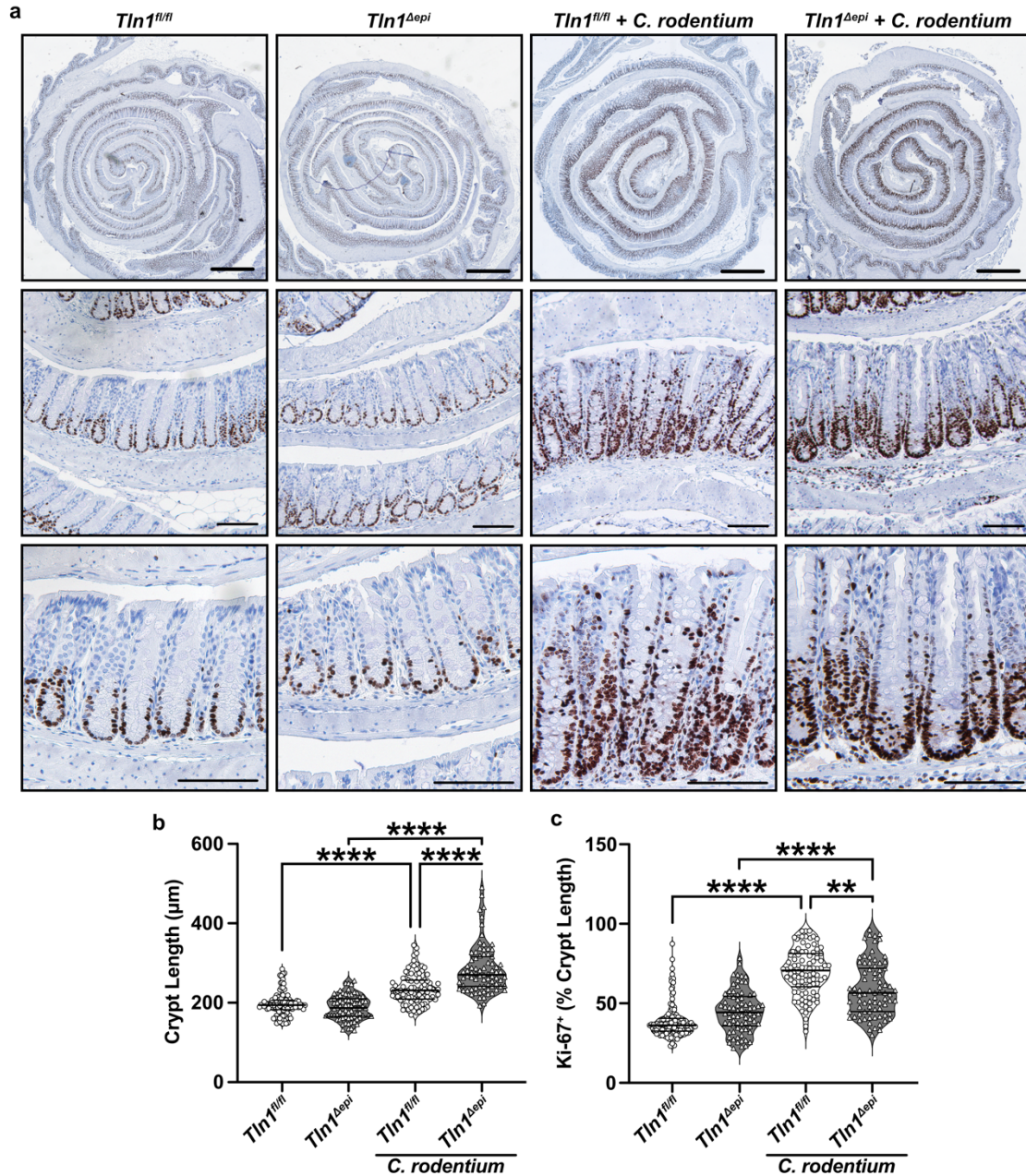
Figure 4.6. Loss of epithelial-specific talin-1 enhances pathogen-induced colonic hyperplasia. (a) Representative images of colon tissues immunoperoxidase-stained for Ki-67. $n = 4$ uninfected mice and $n = 4$-5 infected mice per genotype. (b) Colonic crypt length. Each dot represents an individual crypt that was visible from base to opening; $n = 70$-107 crypts counted from 4 different mice per group. (c) The proportion of the individual crypts that contained Ki-67^{+} nuclei determined by measuring from the base of the crypt to the last positive nuclei. All values reported with the median depicted as a thick line and the upper and lower quartiles as thin lines. Statistical analyses, where shown; **$P<0.01$ and ****$P<0.0001$ determined by 1-way ANOVA and Kruskal-Wallis test. Thick scale bars represent 1000 μm and thin scale bars represent 100 μm.
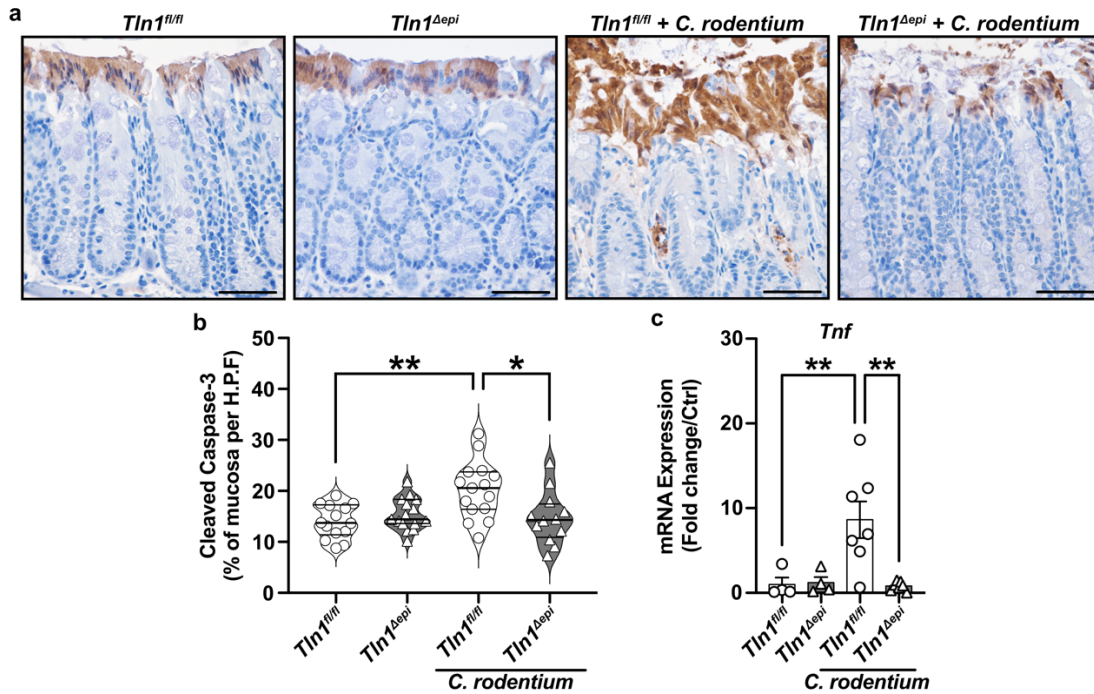
Figure 4.7. Loss of epithelial-specific talin-1 suppresses pathogen-induced epithelial apoptosis. (a) Representative images of colon tissues immunoperoxidase-stained for cleaved caspase-3. (b) The proportion of cleaved caspase-3-positive mucosa determined by measuring the total height of the mucosa and the height of the region with positive staining. Each dot represents measurements from a high-powered field; n = 12-15 fields from 3 different mice per group. All values reported with the median depicted as a thick line and the upper and lower quartiles as thin lines. (c) Expression of the gene encoding TNF-α analyzed by RT-qPCR. n = 4 uninfected mice and n = 6-7 infected mice per genotype. Each symbol is a different mouse. Values are reported as mean ± SEM. *$P<0.05$ and **$P<0.01$ determined by (b) 1-way ANOVA and Tukey test and (c) 1-way ANOVA with Kruskal-Wallis test, followed by a Mann-Whitney U test. Scale bars represent 100 μm.

Epithelial talin-1 deficiency inhibits epithelial cell mobility.

To assess epithelial motility, we generated 3D organoids (colonoids) from colonic crypts isolated from *Tln1^{fl/fl}* and *Tln1^{Δepi}* mice. The colonoids were cultured for 3 days and then passaged and followed daily. The morphology of the *Tln1^{fl/fl}* and *Tln1^{Δepi}* colonoids appeared comparable prior to passage (Figure 4.8). Post-passage, the colonoids from *Tln1^{fl/fl}* mice formed irregular structures and buds that protruded into the extracellular growth matrix over time (Figure 4.8). Conversely, the colonoids derived from *Tln1^{Δepi}* mice maintained a uniform spherical shape with minimal to no budding structures and less overall growth (Figure 4.8).
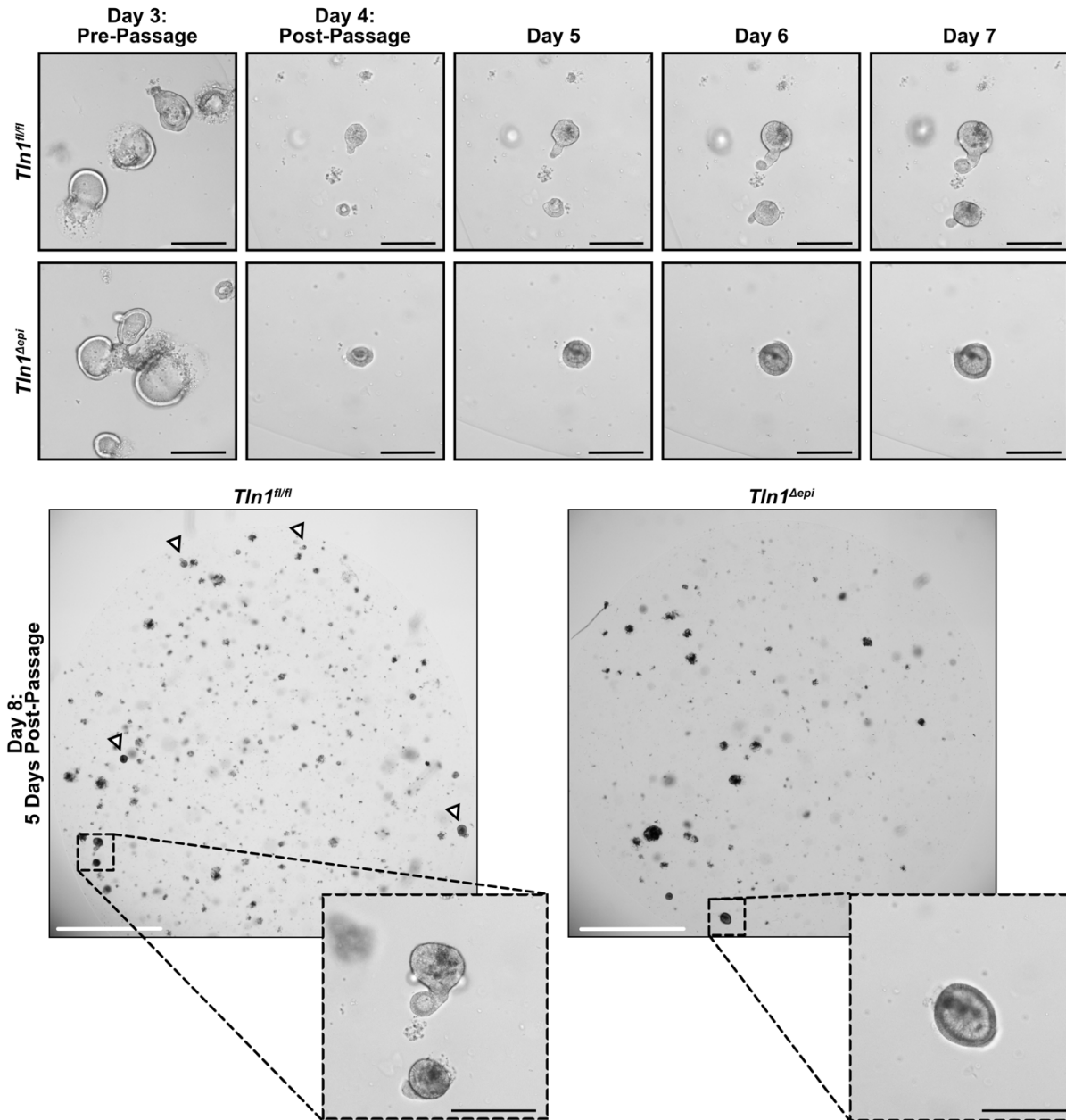
90

Figure 4.8. Epithelial talin-1 deficiency inhibits epithelial cell mobility in vitro. Representative images of colon organoids (colonoids) generated from crypts isolated from *Tln1^fl/fl^* and *Tln1^Δepi^* mice and imaged daily for 8 days; *n* = 3 mice per genotype. Arrowheads highlight colonoids with budding. White scale bars represent 2000 μm and black scale bars represent 100 μm.

4.5 Discussion

Talin-1 provides a two-way bridge between the extracellular environment and intracellular networks. Through inside-out signaling, talin-1 induces a conformational change to the integrin heterodimer and increases ligand affinity while also biding to F-actin and vinculin to facilitate focal adhesion assembly and cell migration.[157,160,161,163,245] Due to the involvement with the cytoskeleton, talin-1 has also been shown to contribute to pedestal formation and actin polymerization in intestinal epithelial cells during infection by A/E pathogens in vitro.[238,239] Thus, we sought to determine if talin-1 is required for bacterial colonization and pathogenesis in the *C. rodentium* mouse model of A/E infection-induced colitis. In this study, we demonstrate that epithelial expression of talin-1 helps contain *C. rodentium* at the luminal surface and protects against mucosal hyperplasia, neutrophil-driven colitis, and death.

C. rodentium shares many of the same virulence factors expressed by EPEC and STEC. One important virulence factor is Tir, which is injected into host cells via the T3SS and triggers actin polymerization following the clustering of bacterial intimin.[141,142] The N-terminal domain of Tir interacts with host focal adhesion molecules including talin-1, however, this interaction is not necessary for A/E lesion formation as deletion of the N-terminus does not diminish pedestal formation.[142,238,246] In addition, phosphorylation of the C-terminus of Tir is required for actin condensation, although the translocation of Tir is sufficient for *C. rodentium* colonization, A/E lesion formation, and colonic hyperplasia.[247] In previous studies, the interaction between bacterial factors and the host cytoskeleton was evaluated using mutant strains. In this study, we directly knocked out an actin binding protein in intestinal epithelial cells. Using *C. rodentium*, we observed that loss of talin-1 attenuated actin polymerization, but did not reduce the ability of *C. rodentium* to colonize the colonic mucosa. In fact, the loss of talin-1 enhanced the depth in which *C. rodentium* inhabited the colonic crypts and increased overall colonization. Therefore, we postulate that talin-1 in CECs strengthens the adherence of *C. rodentium* to host cells by enabling actin rearrangement and preventing detachment and movement of the pathogen further into the glands.

C. rodentium has adapted multiple mechanisms to hijack the host machinery to increase survival in addition to A/E lesions. A hallmark of *C. rodentium* pathology is transmissible murine crypt hyperplasia.[141,222] Under homeostatic conditions, colonic epithelial regeneration begins with the proliferation of colonic stem cells followed

by maturation of the transit amplifying cells as they migrate up the crypt to the luminal surface. Finally, the terminal cells undergo apoptosis and are shed into the lumen.[248] This process is accelerated by *C. rodentium* infection and can potentially benefit the bacteria via increased oxygenation of the mucosa as the cells at the apex of the crypts ferment glucose to lactate instead of oxygen.[249] However, cell extrusion is detrimental to the pathogen as those bacteria attached to the dying cells are shed out into the lumen, which is protective for the host. Not only did we observe a decrease in apoptotic cells at the luminal surface in talin-1 deficient mice, but also crowding of proliferating cells at the base of the crypt with reduced movement of proliferating cells up the sides of the crypts. This resulted in increased crypt elongation that may also contribute to the increased *C. rodentium* colonization. In addition, colonoids derived from *Tln1$^{\Delta epi}$* mice grew over time, but remained spherical and did not show signs of budding or extension into the ECM substrate. In prior studies of the small intestine, cell proliferation was the primary force that drove enterocyte migration up the villus, a movement that required integrins.[250,251] Moreover, the relationship of talin-1 with both integrins and actin filaments contributes to cell adhesion and ECM traction for movement.[252,253] Thus, our data indicates that talin-1 expression in CECs is essential for cell turnover and the movement of proliferating cells up the colonic crypts in a model of infectious colitis.

Interestingly, in addition to the changes we observed in the epithelial cell compartment, the deletion of *Tln1* in CECs also modulated the mucosal immune response. The increased histologic injury scores that *Tln1$^{\Delta epi}$* mice exhibited was driven by the infiltration of immune cells. *C. rodentium* elicits a robust inflammatory response, recently identified as type 3.[224] We found that mice lacking epithelial talin-1 displayed higher numbers of MPO$^+$ cells recruited to the mucosa, which might seem counterintuitive since there was an increase in bacterial burden. However, mice that do not express TLR4 have decreased recruitment of GR-1$^+$ neutrophils and F4/80$^+$ macrophages to the infected tissues, and are less susceptible to *C. rodentium* pathogenesis, which would be consistent with our findings of increased disease with more infiltration of innate inflammatory cells.[225] Moreover, in combination with our data, these findings suggest that innate cells are not sufficient to control bacterial growth, and that the presence of *C. rodentium* maintains the pool of MPO-expressing cells in the tissue. Further, immunocompromised *Rag$^{-/-}$* mice do not display the classic signs of *C. rodentium* pathogenesis, but do exhibit impaired bacterial clearance, all

of which are reversed with reconstitution of CD4^{+} cells.[227,228] In this present study, we observed that CEC-specific deletion of *Tln1* led to decreased T cell recruitment, expression of T cell-attracting chemokines, and expression of the genes encoding IFN-g, IL-17a, and IL-22. Our findings align with previous studies that found loss of IL-22 and specifically IL-22 expressed by T cells, results in decreased survival, increased weight loss, increased crypt hyperplasia, and increased *C. rodentium* colonization deep into colonic crypts.[229,231,232]

In conclusion, the results from our study demonstrate that talin-1 plays a pivotal role in host response to infection by *C. rodentium*. Talin-1 expression by CECs not only influences the epithelial compartment, but also affects the immune cell population during bacterial insult. These findings provide insight into the interaction of A/E lesion-forming pathogens with host cell proteins. Contrary to the conventional paradigm that the intimate attachment of A/E pathogens is associated with increased virulence, our data suggest that this process is also to the advantage of the infected host by limiting bacterial invasion of colonic crypts.

CHAPTER 5

Discussion

5.1 Summary and Future Directions

The field of immunology is ever expending with the discovery of previously uncharacterized cell types, the emergence of new diseases, and more in-depth understanding of well-established immune responses. Dr. Elias Metchnikoff first conceived the concept of phagocytes in 1883 and later, the macrophage in 1875.[254] Ever since, macrophages have become a major focus of immunological research and rightfully so. Macrophages are a critical component of mammalian life and wear many hats. The role of macrophages in health and disease spans a broad spectrum from tissue homeostasis and repair to bacterial killing with immune surveillance in between. Although macrophages have been studied for over a century, new insights into their function and physiology are discovered continuously. The studies presented in Chapters 2 and 3 of this dissertation are no exception.

CTH as a regulator of macrophage function

Chapter 2 outlines the role of CTH in macrophages during *H. pylori*-induced immunopathogenesis. *H. pylori* is a highly prevalent human pathogen that colonizes the gastric mucosa and stimulates a robust but ineffective immune response that culminates in chronic inflammation and risk of cancer development.[24] The identification of novel strategies to both combat the infection and reduce the overzealous immune response while avoiding antibiotic resistance is needed. CTH has been studied in macrophages in the context of inflammation for its ability to produce H_2S, however, the study outlined in Chapter 2 approaches CTH from its other metabolic properties. We found that *H. pylori* induces CTH gene expression in primary macrophages ex vivo. Interestingly, CTH expression was not induced by another Gram-negative pathogen or cytokine stimulation. When I assessed the in vivo expression of CTH during *H. pylori* infection, I confirmed that CTH was upregulated with infection and found that CTH expression co-localized with a macrophage marker but not a neutrophil or T cell marker in gastric tissues. These

data indicate that the role of CTH in inflammation is highly context dependent and not only relies on the stimuli but is also on the cell type.

By using *Cth*-deficient mice, I demonstrate that CTH contributes to the inflammatory response mounted against *H. pylori*. Mice lacking *Cth* exhibited less histologic gastritis as early as 4 weeks and as late as 16 weeks post-inoculation. The decrease in histologic gastritis was also accompanied by a decrease in the gene expression of both proinflammatory and antiinflammatory markers that are induced by *H. pylori*, including markers of T cell activation. This suggests that the presence of CTH is supportive of the immune response to *H. pylori* and if we can find a way to suppress CTH activity, we may be able to exogenously regulate the pathogenic immunity. Unfortunately, there are no known inhibitors of CTH that are selective enough to be used therapeutically since the currently available ones also target other PLP-dependent enzymes.[203] With that in mind, I used unbiased omics approaches to identify targets either upstream or downstream of CTH that I could manipulate and produce the same protective phenotype. I first assessed differences in the transcriptome between WT and *Cth*-deficient gastric macrophages. As expected with the gene expression I observed in the whole gastric tissues of infected mice, the macrophages from *Cth*-deficient mice exhibited downregulation of pathways associated with immune activation and function. This was promising and confirmed the clinical findings. Pathway analysis also revealed dysregulated expression of transcripts involved in general metabolic pathways, SAM metabolism, and activity of methyltransferases. To expand on these findings, I next performed an untargeted metabolomics analysis. Consistent with the transcriptomics analysis and what is known about the RTP, the metabolic pathways that were different in the gastric tissues from WT and *Cth*-deficient mice were polyamine synthesis and SAM utilization. These findings prompted me to test whether SAM supplementation or SAMDC inhibition influenced macrophage activation and *H. pylori*-induced inflammation but there no effect in vivo. These data suggested that the pathways upstream of CTH did not contribute to the protective phenotype that I observed in *Cth*-deficient mice.

In order to dig deeper into the mechanism in which CTH can regulate inflammation, I moved into an ex vivo model of infection using primary BMmacs derived from WT and *Cth*-deficient mice. Overall, I was able to demonstrate that *Cth*-deficient macrophages have impaired activation and polarization due to a decrease in the concentration of available cysteine, the rate limiting precursor of GSH synthesis. Glutathione is a major antioxidant

that is used by cells to counteract the production of ROS.[110,111] ROS is generated by cellular respiration and part of the antimicrobial activity of macrophages is to produce high levels of ROS in an oxidative burst. Excessive amounts of ROS can impede mitochondrial function and cause cellular damage.[209,210] Since *H. pylori* employs multiple mechanisms to avoid killing by the immune response, including neutralizing ROS, I speculate that macrophages upregulate the expression of CTH in order to maintain a proinflammatory state to control infection. Thus, the induction of CTH by *H. pylori* signifies yet another method in which *H. pylori* contributes to chronic inflammation.

Cell specific role of talin-1 in colitis

The overarching goal of my research is to investigate all aspects of macrophage biology in GI inflammation. An important step in inflammation is the trafficking of immune cells to the site of injury or infection. Circulating monocytes must be able to fight the current infections in blood vessels and pull themselves through the endothelial cell lined walls into the underlying tissue. This process is assisted by the binding of integrins on the surface of monocytes to adhesion molecules presented on endothelial cells.[213–215] Talin-1 is a mechanosensory protein that is a crucial member of intercellular adhesion complexes and links the actin cytoskeleton to integrins.[150] The role of talin-1 has previously been assessed in neutrophils, T cells, and dendritic cells,[167,235,255] but the study presented in Chapter 3 of this dissertation is the first time that talin-1 has been directly implicated in macrophage trafficking, particularly in the context of colitis. Using mice with myeloid-specific knockdown of *Tln1*, I demonstrate that talin-1 is essential in the recruitment of macrophages to the colonic mucosa. When infected with the mouse pathogen *C. rodentium*, mice that lacked expression of *Tln1* in myeloid cells exhibited deceased numbers of CD68$^+$ cells in the mucosa while maintaining similar numbers of neutrophils, dendritic cells, and CD4$^+$ T cells to their genetically normal littermates. This finding was associated with lower histologic injury scores and a decrease in both proinflammatory and antiinflammatory gene expression in the colonic tissues. I next evaluated whether this phenotype is the result of impaired macrophage activation and found that talin-1 does not have a cell-intrinsic role in macrophages as the loss of *Tln1* did not affect gene expression, NO production, or phagocytosis of *C. rodentium* ex vivo. Collectively, these results suggest that talin-1 is a promising target to limit the recruitment of macrophages during infectious colitis.

Talin-1 has also been implicated in the immune response of colonocytes in the same model of infectious colitis.[170] The Wilson Lab found that shRNA knockdown of *Tln1* in YAMC cells reduced actin rearrangement, an indicator of A/E lesion formation. We therefore hypothesized that loss of talin-1 in colonic epithelial cells would also protect mice from *C. rodentium*-induced histologic injury and decrease the bacterial burden. Outlined in Chapter 4, using mice with epithelial cell-specific knockdown of *Tln1*, I demonstrate the opposite result. Mice that lacked *Tln1* expression in epithelial cells exhibited increased *C. rodentium* colonization that extended deep into the colonic crypts. I performed a FAS test to confirm that talin-1 is involved in the rearrangement of actin under bound *C. rodentium*. We speculate that instead of *C. rodentium* hijacking host cell cytoskeletal proteins to ensure adherence to the epithelial lining, that it is more beneficial to the host to tightly bind the bacteria and carry it away into the lumen as the apical cells shed off. In addition, I found that epithelial talin-1 is also essential in T cell recruitment and activation in the *C. rodentium* model of colitis. Taken together with the data from the myeloid-specific mice, I demonstrate that the role of talin-1 in the intestinal immune response is multifaceted and the differing disease outcomes based on the cellular source needs to be considered when proposing therapeutic interventions.

5.2 Limitations and Future Directions

Through my thesis research presented in this dissertation, I have demonstrated that CTH activity is a regulator of macrophage activation and function, and that myeloid-derived talin-1 facilitates the recruitment of macrophages while epithelial cell talin-1 supports the recruitment of T cells to the colonic mucosa. Yet, there are still many remaining questions regarding the roles of CTH and talin-1 in the GI immune response. The following sections are outstanding questions and how I propose to address them.

Is the protective phenotype in *Cth*$^{-/-}$ mice macrophage specific?

A limitation of the study presented in Chapter 2 is the use of a whole-body genetic knockout mouse. On one hand the full-body knockout is more clinically relevant since the findings are more indicative of a what would happen with a chemical inhibitor. On the other hand, it is hard to conclude that the protective phenotype that we

observe in $Cth^{-/-}$ mice is not due to a combination of cell types. The in vivo experiments that I performed in Chapter 2 should be repeated in mice with cell-specific knockdown of *Cth*. The Wilson Lab has extensive experience using floxed mice crossed to *Lyz2*-cre driver mice to generate myeloid-specific knockout mice.[218] Additional cre-driver mice that could be used to target macrophages include but are not limited to *Cxc3cr1*-cre, *Cd64*-cre, and *Csf1e*-cre.[256] A caveat to using these cre mice is that none are 100% efficient at knocking down gene expression or are 100% specific to macrophages. Another method that could be used to assess the specific role of macrophage CTH in vivo is adoptive transfer of WT or $Cth^{-/-}$ macrophages into irradiated mice. This would ensure that *Cth* is only lost in the macrophage population.

In addition, this body of work could also benefit from studying the role of CTH in other immune cells. I have shown that in the gastric mucosa, CTH is not upregulated in neutrophils or T cells and that the loss of *Cth* does not impact T cell function in vitro. However, I did not address dendritic cells which share a common myeloid precursor with macrophages. I have performed preliminary studies in bone marrow-derived dendritic cells (BMDCs) and found that BMDCs also upregulate the expression of *Cth* during infection with *H. pylori*. Follow up functional studies assessing the role of *Cth* in dendritic cells may be a useful area of investigation.

The role of CTH in gastric carcinogenesis.

The primary theme of this dissertation is the immunopathogenesis of gastrointestinal infections. *H. pylori* infection is the greatest risk factor for gastric adenocarcinoma with 1-3% of infected individuals developing cancer, but around 85% of infected individuals remaining asymptomatic. Understanding how chronic inflammation causes more severe disease can contribute to the prediction and management of disease outcome. There are two gold standard animal models used for studying the development of *H. pylori*-induced dysplasia and carcinoma. The insulin-gastrin (INS-GAS) mouse overexpresses human gastrin regulated by the rat insulin promoter. Hypergastrinemia is associated with the development of gastric cancer in humans and older INS-GAS mice spontaneously exhibit signs of the precancerous cascade including loss of gastric parietal cells, gastric atrophy, metaplasia, and dysplasia that is accelerated by the infection with *H. pylori*.[257] The benefit of using INS-GAS mice is the continued use of genetic and cell-specific tools. The downside of using INS-GAS mice is that they are not a

natural model of *H. pylori*-induced gastric cancer. Conversely, Mongolian gerbils do develop gastric cancer in addition to the precancerous cascade when infected with *H. pylori*. This model does come with its own limitations. Mongolian gerbils cannot be in-bred, therefore, transgenic animals is not an option so all studies require drug treatment or dietary manipulation. Since there are no specific inhibitors of CTH, studies in Mongolian gerbils are not currently feasible. In addition, the Mongolian gerbil genome is not fully sequenced limiting gene and protein expression assessment tools. The Wilson Lab has begun generating $Cth^{-/-}$ FVB/N INS-GAS mice that should be ready for study soon. These mice will be chronically infected with *H. pylori* and histologic gastritis, hyperplasia, dysplasia, and carcinoma will be assessed. Studies using $Cth^{-/-}$ FVB/N INS-GAS mice will address whether the decreased gastritis observed in the $Cth^{-/-}$ mice translates to protection from cancer development.

How does *H. pylori* induce *Cth* expression?

The gene that encodes CTH is under the regulation of multiple transcription factors and downstream of different signaling cascades. The Wilson Lab has demonstrated using chemical inhibitors that *Cth* expression is induced in RAW264.7 macrophages through the transcription factor SP1, which is downstream of the phosphatidylinositol 3-kinase (PI3K)/mTOR signaling axis.[136] These studies need to be repeated in primary macrophages such as BMmacs to confirm biological relevance. Since CTH generates cysteine, it is part of the cellular response to oxidative stress and the maintenance of redox homeostasis. These responses are regulated through activation of the transcriptional factors ATF4 or NRF2 in immune cells.[210,258–260] The use of chemical inhibitors to block components of the signaling cascade upstream of ATF4 and NRF2 in macrophages during *H. pylori* infection will elucidate which cellular response is turned on. In addition to these proposed signaling studies, I think it is also important to determine how *H. pylori* actually triggers these signaling cascades. This can be done using mutant *H. pylori* strains missing different virulence factors, such as CagA, that are known to activate macrophages and using non-viable *H. pylori* or *H. pylori* lysates to determine if *Cth* induction is dependent on active infection or cell contact.

The role of CTH in APC mediated CD4 T cell activation.

A function of macrophages that I did not address in Chapter 2 is antigen presentation and direct activation of T cells. Cysteine is classified as a semi-essential amino acid since it be generated *de novo* in cells by CTH or it can be acquired extracellular with transporters (Figure 5.1). There are two main transporters of cysteine, the neutral amino acid transporter ASCT2 (SLC5A1),[261] or system X_C^-.[262] Around 90% of extracellular cysteine is in the disulfide form cystine and cannot be readily transported through ASCT2.[263,264] System X_C^- is a glutamate/cystine antiporter composed of two subunits, the light chain transporter xCT (SLC7A11) and the extracellular regulatory component 4F2 heavy chain (4F2hc, SLC3A2).[262] It has been reported that naïve T cells do not express CTH or xCT prior to activation, thus, naïve T cells rely on antigen presenting cells (APCs) such as macrophages and dendritic cells, which express both CTH and xCT, in close proximity to export cysteine through ASCT2 into the surrounding microenvironment.[265–267]
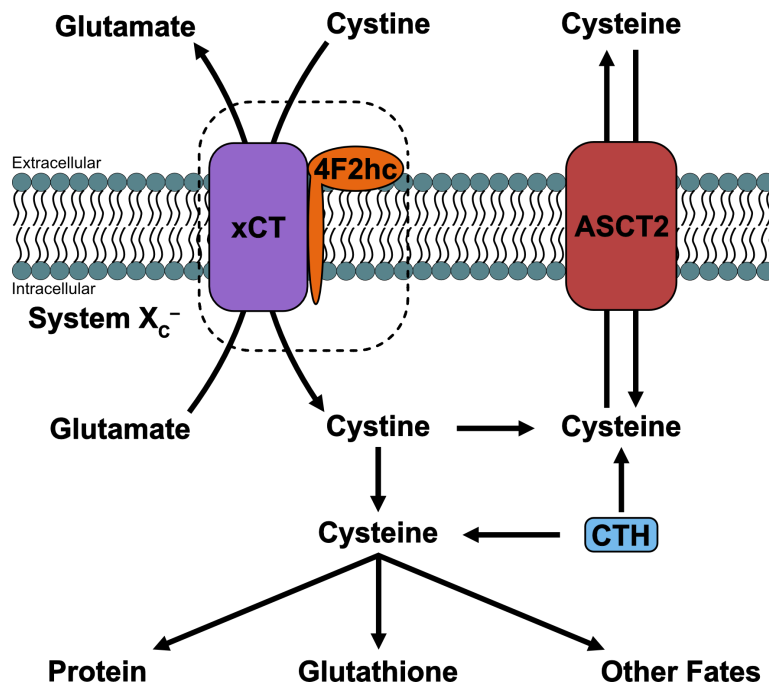

Figure 5.1 Methods of cellular cysteine acquisition.

Since I found that *Cth* expression was also induced in BMDCs by *H. pylori*, I propose to use BMmacs and BMDCs from WT, *Cth*$^{-/-}$, and *Slc7a11*$^{-/-}$ mice for the following experiments to test the impact of CTH on APC function. The addition of *Slc7a11*$^{-/-}$ mice will also help elucidate if the source of cysteine is important in APC function. Naive CD4$^+$ T cells would be isolated from the spleens of uninfected mice, cultured with plate-bound anti-CD3 and soluble anti-CD28 antibodies to activate the cells in an antigen independent-manner. To address if APC derived cysteine during T cell activation is dependent on direct interactions with APCs, CD4$^+$ T cells will then be co-cultured with APCs from WT, *Cth*$^{-/-}$, or *Slc7a11*$^{-/-}$ mice that were infected ex vivo with *H. pylori*. Next, CD4$^+$ T cells will be indirectly cultured with infected APCs using a Transwell Filter system. Transwell inserts would be placed in each well and activated APCs will be added to the Transwell cavity while the T cells sit underneath. Lastly, CD4$^+$ T cells would be cultured in filtered conditioned media from activated APCs. Gene expression and flow cytometry would be used to analyze various markers of T cell subtypes and proliferation using RT-qPCR, flow cytometry, and Luminex multiplex array.

Does talin-1 have a role in other models of GI inflammation?

Finally, Chapters 3 and 4 present talin-1 as a regulator of macrophage trafficking and epithelial immunity but only in a single model of GI inflammation. Future studies should utilize other models of pathogenic infection such as *H. pylori* or the DSS (dextran sodium sulfate) model of chemically induced colitis.

REFERENCES

1. Marshall JS, Warrington R, Watson W, et al. An introduction to immunology and immunopathology. *Allergy Asthma Clin Immunol*. 2018;14:49.
2. Freitag J, Berod L, Kamradt T, et al. Immunometabolism and autoimmunity. *Immunol Cell Biol*. 2016;94:925–934.
3. Medzhitov R. Origin and physiological roles of inflammation. *Nature*. 2008;454:428–435.
4. Barton GM. A calculated response: control of inflammation by the innate immune system. *J Clin Invest*. 2008;118:413–420.
5. Shi C, Pamer EG. Monocyte recruitment during infection and inflammation. *Nat Rev Immunol*. 2011;11:762–774.
6. Gordon S, Taylor PR. Monocyte and macrophage heterogeneity. *Nat Rev Immunol*. 2005;5:953–964.
7. Benoit M, Desnues B, Mege J-L. Macrophage polarization in bacterial infections. *J Immunol*. 2008;181:3733 LP – 3739.
8. Anderson CF, Mosser DM. A novel phenotype for an activated macrophage: the type 2 activated macrophage. *J Leukoc Biol*. 2002;72:101–106.
9. Turner JR. Intestinal mucosal barrier function in health and disease. *Nat Rev Immunol*. 2009;9:799–809.
10. Zhang K, Hornef MW, Dupont A. The intestinal epithelium as guardian of gut barrier integrity. *Cell Microbiol*. 2015;17:1561–1569.
11. Ross KF, Herzberg MC. Autonomous immunity in mucosal epithelial cells: fortifying the barrier against infection. *Microbes Infect*. 2016;18:387–398.
12. Tindemans I, Joosse ME, Samsom JN. Dissecting the heterogeneity in T-cell mediated inflammation in IBD. *Cells*. 2020;9:110.
13. Kotas ME, Medzhitov R. Homeostasis, inflammation, and disease susceptibility. *Cell*. 2015;160:816–827.
14. Germolec DR, Shipkowski KA, Frawley RP, et al. Markers of Inflammation. In: DeWitt JC, Rockwell CE, Bowman CC (eds) Immunotoxicity Testing: Methods and Protocols. New York, NY: Springer New York:57–79.
15. Hooi JKY, Lai WY, Ng WK, et al. Global prevalence of *Helicobacter pylori* infection: Systematic review and meta-analysis. *Gastroenterology*. 2017;153:420–429.
16. Wroblewski LE, Peek RMJ, Wilson KT. *Helicobacter pylori* and gastric cancer: factors that modulate disease risk. *Clin Microbiol Rev*. 2010;23:713–739.
17. Sung H, Ferlay J, Siegel RL, et al. Global Cancer Statistics 2020: GLOBOCAN estimates of incidence and mortality worldwide for 36 cancers in 185 countries. *CA Cancer J Clin*. 2021;71:209–249.
18. Parsonnet J. Bacterial infection as a cause of cancer. *Environ Health Perspect*. 1995;103:263–268.
19. Cogliano VJ, Baan R, Straif K, et al. Preventable exposures associated with human cancers. *J Natl Cancer Inst*. 2011;103:1827–1839.
20. Reshetnyak VI, Burmistrov AI, Maev IV. *Helicobacter pylori*: Commensal, symbiont or pathogen? *World J Gastroenterol*. 2021;27:545.
21. Huang RJ, Koh H, Hwang JH. A summary of the 2020 Gastric Cancer Summit at Stanford University. *Gastroenterology*. 2020;159:1221–1226.

22. Hardbower DM, de Sablet T, Chaturvedi R, et al. Chronic inflammation and oxidative stress: The smoking gun for *Helicobacter pylori*-induced gastric cancer? *Gut Microbes*. 2013;4:475–81.

23. Camargo MC, Piazuelo MB, Mera RM, et al. Effect of smoking on failure of *H. pylori* therapy and gastric histology in a high gastric cancer risk area of Colombia. *Acta Gastroenterol Latinoam*. 2007;37:238–45.

24. Hardbower DM, Peek RMJ, Wilson KT. At the Bench: *Helicobacter pylori*, dysregulated host responses, DNA damage, and gastric cancer. *J Leukoc Biol*. 2014;96:201–212.

25. Zambon C-F, Basso D, Navaglia F, et al. Pro- and anti-inflammatory cytokines gene polymorphisms and *Helicobacter pylori* infection: interactions influence outcome. *Cytokine*. 2005;29:141–152.

26. Romano M, Ricci V, Zarrilli R. Mechanisms of Disease: *Helicobacter pylori*-related gastric carcinogenesis—implications for chemoprevention. *Nat Clin Pract Gastroenterol Hepatol*. 2006;3:622–632.

27. Parsonnet J, Friedman GD, Orentreich N, et al. Risk for gastric cancer in people with CagA positive or CagA negative *Helicobacter pylori* infection. *Gut*. 1997;40:297–301.

28. Blaser MJ, Perez-Perez GI, Kleanthous H, et al. Infection with *Helicobacter pylori* strains possessing CagA Is associated with an increased risk of developing adenocarcinoma of the stomach. *Cancer Res*. 1995;55:2111–2115.

29. Israel DA, Salama N, Arnold CN, et al. *Helicobacter pylori* strain-specific differences in genetic content, identified by microarray, influence host inflammatory responses. *J Clin Invest*. 2001;107:611–620.

30. Palframan S, Kwok T, Gabriel K. Vacuolating cytotoxin A (VacA), a key toxin for *Helicobacter pylori* pathogenesis. *Front Cell Infect Microbiol*;2 Available from: https://www.frontiersin.org/articles/10.3389/fcimb.2012.00092. 2012.

31. Rassow J, Meinecke M. *Helicobacter pylori* VacA: a new perspective on an invasive chloride channel. *Microbes Infect*. 2012;14:1026–1033.

32. Boquet P, Ricci V, Galmiche A, et al. Gastric cell apoptosis and *H. pylori*: Has the main function of VacA finally been identified? *Trends Microbiol*. 2003;11:410–413.

33. Sören S, Roland B, Claudia G, et al. Rapid loss of motility of *Helicobacter pylori* in the gastric lumen in vivo. *Infect Immun*. 2005;73:1584–1589.

34. Montecucco C, Rappuoli R. Living dangerously: how *Helicobacter pylori* survives in the human stomach. *Nat Rev Mol Cell Biol*. 2001;2:457–466.

35. Celli JP, Turner BS, Afdhal NH, et al. *Helicobacter pylori* moves through mucus by reducing mucin viscoelasticity. *Proc Natl Acad Sci USA*. 2009;106:14321–14326.

36. Celli JP, Turner BS, Afdhal NH, et al. Rheology of gastric mucin exhibits a pH-dependent sol−gel transition. *Biomacromolecules*. 2007;8:1580–1586.

37. Gewirtz AT, Yu Y, Krishna US, et al. *Helicobacter pylori* flagellin evades toll-like receptor 5-mediated innate immunity. *J Infect Dis*. 2004;189:1914–1920.

38. Cullen TW, Giles DK, Wolf LN, et al. *Helicobacter pylori* versus the host: remodeling of the bacterial outer membrane is required for survival in the gastric mucosa. *PLoS Pathog*. 2011;7:e1002454-.

39. Moran AP, Lindner B, Walsh EJ. Structural characterization of the lipid A component of *Helicobacter pylori rough*- and smooth-form lipopolysaccharides. *J Bacteriol*. 1997;179:6453–6463.

40.   Sayi A, Kohler E, Toller IM, et al. TLR-2–activated B cells suppress *Helicobacter*-induced preneoplastic gastric immunopathology by inducing T regulatory-1 cells. *J Immunol*. 2011;186:878.

41.   Rad R, Ballhorn W, Voland P, et al. Extracellular and intracellular pattern recognition receptors cooperate in the recognition of *Helicobacter pylori*. *Gastroenterology*. 2009;136:2247–2257.

42.   Otani K, Tanigawa T, Watanabe T, et al. Toll-like receptor 9 signaling has anti-inflammatory effects on the early phase of *Helicobacter pylori*-induced gastritis. *Biochem Biophys Res Commun*. 2012;426:342–349.

43.   Wang G, Alamuri P, Maier RJ. The diverse antioxidant systems of *Helicobacter pylori*. *Mol Microbiol*. 2006;61:847–860.

44.   Ramarao N, Gray-Owen SD, Meyer TF. *Helicobacter pylori* induces but survives the extracellular release of oxygen radicals from professional phagocytes using its catalase activity. *Mol Microbiol*. 2000;38:103–113.

45.   Peek RM, Fiske C, Wilson KT. Role of innate immunity in *Helicobacter pylori*-induced gastric malignancy. *Physiol Rev*. 2010;90:831–858.

46.   Eaton KA, Mefford M, Thevenot T. The role of T cell subsets and cytokines in the pathogenesis of *Helicobacter pylori* gastritis in mice. *J Immunol*. 2001;166:7456.

47.   Shi Y, Liu X-F, Zhuang Y, et al. *Helicobacter pylori*-induced Th17 responses modulate Th1 cell responses, benefit bacterial growth, and contribute to pathology in mice. *J Immunol*. 2010;184:5121.

48.   Robinson K, Kenefeck R, Pidgeon EL, et al. *Helicobacter pylori*-induced peptic ulcer disease is associated with inadequate regulatory T cell responses. *Gut*. 2008;57:1375.

49.   Peterson II RA, Hoepf T, Eaton KA. Adoptive transfer of splenocytes in SCID mice implicates CD4+ T cells in apoptosis and epithelial proliferation associated with *Helicobacter pylori*-induced gastritis. *Comp Med*. 2003;53:498–509.

50.   Hitzler I, Oertli M, Becher B, et al. Dendritic cells prevent rather than promote immunity conferred by a *Helicobacter* vaccine using a mycobacterial adjuvant. *Gastroenterology*. 2011;141:186-196.e1.

51.   Sundrud MS, Torres VJ, Unutmaz D, et al. Inhibition of primary human T cell proliferation by *Helicobacter pylori* vacuolating toxin (VacA) is independent of VacA effects on IL-2 secretion. *Proc Natl Acad Sci USA*. 2004;101:7727–7732.

52.   Gebert B, Fischer W, Weiss E, et al. *Helicobacter pylori* vacuolating cytotoxin inhibits T lymphocyte activation. *Science (1979)*. 2003;301:1099–1102.

53.   Gerhard M, Schmees C, Voland P, et al. A secreted low--molecular-weight protein from *Helicobacter pylori* induces cell-cycle arrest of T cells. *Gastroenterology*. 2005;128:1327–1339.

54.   Schmees C, Prinz C, Treptau T, et al. Inhibition of T-cell proliferation by *Helicobacter pylori* γ-glutamyl transpeptidase. *Gastroenterology*. 2007;132:1820–1833.

55.   Kaparakis M, Walduck AK, Price JD, et al. Macrophages are mediators of gastritis in acute *Helicobacter pylori* infection in C57BL/6 mice. *Infect Immun*. 2008;76:2235–2239.

56.   Wilson KT, Crabtree JE. Immunology of *Helicobacter pylori*: insights into the failure of the immune response and perspectives on vaccine studies. *Gastroenterology*. 2007;133:288–308.

57.   Martinez FO, Gordon S. The M1 and M2 paradigm of macrophage activation: time for reassessment. *F1000Prime Rep*. 2014;6:13.

58.   Mosser DM, Edwards JP. Exploring the full spectrum of macrophage activation. *Nat Rev Immunol*. 2008;8:958–969.

59. Strauss-Ayali D, Conrad SM, Mosser DM. Monocyte subpopulations and their differentiation patterns during infection. *J Leukoc Biol*. 2007;82:244–252.

60. Mosser DM. The many faces of macrophage activation. *J Leukoc Biol*. 2003;73:209–212.

61. Murray PJ, Wynn TA. Protective and pathogenic functions of macrophage subsets. *Nat Rev Immunol*. 2011;11:723–737.

62. Fleming BD, Mosser DM. Regulatory macrophages: setting the threshold for therapy. *Eur J Immunol*. 2011;41:2498–2502.

63. Yang L, Zhang Y. Tumor-associated macrophages: from basic research to clinical application. *J Hematol Oncol*. 2017;10:58.

64. Gabrilovich DI, Nagaraj S. Myeloid-derived suppressor cells as regulators of the immune system. *Nat Rev Immunol*. 2009;9:162–174.

65. Lech M, Anders H-J. Macrophages and fibrosis: How resident and infiltrating mononuclear phagocytes orchestrate all phases of tissue injury and repair. *Biochimica et Biophysica Acta (BBA) - Molecular Basis of Disease*. 2013;1832:989–997.

66. Galli SJ, Borregaard N, Wynn TA. Phenotypic and functional plasticity of cells of innate immunity: macrophages, mast cells and neutrophils. *Nat Immunol*. 2011;12:1035–1044.

67. Wynn TA, Chawla A, Pollard JW. Macrophage biology in development, homeostasis and disease. *Nature*. 2013;496:445.

68. Lichtnekert J, Kawakami T, Parks WC, et al. Changes in macrophage phenotype as the immune response evolves. *Curr Opin Pharmacol*. 2013;13:555–564.

69. Hardbower DM, Asim M, Luis PB, et al. Ornithine decarboxylase regulates M1 macrophage activation and mucosal inflammation via histone modifications. *Proc Natl Acad Sci USA*. 2017;114:E751–E760.

70. Coburn LA, Singh K, Asim M, et al. Loss of solute carrier family 7 member 2 exacerbates inflammation-associated colon tumorigenesis. *Oncogene*. 2018;1.

71. Singh K, Coburn LA, Asim M, et al. Ornithine decarboxylase in macrophages exacerbates colitis and promotes colitis-associated colon carcinogenesis by impairing M1 immune responses. *Cancer Res*. 2018;78:4303–4315.

72. Langston PK, Shibata M, Horng T. Metabolism supports macrophage activation. *Front Immunol*. 2017;8:61.

73. Wang F, Zhang S, Vuckovic I, et al. Glycolytic stimulation is not a requirement for M2 macrophage differentiation. *Cell Metab*. 2018;28:463-475.e4.

74. Freemerman AJ, Johnson AR, Sacks GN, et al. Metabolic reprogramming of macrophages: glucose transporter 1 (GLUT1)-mediated glucose metabolism drives a proinflammatory phenotype. *J Biol Chem*. 2014;289:7884–7896.

75. Jha AK, Huang SC-C, Sergushichev A, et al. Network integration of parallel metabolic and transcriptional data reveals metabolic modules that regulate macrophage polarization. *Immunity*. 2015;42:419–430.

76. Lampropoulou V, Sergushichev A, Bambouskova M, et al. Itaconate links inhibition of succinate dehydrogenase with macrophage metabolic remodeling and regulation of inflammation. *Cell Metab*. 2016;24:158–166.

77. Tannahill GM, Curtis AM, Adamik J, et al. Succinate is an inflammatory signal that induces IL-1β through HIF-1α. *Nature*. 2013;496:238–242.

78. Lauterbach MA, Hanke JE, Serefidou M, et al. Toll-like receptor signaling rewires macrophage metabolism and promotes histone acetylation via ATP-citrate lyase. *Immunity*. 2019;51:997-1011.e7.

79. Huang SC-C, Smith AM, Everts B, et al. Metabolic reprogramming mediated by the mTORC2-IRF4 signaling axis is essential for macrophage alternative activation. *Immunity*. 2016;45:817–830.

80. Viola A, Munari F, Sánchez-Rodríguez R, et al. The metabolic signature of macrophage responses. *Front Immunol*. 2019;10:1462.

81. Pegg AE, McCann PP. Polyamine metabolism and function. *Amer J Phys, Cell Physiol*. 1982;243:C212–C221.

82. Pegg AE. Mammalian polyamine metabolism and function. *IUBMB Life*. 2009;61:880–894.

83. Kakuda DK, Sweet MJ, mac Leod CL, et al. CAT2-mediated L-arginine transport and nitric oxide production in activated macrophages. *Biochem J*. 1999;340 (Pt 2:549–553.

84. Pegg AE. Regulation of ornithine decarboxylase. *J Biol Chem*. 2006;281:14529–14532.

85. Asim M, Chaturvedi R, Hoge S, et al. *Helicobacter pylori* induces ERK-dependent formation of a phospho-c-Fos c-Jun activator protein-1 complex that causes apoptosis in macrophages. *J Biol Chem*. 2010;285:20343–20357.

86. Hobbs CA, Gilmour SK. High levels of intracellular polyamines promote histone acetyltransferase activity resulting in chromatin hyperacetylation. *J Cell Biochem*. 2000;77:345–360.

87. Huang Y, Marton LJ, Woster PM, et al. Polyamine analogues targeting epigenetic gene regulation. *Essays Biochem*. 2009;46:95–110.

88. Brooks WH. Increased polyamines alter chromatin and stabilize autoantigens in autoimmune diseases. *Front immunol*. 2013;4:91.

89. Pasini A, Caldarera CM, Giordano E. Chromatin remodeling by polyamines and polyamine analogs. *Amino Acids*. 2014;46:595–603.

90. Linsalata M, Orlando A, Russo F. Pharmacological and dietary agents for colorectal cancer chemoprevention: Effects on polyamine metabolism. *Int J Oncol*. 2014;45:1802–1812.

91. Chaturvedi R, de Sablet T, Asim M, et al. Increased *Helicobacter pylori*-associated gastric cancer risk in the Andean region of Colombia is mediated by spermine oxidase. *Oncogene*. 2015;34:3429.

92. Saulnier Sholler GL, Gerner EW, Bergendahl G, et al. A Phase I trial of DFMO targeting polyamine addiction in patients with relapsed/refractory neuroblastoma. *PLoS One*. 2015;10:e0127246–e0127246.

93. Bassiri H, Benavides A, Haber M, et al. Translational development of difluoromethylornithine (DFMO) for the treatment of neuroblastoma. *Transl Pediatr*. 2015;4:226–238.

94. Hayashi S, Murakami Y, Matsufuji S. Ornithine decarboxylase antizyme: a novel type of regulatory protein. *Trends Biochem Sci*. 1996;21:27–30.

95. Chaturvedi R, Asim M, Barry DP, et al. Spermine oxidase is a regulator of macrophage host response to *Helicobacter pylori*: enhancement of antimicrobial nitric oxide generation by depletion of spermine. *Amino Acids*. 2014;46:531–542.

96. Chaturvedi R, Asim M, Hoge S, et al. Polyamines impair immunity to *Helicobacter pylori* by inhibiting L-arginine uptake required for nitric oxide production. *Gastroenterology*. 2010;139:1686–1698.

97. Chaturvedi R, Asim M, Romero–Gallo J, et al. Spermine oxidase mediates the gastric cancer risk associated with *Helicobacter pylori* CagA. *Gastroenterology*. 2011;141:1696–1708.

98. Gobert AP, Cheng Y, Wang J-Y, et al. *Helicobacter pylori* induces macrophage apoptosis by activation of arginase II. *J Immunol*. 2002;168:4692–4700.

99. Lewis ND, Asim M, Barry DP, et al. Arginase II restricts host defense to *Helicobacter pylori* by attenuating inducible nitric oxide synthase translation in macrophages. *J Immunol*. 2010;5:2572–2582.

100. Chaturvedi R, de Sablet T, Peek RM, et al. Spermine oxidase, a polyamine catabolic enzyme that links *Helicobacter pylori* CagA and gastric cancer risk. *Gut Microbes*. 2012;3:48–56.

101. Yeramian A, Martin L, Serrat N, et al. Arginine transport via cationic amino acid transporter 2 plays a critical regulatory role in classical or alternative activation of macrophages. *J Immunol*. 2006;176:5918–5924.

102. Lewis ND, Asim M, Barry DP, et al. Immune evasion by *Helicobacter pylori* is mediated by induction of macrophage arginase II. *J Immunol*. 2011;186:3632–3641.

103. Hardbower DM, Asim M, Murray-Stewart T, et al. Arginase 2 deletion leads to enhanced M1 macrophage activation and upregulated polyamine metabolism in response to *Helicobacter pylori* infection. *Amino Acids*. 2016;48:2375–2388.

104. Chaturvedi R, Asim M, Lewis ND, et al. L-arginine availability regulates inducible nitric oxide synthase-dependent host defense against *Helicobacter pylori*. *Infect Immun*. 2007;75:4305–4315.

105. Bussière FI, Chaturvedi R, Cheng Y, et al. Spermine causes loss of innate immune response to *Helicobacter pylori* by inhibition of inducible nitric-oxide synthase translation. *Journal of Biological Chemistry*. 2005;280:2409–2412.

106. Georgopoulos K. Haematopoietic cell-fate decisions, chromatin regulation and ikaros. *Nat Rev Immunol*. 2002;2:162.

107. Shlyueva D, Stampfel G, Stark A. Transcriptional enhancers: from properties to genome-wide predictions. *Nat Rev Genet*. 2014;15:272.

108. Chaturvedi R, Cheng Y, Asim M, et al. Induction of polyamine oxidase 1 by *Helicobacter pylori* causes macrophage apoptosis by hydrogen peroxide release and mitochondrial membrane depolarization. *J Biol Chem*. 2004;279:40161–73.

109. Gobert AP, Finley JL, Latour YL, et al. Hypusination orchestrates the antimicrobial response of macrophages. *Cell Rep*. 2020;33:108510.

110. Chiku T, Padovani D, Zhu W, et al. H2S biogenesis by human cystathionine γ-lyase leads to the novel sulfur metabolites lanthionine and homolanthionine and is responsive to the grade of hyperhomocysteinemia. *J Biol Chem*. 2009;284:11601–11612.

111. Singh S, Padovani D, Leslie RA, et al. Relative contributions of cystathionine β-synthase and γ-cystathionase to H2S biogenesis via alternative trans-sulfuration reactions. *J Bio Chem*. 2009;284:22457–22466.

112. Stipanuk MH. Sulfur amine acid metabolism: Pathways for production and removal of homocysteine and cysteine. *Annu Rev Nutr*. 2004;24:539–577.

113. Aitken SM, Kirsch JF. The enzymology of cystathionine biosynthesis: Strategies for the control of substrate and reaction specificity. *Arch Biochem Biophys*. 2005;433:166–175.

114. Abe K, Kimura H. The possible role of hydrogen sulfide as an endogenous neuromodulator. *J Neurosci*. 2018;16:1066–1071.

115. Yang G, Wu L, Jiang B, et al. H2S as a physiologic vasorelaxant: Hypertension in mice with deletion of cystathionine γ-lyase. *Science (1979)*. 2008;322:587–590.

116. Cantoni GL. Biological methylation: selected aspects. *Annu Rev Biochem*. 1975;44:435–451.

117. Lio C-WJ, Huang SC-C. Circles of Life: linking metabolic and epigenetic cycles to immunity. *Immunology*. 2020;161:165–174.

118. Parkhitko AA, Jouandin P, Mohr SE, et al. Methionine metabolism and methyltransferases in the regulation of aging and lifespan extension across species. *Aging Cell*. 2019;18:e13034.

119. Caudill MA, Wang JC, Melnyk S, et al. Intracellular S-adenosylhomocysteine concentrations predict global DNA hypomethylation in tissues of methyl-deficient cystathionine β-synthase heterozygous mice. *J Nutr*. 2001;131:2811–2818.

120. Hoffman DR, Cornatzer WE, Duerre JA. Relationship between tissue levels of S-adenosylmethionine, S-adenosylhomocysteine, and transmethylation reactions. *Can J Biochem*. 1979;57:56–64.

121. Gemici B, Wallace JL. Anti-inflammatory and cytoprotective properties of hydrogen sulfide. In: Methods in Enzymology. 2015:169–193.

122. Yang G, Cao K, Wu L, et al. Cystathionine γ-lyase overexpression inhibits cell proliferation via a H_2S-dependent modulation of ERK1/2 phosphorylation and p21 Cip/WAK-1. *J Biol Chem*. 2004;279:49199–49205.

123. Pal VK, Bandyopadhyay P, Singh A. Hydrogen sulfide in physiology and pathogenesis of bacteria and viruses. *IUBMB Life*. 2018;70:393–410.

124. Luhachack L, Nudler E. Bacterial gasotransmitters: an innate defense against antibiotics. *Curr Opin Microbiol*. 2014;21:13–17.

125. Dilek N, Papapetropoulos A, Toliver-Kinsky T, et al. Hydrogen sulfide: An endogenous regulator of the immune system. *Pharmacol Res*. 2020;161:105119.

126. Li L, Whiteman M, Moore PK. Dexamethasone inhibits lipopolysaccharide-induced hydrogen sulphide biosynthesis in intact cells and in an animal model of endotoxic shock. *J Cell Mol Med*. 2009;13:2684–2692.

127. Zhang H, Guo C, Wu D, et al. Hydrogen sulfide inhibits the development of atherosclerosis with suppressing CX3CR1 and CX3CL1 expression. *PLoS One*. 2012;7:e41147-.

128. Velmurugan G v, Huang H, Sun H, et al. Depletion of H2S during obesity enhances store-operated Ca2+ entry in adipose tissue macrophages to increase cytokine production. *Sci Signal*. 2015;8:ra128–ra128.

129. Brancaleone V, Mitidieri E, Flower RJ, et al. Annexin A1 mediates hydrogen sulfide properties in the control of inflammation. *J Pharmacol Exp Ther*. 2014;351:96.

130. Oh G-S, Pae H-O, Lee B-S, et al. Hydrogen sulfide inhibits nitric oxide production and nuclear factor-κB via heme oxygenase-1 expression in RAW264.7 macrophages stimulated with lipopolysaccharide. *Free Radic Biol Med*. 2006;41:106–119.

131. Badiei A, Chambers ST, Gaddam RR, et al. Cystathionine-γ-lyase gene silencing with siRNA in monocytes/macrophages attenuates inflammation in cecal ligation and puncture-induced sepsis in the mouse. *J Biosci*. 2016;41:87–95.

132. Gaddam RR, Fraser R, Badiei A, et al. Cystathionine-gamma-lyase gene deletion protects mice against inflammation and liver sieve injury following polymicrobial sepsis. *PLoS One*. 2016;11:e0160521.

133. Badiei A, Muniraj N, Chambers S, et al. Inhibition of hydrogen sulfide production by gene silencing attenuates inflammatory activity by downregulation of NF-κB and MAP kinase activity in LPS-activated RAW 264.7 cells. *Biomed Res Int*. 2014;2014:848570.

134. Badiei A, Rivers-Auty J, Ang AD, et al. Inhibition of hydrogen sulfide production by gene silencing attenuates inflammatory activity of LPS-activated RAW264.7 cells. *Appl Microbiol Biotechnol*. 2013;97:7845–7852.

135. Liu S, Wang X, Pan L, et al. Endogenous hydrogen sulfide regulates histone demethylase JMJD3-mediated inflammatory response in LPS-stimulated macrophages and in a mouse model of LPS-induced septic shock. *Biochem Pharmacol*. 2018;149:153–162.

136. Gobert AP, Latour YL, Asim M, et al. Bacterial pathogens hijack the innate immune response by activation of the reverse transsulfuration pathway. *mBio*. 2019;10:e02174-19.

137. Meng J, LeJeune JT, Zhao T, et al. Enterohemorrhagic *Escherichia coli*. In: Food Microbiology:287–309.

138. Kotloff KL, Nataro JP, Blackwelder WC, et al. Burden and aetiology of diarrhoeal disease in infants and young children in developing countries (the Global Enteric Multicenter Study, GEMS): a prospective, case-control study. *The Lancet*. 2013;382:209–222.

139. Pakbin B, Brück WM, Rossen JWA. Virulence factors of enteric pathogenic *Escherichia coli*: A review. *Int J Mol Sci*. 2021;22:9922.

140. Nataro JP, Kaper JB. Diarrheagenic Escherichia coli. *Clin Microbiol Rev*. 1998;11:142–201.

141. Collins JW, Keeney KM, Crepin VF, et al. *Citrobacter rodentium*: infection, inflammation and the microbiota. *Nat Rev Microbiol*. 2014;12:612–623.

142. Freeman NL, Zurawski D v, Chowrashi P, et al. Interaction of the enteropathogenic *Escherichia coli* protein, translocated intimin receptor (Tir), with focal adhesion proteins. *Cell Motil Cytoskeleton*. 2000;47:307–318.

143. Goosney DL, DeVinney R, Finlay BB. Recruitment of cytoskeletal and signaling proteins to enteropathogenic and enterohemorrhagic *Escherichia coli* pedestals. *Infect Immun*. 2001;69:3315–3322.

144. Ruchaud-Sparagano M-H, Maresca M, Kenny B. Enteropathogenic *Escherichia coli* (EPEC) inactivate innate immune responses prior to compromising epithelial barrier function. *Cell Microbiol*. 2007;9:1909–1921.

145. Zhuang X, Chen Z, He C, et al. Modulation of host signaling in the inflammatory response by enteropathogenic *Escherichia coli* virulence proteins. *Cell Mol Immunol*. 2017;14:237–244.

146. Chloé M-LH, Andrew VB, Angeliki KK, et al. *Escherichia coli* pathobionts associated with inflammatory bowel disease. *Clin Microbiol Rev*. 2019;32:e00060-18.

147. Mancuso G, Midiri A, Gerace E, et al. Bacterial antibiotic resistance: The most critical pathogens. *Pathogens*;10 . Epub ahead of print 2021. DOI: 10.3390/pathogens10101310.

148. Julian D, Dorothy D. Origins and evolution of antibiotic resistance. *Microbiol Mol Biol Rev*. 2010;74:417–433.

149. Burridge K, Connell L. A new protein of adhesion plaques and ruffling membranes. *J Cell Biol*. 1983;97:359–367.

150. Critchley DR. Biochemical and structural properties of the integrin-associated cytoskeletal protein talin. *Annu Rev Biophys*. 2009;38:235–254.

151. Gough RE, Goult BT. The tale of two talins – two isoforms to fine-tune integrin signalling. *FEBS Lett*. 2018;592:2108–2125.

152. Debrand E, Conti FJ, Bate N, et al. Mice carrying a complete deletion of the talin2 coding sequence are viable and fertile. *Biochem Biophys Res Commun*. 2012;426:190–195.

153. Monkley SJ, Zhou X-H, Kinston SJ, et al. Disruption of the talin gene arrests mouse development at the gastrulation stage. *Dev Dyn*. 2000;219:560–574.

154. Kukkurainen S, Azizi L, Zhang P, et al. The F1 loop of the talin head domain acts as a gatekeeper in integrin activation and clustering. *J Cell Sci*. 2020;133:jcs239202.

155. Elliott PR, Goult BT, Kopp PM, et al. The Structure of the talin head reveals a novel extended conformation of the FERM domain. *Structure*. 2010;18:1289–1299.

156. Bosanquet DC, Ye L, Harding KG, et al. FERM family proteins and their importance in cellular movements and wound healing. *Int J Mol Med*. 2014;34:3–12.

157. Calderwood DA, Zent R, Grant R, et al. The talin head domain binds to integrin β subunit cytoplasmic tails and regulates integrin activation. *J Biol Chem*. 1999;274:28071–28074.

158. Klapholz B, Brown NH. Talin – the master of integrin adhesions. *J Cell Sci*. 2017;130:2435–2446.

159. Vinogradova O, Velyvis A, Velyviene A, et al. A structural mechanism of integrin αIIbβ3 "inside-out" activation as regulated by its cytoplasmic face. *Cell*. 2002;110:587–597.

160. Tadokoro S, Shattil SJ, Eto K, et al. Talin binding to integrin ß tails: a final common step in integrin activation. *Science (1979)*. 2003;302:103–106.

161. Kopp PM, Bate N, Hansen TM, et al. Studies on the morphology and spreading of human endothelial cells define key inter-and intramolecular interactions for talin1. *Eur J Cell Biol*. 2010;89:661–673.

162. Zhang X, Jiang G, Cai Y, et al. Talin depletion reveals independence of initial cell spreading from integrin activation and traction. *Nat Cell Biol*. 2008;10:1062–1068.

163. Giannone G, Jiang G, Sutton DH, et al. Talin1 is critical for force-dependent reinforcement of initial integrin–cytoskeleton bonds but not tyrosine kinase activation. *J Cell Biol*. 2003;163:409–419.

164. Hytönen VP, Wehrle-Haller B. Mechanosensing in cell–matrix adhesions – Converting tension into chemical signals. *Exp Cell Res*. 2016;343:35–41.

165. Harburger DS, Calderwood DA. Integrin signalling at a glance. *J Cell Sci*. 2009;122:159–163.

166. Lim TJF, Su I-H. Talin1 methylation is required for neutrophil infiltration and lipopolysaccharide-induced lethality. *J Immunol*. 2018;201:3651.

167. Lim TJF, Bunjamin M, Ruedl C, et al. Talin1 controls dendritic cell activation by regulating TLR complex assembly and signaling. *J Exp Med*. 2020;217:e20191810.

168. Yago T, Petrich BG, Zhang N, et al. Blocking neutrophil integrin activation prevents ischemia–reperfusion injury. *J Exp Med*. 2015;212:1267–1281.

169. Lämmermann T, Bader BL, Monkley SJ, et al. Rapid leukocyte migration by integrin-independent flowing and squeezing. *Nature*. 2008;453:51–55.

170. Singh K, Al-Greene NT, Verriere TG, et al. The L-arginine transporter solute carrier family 7 member 2 mediates the immunopathogenesis of attaching and effacing bacteria. *PLoS Pathog*. 2016;12:e1005984.

171. Wilson KT, Ramanujam KS, Mobley HLT, et al. *Helicobacter pylori* stimulates inducible nitric oxide synthase expression and activity in a murine macrophage cell line. *Gastroenterology*. 1996;111:1524–1533.

172. Gobert AP, McGee DJ, Akhtar M, et al. *Helicobacter pylori* arginase inhibits nitric oxide production by eukaryotic cells: a strategy for bacterial survival. *Proc Natl Acad Sci USA*. 2001;98:13844–13849.

173. Hardbower DM, Singh K, Asim M, et al. EGFR regulates macrophage activation and function in bacterial infection. *J Clin Invest*. 2016;9:3296–3312.

174. Shapouri-Moghaddam A, Mohammadian S, Vazini H, et al. Macrophage plasticity, polarization, and function in health and disease. *J Cell Physiol*. 2018;233:6425–6440.

175. Plummer M, Franceschi S, Vignat J, et al. Global burden of gastric cancer attributable to Helicobacter pylori. *Int J Cancer*. 2015;136:487–490.

176. Mannion A, Dzink-Fox J, Shen Z, et al. *Helicobacter pylori* antimicrobial resistance and gene variants in high- and low-gastric-cancer-risk populations. *J Clin Microbiol*;59 . Epub ahead of print April 2021. DOI: 10.1128/JCM.03203-20.

177. Saracino IM, Pavoni M, Zullo A, et al. Next generation sequencing for the prediction of the antibiotic resistance in *Helicobacter pylori*: A literature review. *Antibiotics (Basel)*;10 . Epub ahead of print April 2021. DOI: 10.3390/antibiotics10040437.

178. Savoldi A, Carrara E, Graham DY, et al. Prevalence of antibiotic resistance in *Helicobacter pylori*: A systematic review and meta-analysis in World Health Organization regions. *Gastroenterology*. 2018;155:1372-1382.e17.

179. Piazuelo MB, Bravo LE, Mera RM, et al. The Colombian Chemoprevention Trial: 20-year follow-up of a cohort of patients with gastric precancerous lesions. *Gastroenterology*. 2021;160:1106-1117.e3.

180. Mera RM, Bravo LE, Camargo MC, et al. Dynamics of *Helicobacter pylori* infection as a determinant of progression of gastric precancerous lesions: 16-year follow-up of an eradication trial. *Gut*. 2018;67:1239–1246.

181. Correa P. Human gastric carcinogenesis: A multistep and multifactorial process-First american cancer society award lecture on cancer epidemiology and prevention. *Cancer Res*. 1992;52:6735–6740.

182. Piazuelo MB, Riechelmann RP, Wilson KT, et al. Resolution of gastric cancer-promoting inflammation: A novel strategy for anti-cancer therapy. *Curr Top Microbiol Immunol*. 2019;421:319–359.

183. Sierra JC, Asim M, Verriere TG, et al. Epidermal growth factor receptor inhibition downregulates *Helicobacter pylori*-induced epithelial inflammatory responses, DNA damage and gastric carcinogenesis. *Gut*. 2018;67:1247–1260.

184. Stoyanov E, Mizrahi L, Olam D, et al. Tumor-suppressive effect of S-adenosylmethionine supplementation in a murine model of inflammation-mediated hepatocarcinogenesis is dependent on treatment longevity. *Oncotarget*. 2017;8:104772–104784.

185. Zabala-Letona A, Arruabarrena-Aristorena A, Martín-Martín N, et al. MTORC1-dependent AMD1 regulation sustains polyamine metabolism in prostate cancer. *Nature*. 2017;547:109–113.

186. Dixon MF, Genta RM, Yardley JH, et al. Classification and grading of gastritis. The updated Sydney System. International Workshop on the Histopathology of Gastritis, Houston 1994. *Am J Surg Pathol*. 1996;20:1161–1181.

187. Chen S, Zhou Y, Chen Y, et al. fastp: an ultra-fast all-in-one FASTQ preprocessor. *Bioinformatics*. 2018;34:i884–i890.

188. Patro R, Duggal G, Love MI, et al. Salmon provides fast and bias-aware quantification of transcript expression. *Nat Methods*. 2017;14:417–419.

189. Love MI, Soneson C, Hickey PF, et al. Tximeta: Reference sequence checksums for provenance identification in RNA-seq. *PLoS Comput Biol*. 2020;16:e1007664.

190. Love MI, Huber W, Anders S. Moderated estimation of fold change and dispersion for RNA-seq data with DESeq2. *Genome Biol*. 2014;15:550.

191. Huang DW, Sherman BT, Lempicki RA. Bioinformatics enrichment tools: Paths toward the comprehensive functional analysis of large gene lists. *Nucleic Acids Res*. 2009;37:1–13.

192. Huang DW, Sherman BT, Lempicki RA. Systematic and integrative analysis of large gene lists using DAVID bioinformatics resources. *Nat Protoc*. 2009;4:44–57.

193. Yu G, Wang L-G, Han Y, et al. clusterProfiler: an R package for comparing biological themes among gene clusters. *OMICS*. 2012;16:284–287.

194. Yu G, Wang L-G, Yan G-R, et al. DOSE: an R/Bioconductor package for disease ontology semantic and enrichment analysis. *Bioinformatics*. 2015;31:608–609.

195. Tautenhahn R, Patti GJ, Rinehart D, et al. XCMS Online: a web-based platform to process untargeted metabolomic data. *Anal Chem*. 2012;84:5035–5039.

196. Haug K, Cochrane K, Nainala VC, et al. MetaboLights: a resource evolving in response to the needs of its scientific community. *Nucleic Acids Res*. 2020;48:D440–D444.

197. Çelik-Uzuner S, Li Y, Peters L, et al. Measurement of global DNA methylation levels by flow cytometry in mouse fibroblasts. *In Vitro Cell Dev Biol Anim*. 2017;53:1–6.

198. Thissen D, Steinberg L, Kuang D. Quick and easy implementation of the Benjamini-Hochberg procedure for controlling the false positive rate in multiple comparisons. *J Educ Behav Stat*. 2002;27:77–83.

199. Perez-Riverol Y, Csordas A, Bai J, et al. The PRIDE database and related tools and resources in 2019: improving support for quantification data. *Nucleic Acids Res*. 2019;47:D442–D450.

200. Schindelin J, Arganda-Carreras I, Frise E, et al. Fiji: an open-source platform for biological-image analysis. *Nat Methods*. 2012;9:676–682.

201. Sierra JC, Piazuelo MB, Luis PB, et al. Spermine oxidase mediates *Helicobacter pylori*-induced gastric inflammation, DNA damage, and carcinogenic signaling. *Oncogene*. 2020;39:4465–4474.

202. Svensson F, Mett H, Persson L. CGP 48664, a potent and specific S-adenosylmethionine decarboxylase inhibitor: effects on regulation and stability of the enzyme. *Biochem*. 1997;322:297–302.

203. Asimakopoulou A, Panopoulos P, Chasapis CT, et al. Selectivity of commonly used pharmacological inhibitors for cystathionine β synthase (CBS) and cystathionine γ lyase (CSE). *Br J Pharmacol*. 2013;169:922–932.

204. Rahman MA, Cumming BM, Addicott KW, et al. Hydrogen sulfide dysregulates the immune response by suppressing central carbon metabolism to promote tuberculosis. *Proc Natl Acad Sci USA*. 2020;117:6663–6674.

205. Lee H, Kho H-S, Chung J-W, et al. Volatile sulfur compounds produced by *Helicobacter pylori*. *J Clin Gastroenterol*. 2006;40:421–426.

206. Yoon S-Y, Hong GH, Kwon H-S, et al. S-adenosylmethionine reduces airway inflammation and fibrosis in a murine model of chronic severe asthma via suppression of oxidative stress. *Exp Mol Med*. 2016;48:e236–e236.

207. Jain N, Shahal T, Gabrieli T, et al. Global modulation in DNA epigenetics during pro-inflammatory macrophage activation. *Epigenetics*. 2019;14:1183–1193.

208. Travers M, Brown SM, Dunworth M, et al. DFMO and 5-azacytidine increase M1 macrophages in the tumor microenvironment of murine ovarian cancer. *Cancer Res*. 2019;79:3445–3454.

209. Tan H-Y, Wang N, Li S, et al. The reactive oxygen species in macrophage polarization: Reflecting its dual role in progression and treatment of human diseases. *Oxid Med Cell Longev*. 2016;2016:2795090.

210. Wang P, Geng J, Gao J, et al. Macrophage achieves self-protection against oxidative stress-induced ageing through the Mst-Nrf2 axis. *Nat Commun*. 2019;10:755.

211. Mowat AM, Agace WW. Regional specialization within the intestinal immune system. *Nat Rev Immunol*. 2014;14:667–685.

212. Lebeis SL, Sherman MA, Kalman D. Protective and destructive innate immune responses to enteropathogenic *Escherichia coli* and related A/E pathogens. *Future Microbiol*. 2008;3:315–328.

213. Jin H, Su J, Garmy-Susini B, et al. Integrin α4β1 promotes monocyte trafficking and angiogenesis in tumors. *Cancer Res*. 2006;66:2146–2152.

214. Weerasinghe D, McHugh KP, Ross FP, et al. A role for the αvβ3 integrin in the transmigration of monocytes. *J Cell Biol*. 1998;142:595–607.

215. Schittenhelm L, Hilkens CM, Morrison VL. β2 integrins as regulators of dendritic cell, monocyte, and macrophage function. *Front Immunol*. 2017;1866.

216. Gobert AP, Al-Greene NT, Singh K, et al. Distinct immunomodulatory effects of spermine oxidase in colitis induced by epithelial injury or infection. *Front Immunol*. 2018;9:1242.

217. Mathew S, Palamuttam RJ, Mernaugh G, et al. Talin regulates integrin β1-dependent and -independent cell functions in ureteric bud development. *Development*. 2017;144:4148–4158.

218. Shi J, Hua L, Harmer D, et al. Cre driver mice targeting macrophages. In: Rousselet G (ed) Macrophages: Methods and Protocols. New York, NY: Springer New York:263–275.

219. Clausen BE, Burkhardt C, Reith W, et al. Conditional gene targeting in macrophages and granulocytes using LysMcre mice. *Transgenic Res*. 1999;8:265–277.

220. Latour YL, Sierra JC, Finley JL, et al. Cystathionine γ-lyase exacerbates *Helicobacter pylori* immunopathogenesis by promoting macrophage metabolic remodeling and activation. *JCI Insight*. 2022;7:e155338.

221. Latour YL, Sierra JC, McNamara KM, et al. Ornithine decarboxylase in gastric epithelial cells promotes the immunopathogenesis of *Helicobacter pylori* infection. *J Immunol*. 2022;209:796–805.

222. Luperchio SA, Schauer DB. Molecular pathogenesis of *Citrobacter rodentium* and transmissible murine colonic hyperplasia. *Microbes Infect*. 2001;3:333–340.

223. Barthold SW, Coleman GL, Bhatt PN, et al. The etiology of transmissible murine colonic hyperplasia. *Lab Anim Sci*. 1976;26:889–894.

224. Silberger DJ, Zindl CL, Weaver CT. Citrobacter rodentium: a model enteropathogen for understanding the interplay of innate and adaptive components of type 3 immunity. *Mucosal Immunol*. 2017;10:1108–1117.

225. Khan MA, Ma C, Knodler LA, et al. Toll-like receptor 4 contributes to colitis development but not to host defense during *Citrobacter rodentium* infection in mice. *Infect Immun*. 2006;74:2522–2536.

226. Gibson DL, Ma C, Rosenberger CM, et al. Toll-like receptor 2 plays a critical role in maintaining mucosal integrity during *Citrobacter rodentium*-induced colitis. *Cell Microbiol*. 2008;10:388–403.

227. Vallance BA, Deng W, Knodler LA, et al. Mice lacking T and B lymphocytes develop transient colitis and crypt hyperplasia yet suffer impaired bacterial clearance during *Citrobacter rodentium* infection. *Infect Immun*. 2002;70:2070–2081.

228. Chan JM, Bhinder G, Sham HP, et al. CD4+ T cells drive goblet cell depletion during *Citrobacter rodentium* infection. *Infect Immun*. 2013;81:4649–4658.

229. Zheng Y, Valdez PA, Danilenko DM, et al. Interleukin-22 mediates early host defense against attaching and effacing bacterial pathogens. *Nat Med*. 2008;14:282–289.

230. Matsunaga Y, Wanek A, Song K, et al. IL-17 receptor and IL-22 receptor signaling in *Citrobacter rodentium* infection. *J Immunol*. 2019;202:192.1.

231. Basu R, O'Quinn DB, Silberger DJ, et al. Th22 cells are an important source of IL-22 for host protection against enteropathogenic bacteria. *Immunity*. 2012;37:1061–1075.

232. Zindl CL, Witte SJ, Laufer VA, et al. A nonredundant role for T cell-derived interleukin 22 in antibacterial defense of colonic crypts. *Immunity*. 2022;55:494-511.e11.

233. Singh S, D'mello V, Henegouwen P van B en, et al. A NPxY-independent β5 integrin activation signal regulates phagocytosis of apoptotic cells. *Biochem Biophys Res Commun*. 2007;364:540–548.

234. Lim J, Wiedemann A, Tzircotis G, et al. An essential role for talin during αMβ2-mediated phagocytosis. *Mol Biol Cell*. 2007;18:976–985.
235. Wernimont SA, Wiemer AJ, Bennin DA, et al. Contact-dependent T cell activation and T cell stopping require talin1. *J Immunol*. 2011;187:6256.
236. Allaire JM, Crowley SM, Law HT, et al. The intestinal epithelium: central coordinator of mucosal immunity. *Trends Immunol*. 2018;39:677–696.
237. Finlay BB, Rosenshine I, Donnenberg MS, et al. Cytoskeletal composition of attaching and effacing lesions associated with enteropathogenic *Escherichia coli* adherence to HeLa cells. *Infect Immun*. 1992;60:2541–2543.
238. Cantarelli V v, Takahashi A, Yanagihara I, et al. Talin, a host cell protein, interacts directly with the translocated intimin receptor, Tir, of enteropathogenic *Escherichia coli*, and is essential for pedestal formation. *Cell Microbiol*. 2001;3:745–751.
239. Singh K, Al-Greene NT, Verriere TG, et al. The L-arginine transporter solute carrier family 7 member 2 mediates the immunopathogenesis of attaching and effacing bacteria. *PLoS Pathog*. 2016;12:e1005984.
240. Petrich BG, Marchese P, Ruggeri ZM, et al. Talin is required for integrin-mediated platelet function in hemostasis and thrombosis. *J Exp Med*. 2007;204:3103–3111.
241. Rutlin M, Rastelli D, Kuo WT, et al. The Villin1 gene promoter drives Cre recombinase expression in extraintestinal tissues. *Cell Mol Gastroenterol Hepatol*. 2020;10:864.
242. Whitehead RH, VanEeden PE, Noble MD, et al. Establishment of conditionally immortalized epithelial cell lines from both colon and small intestine of adult H-2Kb-tsA58 transgenic mice. *Proc Natl Acad Sci USA*. 1993;90:587–591.
243. Gobert AP, Finley JL, Latour YL, et al. Hypusination orchestrates the antimicrobial response of macrophages. *Cell Rep*. 2020;33:108510.
244. Watson AJM, Hughes KR. TNF-α–induced intestinal epithelial cell shedding: implications for intestinal barrier function. *Ann N Y Acad Sci*. 2012;1258:1–8.
245. Wang P, Ballestrem C, Streuli CH. The C terminus of talin links integrins to cell cycle progression. *J Cell Biol*. 2011;195:499–513.
246. Campellone KG, Rankin S, Pawson T, et al. Clustering of Nck by a 12-residue Tir phosphopeptide is sufficient to trigger localized actin assembly. *J Cell Biol*. 2004;164:407–416.
247. Deng W, Vallance BA, Li Y, et al. *Citrobacter rodentium* translocated intimin receptor (Tir) is an essential virulence factor needed for actin condensation, intestinal colonization and colonic hyperplasia in mice. *Mol Microbiol*. 2003;48:95–115.
248. Barker N, van de Wetering M, Clevers H. The intestinal stem cell. *Genes Dev*. 2008;22:1856–1864.
249. Lopez CA, Miller BM, Rivera-Chávez F, et al. Virulence factors enhance *Citrobacter rodentium* expansion through aerobic respiration. *Science (1979)*. 2016;353:1249–1253.
250. Kaemmerer E, Kuhn P, Schneider U, et al. Beta-7 integrin controls enterocyte migration in the small intestine. *World J Gastroenterol*. 2015;21:1759.
251. Parker A, Maclaren OJ, Fletcher AG, et al. Cell proliferation within small intestinal crypts is the principal driving force for cell migration on villi. *The FASEB Journal*. 2017;31:636–649.
252. Zhang X, Jiang G, Cai Y, et al. Talin depletion reveals independence of initial cell spreading from integrin activation and traction. *Nat Cell Biol*. 2008;10:1062–1068.
253. Rankin CR, Hilgarth RS, Leoni G, et al. Annexin A2 regulates β1 integrin internalization and intestinal epithelial cell migration. *J Biol Chem*. 2013;288:15229–15239.

254. Kaufmann SHE. Immunology's coming of age. *Front Immunol*;10 Available from: https://www.frontiersin.org/articles/10.3389/fimmu.2019.00684. 2019.

255. Lefort CT, Rossaint J, Moser M, et al. Distinct roles for talin-1 and kindlin-3 in LFA-1 extension and affinity regulation. *Blood*. 2012;119:4275–4282.

256. Shi J, Hua L, Harmer D, et al. Cre Driver Mice Targeting Macrophages. In: Rousselet G (ed) Macrophages: Methods and Protocols. New York, NY: Springer New York:263–275.

257. Wang TC, Dangler CA, Chen D, et al. Synergistic interaction between hypergastrinemia and Helicobacter infection in a mouse model of gastric cancer. *Gastroenterology*. 2000;118:36–47.

258. Yang X, Xia R, Yue C, et al. ATF4 regulates CD4(+) T cell immune responses through metabolic reprogramming. *Cell Rep*. 2018;23:1754–1766.

259. Quirós PM, Prado MA, Zamboni N, et al. Multi-omics analysis identifies ATF4 as a key regulator of the mitochondrial stress response in mammals. *J Cell Biol*. 2017;216:2027–2045.

260. Sha LK, Sha W, Kuchler L, et al. Loss of Nrf2 in bone marrow-derived macrophages impairs antigen-driven CD8+ T cell function by limiting GSH and Cys availability. *Free Radic Biol Med*. 2015;83:77–88.

261. Kanai Y, Hediger MA. The glutamate/neutral amino acid transporter family SLC1: molecular, physiological and pharmacological aspects. *Pflugers Arch*. 2004;447:469–479.

262. Lewerenz J, Hewett SJ, Huang Y, et al. The cystine/glutamate antiporter system x(c)(-) in health and disease: from molecular mechanisms to novel therapeutic opportunities. *Antioxid Redox Signal*. 2013;18:522–555.

263. Yan Z, Banerjee R. Redox remodeling as an immunoregulatory strategy. *Biochemistry*. 2010;49:1059–1066.

264. Mansoor MA, Svardal AM, Ueland PM. Determination of the in vivo redox status of cysteine, cysteinylglycine, homocysteine, and glutathione in human plasma. *Anal Biochem*. 1992;200:218–229.

265. Garg SK, Yan Z, Vitvitsky V, et al. Differential dependence on cysteine from transsulfuration versus transport during T cell activation. *Antioxid Redox Signal*. 2011;15:39–47.

266. Srivastava MK, Sinha P, Clements VK. Myeloid-derived suppressor cells inhibit T-cell activation by depleting cystine and cysteine. *Canc Res*. 2010;70:68–77.

267. Angelini G, Gardella S, Ardy M, et al. Antigen-presenting dendritic cells provide the reducing extracellular microenvironment required for T lymphocyte activation. *Proc Natl Acad Sci USA*. 2002;99:1491 LP – 1496.
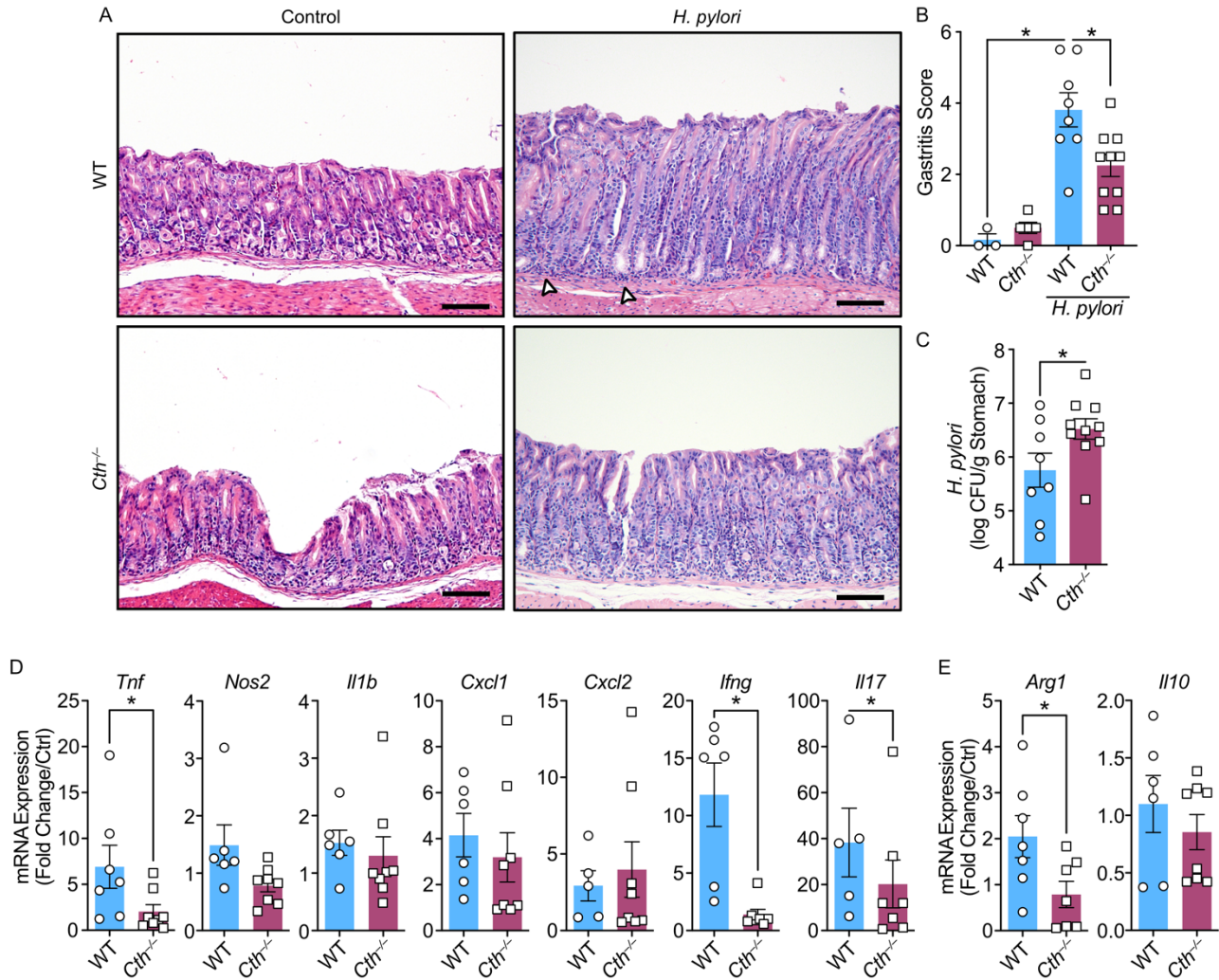
Supplementary Figures for Chapter 2

Figure 1. *Cth$^{-/-}$* **mice exhibit decreased inflammation that is associated with decreased inflammatory gene expression.** WT and *Cth$^{-/-}$* mice were infected or not with *H. pylori* PMSS1 for 4 wk. (A) Representative H&E images of the gastric tissue. (B) Histologic gastritis scores, each symbol is a different mouse. (C) *H. pylori* colonization in gastric tissues from *B*. mRNA expression of (D) Proinflammatory, and (E) antiinflammatory genes were assessed in the gastric tissues of WT and *Cth$^{-/-}$* mice by RT-real-time PCR, *n* = 3-5 uninfected and 5-9 infected mice per genotype. All values are means ± SEM. Statistical analyses where shown: (B), (D), and (E) One-way ANOVA with Kruskal-Wallis test, followed by a Mann-Whitney *U* test; (C) Student's *t* test; *$p < 0.05$, **$p < 0.01$, and ***$p < 0.001$. Scale bars in (A), 50 μm.
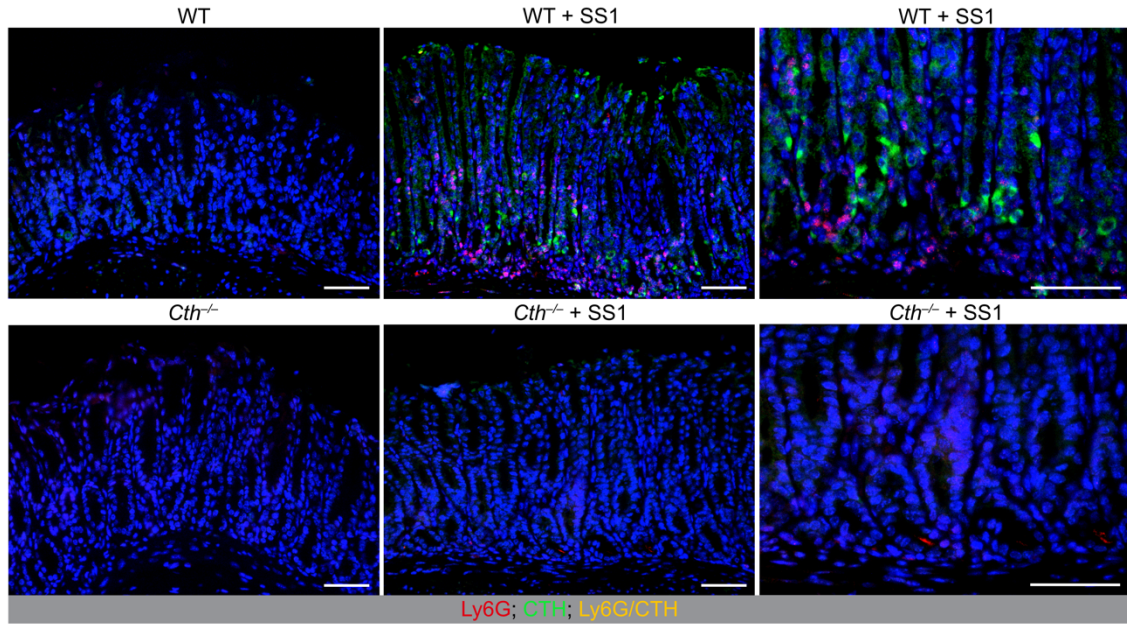
Figure 2. Gastric neutrophils do not express CTH. Representative immunofluorescence images of gastric tissues from WT and *Cth*$^{-/-}$ mice infected or not with *H. pylori* SS1 for 16 wk; *n* = 3 mice per genotype. CTH (green); Ly6G (red); DAPI (blue). Scale bars; 50 μm.
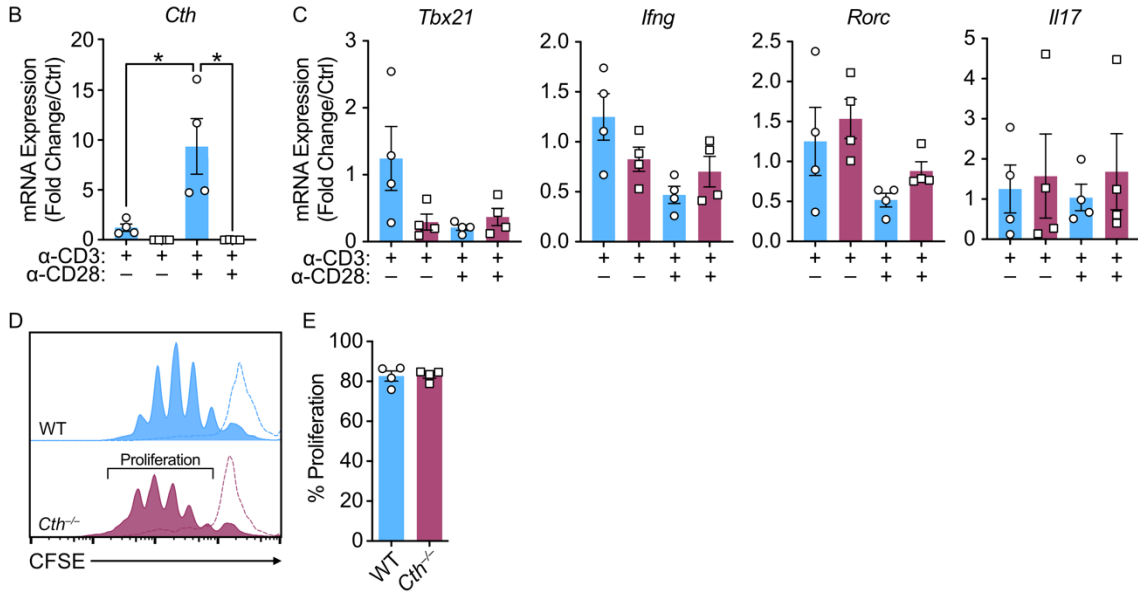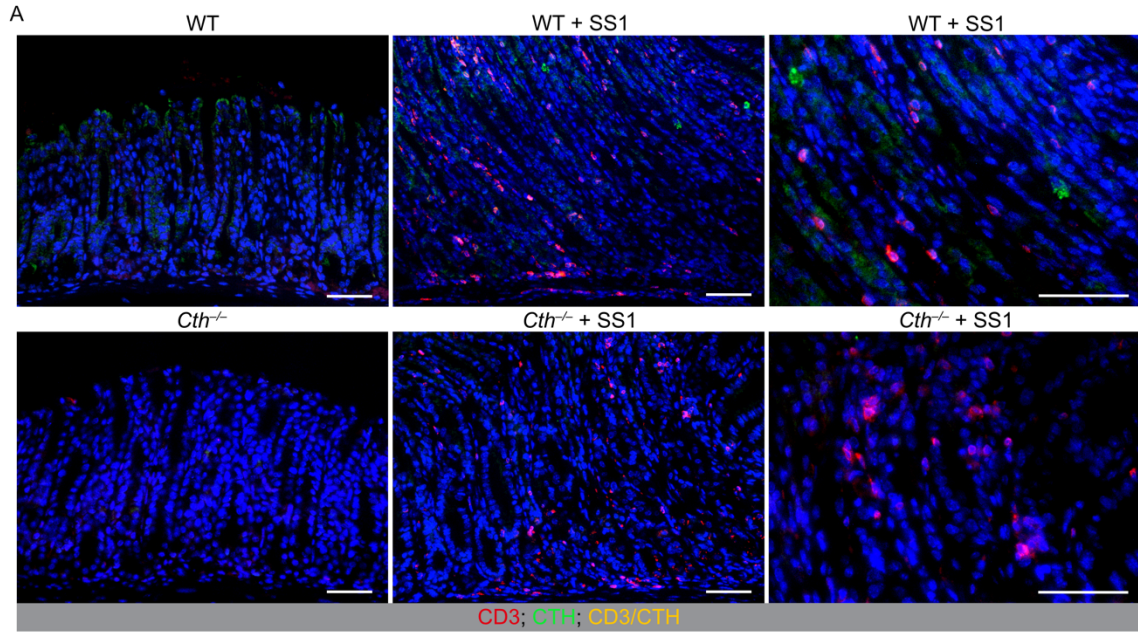
Figure 3. Gastric T lymphocytes do not exhibit induced expression of CTH, and CD4+ T cells do not rely on CTH for activation. (A) Representative immunofluorescence images of gastric tissues from WT and *Cth⁻/⁻* mice infected or not with *H. pylori* SS1 for 16 wk; *n* = 3 mice per genotype. CTH (green); CD3 (red); DAPI (blue). (B-E) Naïve CD4+ splenocytes were isolated from WT and *Cth⁻/⁻*. Cells were activated with α-CD3 or α-CD3+α-CD28 for 72 h; *n* = 4 mice per genotype. (B) mRNA expression of *Cth*. (C) mRNA expression of Th1 and Th17 transcription factors and cytokines. (D) Representative plot and (E) and quantification of proliferation as a percent of CFSE positive cells below baseline. Scale bars in (A), 50 μm.

119
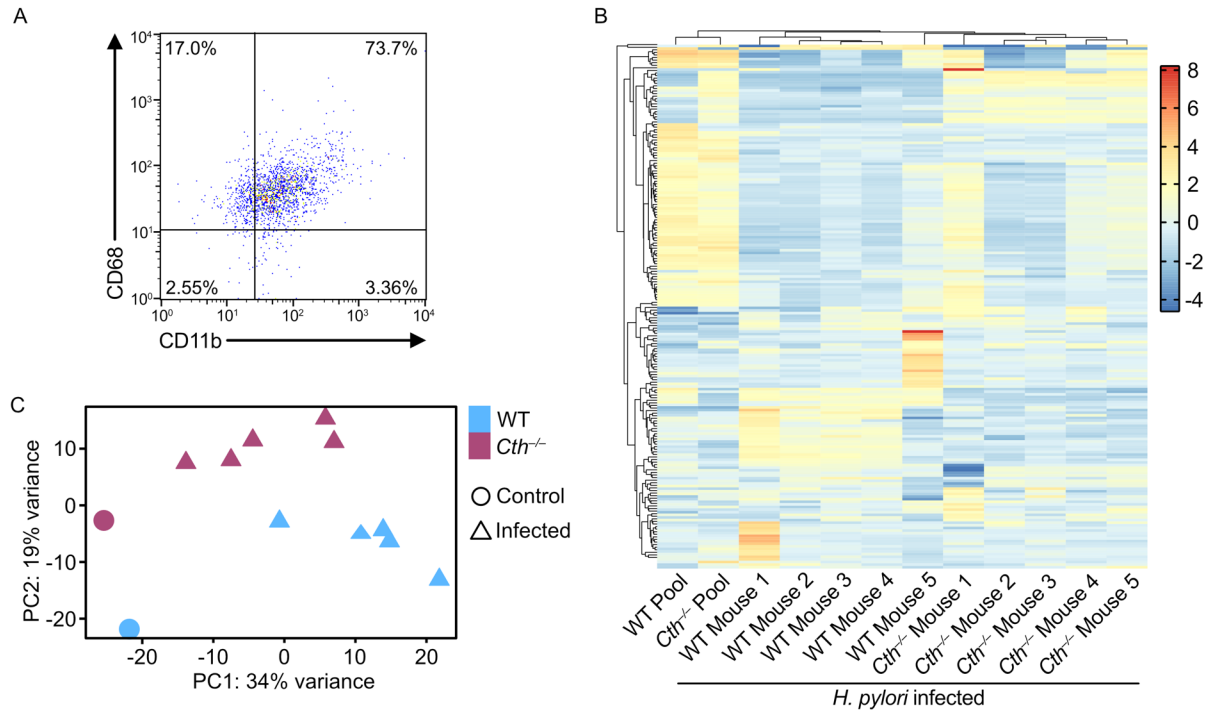
Figure 4. RNA sequencing of F4/80+-enriched gastric macrophages. (A) Representative plot of CD68 and CD11b expression from cells post-F4/80 positive selection from the gastric lamina propria. (B) Top 200 most variable genes at 16 wk p.i. with *H. pylori* SS1, *n* = pooled cells from uninfected mice and 5 individual infected mice per genotype. (C) PCA showing separate overall distribution between samples with different genotypes and infection status.
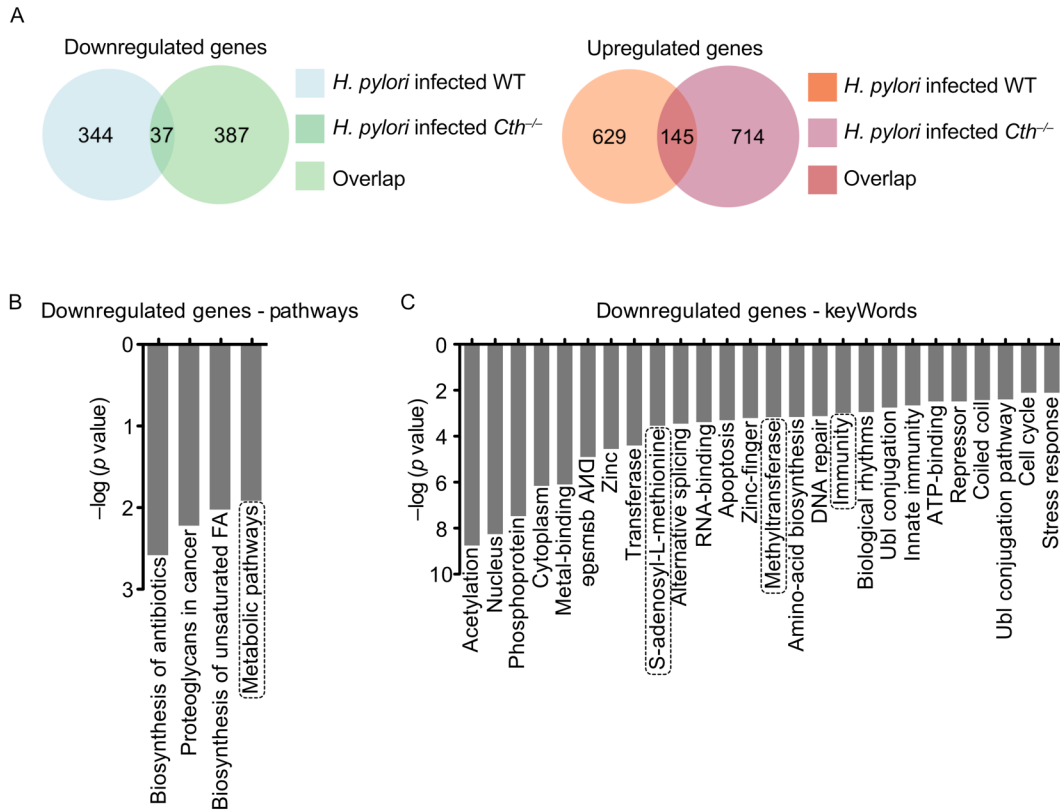
Figure 5. Pathway analysis of DEGs downregulated by *H. pylori* infection using DAVID. (A) Venn diagrams showing abundance of commonly downregulated and upregulated genes in infected WT and *Cth*$^{-/-}$ mice compared to uninfected controls. (B) Significantly downregulated KEGG pathways. (C) Significantly downregulated KeyWords.
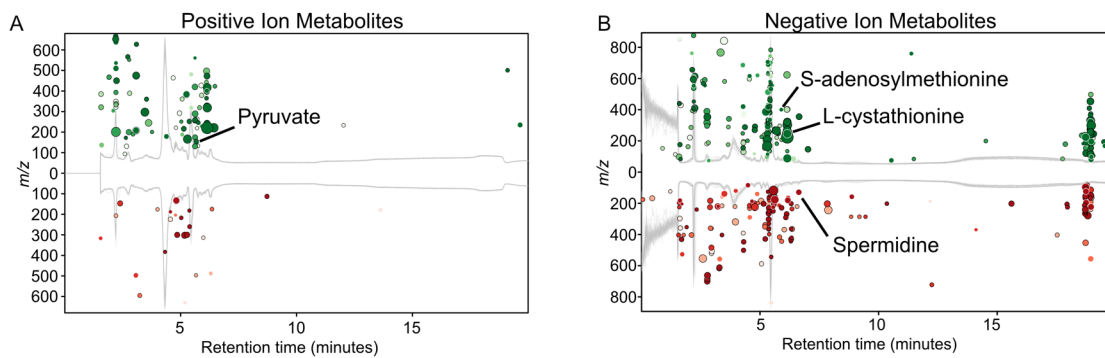
Figure 6. Untargeted metabolomics and polyamine levels of WT and *Cth*^{−/−} gastric tissues. Metabolomic analysis of gastric tissues from WT and *Cth*^{−/−} mice at 8 wk p.i. with *H. pylori* PMSS1, *n* = 8 *H. pylori* PMSS1-infected mice per genotype. Cloud plots for the (A) positive ion and (B) negative ion metabolites downregulated (red) and upregulated (green) generated using XCMS. The x-axis represents the retention time, and the y-axis represents mass-to-charge ration (m/z). The fold change and *p* value are represented by dot size and shade, respectively.
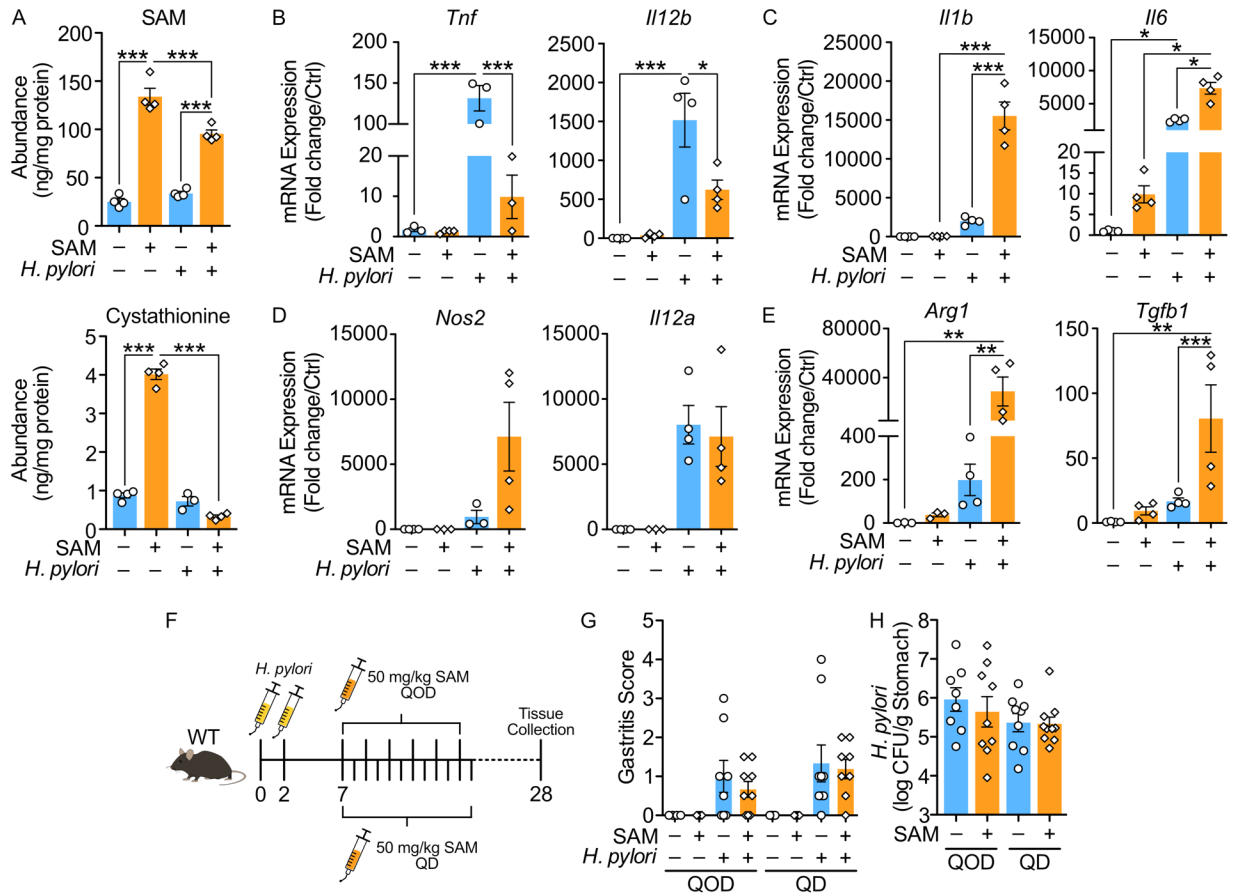
Figure 7. SAM treatment does not confer protection against *H. pylori*-induced gastritis. (A) SAM and cystathionine levels in BMmacs 24 h p.i. with *H. pylori* ± 0.5 mM SAM; *n* = 4 biological replicates. Expression of proinflammatory genes (B) decreased, (C) increased, and (D) unchanged by SAM treatment 24 h p.i. with *H. pylori*, *n* = 4 biological replicates. (E) Expression of antiinflammatory genes increased with by SAM treatment treatment 24 h p.i. with *H. pylori*, *n* = 4 biological replicates. (F) C57BL/6 mice infected or not with *H. pylori* PMSS1 ± 50 mg/kg SAM every other day (QOD) or every day (QD) for 4 wk; *n* = 9-10 infected mice per treatment. (G) Histologic gastritis scores. (H) *H. pylori* colonization in gastric tissues from *G*. All values are means ± SEM. Statistical analyses where shown: (A-C) and (E) One-way ANOVA with Kruskal-Wallis test, followed by a Mann-Whitney *U* test; *$p < 0.05$, **$p < 0.01$, and ***$p < 0.001$.
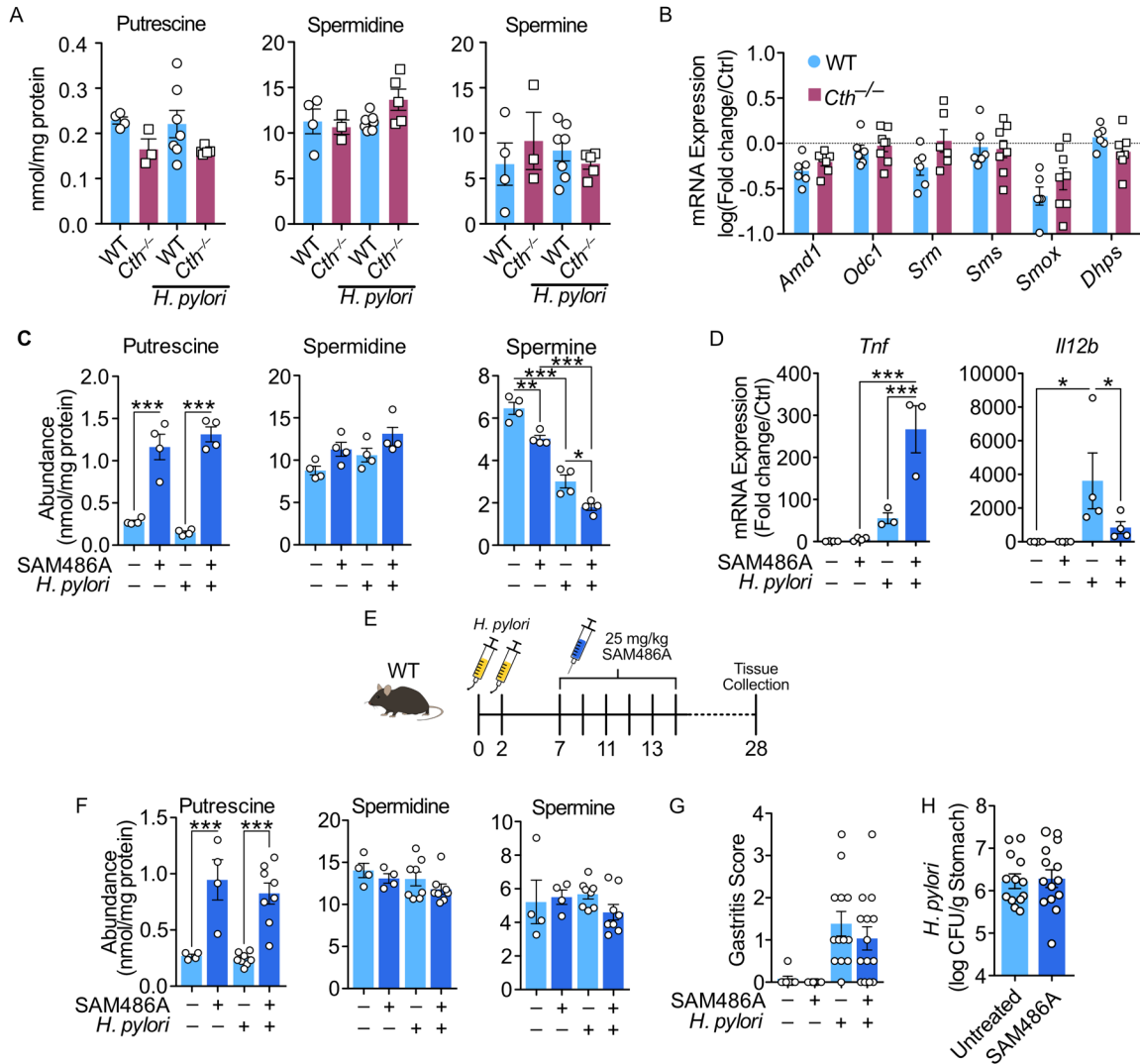
Figure 8. SAM486A treatment does not confer protection against *H. pylori*-induced gastritis. (A) Polyamine levels were measured by LC-MS in the gastric tissues of WT and *Cth*^{-/-} mice at 16 wk p.i. with *H. pylori* SS1, *n* = 3-4 uninfected and 5-6 *H. pylori* SS1-infected mice per genotype. (B) mRNA expression of enzymes involved in polyamine biosynthesis and metabolism in the gastric tissues of WT and *Cth*^{-/-} mice at 4 wk p.i. with *H. pylori* PMSS1, *n* = 3-5 uninfected and 6-8 infected mice per genotype. (C) Polyamine levels in BMmacs 24 h p.i. with *H. pylori* ± 1 μM SAM486A; *n* = 4 biological replicates. (D) Gene expression of proinflammatory genes upregulated by SAM486A treatment 24 h p.i. with *H. pylori*; *n* = 4 biological replicates. (E) C57BL/6 mice infected or not with *H. pylori* PMSS1 ± 5 mg/kg SAM486A for 4 wk; n = 4-6 uninfected and 8-10 infected mice per treatment from 2 independent experiments. (F) Polyamine levels in gastric tissues; n = 4 uninfected and 8 infected mice per treatment. (G) Histologic gastritis scores. (H) *H. pylori* colonization of in gastric tissues in *G* All values are means ± SEM. Statistical analyses where shown: (C) and (F), One-way ANOVA with Newman-Keuls post hoc test; (D), One-way ANOVA with Kruskal-Wallis test, followed by a Mann-Whitney *U* test; *p < 0.05, **p < 0.01, and ***p < 0.001.
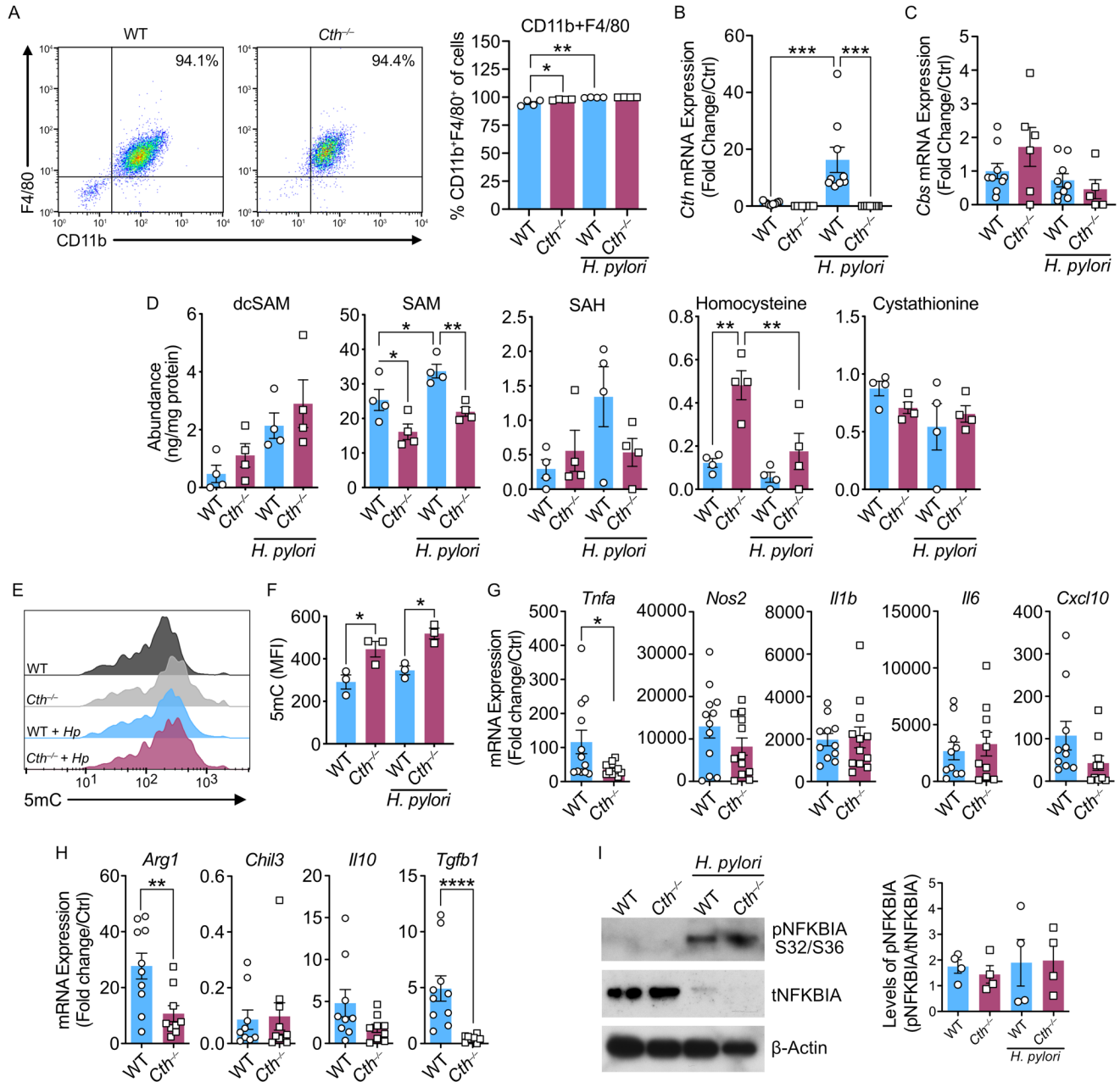
Figure 9. (A) Representative plot of uninfected cells and quantification of the precent of CD11b⁺F4/80⁺ cells shown in Figure 6B, $n = 4$ biological replicate per genotype. (B) Expression of *Cth* by WT and *Cth*⁻/⁻ BMmacs 24 h p.i. with *H. pylori*, $n = 9$ biological replicates from 3 independent experiments (WT are the same as in Figure 6A). (C) Expression of *Cbs* by WT and *Cth*⁻/⁻ BMmacs 24 h p.i. with *H. pylori*, $n = 6$-9 biological replicates from 3 independent experiments. (D) Abundance of metabolites shown in Figure 6C. $n = 4$ biological replicates. (E) Representative plot of WT and *Cth*⁻/⁻ BMmacs stained with 5mC 24 h p.i. with *H. pylori*. (F) Quantification of the MFI in *E*. $n = 3$ biological replicates per genotype. mRNA expression of proinflammatory (G) and antiinflammatory (H) genes by WT and *Cth*⁻/⁻ BMmacs 24 h p.i. with *H. pylori*, $n = 4$-10 biological replicates per genotype from 3 independent experiments. (I) pNFKBIA immunoblots and densitometric analysis of WT and *Cth*⁻/⁻ BMmacs 30 min p.i. with *H. pylori*, $n = 3$-4 biological replicates from 2 independent experiments. All values are means ± SEM. Statistical analyses where shown: One-way ANOVA with Newman-Keuls test, followed by a Mann-Whitney *U* test; *$p < 0.05$, **$p < 0.01$, ***$p < 0.001$.
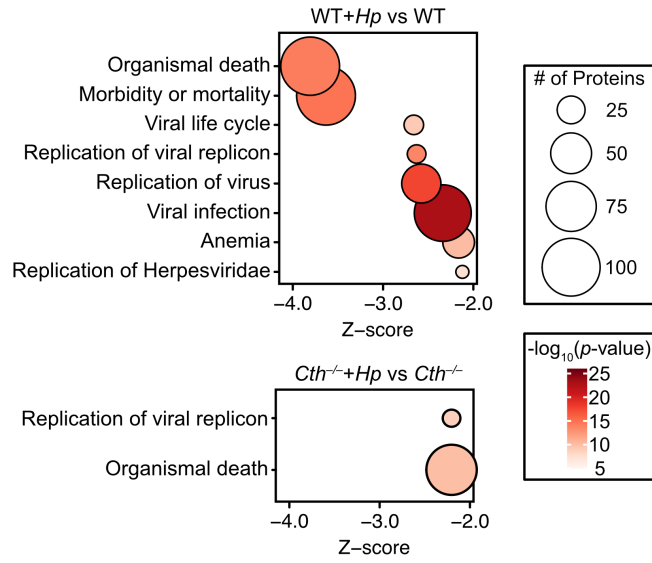
Figure 10. Proteomic pathways downregulated by *H. pylori* infection in BMmacs. Enrichment analysis of pathways inhibited by *H. pylori* infection in WT and *Cth*$^{-/-}$ BMmacs., *n* = 4 biological replicates per genotype. (FDR <0.05, z-score <-2).
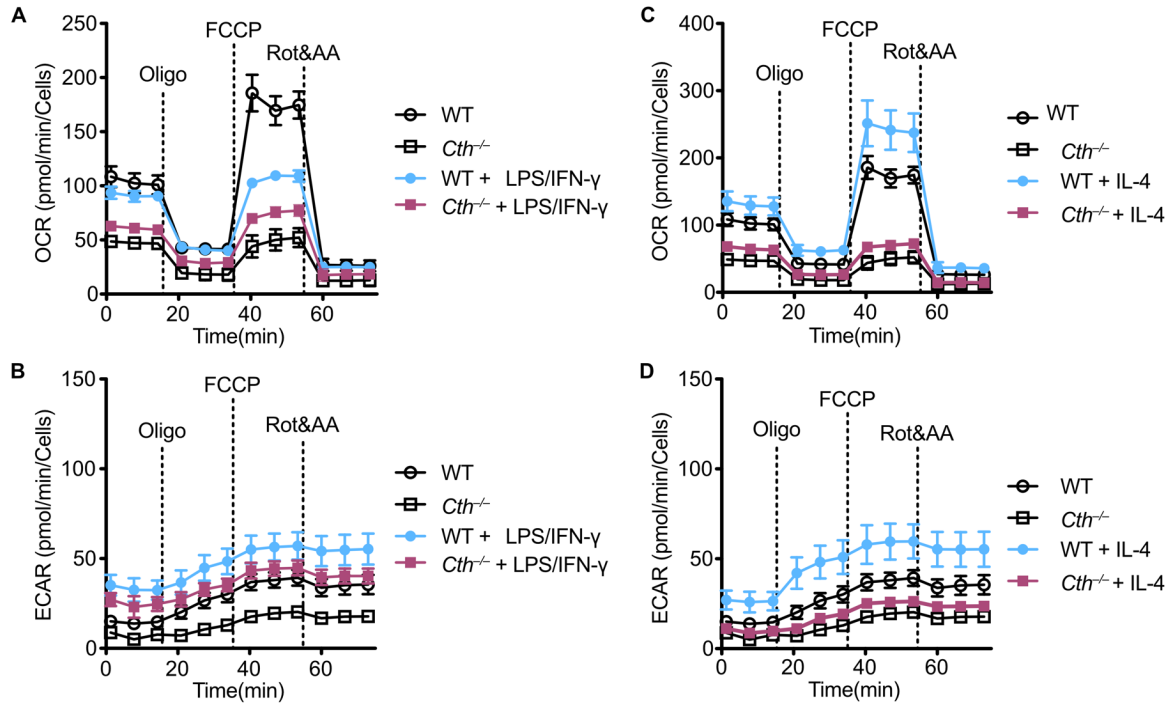
Figure 11. Cellular respiration of classically stimulated WT and *Cth*$^{-/-}$ BMmacs. (A-B) WT and *Cth*$^{-/-}$ BMmacs stimulated with LPS (10 ng/mL) and IFNγ (200 U/mL). (A) Oxygen consumption rate and (B) extracellular acidification rate assessed 24 h post-stimulation, *n* = 5 from 2 independent experiments. (C-D) WT and *Cth*$^{-/-}$ BMmacs stimulated with IL-4 (10 ng/mL). (C) Oxygen consumption rate and (D) extracellular acidification rate assessed 24 h post-stimulation, *n* = 5 from 2 independent experiments. Vertical dashed lines indicated the sequential addition of oligomycin (Oligo), FCCP, and Rot/AA (The controls are the same as in Figure 9). All values are means ± SEM.
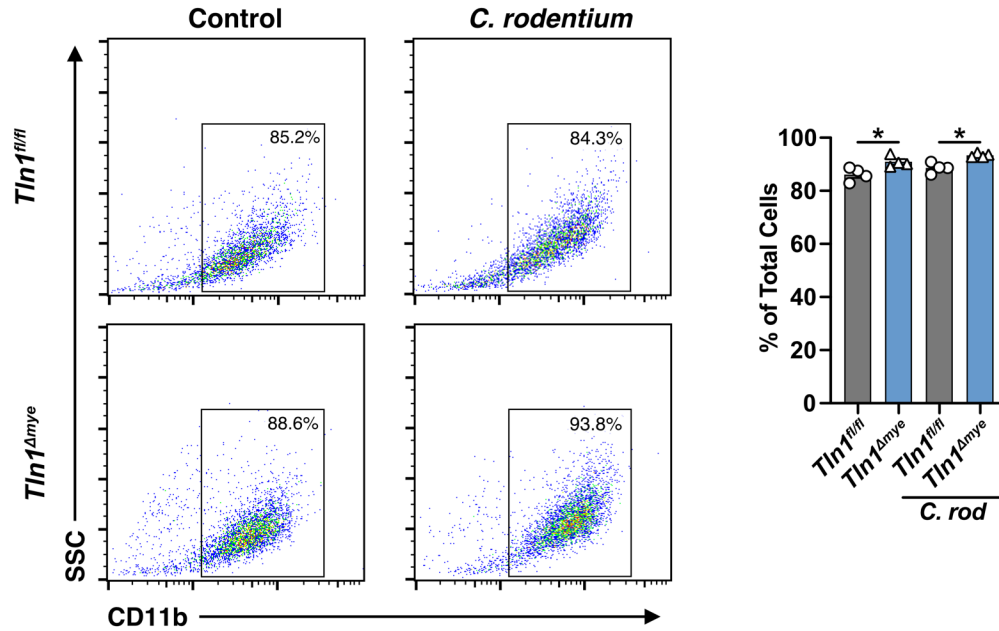
Supplementary Figures for Chapter 3

Figure 1. The surface expression of CD11b. Representative flow plots and graph depicting the surface expression and percent of CD11b-expressing BMmacs derived from *Tln1$^{fl/fl}$* and *Tln1$^{\Delta mye}$* mice. All values are reported as mean ± SEM. *$P<0.05$ determined by 1-way ANOVA and Tukey post hoc test.

APPENDIX C

Ornithine Decarboxylase in Gastric Epithelial Cells Promotes the Immunopathogenesis of

Helicobacter pylori Infection

The original publication (listed below) is included as a PDF, as it relates to the immunopathogenesis of *H. pylori* infection.

Latour YL*, Sierra JC*, McNamara KM, Smith TM, Luis PB, Schneider C, Delgado AG, Barry DP, Allaman MM, Calcutt MW, Schey KL, Piazuelo MB, Gobert AP, Wilson KT. (2022). Ornithine Decarboxylase in Gastric Epithelial Cells Promotes the Immunopathogenesis of *Helicobacter pylori* Infection. *J Immunol.* 209 (4) 796-805. doi: 10.4049/jimmunol.2100795; PMID: 35896340; PMCID: PMC9378675.

*These authors contributed equally to this work and are co-first authors

The Journal *of* Immunology

This information is current as of August 19, 2022.

Ornithine Decarboxylase in Gastric Epithelial Cells Promotes the Immunopathogenesis of *Helicobacter pylori* Infection

Yvonne L. Latour, Johanna C. Sierra, Kara M. McNamara, Thaddeus M. Smith, Paula B. Luis, Claus Schneider, Alberto G. Delgado, Daniel P. Barry, Margaret M. Allaman, M. Wade Calcutt, Kevin L. Schey, M. Blanca Piazuelo, Alain P. Gobert and Keith T. Wilson

---

Supplementary Material	http://www.jimmunol.org/content/suppl/2022/07/27/jimmunol.2100795.DCSupplemental
References	This article **cites 47 articles**, 10 of which you can access for free at: http://www.jimmunol.org/content/209/4/796.full#ref-list-1

Why *The JI*? Submit online.

- **Rapid Reviews! 30 days*** from submission to initial decision

- **No Triage!** Every submission reviewed by practicing scientists

- **Fast Publication!** 4 weeks from acceptance to publication

*average

Subscription	Information about subscribing to *The Journal of Immunology* is online at: http://jimmunol.org/subscription
Permissions	Submit copyright permission requests at: http://www.aai.org/About/Publications/JI/copyright.html
Email Alerts	Receive free email-alerts when new articles cite this article. Sign up at: http://jimmunol.org/alerts

---

Ornithine Decarboxylase in Gastric Epithelial Cells Promotes the Immunopathogenesis of *Helicobacter pylori* Infection

Yvonne L. Latour,*,†,1 Johanna C. Sierra,*,‡,1 Kara M. McNamara,*,§ Thaddeus M. Smith,* Paula B. Luis,¶ Claus Schneider,¶ Alberto G. Delgado,* Daniel P. Barry,* Margaret M. Allaman,* M. Wade Calcutt,∥ Kevin L. Schey,∥ M. Blanca Piazuelo,*,‡ Alain P. Gobert,*,‡ and Keith T. Wilson*,†,‡,§,#

Colonization by *Helicobacter pylori* is associated with gastric diseases, ranging from superficial gastritis to more severe pathologies, including intestinal metaplasia and adenocarcinoma. The interplay of the host response and the pathogen affect the outcome of disease. One major component of the mucosal response to *H. pylori* is the activation of a strong but inefficient immune response that fails to control the infection and frequently causes tissue damage. We have shown that polyamines can regulate *H. pylori*–induced inflammation. Chemical inhibition of ornithine decarboxylase (ODC), which generates the polyamine putrescine from ʟ-ornithine, reduces gastritis in mice and adenocarcinoma incidence in gerbils infected with *H. pylori*. However, we have also demonstrated that *Odc* deletion in myeloid cells enhances M1 macrophage activation and gastritis. Here we used a genetic approach to assess the specific role of gastric epithelial ODC during *H. pylori* infection. Specific deletion of the gene encoding for ODC in gastric epithelial cells reduces gastritis, attenuates epithelial proliferation, alters the metabolome, and downregulates the expression of immune mediators induced by *H. pylori*. Inhibition of ODC activity or *ODC* knockdown in human gastric epithelial cells dampens *H. pylori*–induced NF-κB activation, *CXCL8* mRNA expression, and IL-8 production. Chronic inflammation is a major risk factor for the progression to more severe pathologies associated with *H. pylori* infection, and we now show that epithelial ODC plays an important role in mediating this inflammatory response. *The Journal of Immunology*, 2022, 209: 796–805.

Infection by *Helicobacter pylori* is the main risk factor for the development of gastric cancer (1), and the inflammatory response induced by this bacterium is considered necessary for the progression to gastric adenocarcinoma (2). Strategies proposed to reduce gastric cancer mortality include global antibiotic eradication and early detection through upper gastrointestinal endoscopy (3, 4). However, both interventions face challenges, including the increased occurrence of antibiotic resistance in *H. pylori* and the cost-effectiveness of screening a significant portion of the population at risk in areas of high gastric cancer incidence (5, 6). Complementary strategies that limit the inflammatory response induced by *H. pylori* may improve disease outcomes for infected individuals.

Polyamines are generated through a process that starts with the synthesis of putrescine from ʟ-ornithine by the action of the rate-limiting enzyme ornithine decarboxylase (ODC) (7, 8). Then, putrescine is sequentially transformed to spermidine and spermine by spermidine synthase and spermine synthase, respectively (7). Polyamines are pleiotropic molecules that have major functions in embryogenesis, homeostasis, and aging (9–11). In addition, polyamines contribute to the regulation of the immune response during inflammation and infection, notably by altering histone modifications and chromatin structure and thus transcription of inducible effectors (12–14). Furthermore, these molecular alterations can also affect DNA stability, and the global metabolism of polyamines has also been shown to support cell proliferation and oxidative damage (15, 16), thus favoring cell transformation and, potentially, carcinogenesis (8, 17). In this context, the ODC inhibitor difluoromethylornithine (DFMO) represents a promising potential treatment or chemopreventive for various cancers, including neuroblastoma, colorectal cancer, or gastric adenocarcinoma in high-risk *H. pylori*–infected populations (16, 18–21).

*Division of Gastroenterology, Hepatology, and Nutrition, Department of Medicine, Vanderbilt University Medical Center, Nashville, TN; †Department of Pathology, Microbiology, and Immunology, Vanderbilt University School of Medicine, Nashville, TN; ‡Center for Mucosal Inflammation and Cancer, Vanderbilt University Medical Center, Nashville, TN; §Program in Cancer Biology, Vanderbilt University School of Medicine, Nashville, TN; ¶Department of Pharmacology, Vanderbilt University School of Medicine, Nashville, TN; ∥Department of Biochemistry, Mass Spectrometry Research Center, Vanderbilt University School of Medicine, Nashville, TN; and #Veterans Affairs Tennessee Valley Healthcare System, Nashville, TN

1Y.L.L. and J.C.S. contributed equally to this work.

ORCIDs: 0000-0001-9347-0009 (K.M.M.); 0000-0001-6729-1023 (P.B.L.); 0000-0003-4215-967X (C.S.); 0000-0002-3972-3914 (D.P.B.); 0000-0002-2803-1365 (M.M.A.); 0000-0002-8002-4699 (M.W.C.); 0000-0001-7535-539X (A.P.G.); 0000-0003-4421-1830 (K.T.W.).

Received for publication August 13, 2021. Accepted for publication June 6, 2022.

This work was supported by National Institutes of Health Grants R21AI142042, R01CA190612, P01CA116087, P01CA028842, and R01DK128200 (K.T.W.); U.S. Department of Veterans Affairs Merit Review Grants I01BX001453 and I01CX002171 (K.T.W.); U.S. Department of Defense Grants W81XWH-18-1-0301 and W81XWH-21-1-0617 (K.T.W.); the Thomas F. Frist Sr. Endowment (K.T.W.); and the Vanderbilt Center for Mucosal Inflammation and Cancer (K.T.W.). Y.L.L. was supported by National Institutes of Health Grant T32AI138932, and K.M.M. was supported by National Institutes of Health Grant T32CA009592. Metabolomic analysis was supported in part by core scholarships from the Vanderbilt University Medical Center Digestive Disease Research Center funded by National Institutes of Health Grant P30DK058404 and Vanderbilt-Ingram Cancer Center Support Grant P30CA068485.

The RNA-sequencing data presented in this article have been submitted to the Gene Expression Omnibus repository (https://www.ncbi.nlm.nih.gov/geo/) using accession number GSE181917. The metabolomic data presented in this article have been submitted to MetaboLights (https://www.ebi.ac.uk/metabolights/) under accession number MTBLS3235.

Address correspondence and reprint requests to Dr. Keith T. Wilson, Division of Gastroenterology, Hepatology, and Nutrition, Department of Medicine, Vanderbilt University Medical Center, Room 1030C MRBIV, 2215 Garland Avenue, Nashville, TN 37232. E-mail address: keith.wilson@vumc.org

The online version of this article contains supplemental material.

Abbreviations used in this article: DFMO, difluoromethylornithine; GEC, gastric epithelial cell; MPO, myeloperoxidase; ODC, ornithine decarboxylase; PMSS1, premouse Sydney strain 1.

We have previously shown that mice with specific deletion in myeloid cells of the gene encoding for ODC, *Odc1*, hereafter termed *Odc*, exhibit increased gastric inflammation and reduced colonization in response to *H. pylori* (13); this is associated with increased polarization of macrophages toward an M1 phenotype (13). However, the specific contribution of ODC in gastric epithelial cells (GECs) to *H. pylori* pathogenesis remains unknown. To test this, we infected mice with specific deletion of the *Odc* gene in GECs and found that epithelial ODC supports *H. pylori* pathogenesis.

Materials and Methods

Model of H. pylori *infection*

C57BL/6 *Odc1^{fl/fl}* mice were crossed with C57BL/6 *Foxa3^{cre/+}* mice containing a single copy of the *Foxa3-cre^{1Khk}* transgene (13, 22). The resulting *Odc1^{+/fl}; Foxa3^{cre/+}* mice were backcrossed once more with *Odc1^{fl/fl}* mice to create *Odc1^{fl/fl};Foxa3^{+/+}* and *Odc1^{fl/fl};Foxa3^{+/cre}* (*Odc^{Δepi}*) mice. Mice were housed in a specific pathogen-free facility with ventilated cage racks and on a 12-h/12-h light/dark cycle. Littermate *Odc^{fl/fl}* and *Odc^{Δepi}* male mice (aged 6 to 12 wk) were provided continuous water, fed ad libitum with 5L0D chow (LabDiet), and infected with 10^9 CFU of *H. pylori* premouse Sydney strain 1 (PMSS1), a *cagA^+* strain with intact type IV secretion system function, as reported (23, 24). After 4 or 12 wk, animals were sacrificed. Colonization was assessed by culture of serial dilutions of the gastric tissue lysates (23, 24). Histologic assessment of longitudinal sections of the gastric tissues stained by H&E was performed by a gastrointestinal pathologist (M.B.P.) in a blinded manner using the modified Sydney system (13, 25). The antrum and corpus regions were each scored 0–3 for acute and chronic inflammation, and the scores for antrum and corpus were added together for a 0–12 scale. In the mice infected for 12 wk, the extent of mucous metaplasia, the loss of parietal cells, and the loss of chief cells were assessed on a 0–3 scale (absent, mild, moderate, marked) on H&E-stained sections containing the entire length of the stomach, using a slightly modified system based on Rogers et al (26). Mucous metaplasia is described as the presence of mucus-producing cells with foamy change, predominantly replacing parietal cells. GECs were isolated by dissociation and dispersion as reported (27).

These experiments were approved by the Vanderbilt University Medical Center Institutional Animal Care and Use Committee under protocols M/14/230, M1600091, and M1900067. Procedures followed institutional policies, American Veterinary Medical Association Guidelines of Euthanasia, American Association for the Accreditation of Laboratory Animal Care guidelines, NIH regulations (Guide for the Care and Use of Laboratory Animals), and the United States Animal Welfare Act (1996).

Cells

AGS cells were obtained from American Type Culture Collection and maintained in RPMI 1640 medium supplemented with 10% FBS and 10 mM HEPES. We also used AGS cells expressing a stable luciferase-based NF-κB reporter pGL4.32(luc2P/NF-κB-RE/Hygro; Promega) (28). Cells were treated with 5 mM DFMO for 7 d; DFMO was removed 24 h before the infection with *H. pylori* PMSS1 at a multiplicity of infection of 10. Putrescine (10 μM) was added 24 h before infection.

For transfections, AGS cells maintained in Opti-MEM I Reduced Serum Media (Invitrogen) were transfected with 100 nM ON-TARGETplus siRNAs (Dharmacon) directed against human *ODC* or *LMNA* (used as a control) using Lipofectamine 2000 (Invitrogen). After 16 h, cells were washed and maintained in fresh media for 36 h prior to infection.
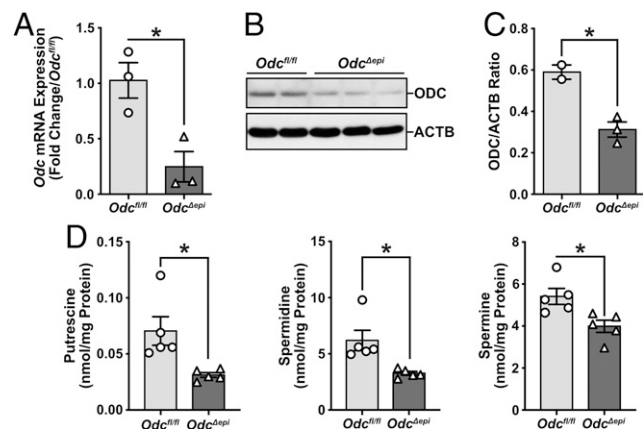

FIGURE 1. ODC expression and polyamine levels in naive mice with specific deletion of *Odc* in GECs. GECs were isolated from the stomach of *Odc^{fl/fl}* and *Odc^{Δepi}* mice. Levels of *Odc* mRNA (**A**), ODC protein (**B**), and polyamines (**D**) were analyzed by real-time PCR, Western blotting, and liquid chromatography–mass spectrometry, respectively; densitometric analysis of the immunoblot is depicted in (**C**); $n = 2$ or 3 mice per genotype. Each symbol is a different mouse. $*p < 0.05$ versus GECs from *Odc^{fl/fl}* mice.
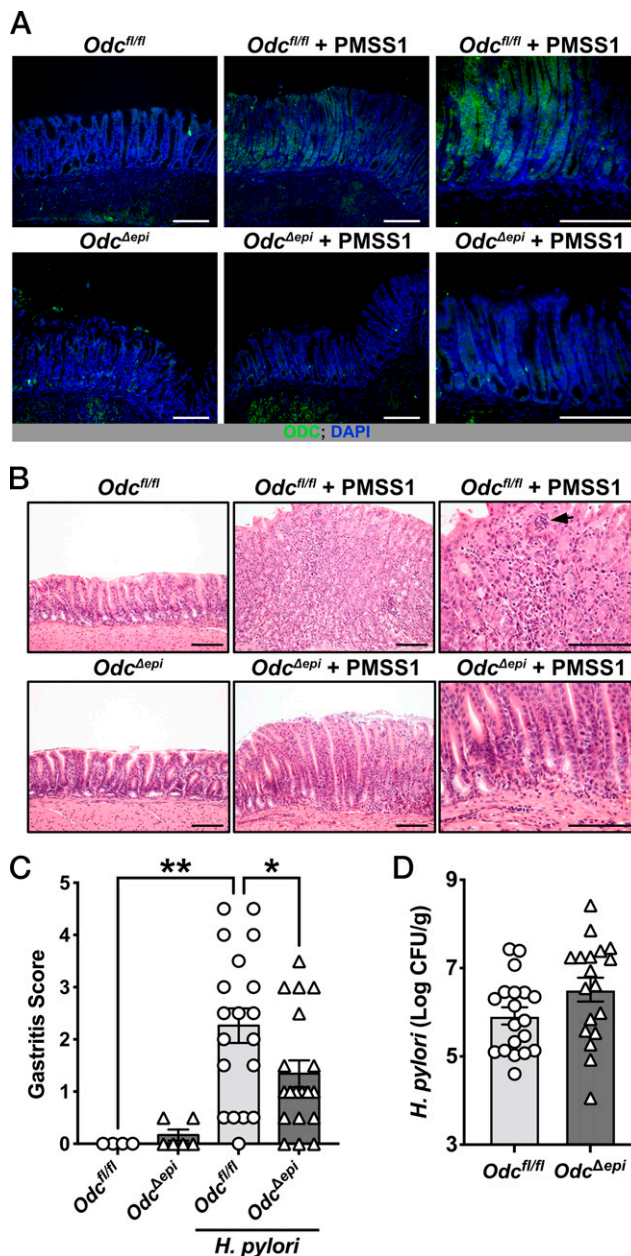

FIGURE 2. Effect of *Odc* deletion in GECs on *H. pylori* pathogenesis. Littermate *Odc^{fl/fl}* and *Odc^{Δepi}* mice were infected with *H. pylori* PMSS1 for 4 wk. (**A**) Representative immunofluorescence images of ODC in gastric tissues of uninfected and infected mice. $n = 5$ mice per group. Note strong DAPI staining of the antral-corpus transition zone in the *Odc^{fl/fl}* mice. (**B**) H&E staining from the gastric tissues of uninfected and infected mice. (**C**) Gastric inflammation scores derived from H&E-stained tissues. $n = 4–6$ uninfected mice and $n = 19$ infected mice per genotype; data pooled from two independent experiments. (**D**) Colonization density was assessed by plating serial dilution of stomach lysates from (C). In (A) and (B), scale bars are 100 μm. $*p < 0.05$, $**p < 0.01$.

NF-κB activation reporter assay

Lysates were prepared using Reporter Lysis Buffer (Promega), then mixed with the Luciferase Assay System (Promega), and luminescence was measured on a Synergy 4 plate reader (BioTek Instruments).

mRNA analysis

Total RNA was isolated from longitudinal sections, encompassing both the antrum and corpus, of gastric tissues using the RNeasy Mini Kit (QIAGEN).

For RNA sequencing, RNA quality control, cDNA libraries, and next-generation sequencing (PE150) were performed using the TapeStation System (Agilent), the NEBNext Ultra II Directional RNA Library Prep kit (New England Biolabs), and Illumina NovaSeq6000 with the NovaSeq 6000 SP Reagent Kit (Illumina), respectively. Adapter sequences were removed, and read quality was checked using *fastp* (29). Transcripts were quantified and mapped to the indexed mouse genome (M23, GRCm38) using *Salmon* (30). Transcript-level quantification was then summarized to the gene level, annotated, and prepared for differential gene expression analysis using the R package *tximeta* (31). The R/Bioconductor package *DESeq2* was then used to identify differentially expressed genes in each condition using a Benjamini-Hochberg test adjusted for false discovery rate (32). Pathway analysis was performed using the DAVID database (Database for Annotation, Visualization, and Integrated Discovery). RNA-sequencing data can be accessed from the Gene Expression Omnibus repository (https://www.ncbi.nlm.nih.gov/geo/) using the accession number GSE181917.

Expression of *Odc*, *Cxcl1*, *Ccl5*, *Ccl3*, *Tnf*, *Ifng*, and *Il17a* was also assessed by real-time PCR as previously described (13, 27).

IL-8 expression

Total RNA was isolated using the RNeasy Mini Kit (QIAGEN) from AGS cells 3 h after infection, and expression of *CXCL8*, the gene that encodes for human IL-8, was assessed by real-time PCR. IL-8 protein levels were determined in AGS cell culture supernatants using the Human IL-8 DuoSet ELISA kit per the manufacturer's instructions (R&D Systems) 6 h after infection. IL-8 concentrations were normalized to the protein concentration of lysed cells from the same well.

Western blot analysis

Protein isolation, electrophoresis separation, transfer to nitrocellulose, and hybridization with rabbit polyclonal anti-ODC Ab (Abcam, 97395; 1:1,000) or a mouse anti-β-actin mAb (Sigma, A1978; 1:10,000) was performed as described (33).

Immunofluorescence

Immunofluorescence staining for ODC was performed as previously described (13) using a rabbit polyclonal anti-ODC (Lisa Shantz, Penn State College of Medicine; and David Feith, University of Virginia; 1:2000) and goat anti-rabbit IgG, Alexa Fluor 488 labeled (Thermo Fisher Scientific, A11008).

Immunohistochemistry and image analysis

Sections of paraffin-embedded tissues were deparaffinized, and Ag retrieval was performed (26). Tissues were incubated with prediluted rabbit polyclonal anti–Ki-67 (Biocare, PRM325AA), prediluted rabbit monoclonal anti-myeloperoxidase (anti-MPO; Biocare, PP023AA), or rabbit polyclonal anti-CD3 (Abcam, ab5690; 1:150) and processed as described (33). Ki-67 slides were imaged and analyzed using a Cytation C10 Confocal Imaging Reader and Gen 5+ software (Agilent BioTek). The average number of MPO- and CD68-positive cells per 5 high-powered fields was quantified by a gastrointestinal pathologist (M.B.P.) in a blinded manner.

Polyamine quantification

The polyamines putrescine, spermidine, and spermine were quantified by liquid chromatography–mass spectrometry as previously described (34).

Metabolomic analysis

Gastric tissues from uninfected and infected mice from each genotype were homogenized and processed as previously described (35). We used XCMS (https://xcmsonline.scripps.edu) to generate chromatographic alignment, peak picking, and statistical comparisons. Metabolomic data have been deposited to MetaboLights (https://www.ebi.ac.uk/metabolights/) with accession number MTBLS3235.

Statistics

Prism 9.3 software (GraphPad Software) was used for statistical analysis, and all the results are expressed as mean ± SEM. Data that were not normally distributed according to the D'Agostino and Pearson normality test were square root transformed, and distribution was reassessed. The Student t test or

ANOVA with the Tukey test was used to determine significant differences between two or multiple groups, respectively. Fisher's exact test was used to determine significant differences between the proportions of two groups.

Results

Reduced gastric inflammation in $Odc^{\Delta epi}$ mice infected with H. pylori

We first found that $Odc^{\Delta epi}$ mice showed a significant reduction in *Odc* mRNA levels (Fig. 1A) and ODC protein expression (Fig. 1B,
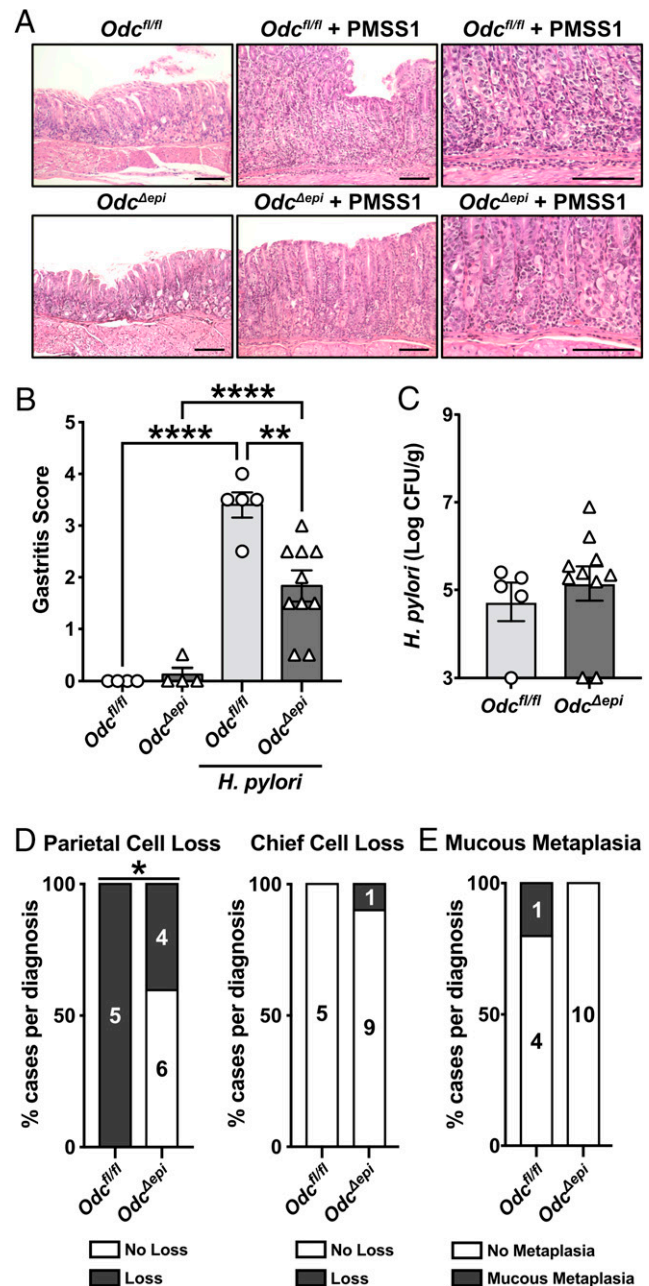

FIGURE 3. Effect of *Odc* deletion in GECs on chronic *H. pylori* pathogenesis. Littermate $Odc^{fl/fl}$ and $Odc^{\Delta epi}$ mice were infected with *H. pylori* PMSS1 for 12 wk. (**A**) H&E staining from the gastric tissues of uninfected and infected mice. (**B**) Gastric inflammation scores derived from H&E-stained tissues. Each symbol is a different mouse; $n = 4$ uninfected mice and $n = 5–10$ infected mice per genotype. (**C**) Colonization density was assessed by plating serial dilution of stomach lysates in B. (**D**) Percentage of cases from B exhibiting no loss or loss of parietal cells and chief cells. (**E**) Percentage of cases from (B) exhibiting mucous metaplasia. In (A), scale bars are 100 μm. *$p < 0.05$, **$p < 0.01$, and ****$p < 0.0001$.

1C) in isolated GECs when compared with littermate $Odc^{fl/fl}$ mice. Polyamine levels in GECs were quantified, and we found a significant reduction in the concentrations of putrescine, spermidine, and spermine in $Odc^{\Delta epi}$ mice compared with $Odc^{fl/fl}$ animals (Fig. 1D).

Next, $Odc^{fl/fl}$ and $Odc^{\Delta epi}$ mice were infected with *H. pylori* strain PMSS1 for 4 wk. We evaluated ODC expression in the gastric mucosa by immunofluorescence. *H. pylori*–infected $Odc^{fl/fl}$ mice exhibited increased expression of ODC throughout the epithelium compared with uninfected mice, which was substantially reduced in the infected $Odc^{\Delta epi}$ mice (Fig. 2A). This confirmed successful knockdown of ODC in the epithelium. Inflammation levels were

evaluated in H&E-stained sections (Fig. 2B). Gastric tissues from $Odc^{fl/fl}$-infected mice exhibited increased epithelial hyperplasia and significant recruitment of immune cells compared with uninfected animals (Fig. 2B). There was an obvious attenuation of inflammation in infected $Odc^{\Delta epi}$ mice (Fig. 2B). Accordingly, when we scored acute and chronic inflammation in the antrum and corpus of infected mice, we found significantly less gastritis in $Odc^{\Delta epi}$ mice than in $Odc^{fl/fl}$ animals (Fig. 2C). However, colonization density was similar between $Odc^{fl/fl}$ and $Odc^{\Delta epi}$ mice (Fig. 2D).

H. pylori–induced disease manifests as chronic active inflammation in infected individuals; therefore, we infected $Odc^{fl/fl}$ and

FIGURE 4. Effect of *Odc* deletion in GECs on cellular proliferation and immune cell infiltration. (**A**) Representative immunohistochemistry images of Ki-67 immunoperoxidase staining and (**B**) quantification of positive nuclei in gastric tissues infected or not with *H. pylori* for 4 wk. $n = 5$ or 6 uninfected mice and $n = 13$–15 infected mice per genotype; data pooled from three independent experiments. (**C**) Representative images of gastric tissues immunoperoxidase-stained for MPO and (**D**) quantification of the number of MPO$^+$ cells per high-power field (H.P.F.). $n = 3$–5 uninfected mice and $n = 5$ or 6 infected mice per genotype; data pooled from three independent experiments. (**E**) Representative images of gastric tissues immunoperoxidase-stained for CD3 and (**F**) quantification of the number of CD3$^+$ T cells per H.P.F. $n = 3$ or 4 uninfected mice and $n = 5$ or 6 infected mice per genotype; data pooled from three independent experiments. In (A), (C), and (E), scale bars are 100 μm. $*p < 0.05$, $**p < 0.01$, $***p < 0.001$.
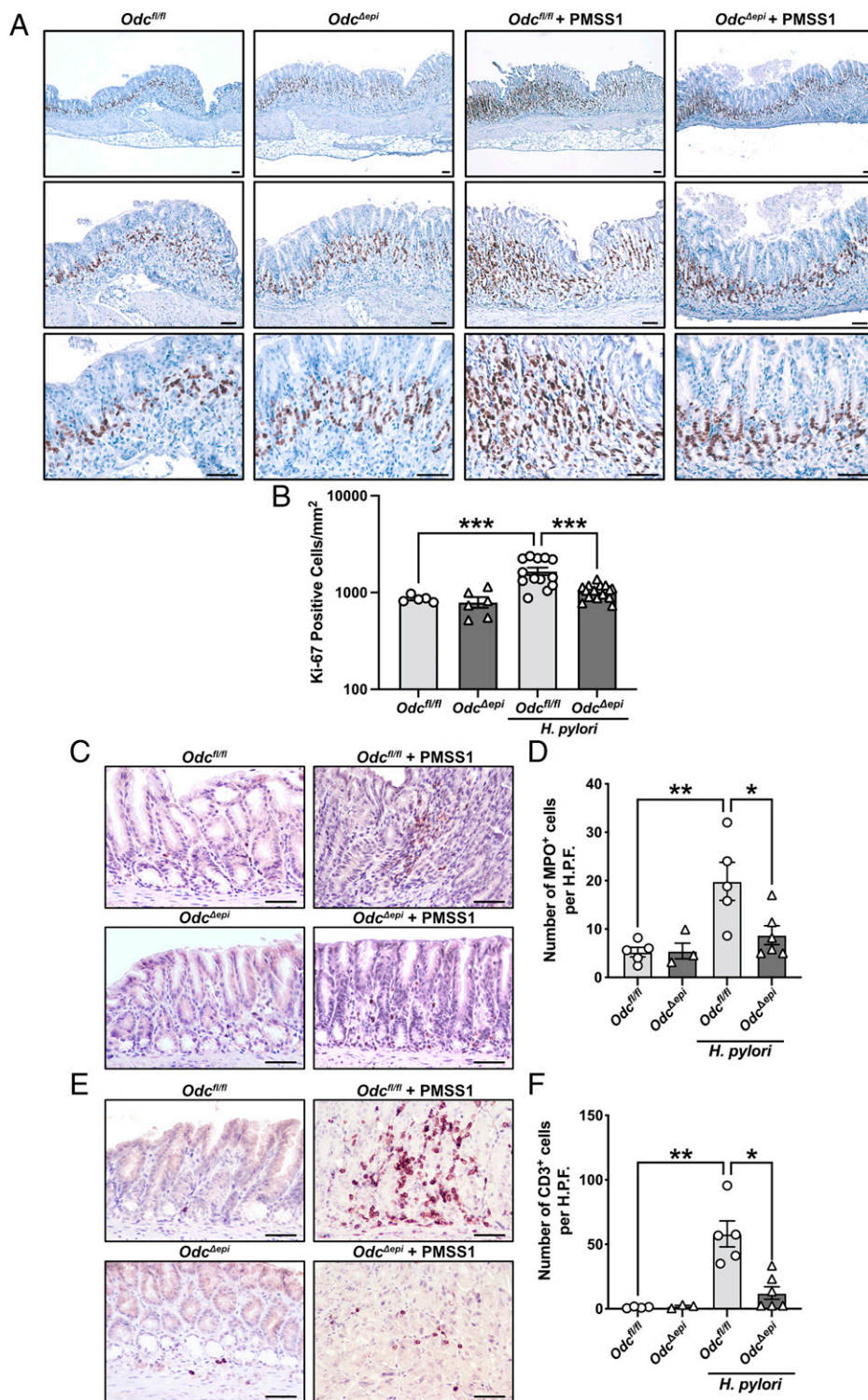
FIGURE 5. Metabolomic changes in gastric tissues affected by *Odc* deletion. Mice were infected or not with *H. pylori* PMSS1. After 4 wk, the metabolome of the gastric tissues was determined by ultra-HPLC. $n = 4$ uninfected mice and $n = 8$ infected mice per genotype. Bubble plots of metabolomic analysis comparing uninfected $Odc^{fl/fl}$ and $Odc^{\Delta epi}$ mice (**A**) and *H. pylori*–infected $Odc^{fl/fl}$ and $Odc^{\Delta epi}$ animals (**B**) were generated using the XCMS website. The full list of pathways is shown in Supplemental Table I. Putrescine, spermidine, and spermine were quantified by liquid chromatography–mass spectrometry in strips of whole-stomach tissues of $Odc^{fl/fl}$ and $Odc^{\Delta epi}$ mice, infected or not with *H. pylori* (**C**). $n = 7$ or 8 uninfected mice and $n = 12$ or 13 infected mice per genotype. **$p < 0.01$, ***$p < 0.001$.
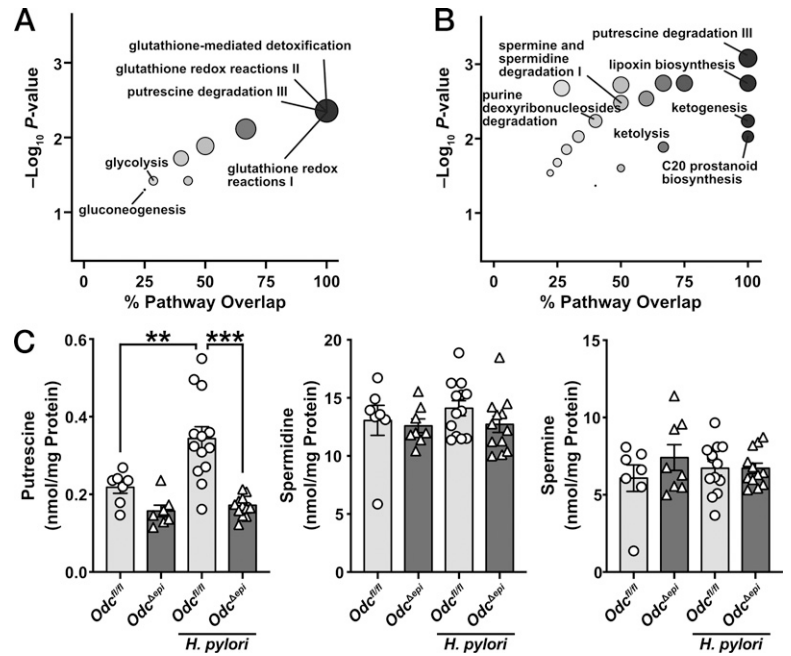
$Odc^{\Delta epi}$ mice for 12 wk to assess the impact of epithelial ODC on chronic gastritis. Similar to our 4-wk model, $Odc^{fl/fl}$ mice exhibited increased inflammation and epithelial hyperplasia compared with uninfected mice, which was attenuated in the $Odc^{\Delta epi}$ mice (Fig. 3A). These findings are reflected in the scored gastric inflammation (Fig. 3B). Additionally, we found no difference in the level of *H. pylori* colonization (Fig. 3C). Loss of parietal cells and loss of chief cells were very mild and predominantly seen in the transitional mucosa of the junction of the antrum and corpus; however, infected $Odc^{\Delta epi}$ mice exhibited significantly less parietal cell loss than infected $Odc^{fl/fl}$ mice (Fig. 3D). Mucous metaplasia, only observed in one $Odc^{fl/fl}$ animal, was mild and located in the proximal corpus (Fig. 3E). There were no observed differences in the epithelium of $Odc^{\Delta epi}$ mice compared with $Odc^{fl/fl}$ mice at baseline.

Reduced gastric hyperplasia and immune infiltration in $Odc^{\Delta epi}$ mice infected with H. pylori

Because polyamines are important for cell survival and inhibition of ODC activity can lead to cytostasis, we evaluated cell proliferation in gastric tissues from $Odc^{fl/fl}$ and $Odc^{\Delta epi}$ mice using immunohistochemistry for Ki-67. There was increased Ki-67 immunostaining of GECs in $Odc^{fl/fl}$ mice infected with *H. pylori* compared with uninfected control animals, and the number of proliferating cells was significantly reduced in *H. pylori*–infected $Odc^{\Delta epi}$ mice (Fig. 4A). These results were confirmed by the quantification of the positive nuclei (Fig. 4B).

To further investigate the alteration in cellular composition and level of inflammation overserved in the gastric mucosa of $Odc^{\Delta epi}$ mice, we assessed the population of MPO-expressing cells (macrophages and neutrophils) and T cells (CD3) by immunohistochemistry. Consistent with the decrease in scored gastric inflammation, infected $Odc^{\Delta epi}$ mice also exhibit a significant decrease in the infiltration of MPO^{+} (Fig. 4C, 4D) and CD3^{+} (Fig. 4E, 4F) cells found in the tissues of infected $Odc^{fl/fl}$ mice.

These data indicate that ODC in GECs controls polyamine levels and supports inflammation and GEC proliferation during *H. pylori* infection.

Metabolic pathways affected by Odc deletion during H. pylori infection

To gain further insight into the functional role of epithelial ODC, we assessed the effect of *Odc* deletion in GECs on the gastric metabolomic signatures of the stomach. We found 282 and 326 metabolites significantly altered (fold change ≥1.5 and $p < 0.05$) by epithelial *Odc* deletion in the gastric tissues of uninfected and *H. pylori*–infected mice, respectively.

Pathway analysis revealed that the putrescine degradation pathway was reduced in $Odc^{\Delta epi}$ gastric tissues at baseline, as expected. We also found that glutathione redox reactions and glycolysis, two pathways potentially related to the propensity for proinflammatory responses (36, 37), were affected in uninfected $Odc^{\Delta epi}$ animals (Fig. 5A; Supplemental Table I). When we compared $Odc^{fl/fl}$ and $Odc^{\Delta epi}$ mice that were infected with *H. pylori*, we also observed a significant downregulation of different polyamine-associated pathways, such as putrescine degradation as well as spermine and spermidine degradation; in addition, the lipoxin biosynthesis pathway, which is known for its anti-inflammatory effects (38, 39), was upregulated in $Odc^{\Delta epi}$ mice (Fig. 5B).

Last, we confirmed by a targeted approach that putrescine concentration was increased in the whole gastric tissues of infected $Odc^{fl/fl}$ mice compared with control animals (Fig. 5C). There was a significant reduction of putrescine to basal levels in *H. pylori*–infected $Odc^{\Delta epi}$ mice (Fig. 5C). However, there was no effect of epithelium-specific *Odc* deletion on the level of spermidine or spermine in the gastric tissues of infected mice (Fig. 5C; Supplemental Table I).

Reduced expression of immune response–associated genes in $Odc^{\Delta epi}$ mice infected with H. pylori

To better understand the effect of epithelial ODC on the transcriptomic changes of gastric tissues during *H. pylori* infection, we performed RNA sequencing from $Odc^{fl/fl}$ and $Odc^{\Delta epi}$ mice. We identified 26,983 sequences in the analysis that comprised 19,084 known genes and 7,899 unknown sequences (Supplemental Table II). The differential expression analysis included genes that were altered twofold or more between the two groups with an adjusted p value <0.05. We found that 148 genes, essentially coding for
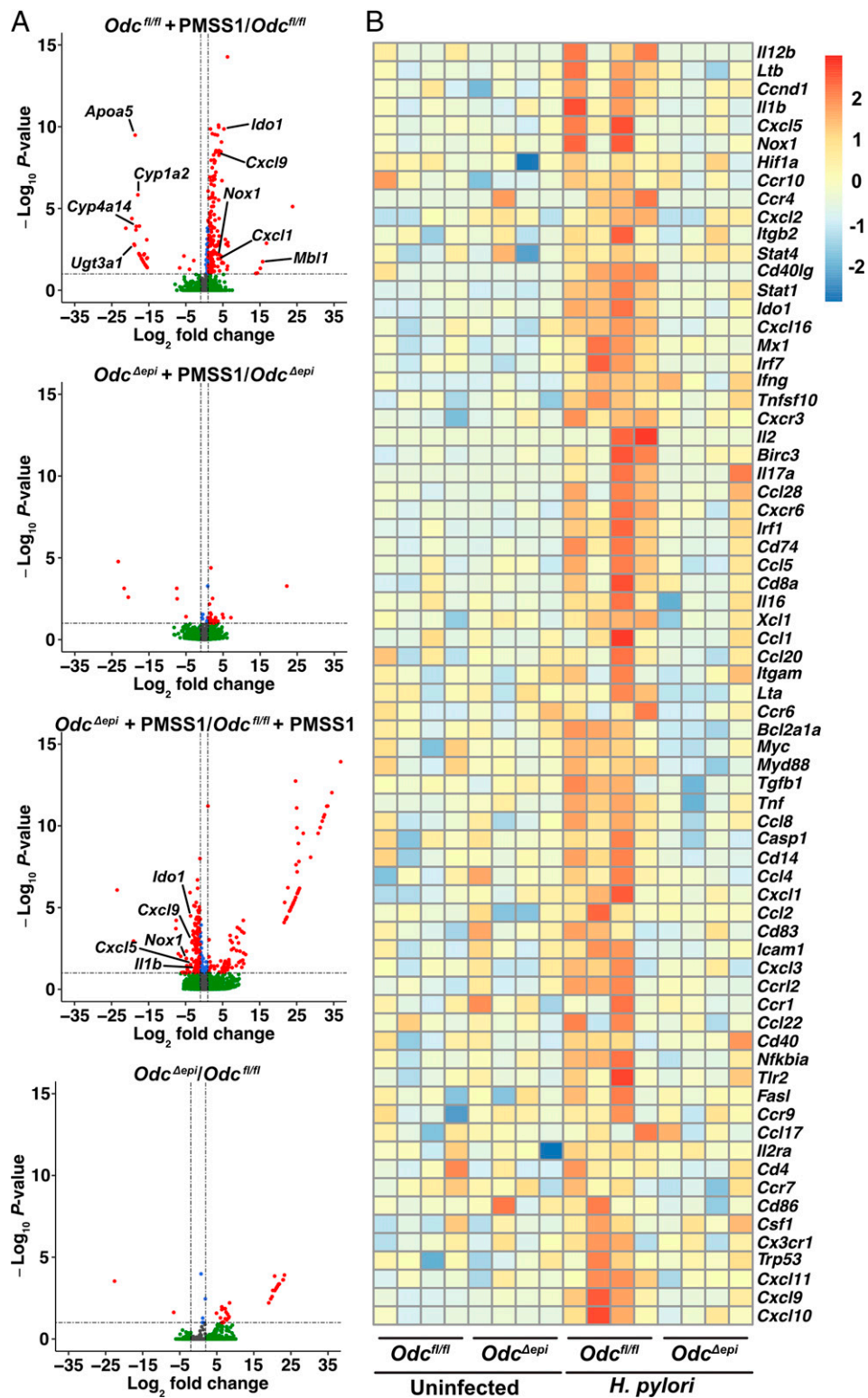
FIGURE 6. Determination of the effect of *Odc* deletion in GECs on the gastric transcriptome. *Odc*^fl/fl^ and *Odc*^Δepi^ mice were infected or not with *H. pylori*. After 4 wk, gastric RNA was analyzed by RNA sequencing. *n* = 4 mice per group. (**A**) Volcano plots for paired comparisons; the full list of differentially expressed genes is shown in Supplemental Table II. (**B**) Heat map representing the level of genes encoding for chemokines, cytokines, and immune effectors.

immune effectors (such as chemokines *Cxcl5* and *Cxcl9* or the defense response-related genes *Mbl1*, *Ido1*, and *Nox1*), were significantly upregulated in infected *Odc*^fl/fl^ mice versus uninfected control animals (Fig. 6A; Supplemental Table II). In addition, 33 genes involved in fatty acid metabolism (*Ugt3a1*, *Apoa5*) or cellular respiration (*Cyp4a14*, *Cyp1a2*) were downregulated with infection (Fig. 6A; Supplemental Table II). In contrast, only 12 and 7 genes were upregulated and downregulated, respectively, in the infected *Odc*^Δepi^ mice compared with the uninfected animals (Fig. 6A; Supplemental

Table II). Thus, when we compared *H. pylori*–infected *Odc*^Δepi^ mice with infected *Odc*^fl/fl^ mice (Fig. 6A; Supplemental Table II), we found 106 genes downregulated, comprising mainly immune effectors (*Il1b*, *Cxcl5*, *Cxcl9*, *Ido1*, and *Nox1*). According to this result, we selectively analyzed the expression of multiple genes involved in the immune response, and we generated the heatmap depicted in Fig. 6B. Overall, cytokines (*Il17a*, *Il1b*, *Il12b*, *Il2*, and *Ifng*), chemokines (*Cxcl3*, *Cxcl19*, *Cxcl10*, *Ccl5*, and *Ccl20*), and immune cell–associated genes (*Ccr4*, *Cxcr6*, *Cd74*, *Cd8a*, *Myd88*, *Cd4*, and
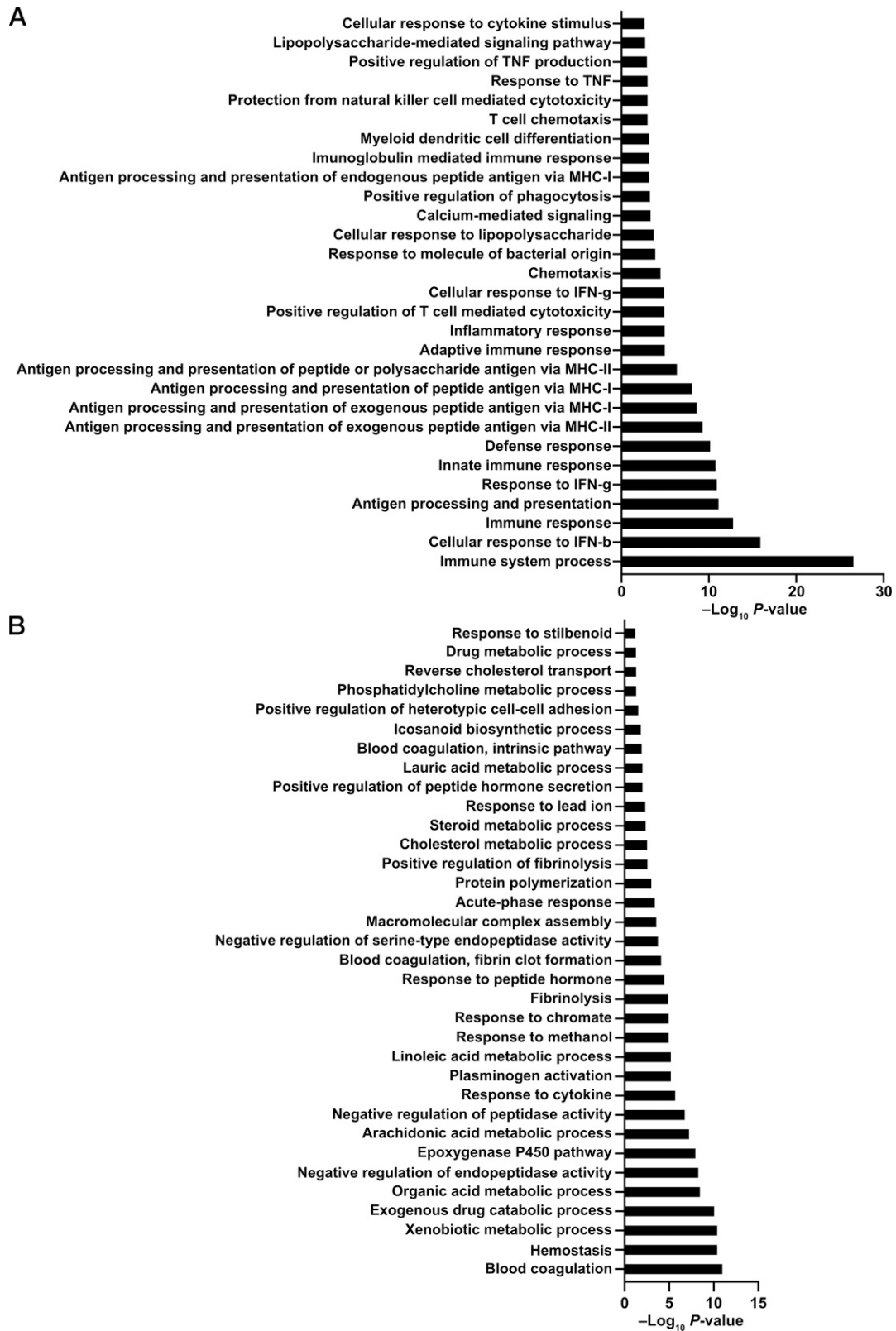
A

B

FIGURE 7. Pathway analysis performed from the transcriptomic analysis, showing the pathways significantly downregulated (**A**) and significantly upregulated (**B**) in the gastric tissues of $Odc^{\Delta epi}$ mice infected with *H. pylori* compared with infected $Odc^{fl/fl}$ animals.

Cd86) exhibited decreased expression in $Odc^{\Delta epi}$ compared with $Odc^{fl/fl}$ mice during infection. Importantly, we identified only 29 genes and 2 unidentified genes upregulated and downregulated, respectively, when comparing uninfected $Odc^{\Delta epi}$ and $Odc^{fl/fl}$ mice without infection (Fig. 6B; Supplemental Table II),

demonstrating that the main transcriptomic changes orchestrated by epithelial ODC occur under pathophysiological conditions and not at the basal level.

Analysis of the differentially expressed genes between $Odc^{fl/fl}$ and $Odc^{\Delta epi}$ mice infected with *H. pylori* using the DAVID software
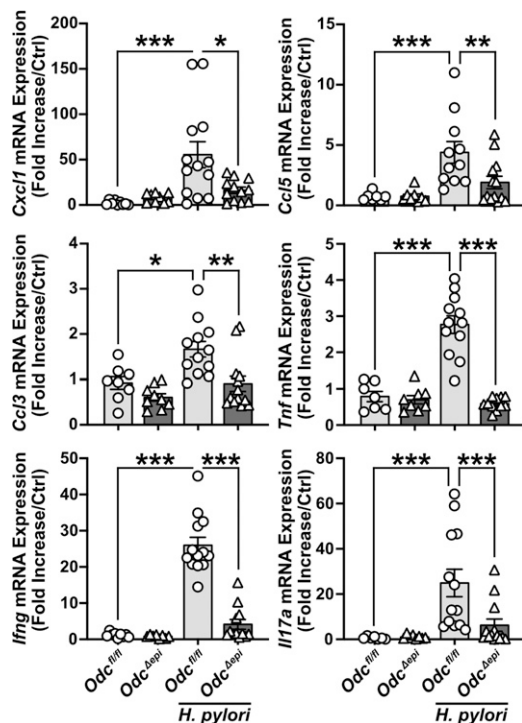
803

FIGURE 8. Targeted mRNA analysis. The expression of genes encoding for different chemokines and cytokines in the gastric tissues of $Odc^{fl/fl}$ and $Odc^{\Delta epi}$ mice, infected or not with *H. pylori*, was analyzed by RT real-time PCR. $n = 7$ or 8 uninfected mice and $n = 12$ or 13 infected mice per genotype. $*p < 0.05$, $**p < 0.01$, $***p < 0.001$.

evidenced that pathways related to innate or specific immune responses (Fig. 7A) were significantly downregulated in the infected $Odc^{\Delta epi}$ mice, confirming that ODC in GECs supports gastric inflammation. Only one pathway related to the immune response, "response to cytokine," was significantly upregulated in the infected $Odc^{\Delta epi}$ mice (Fig. 7B).

These alterations were further confirmed when we quantified selected chemokine and cytokine mRNA expression levels in the tissues of $Odc^{fl/fl}$ and $Odc^{\Delta epi}$ mice. *Cxcl1*, *Ccl5*, *Ccl3*, *Tnf*, *Ifng*, and *Il17a* mRNA expression was significantly induced after *H. pylori* infection in $Odc^{fl/fl}$ mice and significantly reduced in infected $Odc^{\Delta epi}$ mice (Fig. 8).

ODC inhibition diminishes the innate response of human GECs to
H. pylori

We then assessed the direct effect of ODC on the innate activation of GECs. We found a marked and significant reduction in the levels of putrescine and spermidine, but not spermine, when uninfected and *H. pylori*–infected AGS cells were treated with the ODC inhibitor DFMO, as previously observed in cell culture (13, 40) (Fig. 9A). In parallel, the activation of NF-κB (Fig. 9B), the expression of the classic proinflammatory GEC *H. pylori* response gene *CXCL8* (Fig. 9C), and the subsequent protein expression of IL-8 (Fig. 9D) induced by *H. pylori* were inhibited by DFMO. These molecular events were restored when DFMO-treated cells were supplemented with the ODC product putrescine (Fig. 9B–9D). Using siRNA directed against *ODC* (Fig. 9E), we confirmed that the reduction of *CXCL8* mRNA and IL-8 protein expression by DFMO was the result of ODC inhibition. Silencing of *ODC* in AGS cells led to a significant reduction in *H. pylori*–stimulated *CXCL8* mRNA expression (Fig. 9F) and IL-8 protein production (Fig. 9G), as was seen with DFMO treatment.

Discussion

Polyamines are ubiquitous molecules, but decades of investigation have shown that their roles in homeostasis and pathophysiology are disease, time, and cell specific. We have previously demonstrated that *H. pylori*–induced ODC expression in myeloid cells attenuates the antimicrobial/proinflammatory response of innate immune cells, thus supporting bacterial persistence and pathogenesis (13). Here, we questioned the role of ODC in GECs because these cells are the first in contact with the bacterium, produce chemokines that attract immune cells to the gastric mucosa, and are prone to malignant transformation. Thus, we found that genetic deletion of *Odc* in GECs reduces polyamine levels and protects mice from *H. pylori*–induced inflammation and proliferation. We also confirmed by metabolomics and transcriptomics substantive effects of epithelial ODC on inflammatory pathways. Together, these data indicate that the expression of ODC in the gastric epithelium supports *H. pylori* pathogenesis and further demonstrate that polyamines can have multiple and varying effects according to the type of cells in which they are generated.

H. pylori induces sustained acute inflammation, characterized by polymorphonuclear cell infiltration of the gastric mucosa in most infected individuals. This response is characterized by the production of multiple proinflammatory chemokines and cytokines. High levels of these proinflammatory mediators are associated with elevated risk of severe disease (41, 42). Global assessment of the gastric transcriptome from $Odc^{fl/fl}$ and $Odc^{\Delta epi}$ mice revealed a significant downregulation in the expression of chemokines, cytokines, and other immune-associated genes in infected $Odc^{\Delta epi}$ mice. We confirmed by RT-PCR that not only the genes encoding for chemokines expressed in epithelial cells but also those encoding for effectors related to the innate immune system (*Tnf*, *Il1b*, *Cxcl1*) and to T cell activation (*Ifng*, *Il17a*, *Il2*) are regulated by epithelium-specific *Odc* deletion. Furthermore, we also found that ODC expression in cultured GECs favors NF-κB activation and chemokine synthesis. In this context, we postulate that ODC in GECs induces and/or sustains chemokine production, resulting in recruitment of leukocytes in the infected gastric mucosa and thus to the development of a robust innate and adaptive immune response. Because we previously reported that putrescine in macrophages dampens the M1 response (13), a future goal is further elucidating the cellular/molecular mechanism by which ODC supports chemokine synthesis in GECs.

Early studies showed that polyamine levels increase during cell cycle progression and that their depletion inhibits G_1- to S-phase transition (15, 43). Here we used Ki-67 as a marker of cell proliferation in gastric tissues, and we observed increased proliferation in infected $Odc^{fl/fl}$ animals, which is consistent with previous studies in *H. pylori*–infected humans and mice (44, 45). It has been shown that *H. pylori* can interact directly with progenitor cells deep in the glands and accelerates their proliferation, leading to hyperplastic changes (46). We showed that GEC proliferation was significantly reduced in infected $Odc^{\Delta epi}$ versus $Odc^{fl/fl}$ mice, suggesting that polyamines are important mediators of epithelial proliferation in the context of *H. pylori* infection and that polyamine depletion may be a logical strategy to prevent uncontrolled proliferation of GECs with carcinogenic potential.

On the basis of data demonstrating that the ODC inhibitor DFMO reduced gastritis and carcinogenesis in *H. pylori*–infected gerbils (16, 21), our group is conducting a clinical trial of this drug in patients with precancerous gastric lesions in Latin America (ClinicalTrials.gov Identifier: NCT02794428). Furthermore, we have shown that DFMO induces direct oxidative DNA damage to *H. pylori* and specific mutations in the *cagY* gene, which result in reduction in the functionality of the type 4 secretion system and
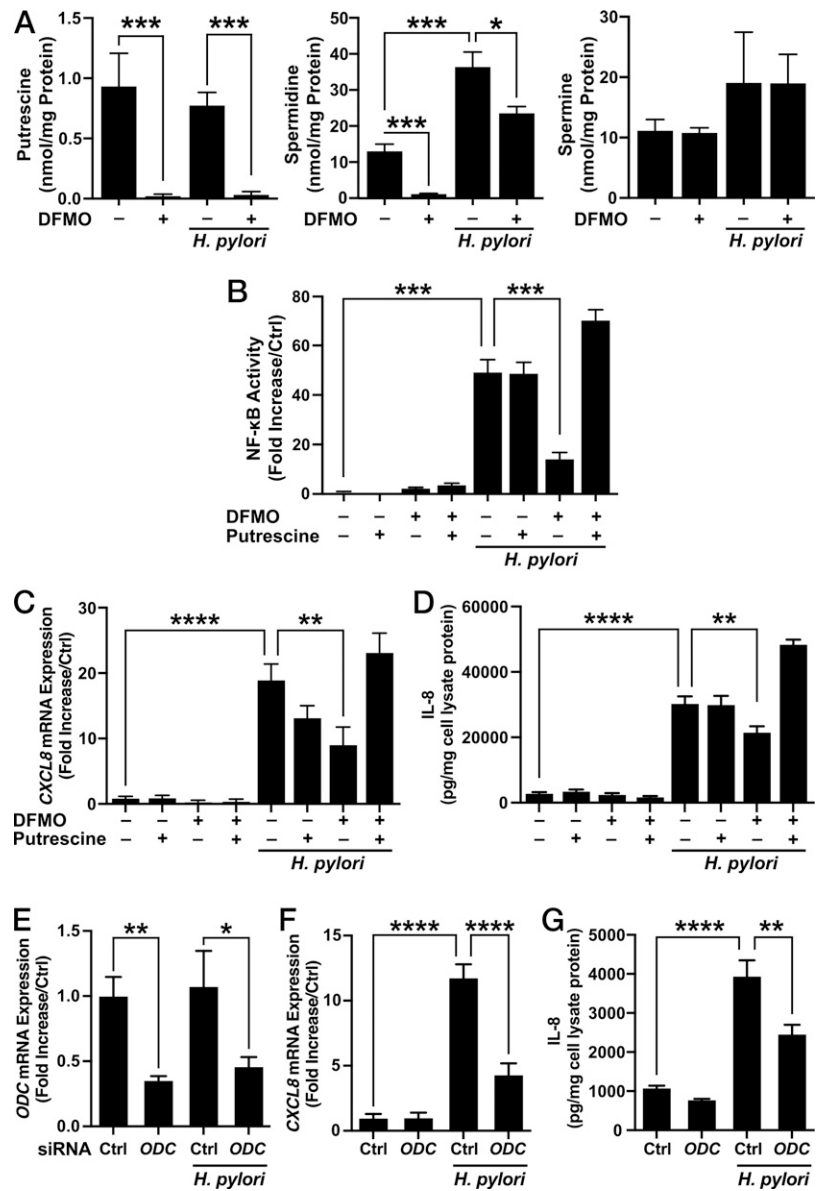
FIGURE 9. Effect of ODC inhibition or knockdown on *H. pylori*–induced innate response in GECs. (**A–D**) AGS cells were treated with DFMO and/or putrescine and then infected or not with *H. pylori* PMSS1. (A) Polyamine levels measured by mass spectrometry. NF-κB activity (B) and *CXCL8* mRNA expression (C) were assessed after infection for 3 h. (D) IL-8 protein concentration was assessed after 6 h. (**E–G**) AGS cells were transfected with siRNA directed against *ODC* or *LMNA* control and then infected or not with *H. pylori* PMSS1. ODC (E) and CXCL8 (F) mRNA expression was assessed after infection for 3 h. (G) IL-8 protein concentration was assessed after 6 h. $*p < 0.05$, $**p < 0.01$, $***p < 0.001$, $****p < 0.0001$. $n = 3–6$.

thus less CagA translocation in GECs (47). This was observed in vitro and in *H. pylori*–infected gerbils treated with DFMO (47). Because we now show an overall protective effect of gastric epithelial *Odc* deletion in *H. pylori*–induced inflammation and a reduction of GEC proliferation, we suggest that a key protective effect of DFMO treatment in *H. pylori* infection is due to the inhibition of epithelial ODC. Moreover, we also show that DFMO treatment or *ODC* knockdown attenuates *H. pylori*–stimulated expression of CXCL8, as well as the IL-8 protein for which it encodes, in human GECs. Therefore, our present work further supports the use of DFMO in *H. pylori*–infected patients to limit the development of more advanced gastric pathology.

Disclosures

The authors have no financial conflicts of interest.

References

1. Uemura, N., S. Okamoto, S. Yamamoto, N. Matsumura, S. Yamaguchi, M. Yamakido, K. Taniyama, N. Sasaki, and R. J. Schlemper. 2001. *Helicobacter pylori* infection and the development of gastric cancer. *N. Engl. J. Med.* 345: 784–789.
2. Correa, P., W. Haenszel, C. Cuello, S. Tannenbaum, and M. Archer. 1975. A model for gastric cancer epidemiology. *Lancet* 306: 58–60.
3. Malfertheiner, P., F. Megraud, C. A. O'Morain, J. Atherton, A. T. Axon, F. Bazzoli, G. F. Gensini, J. P. Gisbert, D. Y. Graham, T. Rokkas, et al; European Helicobacter Study Group. 2012. Management of *Helicobacter pylori* infection— the Maastricht IV/Florence consensus report. *Gut* 61: 646–664.
4. Yada, T., C. Yokoi, and N. Uemura. 2013. The current state of diagnosis and treatment for early gastric cancer. *Diagn. Ther. Endosc.* 2013: 241320.
5. Morgan, D. R., J. Torres, R. Sexton, R. Herrero, E. Salazar-Martínez, E. R. Greenberg, L. E. Bravo, R. L. Dominguez, C. Ferreccio, E. C. Lazcano-Ponce, et al. 2013. Risk of recurrent *Helicobacter pylori* infection 1 year after initial eradication therapy in 7 Latin American communities. *JAMA* 309: 578–586.
6. Areia, M., R. Carvalho, A. T. Cadime, F. Rocha Gonçalves, and M. Dinis-Ribeiro. 2013. Screening for gastric cancer and surveillance of premalignant lesions: a systematic review of cost-effectiveness studies. *Helicobacter* 18: 325–337.
7. Pegg, A. E. 2016. Functions of polyamines in mammals. *J. Biol. Chem.* 291: 14904–14912.
8. McNamara, K. M., A. P. Gobert, and K. T. Wilson. 2021. The role of polyamines in gastric cancer. *Oncogene* 40: 4399–4412.
9. Eisenberg, T., H. Knauer, A. Schauer, S. Büttner, C. Ruckenstuhl, D. Carmona-Gutierrez, J. Ring, S. Schroeder, C. Magnes, L. Antonacci, et al. 2009. Induction of autophagy by spermidine promotes longevity. *Nat. Cell Biol.* 11: 1305–1314.
10. Zhao, Y. C., Y. J. Chi, Y. S. Yu, J. L. Liu, R. W. Su, X. H. Ma, C. H. Shan, and Z. M. Yang. 2008. Polyamines are essential in embryo implantation: expression and function of polyamine-related genes in mouse uterus during peri-implantation period. *Endocrinology* 149: 2325–2332.
11. Timmons, J., E. T. Chang, J. Y. Wang, and J. N. Rao. 2012. Polyamines and gut mucosal homeostasis. *J Gastrointest Dig Syst* 2(Suppl 7): 001.

12. Hobbs, C. A., and S. K. Gilmour. 2000. High levels of intracellular polyamines promote histone acetyltransferase activity resulting in chromatin hyperacetylation. *J. Cell. Biochem.* 77: 345–360.

13. Hardbower, D. M., M. Asim, P. B. Luis, K. Singh, D. P. Barry, C. Yang, M. A. Steeves, J. L. Cleveland, C. Schneider, M. B. Piazuelo, et al. 2017. Ornithine decarboxylase regulates M1 macrophage activation and mucosal inflammation via histone modifications. *Proc. Natl. Acad. Sci. USA* 114: E751–E760.

14. Latour, Y. L., A. P. Gobert, and K. T. Wilson. 2020. The role of polyamines in the regulation of macrophage polarization and function. *Amino Acids* 52: 151–160.

15. Heby, O., G. P. Sarna, L. J. Marton, M. Omine, S. Perry, and D. H. Russell. 1973. Polyamine content of AKR leukemic cells in relation to the cell cycle. *Cancer Res.* 33: 2959–2964.

16. Chaturvedi, R., T. de Sablet, M. Asim, M. B. Piazuelo, D. P. Barry, T. G. Verriere, J. C. Sierra, D. M. Hardbower, A. G. Delgado, B. G. Schneider, et al. 2015. Increased *Helicobacter pylori*-associated gastric cancer risk in the Andean region of Colombia is mediated by spermine oxidase. *Oncogene* 34: 3429–3440.

17. Erdman, S. H., N. A. Ignatenko, M. B. Powell, K. A. Blohm-Mangone, H. Holubec, J. M. Guillén-Rodriguez, and E. W. Gerner. 1999. APC-dependent changes in expression of genes influencing polyamine metabolism, and consequences for gastrointestinal carcinogenesis, in the Min mouse. *Carcinogenesis* 20: 1709–1713.

18. Saulnier Sholler, G. L., E. W. Gerner, G. Bergendahl, R. B. MacArthur, A. VanderWerff, T. Ashikaga, J. P. Bond, W. Ferguson, W. Roberts, R. K. Wada, et al. 2015. A phase I trial of DFMO targeting polyamine addiction in patients with relapsed/refractory neuroblastoma. *PLoS One* 10: e0127246.

19. Meyskens, F. L., Jr., C. E. McLaren, D. Pelot, S. Fujikawa-Brooks, P. M. Carpenter, E. Hawk, G. Kelloff, M. J. Lawson, J. Kidao, J. McCracken, et al. 2008. Difluoromethylornithine plus sulindac for the prevention of sporadic colorectal adenomas: a randomized placebo-controlled, double-blind trial. *Cancer Prev. Res. (Phila.)* 1: 32–38.

20. Linsalata, M., A. Orlando, and F. Russo. 2014. Pharmacological and dietary agents for colorectal cancer chemoprevention: effects on polyamine metabolism (review). *Int. J. Oncol.* 45: 1802–1812.

21. Chaturvedi, R., M. Asim, S. Hoge, N. D. Lewis, K. Singh, D. P. Barry, T. de Sablet, M. B. Piazuelo, A. R. Sarvaria, Y. Cheng, et al. 2010. Polyamines impair immunity to *Helicobacter pylori* by inhibiting L-arginine uptake required for nitric oxide production. *Gastroenterology* 139: 1686–1698.e6.

22. Shibata, W., S. Takaishi, S. Muthupalani, D. M. Pritchard, M. T. Whary, A. B. Rogers, J. G. Fox, K. S. Betz, K. H. Kaestner, M. Karin, and T. C. Wang. 2010. Conditional deletion of IκB-kinase-β accelerates *Helicobacter*-dependent gastric apoptosis, proliferation, and preneoplasia. *Gastroenterology* 138: 1022–1034.e10.

23. Hardbower, D. M., K. Singh, M. Asim, T. G. Verriere, D. Olivares-Villagómez, D. P. Barry, M. M. Allaman, M. K. Washington, R. M. Peek, Jr., M. B. Piazuelo, and K. T. Wilson. 2016. EGFR regulates macrophage activation and function in bacterial infection. *J. Clin. Invest.* 126: 3296–3312.

24. Sierra, J. C., M. Asim, T. G. Verriere, M. B. Piazuelo, G. Suarez, J. Romero-Gallo, A. G. Delgado, L. E. Wroblewski, D. P. Barry, R. M. Peek, et al. 2018. Epidermal growth factor receptor inhibition downregulates *Helicobacter pylori*-induced epithelial inflammatory responses, DNA damage and gastric carcinogenesis. *Gut* 67: 1247–1260.

25. Dixon, M. F., R. M. Genta, J. H. Yardley, and P. Correa. 1996. Classification and grading of gastritis. The updated Sydney System. International Workshop on the Histopathology of Gastritis, Houston 1994. *Am. J. Surg. Pathol.* 20: 1161–1181.

26. Rogers, A. B., N. S. Taylor, M. T. Whary, E. D. Stefanich, T. C. Wang, and J. G. Fox. 2005. *Helicobacter pylori* but not high salt induces gastric intraepithelial neoplasia in B6129 mice. *Cancer Res.* 65: 10709–10715.

27. Chaturvedi, R., M. Asim, J. Romero-Gallo, D. P. Barry, S. Hoge, T. de Sablet, A. G. Delgado, L. E. Wroblewski, M. B. Piazuelo, F. Yan, et al. 2011. Spermine oxidase mediates the gastric cancer risk associated with *Helicobacter pylori* CagA. *Gastroenterology* 141: 1696–1708.e2.

28. Suarez, G., J. Romero-Gallo, M. B. Piazuelo, G. Wang, R. J. Maier, L. S. Forsberg, P. Azadi, M. A. Gomez, P. Correa, and R. M. Peek, Jr. 2015. Modification of *Helicobacter pylori* peptidoglycan enhances NOD1 activation and promotes cancer of the stomach. *Cancer Res.* 75: 1749–1759.

29. Chen, S., Y. Zhou, Y. Chen, and J. Gu. 2018. fastp: an ultra-fast all-in-one FASTQ preprocessor. *Bioinformatics* 34: i884–i890.

30. Patro, R., G. Duggal, M. I. Love, R. A. Irizarry, and C. Kingsford. 2017. Salmon provides fast and bias-aware quantification of transcript expression. *Nat. Methods* 14: 417–419.

31. Love, M. I., C. Soneson, P. F. Hickey, L. K. Johnson, N. T. Pierce, L. Shepherd, M. Morgan, and R. Patro. 2020. Tximeta: reference sequence checksums for provenance identification in RNA-seq. *PLoS Comput. Biol.* 16: e1007664.

32. Love, M. I., W. Huber, and S. Anders. 2014. Moderated estimation of fold change and dispersion for RNA-seq data with DESeq2. *Genome Biol.* 15: 550.

33. Chaturvedi, R., M. Asim, M. B. Piazuelo, F. Yan, D. P. Barry, J. C. Sierra, A. G. Delgado, S. Hill, R. A. Casero, Jr., L. E. Bravo, et al. 2014. Activation of EGFR and ERBB2 by *Helicobacter pylori* results in survival of gastric epithelial cells with DNA damage. *Gastroenterology* 146: 1739–1751.e14.

34. Gobert, A. P., N. T. Al-Greene, K. Singh, L. A. Coburn, J. C. Sierra, T. G. Verriere, P. B. Luis, C. Schneider, M. Asim, M. M. Allaman, et al. 2018. Distinct immunomodulatory effects of spermine oxidase in colitis induced by epithelial injury or infection. *Front. Immunol.* 9: 1242.

35. Gobert, A. P., J. L. Finley, Y. L. Latour, M. Asim, T. M. Smith, T. G. Verriere, D. P. Barry, M. M. Allaman, A. G. Delagado, K. L. Rose, et al. 2020. Hypusination orchestrates the antimicrobial response of macrophages. *Cell Rep.* 33: 108510.

36. Haddad, J. J. 2002. Redox regulation of pro-inflammatory cytokines and IκB-alpha/NF-κB nuclear translocation and activation. *Biochem. Biophys. Res. Commun.* 296: 847–856.

37. Tannahill, G. M., A. M. Curtis, J. Adamik, E. M. Palsson-McDermott, A. F. McGettrick, G. Goel, C. Frezza, N. J. Bernard, B. Kelly, N. H. Foley, et al. 2013. Succinate is an inflammatory signal that induces IL-1β through HIF-1α. *Nature* 496: 238–242.

38. Gewirtz, A. T., L. S. Collier-Hyams, A. N. Young, T. Kucharzik, W. J. Guilford, J. F. Parkinson, I. R. Williams, A. S. Neish, and J. L. Madara. 2002. Lipoxin a4 analogs attenuate induction of intestinal epithelial proinflammatory gene expression and reduce the severity of dextran sodium sulfate-induced colitis. *J. Immunol.* 168: 5260–5267.

39. Hogaboam, C. M., E. Y. Bissonnette, B. C. Chin, A. D. Befus, and J. L. Wallace. 1993. Prostaglandins inhibit inflammatory mediator release from rat mast cells. *Gastroenterology* 104: 122–129.

40. Casero, R. A., Jr., and L. J. Marton. 2007. Targeting polyamine metabolism and function in cancer and other hyperproliferative diseases. *Nat. Rev. Drug Discov.* 6: 373–390.

41. Peek, R. M., Jr., G. G. Miller, K. T. Tham, G. I. Perez-Perez, X. Zhao, J. C. Atherton, and M. J. Blaser. 1995. Heightened inflammatory response and cytokine expression in vivo to *cagA*+ *Helicobacter pylori* strains. *Lab. Invest.* 73: 760–770.

42. El-Omar, E. M., C. S. Rabkin, M. D. Gammon, T. L. Vaughan, H. A. Risch, J. B. Schoenberg, J. L. Stanford, S. T. Mayne, J. Goedert, W. J. Blot, et al. 2003. Increased risk of noncardia gastric cancer associated with proinflammatory cytokine gene polymorphisms. *Gastroenterology* 124: 1193–1201.

43. Fredlund, J. O., M. C. Johansson, E. Dahlberg, and S. M. Oredsson. 1995. Ornithine decarboxylase and S-adenosylmethionine decarboxylase expression during the cell cycle of Chinese hamster ovary cells. *Exp. Cell Res.* 216: 86–92.

44. Peek, R. M., Jr., S. F. Moss, K. T. Tham, G. I. Pérez-Pérez, S. Wang, G. G. Miller, J. C. Atherton, P. R. Holt, and M. J. Blaser. 1997. *Helicobacter pylori cagA*+ strains and dissociation of gastric epithelial cell proliferation from apoptosis. *J. Natl. Cancer Inst.* 89: 863–868.

45. Bertaux-Skeirik, N., R. Feng, M. A. Schumacher, J. Li, M. M. Mahe, A. C. Engevik, J. E. Javier, R. M. Peek, Jr., K. Ottemann, V. Orian-Rousseau, et al. 2015. CD44 plays a functional role in *Helicobacter pylori*-induced epithelial cell proliferation. *PLoS Pathog.* 11: e1004663.

46. Sigal, M., M. E. Rothenberg, C. Y. Logan, J. Y. Lee, R. W. Honaker, R. L. Cooper, B. Passarelli, M. Camorlinga, D. M. Bouley, G. Alvarez, et al. 2015. *Helicobacter pylori* activates and expands LGR5+ stem cells through direct colonization of the gastric glands. *Gastroenterology* 148: 1392–404.e21.

47. Sierra, J. C., G. Suarez, M. B. Piazuelo, P. B. Luis, D. R. Baker, J. Romero-Gallo, D. P. Barry, C. Schneider, D. R. Morgan, R. M. Peek, Jr., et al. 2019. α-Difluoromethylornithine reduces gastric carcinogenesis by causing mutations in *Helicobacter pylori cagY*. *Proc. Natl. Acad. Sci. USA* 116: 5077–5085.